

# **Synthesis of Controlled-Structure Methacrylic Copolymers via Aqueous RAFT Polymerisation**



**Craig Peter Jesson**

**Department of Chemistry**

**The University of Sheffield**

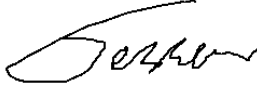
**Submitted to the University of Sheffield in fulfilment of the  
requirements for the award of Doctor of Philosophy**

**July 2019**

Date Submitted: 12.07.19

## Declaration

The work described in this Thesis was carried out at the University of Sheffield under the supervision of Professor Steven P. Armes FRS between October 2015 and July 2019 and has not been submitted, either wholly or in part, for this or any other degree. All the work is the original work of the author, except where acknowledged by references.

Signature:.....

Craig Peter Jesson

July 2019

## Acknowledgements

Anyone who has known me during my PhD, knows that it has not been an easy journey, with life adamant on trying to stop me getting to the end. But fortunately, I've finally made it and there are many people who I need to thank for getting me there.

First and foremost, I would like to thank Prof. Steve Armes for allowing me to do my PhD in his group. He has been an unrivalled measure of support and knowledge for the whole 4 years I've been in his group. In particular, thanks for keeping things going and bringing the PhD to me when I couldn't make it to you!

To the rest of the Armes group, thanks for all the assistance over the years. Thanks for teaching me the basics, coaching me when I started and making downstairs office life entertaining (Joe, Nick, Vicki, Lizzy). And thanks for making my PhD years fun both in and out of the department (Reb, Olly, Erik, Shannon, Deb). Sarah and Erik, we started this PhD together, I enjoyed stumbling through the unknowns with you guys.

Thanks to all the other staff in the department who helped things run smoothly. Denise and Louise, thanks for the help with financial matters and never being annoyed when I turned up with another issue. Thank you Dean for helping with all the computer and IT matters (of which there were many!). Thanks to Sandra for helping me design and run NMR experiments over the years. And thanks the Stephen Atkin for helping fix things in the Lab and just generally being a nice guy to chat to.

Thanks to the Leggett group (Brice) and Gary who helped me discover the world of ATRP and polymer brushes. It was short but I learned a lot, thanks for being patient with me.

To the staff of GEO specialty chemicals, thanks for being so friendly and welcoming me into your ranks for my time in Hythe. You were all so friendly, despite barely knowing me. I am especially grateful for your efforts in fundraising after hearing about my accident, your kindness means so much! In particular, thanks to the R+D team (George, Léon, Becky, Jeremy, Nat, Matt, Mel, Mike, Andy and Mark). You guys made my time at GEO enjoyable, thanks for answering all my questions and putting up with me, I hope we stay in touch!

Reb, I promised you a special mention and here it is bestie! Thanks for being there through the good times and the bad, you really made the work a lot more fun than it should have been. I'll especially remember all the hours spent convincing you that you can make it to. Craig and the Spheres wouldn't be the same without you.

Claire, you have been my rock since day one. Thanks for sticking by me through the years in Sheffield, even though I know you didn't really want to be there. You are my reason for carrying on and I wouldn't have been able to bounce back without your love and support.

Thanks to my family whose unyielding support knows know bounds. Thanks for everything growing up and for giving up so much time to keep me company during my recovery, it meant a lot. To Mum, Dad and Liz, thanks for adapting your houses for me and giving me a place to live and write up my PhD. I'm sorry for all the scratches to skirting boards and cupboards!

Finally, thanks goes to The University of Sheffield, EPSRC and GEO Specialty Chemicals for funding my CDT studentship and to GEO for supplying the monomers used in these studies. None of this work would have been possible without it.

## **Dissemination of Research Findings**

### **Primary publications resulting from work presented in this thesis**

“H<sub>2</sub>O<sub>2</sub> Enables Convenient Removal of RAFT End-Groups from Block Copolymer Nano-Objects Prepared via Polymerization-Induced Self-Assembly in Water” C. P. Jesson, C. M. Pearce, H. Simon, A. Werner, V. J. Cunningham, J. R. Lovett, M. J. Smallridge, N. J. Warren and S. P. Armes, *Macromolecules*, **2017**, *50*, 182-191.

“Synthesis of high molecular weight poly(glycerol monomethacrylate) via RAFT emulsion polymerization of isopropylidenglycerol methacrylate” C. P. Jesson, V. J. Cunningham, M. J. Smallridge and S. P. Armes, *Macromolecules*, **2018**, *51*, 3221-3232.

### **Publications resulting from work conducted on other projects**

“Using Host-Guest Chemistry to Tune the Kinetics of Morphological Transitions Undertaken by Block Copolymer Vesicles” H. Yao, Y. Ning, C. P. Jesson, J. He, R. Deng, T. Wei and S. P. Armes, *ACS Macro Lett.*, **2017**, *6* (12), 1379-1385

### **Poster presentations at conferences**

“End-Group Removal for RAFT-synthesised Nanoparticles using Hydrogen Peroxide” The Polymer Conference, 10<sup>th</sup>-14<sup>th</sup> July 2016, Warwick, UK.

“End-Group Removal for RAFT-synthesised Nanoparticles using Hydrogen Peroxide” Advanced Polymers via Macromolecular Engineering, 21<sup>st</sup>-25<sup>th</sup> May 2017, Ghent, Belgium.

“End-Group Removal for RAFT-synthesised Nanoparticles using Hydrogen Peroxide” American Chemical Society National Meeting and Exposition, 20<sup>th</sup>-24<sup>th</sup> August 2017, Washington, DC, USA.

**Abstract.** Over the past two decades, reversible addition-fragmentation chain transfer (RAFT) polymerization has become widely recognized as a powerful technique for the synthesis of controlled-structure polymers. However, RAFT-synthesized polymers are typically colored and malodorous owing to the presence of the organosulfur-based RAFT end-group(s). It is well-known that such end-groups can be removed by treating *molecularly-dissolved copolymer chains* with excess free radical initiators, amines or oxidants. Herein we report a convenient method for the removal of RAFT end-groups from *aqueous dispersions of diblock copolymer nano-objects* using H<sub>2</sub>O<sub>2</sub>. This oxidant is relatively cheap, has minimal impact on the copolymer morphology and produces benign side-products that can be readily removed via dialysis. We investigate the efficiency of end-group removal for various diblock copolymer nano-objects prepared with either dithiobenzoate- or trithiocarbonate-based RAFT chain transfer agents. It is demonstrated that UV GPC offers a decisive advantage over UV spectroscopy for assessing both the kinetics and extent of end-group removal.

High molecular weight water-soluble polymers are widely used as flocculants or thickeners. However, their synthesis via solution polymerization invariably results in highly viscous fluids, which makes subsequent processing somewhat problematic. Alternatively, such polymers can be prepared as colloidal dispersions; in principle, this is advantageous because the particulate nature of the polymer chains ensures a much lower fluid viscosity. Herein we exemplify the latter approach by reporting the convenient one-pot synthesis of high molecular weight poly(glycerol monomethacrylate) (PGMA) via RAFT aqueous emulsion polymerization of a water-immiscible protected monomer, isopropylidenglycerol methacrylate (IPGMA), at 70 °C, using a water-soluble poly(glycerol monomethacrylate) (PGMA) chain transfer agent as a steric stabilizer. This formulation produces a low-viscosity aqueous dispersion of PGMA-PIPGMA diblock copolymer spheres at 20% solids. Subsequent acid deprotection of the hydrophobic core-forming PIPGMA block leads to nanoparticle dissolution and affords a viscous aqueous solution comprising high molecular weight PGMA homopolymer chains with a relatively narrow molecular weight distribution. Moreover, it is shown that this latex precursor route offers an important advantage over the RAFT aqueous solution polymerization of glycerol monomethacrylate because it provides a significantly faster rate of polymerization (and hence higher monomer conversion) under comparable conditions. This latex precursor route has been extended to include aqueous emulsion polymerization of IPGMA using conventional free radical chemistry combined with an anionic surfactant. In this case, monomer-starved conditions are required to minimize gel formation when converting the PIPGMA latex into water-soluble PGMA chains via acid hydrolysis. Moreover, significantly higher molecular weight PGMA chains can be prepared compared to that obtained via RAFT aqueous emulsion polymerization. Finally, a one-pot synthetic protocol in which the intermediate PIPGMA latex is directly converted into PGMA at low pH appears to be feasible.

Finally, a *cis*-diol-capped analogue of oligo(ethylene glycol) methacrylate (OEGMA) known as ‘GEO5MA’ has been prepared on a 1.2 kg scale via a four-step synthesis performed while on secondment at GEO Specialty Chemicals. Preliminary experiments confirm that this monomer can be polymerized with good control by RAFT solution polymerization to produce PGEO5MA. The pendent *cis*-diol groups on this precursor can be selectively oxidized using sodium periodate in aqueous solution at ambient temperature to afford a rare example of an *aldehyde-functional water-soluble polymer*. A similar approach can be used to prepare *aldehyde-functionalized diblock copolymer nano-objects* via aqueous PISA.

## Common Abbreviations

ACVA	4,4'-azobis(4-cyanopentanoic acid)
ARGET	Activators Regenerated by Electron Transfer
ATRP	Atom Transfer Radical Polymerisation
BzMA	Benzyl methacrylate
CPDB	2-cyano-2-propyl dithiobenzoate
CRP	Controlled Radical Polymerisation
CTA	Chain Transfer Agent
DLS	Dynamic Light Scattering
DMF	Dimethyl formamide
DP	Degree of Polymerisation
FESEM	Field Emission Scanning Electron Microscopy
FRP	Free Radical Polymerisation
GMA	Glycerol monomethacrylate
GPC	Gel Permeation Chromatography
HPLC	High Performance Liquid Chromatography
HPMA	2-hydroxypropyl methacrylate
IPGMA	Isopropylidene glycerol methacrylate
$k_i$	Rate of Initiation
$k_p$	Rate of Propagation
$k_t$	Rate of Termination
LAM	Less Activated Monomer
Macro-CTA	Macromolecular Chain Transfer Agent
MAM	More Activated Monomer
$M_n$	Number-average Molecular Weight
$M_w$	Weight-average Molecular Weight
MWD	Molecular Weight Distribution

$M_w/M_n$	Dispersity
NMP	Nitroxide Mediated Polymerisation
NMR	Nuclear Magnetic Resonance
PBzMA	poly(benzyl methacrylate)
PDI	Polydispersity index
PEG	Poly(ethylene glycol)
PETTC	4-cyano-4-(2-phenylethanesulfanylthiocarbonyl)- sulfanylpentanoic acid)
PGMA	poly(glycerol monomethacrylate)
PHPMA	poly(2-hydroxypropyl methacrylate)
PIPGMA	poly(isopropylidene glycerol monomethacrylate)
PISA	Polymerisation-induced self-assembly
PS	Polystyrene
RAFT	Reversible Addition Fragmentation Chain-Transfer
$R_i$	Rate of Initiation
$R_p$	Rate of Propagation
$R_{\text{Polym}}$	Rate of Polymerisation
$R_t$	Rate of Termination
SEM	Scanning electron microscopy
TEM	Transmission electron microscopy
$T_g$	Glass transition temperature
TGA	Thermogravimetric analysis
UV-Vis	Ultraviolet-visible

# Contents

## **Chapter One - Introduction..... 1**

Free Radical Polymerisation (FRP) .....	4
Bulk/Solution Polymerisation .....	7
Precipitation Polymerisation .....	7
Dispersion Polymerisation .....	7
Aqueous Emulsion Polymerisation .....	9
Living Polymerisations .....	11
Living anionic polymerisation .....	12
Controlled Radical Polymerisation (CRP) .....	14
Atom Transfer Radical Polymerisation (ATRP) .....	14
Reversible Addition-Fragmentation chain Transfer (RAFT) Polymerisation .....	19
Modification and Removal of RAFT End-Groups.....	22
Polymer Brushes .....	25
Self-Assembly of Amphiphiles .....	25
Polymerisation-Induced Self-Assembly (PISA) .....	28
Aims of this PhD Project.....	38
References .....	41

## **Chapter 2 - H<sub>2</sub>O<sub>2</sub> enables convenient removal of RAFT end-groups from block copolymer nano-objects prepared via polymerisation-induced self-assembly in water ..... 53**

Introduction .....	54
Experimental .....	55
Results and Discussion.....	62
Conclusions .....	79
References .....	80



**Chapter 3 - Synthesis of high molecular weight poly(glycerol monomethacrylate) via RAFT emulsion polymerisation of isopropylidenglycerol methacrylate ..... 86**

Introduction .....	87
Experimental .....	90
Results and Discussion.....	94
Conclusions .....	112
References .....	113

**Chapter Four - Synthesis of high molecular weight poly(glycerol monomethacrylate) via conventional aqueous emulsion polymerisation of isopropylidenglycerol methacrylate ..... 122**

Introduction .....	123
Experimental .....	125
Results and Discussion.....	128
Conclusions .....	141
Future Work .....	142
References .....	144

**Chapter Five – Synthesis and characterisation of aldehyde-functional homopolymers, block copolymers and brushes ..... 145**

Introduction .....	146
Experimental .....	148
Results and Discussion.....	152
Conclusions .....	166
Future Work .....	167
References .....	168

**Chapter Six - Conclusions and Prospect ..... 170**

Conclusions and Prospect ..... 171

References ..... 175

**Chapter Seven – Appendix ..... 178**

# **Chapter One - Introduction**

## Introduction

In recent years, the use of polymers in modern society has become ubiquitous. With ever-increasing applications, polymer science has had to adapt and evolve to meet a wide range of complex requirements. It was less than 100 years ago when Staudinger first proposed that polymers were long-chain molecules made up of covalently-bound building blocks or repeat units called monomers.<sup>1</sup> When this revolutionary and controversial concept was finally established in 1929, Carothers proposed that there were two categories of synthetic polymers: ‘addition’ polymers and ‘condensation’ polymers.<sup>2</sup> While the repeat unit of an ‘addition’ polymer is identical to that of the monomer being polymerised, ‘condensation’ polymers are typically formed via elimination of a small molecule such as water, with one such side-product being eliminated for every repeat unit linkage. This initial classification system worked well for the majority of polymers but over time it became apparent that there were some obvious exceptions, such as polyurethanes. In 1953, this system was updated by Flory, who proposed that polymers should be classified as either ‘step’ or ‘chain’ depending on their reaction mechanisms.<sup>3</sup> Step-growth polymers involve the gradual build-up of long-chain polymers via dimers, trimers, oligomers etc., whereas the formation of chain-growth polymers proceeds by sequential addition of a single (monomer) unit. The latter mechanism is used for the polymerisation of vinyl monomers, as discussed in this thesis.

Unlike small molecules, synthetic polymers do not exhibit a single unique molecular weight. Instead, they possess a range of molecular weights and hence a molecular weight distribution (MWD). In this situation, it is useful to define certain moments of the MWD. For example, the number average molecular weight ( $M_n$ ) is defined as follows:

$$\langle M_n \rangle = \frac{\sum n_i M_i}{\sum n_i} \quad (1)$$

Where  $M$  is the molecular weight of a polymeric fragment and  $n$  is the number of fragments of this molecular weight.<sup>4</sup> Another important moment of the MWD is the weight-average molecular weight ( $M_w$ ), which is defined as:

$$\langle M_w \rangle = \frac{\sum n_i M_i^2}{\sum n_i M_i} \quad (2)$$

According to equations (1) and (2),  $M_w$  is more biased towards higher molecular weight species than  $M_n$ .  $M_w/M_n$  is known as the polydispersity index, or dispersity, and is always greater than unity. This parameter provides a crude measure of the breadth of the MWD.<sup>4</sup>

Over the past fifty years or so, synthetic polymer chemists have designed a remarkably wide range of complex architectures. Initially, the evolution of polymer architecture involved the use of multiple monomer feeds and monomers with multiple reactive sites to give rise to homopolymers, statistical copolymers, alternating copolymers and branched copolymers (see Figure 1.1)

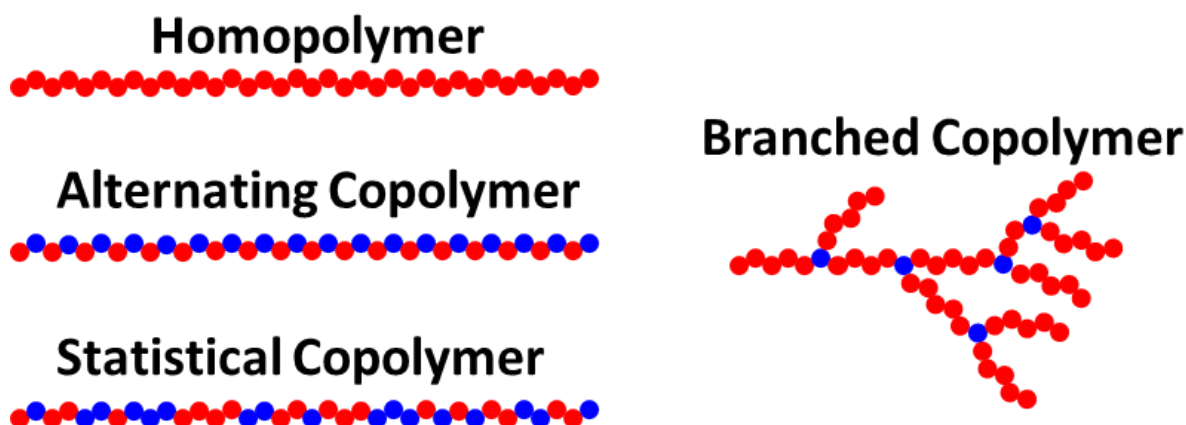


**Figure 1.1.** Examples of simple polymer architectures obtainable by non-living polymerisation techniques

Although some degree of control over copolymer architecture is possible with conventional polymerisation techniques, the use of so-called living polymerisations offers superior control, as discussed below.

### Free Radical Polymerisation (FRP)

Free radical polymerisation (FRP) is a type of chain-growth polymerisation.<sup>3</sup> It is an extremely versatile technique and is used for the polymerisation of many vinyl monomers in industrial applications. FRP is applicable to a wide range of functional monomers in various solvents and usually does not require protecting group chemistry.<sup>5</sup> Moreover, FRP is unaffected by impurities or by the presence of protic solvents such as water. This enables FRP to be conducted under bulk, solution, suspension, emulsion or dispersion polymerisation conditions. One disadvantage of FRP is its susceptibility to oxygen; polymerisations must be carried out under an inert atmosphere in order to eliminate oxygen, which would otherwise cause retardation. FRP comprises four distinct stages: initiation, propagation, termination and transfer, as summarised in Figure 1.2.<sup>4-6</sup>

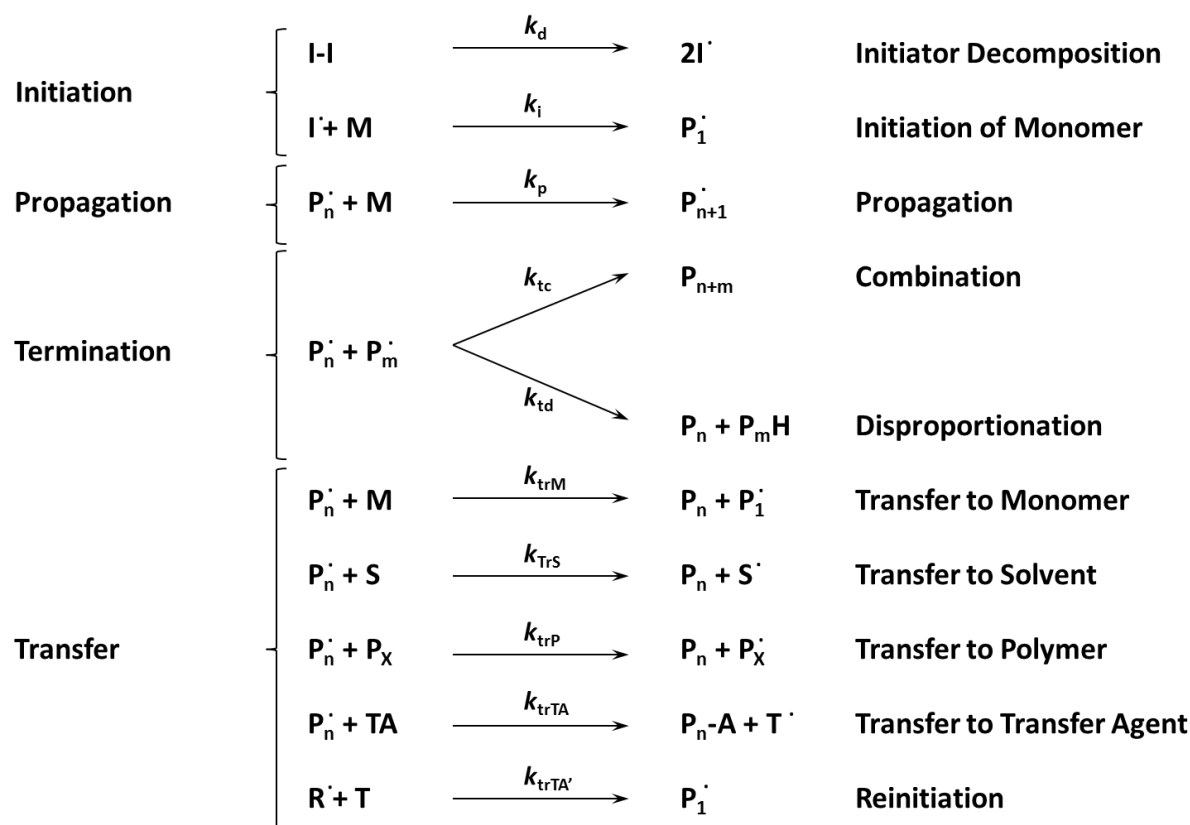


**Figure 1.2.** The four distinct stages of free radical polymerisation (FRP)<sup>6</sup>

During initiation, an initiator (I-I), commonly a peroxide or an azo compound, undergoes homolytic cleavage triggered by thermal degradation or irradiative decay to produce two primary radicals ( $2I^{\cdot}$ ). This is the relatively slow, rate-limiting step. These  $I^{\cdot}$  species then react rapidly with a vinyl monomer, M, to commence polymerisation by forming a new active radical

$P_1\cdot$  with a number-average degree of polymerisation ( $DP_n$ ) of unity. As the rate of initiator decomposition is relatively slow compared to that of the radical reacting with a monomer unit, the overall rate of initiation is given by Equation ( 3 ):

$$R_i = \frac{d[P_1\cdot]}{dt} = 2k_d f [I] \quad (3)$$

Here  $k_d$  is the rate constant for the thermal decomposition of the initiator,  $f$  is the efficiency of the initiator and the factor of two is required because two radicals are generated from the homolytic cleavage of every initiator molecule. The initiator efficiency is a fractional quantity that is a measure of the probability of the initiator radicals reacting with monomer. After initiation, polymer chains grow rapidly via addition of many monomer units to the active radical centre. This is known as the propagation step. The growth of individual chains during propagation typically occurs within a fraction of a second. It is assumed that the rate constant of propagation ( $k_p$ ) is independent of the size of the radical species  $P_n\cdot$ . Hence the rate of monomer consumption is given by Equation ( 4 ).

$$R_p = -\frac{d[M]}{dt} = k_p [P_n\cdot][M] \quad (4)$$

Owing to substantial temporal overlap between initiation and propagation, polymers with relatively broad molecular weight distributions are formed (typical  $M_w/M_n < 2.0$ ).<sup>7</sup> When two propagating polymer radicals meet, they undergo termination either by *combination* (which is favoured for less hindered monomers such as acrylates or styrene) or by *disproportionation* (which is favoured for more hindered monomers such as methacrylates). The latter pathway involves abstraction of a hydrogen atom from the carbon adjacent to the radical centre to form a polymer chain with an unsaturated end-group, or macromonomer. The predominant termination mechanism influences the final molecular weight: polymers that undergo termination solely by combination exhibit twice the molecular weight of those that solely undergo disproportionation.<sup>6</sup> The overall rate of termination is given by Equation ( 5 ).

$$R_t = 2k_t [P\cdot]^2 \quad (5)$$

Finally, polymer radicals can undergo chain transfer reactions. This involves reaction of the active radical centre with either monomer, polymer, solvent or a deliberately added transfer agent. Typically, transfer does not affect the overall kinetics of polymerisation owing to fast reinitiation and no net loss of radicals.<sup>4</sup> However, chain transfer can lead to significant branching, which affects the molecular weight and dispersity of the final polymer.<sup>6</sup>

During FRP, the instantaneous free radical concentration is usually very low and approximately constant. Therefore, it is valid to apply the steady-state approximation and assume that the rate of initiation ( $R_i$ ) is equal to the rate of termination ( $R_t$ ). Combining equations ( 3 ) and ( 5 ) gives an expression for the concentration of polymer radicals  $[P\cdot]$ :

$$[P\cdot] = \sqrt{\frac{fk_d[I]}{k_t}} \quad (6)$$

In addition, the rate of propagation ( $R_p$ ) is significantly larger than that of either initiation or termination, so an expression for the rate of polymerisation can be obtained by substituting equation ( 6 ) into equation ( 4 ):

$$R_{polym} = k_p[M] \sqrt{\frac{fk_d[I]}{k_t}} \quad (7)$$

Thus the rate of polymerisation is first order with respect to the monomer concentration and proportional to the square root of the initiator concentration. Towards the end of the reaction, an ‘auto-acceleration’ effect can be observed for FRP syntheses conducted either in the bulk or at relatively high monomer concentration.<sup>4</sup> This is associated with the relatively high viscosity of concentrated polymer solutions. Diffusion of large polymer chains is retarded under such conditions, which lowers the rate of termination ( $k_t$ ). However, small molecules (e.g. monomer) can still diffuse freely. Thus the rate of propagation ( $k_p$ ) remains relatively high, leading to an overall increase in the rate of polymerisation.<sup>6</sup> If chain transfer to polymer occurs under such conditions, this can sometimes lead to macroscopic gelation.



### **Bulk/Solution Polymerisation**

Bulk polymerisation is the simplest type of polymerisation. Such formulations comprise liquid monomer and a monomer-soluble polymerisation agent such as an initiator or catalyst. The product of this polymerisation is typically either a solid casting (e.g. an acrylic bath) or an extremely viscous solution or gel (e.g. a soft contact lens). However, the polymerising solution becomes highly viscous which can make efficient heat dissipation somewhat problematic; extremely broad molecular weight distributions are very common. These issues are often best addressed by addition of a suitable solvent, transforming the formulation into a solution polymerisation. Solution polymerisation involves reacting a miscible monomer with a soluble initiator to form a soluble polymer in a suitable, non-reactive solvent, allowing much greater control over the solution viscosity and heat dissipation. An important consideration is the boiling point of the solvent, as this limits the polymerisation temperature. Unfortunately, there are few truly inert solvents when it comes to radical polymerisation, and transfer to solvent is almost always observed to some extent. Solution polymerisation may still lead to high viscosity when targeting high molecular weight polymers, but this problem is significantly reduced compared to bulk polymerisation. Depending on the final intended application, one disadvantage of solution polymerisation can be isolation of the desired polymer and its purification (e.g. removal of unreacted monomer and solvent).<sup>8</sup>

### **Precipitation Polymerisation**

If a polymerisation is conducted in a solvent that is a bad solvent for the polymer, the result is a precipitation polymerisation. The precipitated particles are typically large and ill-defined and it is usually difficult to obtain high monomer conversions or to be able to target high molecular weights.<sup>5,9</sup> More well-defined particles can be obtained by adding a suitable steric stabiliser to the formulation, which leads to a dispersion polymerisation (see below).

### **Dispersion Polymerisation**

Dispersion polymerisation involves use of a preformed polymeric stabiliser to form latex particles. The monomer is miscible with the solvent and the initiator is soluble in the continuous phase. At a critical  $DP_n$ , the growing polymer chains become insoluble and phase separate. In the absence of any polymeric stabiliser, a macroscopic precipitate is obtained. In the presence of a suitable polymeric stabiliser, a colloidal dispersion of sterically-stabilised latex is obtained.

Dispersion polymerisation has been conducted utilising a wide range of solvents, including polar solvents such as alcohols,<sup>10-12</sup> non-polar solvents such as n-alkanes<sup>13-14</sup> and also supercritical carbon dioxide<sup>15-18</sup> or ionic liquids.<sup>19</sup> In the specific case of aqueous dispersion polymerisation, there are relatively few water-miscible monomers that form water-insoluble polymers, which is a prerequisite for such formulations. Nevertheless, various examples have been reported in the literature, particularly over the past decade or so. These include the polymerisation of pyrrole (Py)<sup>20-22</sup>, *N*-isopropylacrylamide (NIPAM),<sup>23-24</sup> *N,N'*-diethylacrylamide (DEAA),<sup>25-26</sup> 2-methoxyethyl acrylate (MEA),<sup>27-28</sup> 2-hydroxypropyl methacrylate (HPMA),<sup>29-31</sup> and di(ethylene glycol) methyl ether methacrylate (DEGMA).<sup>32</sup>

The Armes group has published numerous papers describing the aqueous dispersion polymerisation of pyrrole.<sup>20-22</sup> In particular, the effect of using various polymeric stabilisers on the mean latex diameter has been explored.<sup>20</sup> For example, pyrrole was polymerised in water using an iron(III) chloride oxidant and either poly(vinyl alcohol-co-vinyl acetate) or poly(2-vinyl pyridine-co-butyl methacrylate) or poly(ethylene oxide), see Figure 1.3. The purified polypyrrole particles were assessed by transmission electron microscopy (TEM) and a technique known as charge-velocity analysis (CVA). Relatively narrow size distributions were obtained and the mean latex diameter could be tuned between 50 and 350 nm depending on the choice of polymeric stabiliser.

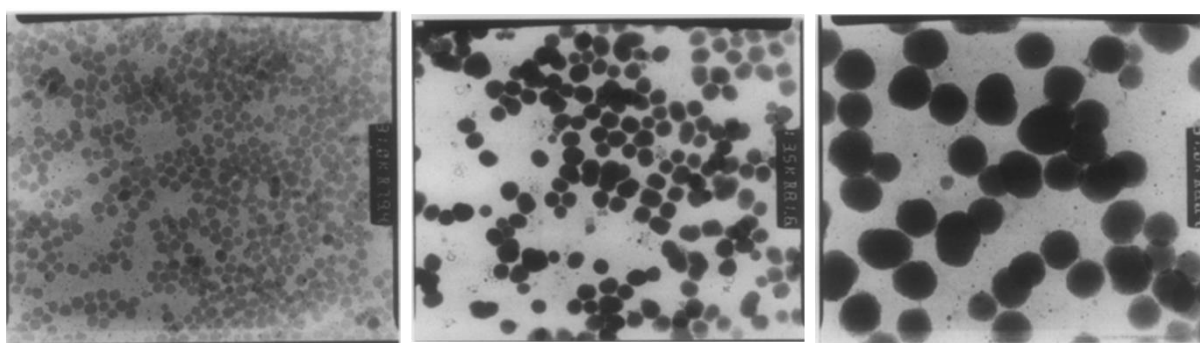


**Figure 1.3.** TEM images of polypyrrole latex particles prepared via aqueous dispersion polymerisation using poly(vinyl alcohol-co-vinyl acetate) (left), poly(2-vinyl pyridine-co-butyl methacrylate) (middle) or poly(ethylene oxide) (right) as the steric stabiliser.<sup>20</sup>

Alternative methods for varying particle size were explored by Ali et al., who examined the aqueous dispersion polymerisation of HPMA using poly(*N*-vinyl pyrrolidone) (PNVP) as a polymeric stabiliser (see Figure 1.4).<sup>31</sup> The initiator type (2,2'-azobis(2-

methylpropionamide) dihydrochloride (AIBA), azobisisobutyronitrile (AIBN), sodium persulfate (SPS), potassium persulfate (KPS), ammonium persulfate (APS)), PNVP stabiliser concentration (from 0 to 10 % w/w) and the presence of low levels of ethyl acrylate comonomer (from 0 to 4 mol. %) were systematically investigated. Purified PHPMA latexes were analysed by DLS to determine particle size distributions. Relatively narrow particle size distributions were obtained, with mean latex diameters varying between 350 and 1100 nm. This is not unexpected for FRP-mediated dispersion polymerisations, which often produce particles in the 1-10  $\mu\text{m}$  range. By adding anionic surfactant (0 to 2 % w/w), particles as small as 110 nm could be achieved.

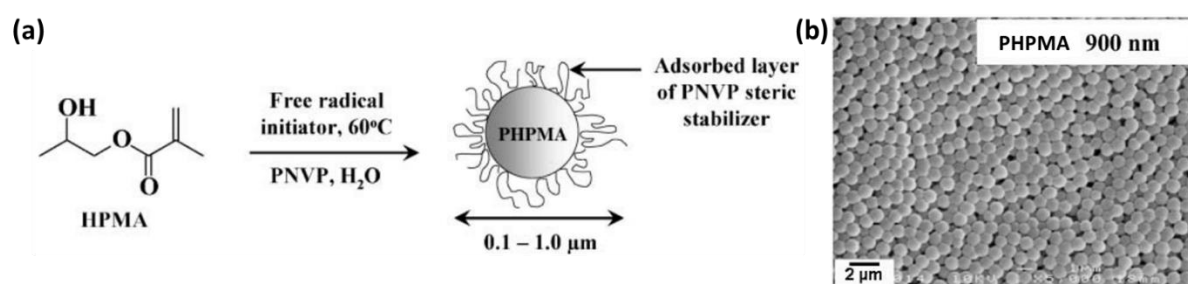


**Figure 1.4.** (a) Schematic for the aqueous dispersion of HPMA using a PNVP stabiliser. (b) Scanning electron microscope (SEM) image of formed PHMA latexes. Conditions: AIBA, 10 % w/w PNVP, 2 mol. % ethyl acetate (EA), 60 °C.<sup>31</sup>

### Aqueous Emulsion Polymerisation

Using water as a solvent for polymerisation has always been desirable in order to avoid large scale use of relatively expensive (and often toxic) organic solvents. However, most vinyl monomers are immiscible with water. This led to the development of new formulations to enable polymerisation of such monomers in aqueous media. The observation that natural rubber was produced in the form of an aqueous colloidal dispersion of latex particles was first made by scientists working at Bayer.<sup>33</sup> In principle, synthesising high molecular weight polymer chains in the form of low-viscosity particles eliminates the problem of high solution viscosity associated with either solution or bulk polymerisation. This led to the first attempt to prepare the synthetic equivalent of synthetic rubber using an emulsified vinyl monomer via a formulation now termed as suspension polymerisation.<sup>34</sup> Following substantial industrial research during WW II, synthetic rubber can now be prepared in the form of water-borne latex.<sup>35</sup>

A typical aqueous emulsion polymerisation consists of a water-immiscible vinyl monomer polymerised in aqueous media in the presence of a water-soluble initiator and a surfactant. The surfactant is required to stabilise the growing polymer latexes and prevent macroscopic precipitation.<sup>36</sup> When the heterogeneous reaction mixture is subjected to high shear, this produces micrometer-sized surfactant-stabilised monomer droplets, much smaller monomer-swollen surfactant micelles and a relatively small amount of molecularly-dissolved monomer. Because the initiator is insoluble within the water-immiscible monomer, no polymerisation can occur within these large monomer droplets. Thermal decomposition of the initiator molecules generates radical species that in principle can react with dissolved monomer (*homogeneous nucleation*) to generate surface-active oligomers that then form micelles *in situ*.<sup>37</sup> Alternatively, if the aqueous monomer solubility is relatively low, these initiator radicals can diffuse into the monomer-swollen surfactant micelles, leading to *heterogeneous nucleation*.<sup>37</sup> In either scenario, the micelles provide the main locus for the vast majority of the polymerisation. Given the relatively high local monomer concentration, polymer radicals propagate rapidly within such micelles. As the supply of monomer becomes depleted, monomer transport from the micrometer-sized surfactant-stabilised droplets into the growing nascent particles occurs. At any given time, either one or zero growing polymer radicals are present in each particle. Thus termination is suppressed relative to propagation and relatively high molecular weight polymer chains can be obtained because of this so-called microcompartmentalisation effect. Eventually, the monomer droplet reservoirs are consumed and colloidally stable latex particles are the final product.<sup>37-38</sup> A schematic representation of an emulsion polymerisation is depicted in Figure 1.5.<sup>37</sup>

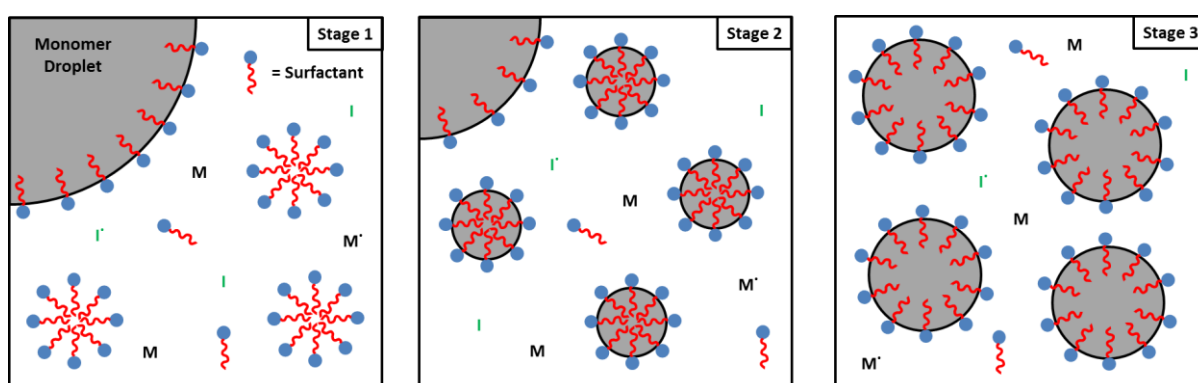


**Figure 1.5.** Schematic representation of the three main stages of emulsion polymerisation: I is the initiator molecule, I' is the corresponding initiator radical, M denotes the monomer and M' indicates the propagating monomeric/polymeric radicals.<sup>37</sup>

### Living Polymerisations

Although FRP is widely utilised on an industrial scale, it offers only limited control over molecular weight, dispersity or copolymer architecture. Living polymerisation resolves these issues by suppressing or eliminating termination with respect to propagation, giving all chains an equal probability of growth. Living polymerisation was discovered by Szwarc and co-workers in 1956,<sup>39-40</sup> where styrene was polymerised in dry tetrahydrofuran via anionic polymerisation. Anionic polymerisation is now used to prepare various controlled-structure copolymers on an industrial scale for various applications, including thermoplastic elastomers,<sup>41-42</sup> polymeric surfactants/dispersants/emulsifiers/stabilisers,<sup>43-44</sup> viscosity modifiers for engine oils<sup>45-46</sup> and diesel soot dispersants.<sup>47-48</sup> Living polymerisations are characterised by a linear evolution in molecular weight against conversion (see Figure 1.6). Moreover, there is either no intrinsic termination or the rate of termination is suppressed relative to that of propagation, which results in much narrower MWDs ( $M_w/M_n \sim 1.10$ ) compared to that achieved using FRP. Such polymerisations also offer convenient access to various complex copolymer architectures, such as block, graft, star and ring copolymers (see Figure 1.7). For example, block copolymers can be prepared via sequential monomer addition. Another advantage of living polymerisation is that a range of desired end-groups can be introduced via post- polymerisation functionalisation.

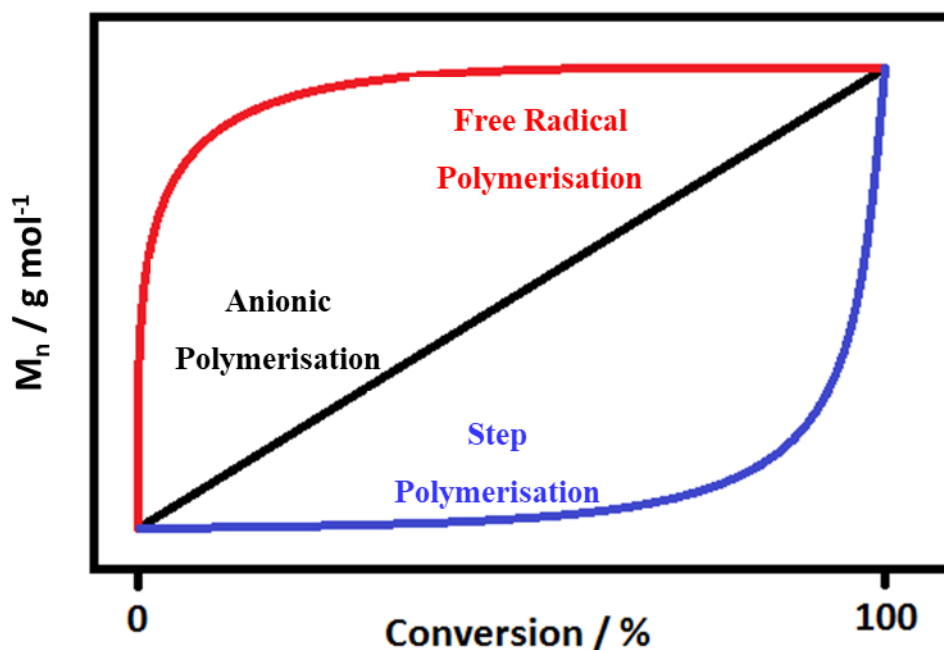


**Figure 1.6.** Evolution in molecular weight with monomer conversion for free radical polymerisation, anionic polymerisation and step polymerisation

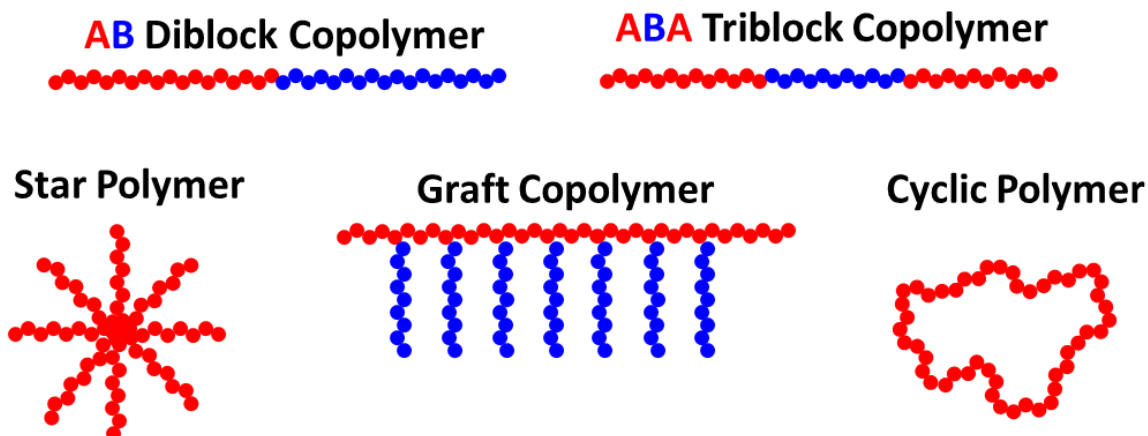


**Figure 1.7.** Examples of well-defined copolymer architectures that can be accessed by living polymerisation.

### Living anionic polymerisation

Anionic polymerisation involves propagation of a carbanion end-group via nucleophilic attack by vinyl monomer. Unlike the polymer radicals present in FRP, such growing carbanions cannot react with each other. Thus, assuming that all protic impurities have been carefully removed, there is no intrinsic termination mechanism. This facilitates the synthesis of polymers with very narrow MWDs and predictable  $M_n$ , where the latter parameter is simply equal to the mass of a monomer unit,  $M$ , multiplied by the monomer/initiator molar ratio, given all initiator undergoes polymerisation, see equation ( 8 ).

$$M_n = M \frac{[M]}{[I]} \quad (8)$$

Similarly,  $DP_n$  is given by the monomer/initiator molar ratio, see equation ( 9 ).

$$DP_n = \frac{[M]}{[I]} \quad (9)$$

An important prerequisite for living anionic polymerisation is that the vinyl monomer (denoted  $\text{CH}_2=\text{CRX}$ ) must be able to stabilise the terminal anionic charge. Hence X should be an electron-withdrawing substituent such as a nitrile, carbonyl or phenyl group. Solvent choice is also important as traces of protic solvents such as water cause premature termination of the

growing polymeric carbanions. Thus meticulous drying of all glassware, solvents and monomer(s) to remove traces of water is essential.

If protic impurities can be eliminated, then in principle the highly reactive terminal carbanions should remain intact indefinitely even under monomer-starved conditions. Hence, addition of further monomer enables the preparation of block copolymers via sequential monomer addition.<sup>42</sup> Alternatively, addition of electrophiles such as CO<sub>2</sub> or ethylene oxide enables chain-end functionalisation. Perhaps the most famous commercial example of a multiblock copolymer produced via living anionic polymerisation is polystyrene-block-polybutadiene-block-polystyrene (PS-PB-PS). This formulation was patented by Holden and Milkovich<sup>49</sup> who synthesised such triblock copolymers using an *n*-butyllithium initiator in an inert hydrocarbon solvent. It was later commercialised by Shell Chemicals (now Kraton) who utilised the enthalpic incompatibility of the two blocks to make microphase-separated elastomers and gels. The high  $T_g$  polystyrene blocks form either spherical or cylindrical domains within a matrix of low  $T_g$  polybutadiene (Figure 1.8).

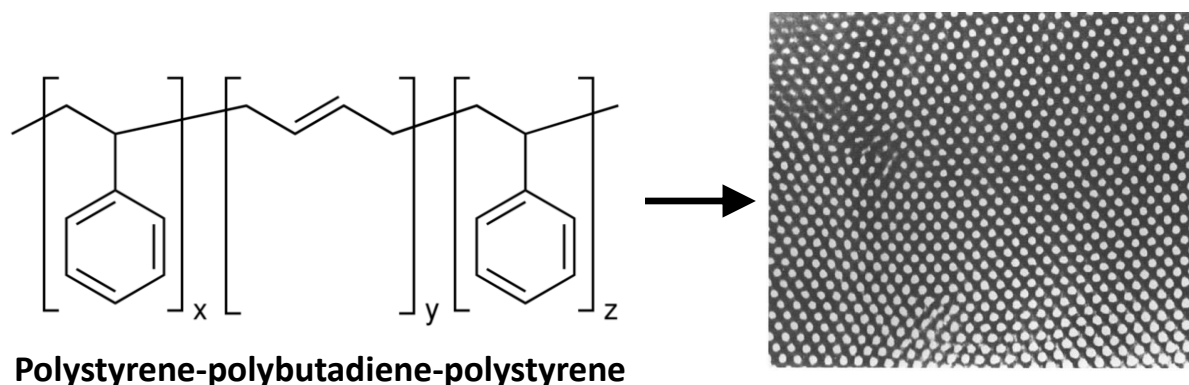


**Figure 1.8.** Electron micrograph of a PS-PB-PS triblock copolymer exhibiting microphase separation (i.e. white PS domains within a black PB matrix).<sup>50</sup>

Heating this material above the  $T_g$  of the polystyrene block allows manipulation of the shape of such elastomers, hence they are known as thermoplastic elastomers. The unsaturated nature of the PB chains means that these materials are susceptible to UV degradation. However, catalytic hydrogenation of this central block confers stabilisation, enabling such synthetic rubbers to be used for footwear, automotive, coatings and adhesives applications.<sup>51-52</sup>

In principle, living anionic polymerisation enables excellent control over both molecular weight distributions and copolymer architecture. However, in practice it requires rigorous purification to remove protic impurities and is not amenable to a wide range of vinyl monomers.

### **Controlled Radical Polymerisation (CRP)**

Controlled radical polymerisation offers most of the benefits and convenience of FRP but the rate of termination is suppressed relative to that of propagation. Unlike living anionic polymerisation, termination is always present at a background level rather than eliminated entirely; this is why CRP is sometimes known as a ‘pseudo-living’ polymerisation. A rapid equilibrium is created between active (propagating) and dormant (unreactive) polymer chains. This lowers the number of active polymer chains at any given time, thus significantly reducing the probability of irreversible termination via radical-radical annihilation. The two most commonly used classes of CRP are discussed below.

### **Atom Transfer Radical Polymerisation (ATRP)**

Since its more or less simultaneous discovery by Sawamoto and co-workers<sup>53</sup> and Wang and Matyjaszewski,<sup>54</sup> ATRP has grown to become one of the most widely-used types of CRP. It is essentially an example of atom transfer radical addition (ATRA), which is a well-known synthetic organic transformation for creating new carbon-carbon bonds (a.k.a. the *Kharasch* reaction). During ATRP, a transition metal catalyst abstracts a halogen atom via reversible redox chemistry. As a result, the catalyst becomes oxidised and a reactive carbon-centred radical is generated from a halogen-capped chain. During its relatively short lifetime, the carbon-centred radical reacts with multiple monomer units to give a short burst of polymerisation before being recapped with a halogen atom (Figure 1.9)<sup>55-56</sup>. Normally, such carbon-centred radicals are prone to bimolecular combination. However, in this case the oxidised transition metal complex reacts rapidly and reversibly to reintroduce the halogen end-group and hence minimises the probability of premature termination. Because ATRP is based on radical chemistry, it is applicable to a much wider range of *functional* (meth)acrylic monomers than anionic polymerisation. This is a potentially decisive advantage for the design of functional polymers with complex architectures.



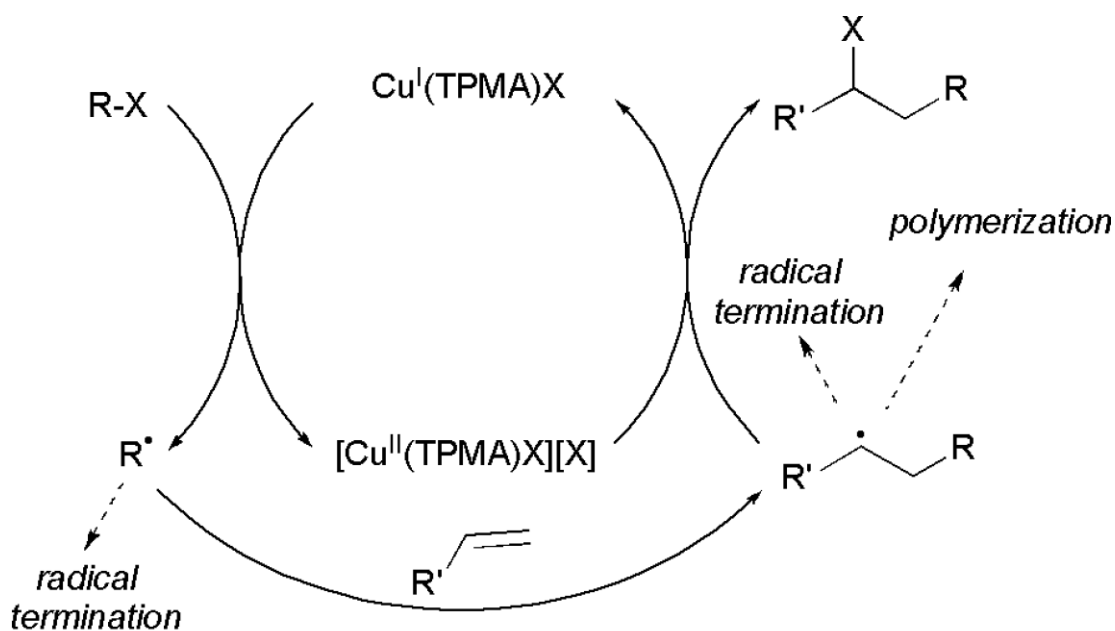


**Figure 1.9.** The mechanism of atom transfer radical polymerisation (ATRP) when  $\text{X} = \text{Cl}$  or  $\text{Br}$ . Tris(2-pyridylmethyl)amine (TPMA) is acting as a ligand.<sup>57</sup>

Two research teams independently recognised the potential for utilising this mechanism for CRP. Sawamoto and co-workers used carbon tetrachloride to initiate the polymerisation of MMA in the presence of a  $\text{RuCl}_2(\text{PPh}_3)_2$  catalyst but found that  $\text{MeAl}(\text{ODBP})_2$  was required to activate the C-Cl bond for polymerisation. They reported a near-linear evolution of molecular weight with conversion and relatively low dispersities ( $M_w/M_n = 1.30\text{-}1.40$ ). In contrast, Wang and Matyjaszewski used 1-phenylethyl chloride to initiate the polymerisation of styrene at  $130^\circ\text{C}$  in the presence of  $\text{Cu}(\text{I})\text{Cl}$  and three equivalents of 2,2'-bipyridine, which served as a solubilising ligand for this transition metal. A linear increase in  $M_n$  with monomer conversion and a final dispersity below 1.50 was observed, which indicated reasonable control.

Subsequent research has shown that optimisation of almost every aspect of an ATRP formulation is important to achieve good control over the target molecular weight and the molecular weight distribution, including the choice of initiator, transition metal, ligand, solvent, and even the order of monomer addition.<sup>58</sup> ATRP initiators are typically alkyl halides, but efficient initiation requires careful consideration of the chemical structures of the initiator and the target monomer.<sup>59</sup> The type of halogen atom in the initiator is also important, with relative reactivity following the trend:  $\text{I} > \text{Br} > \text{Cl}$ . In addition, it is vital that the initiator contains suitable radical-stabilising substituents, with adjacent nitrile ( $-\text{CN}$ ) groups usually being the most effective followed by phenyl groups and esters (see Figure 1.10).<sup>58-59</sup>

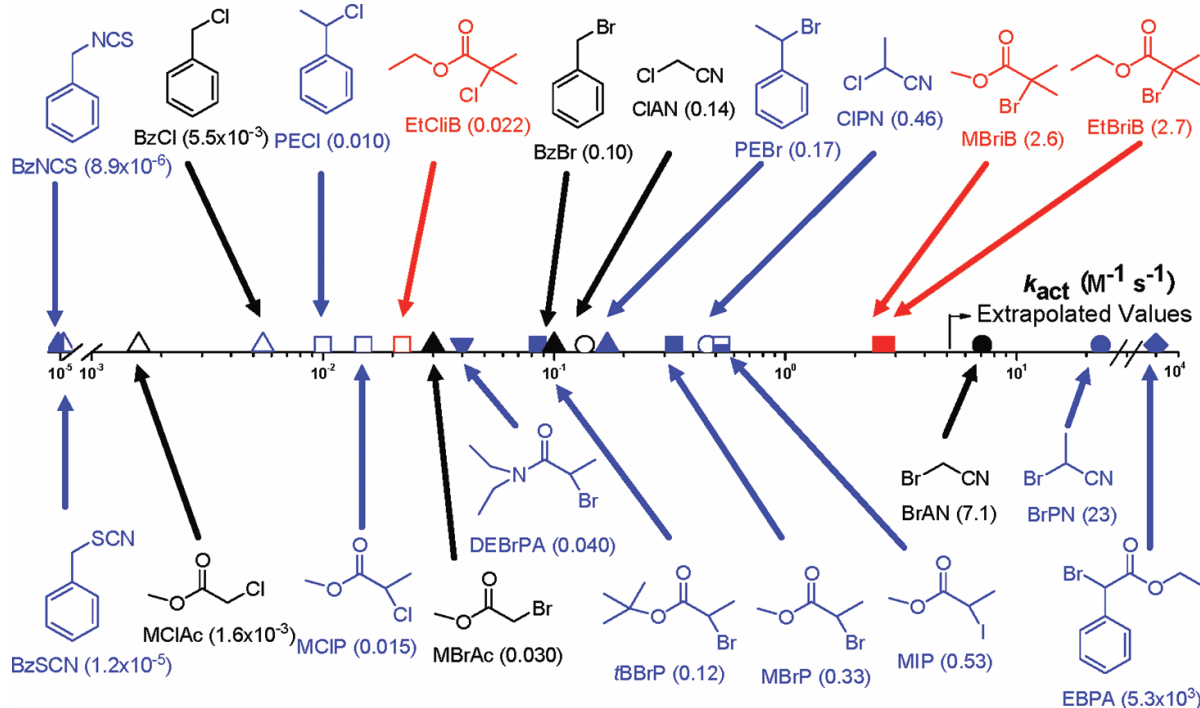


**Figure 1.10.** Chemical structures of various ATRP initiators illustrating the effect of strong radical stabilisation on the rate constant for activation.<sup>58-59</sup>

In principle, any transition metal that has two accessible oxidation states may be suitable as an ATRP catalyst. Transition metals successfully employed for this type of CRP include ruthenium, iron, osmium or molybdenum but the most common example is copper.<sup>60-61</sup> Another important parameter for influencing the activity of the transition metal catalyst is the choice of solubilising ligand(s). The effect of ligand structure on the rate constant for activation is shown in Figure 1.11.

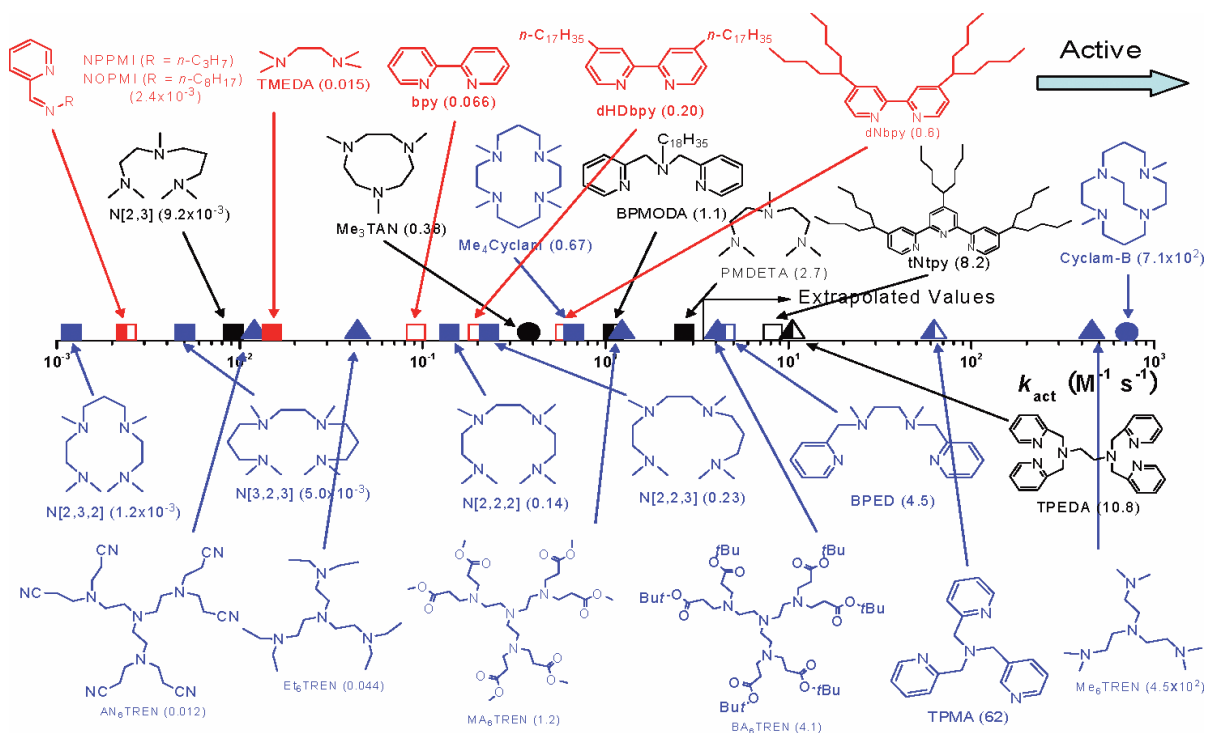


**Figure 1.11.** Chemical structures of various ATRP ligands illustrating the effect of ligand structure on the rate constant for activation.<sup>58, 62</sup>

In general, ligands for copper-based ATRP catalysts are almost exclusively nitrogen donor ligands.<sup>62</sup> Multidentate ligands tend to afford much more active catalysts (tetradentate > tridentate > bidentate).<sup>62</sup> In addition, cyclic and bridged ligands produce higher activities than the equivalent linear ligands.<sup>62</sup>

In ATRP, if a polymer radical undergoes irreversible termination then the associated metal complex can no longer undergo reduction, resulting in a gradual reduction in catalytic activity. One strategy to address this problem is to regenerate the spent catalyst by adding an external reducing agent (Figure 1.12). This strategy is known as ‘activator regenerated by electron transfer’ (ARGET) ATRP.<sup>63</sup> One important advantage of ARGET ATRP is that no external radical source is required. It is also considered to be a more environmentally-friendly type of polymerisation because much less transition metal catalyst is required compared to a conventional ATRP formulation (typically just ppm levels relative to the alkyl halide initiator, rather than stoichiometric levels). Common reducing agents that work effectively in this context are tin(II) 2-ethylhexanoate (Sn(EH)<sub>2</sub>),<sup>64-65</sup> ascorbic acid<sup>65</sup> and glucose.<sup>66</sup>

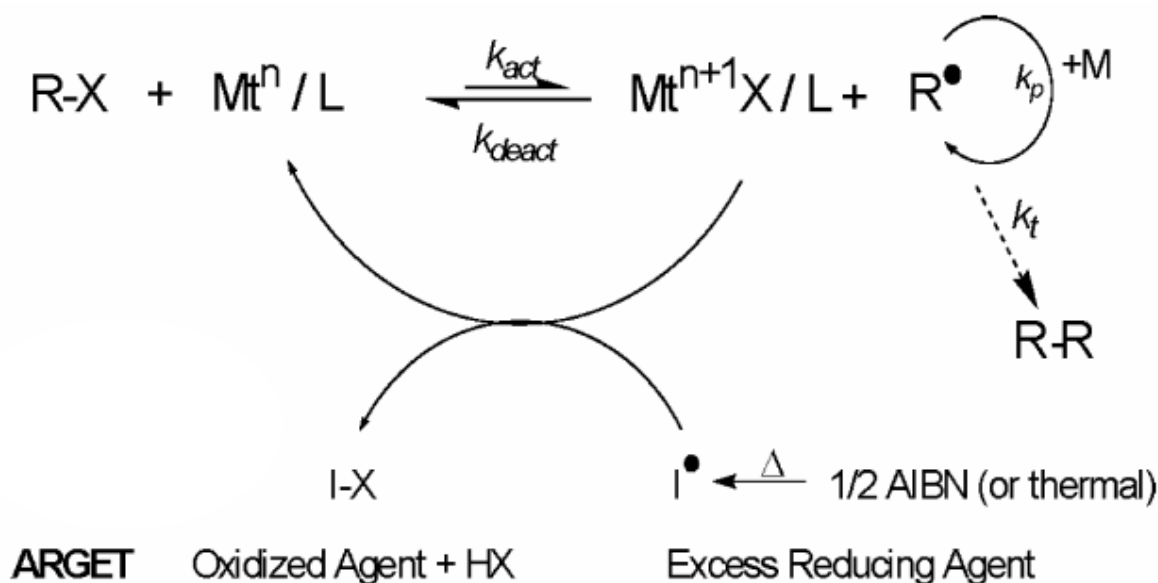


**Figure 1.12.** Mechanism for ARGET ATRP whereby the active catalyst is continuously regenerated by excess reducing agent.<sup>58</sup>

Finally, if the concentration of the reducing agent is high enough, then the generated active catalyst can effectively scavenge dissolved oxygen. This was demonstrated by Matyjaszewski and co-workers when polymerising styrene in the presence of only 5 ppm  $\text{CuCl}_2/\text{Me}_6\text{TREN}$  (TREN = tris(2-aminoethyl)amine) plus 500 ppm of a  $\text{Sn}(\text{EH})_2$  reducing agent.<sup>66</sup> Gel permeation chromatography (GPC) indicated a  $M_n$  of  $12,500 \text{ g mol}^{-1}$  (theoretical  $M_n = 12,600 \text{ g mol}^{-1}$ ) and an  $M_w/M_n$  of 1.28, suggesting a reasonably good level of control.

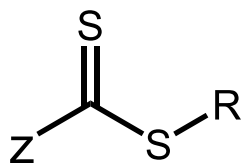
One of the major disadvantages of ATRP is the presence of a toxic, coloured transition metal in the final product. Although ARGET ATRP enables a significant reduction in the catalyst concentration, many applications require even lower levels of residual catalyst. Fortunately, various methods have been developed for removing the spent catalyst, including precipitation into a non-solvent, column chromatography using either alumina or silica as the stationary phase or the judicious use of an ion exchange resin.<sup>61, 67</sup>

In summary, ATRP is a versatile polymerisation technique that can polymerise a wide range of functional monomers and is tolerant of many types of solvents (including water). When ARGET ATRP is employed, even dissolved oxygen present in the formulation can be tolerated. Optimisation of reaction conditions and reagents can be complicated, particularly for new

systems. However, once an appropriate formulation has been identified, well-controlled polymerisations can be achieved with good reproducibility.

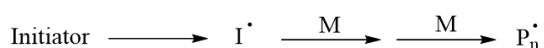
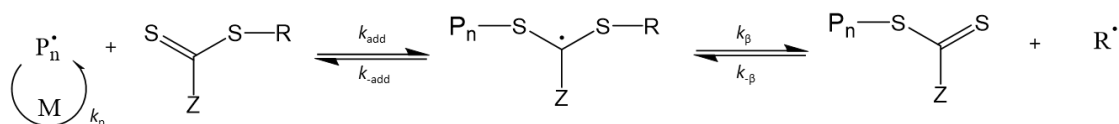
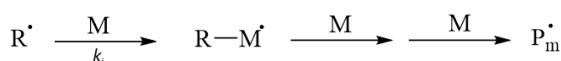
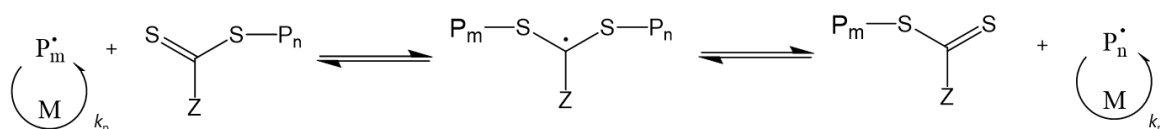
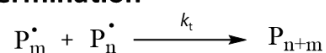
### Reversible Addition-Fragmentation chain Transfer (RAFT) Polymerisation

Various types of controlled radical polymerisation are now known, but reversible addition-fragmentation chain transfer (RAFT) polymerisation has become increasingly popular over the past decade owing to its versatility and relatively simple formulations compared to ATRP. RAFT polymerisation was first reported in 1998 by Rizzardo and co-workers: a series of dithiobenzoate compounds were added to otherwise conventional FRP formulations, yielding (co)polymers with remarkably narrow molecular weight distributions.<sup>68</sup> It was hypothesised that RAFT displays living characteristics as a result of the rapid reversible chain transfer of polymer radicals to an organosulfur-based chain transfer agent (CTA). Such efficient chain transfer suppresses termination of active polymer radicals. Rizzardo and co-workers emphasised that an effective RAFT CTA requires both a stabilising group (Z) and also a good radical leaving group (R) (see Figure 1.13).



**Figure 1.13.** Generic chemical structure of a RAFT chain transfer agent, where Z is a stabilising group and R is a good radical leaving group.<sup>68</sup>

The RAFT mechanism differs from that of other controlled radical polymerisations. In ATRP, rapid reversible chain-capping by halogen atoms suppresses termination and hence ensures pseudo-living character. In contrast, rapid reversible addition-fragmentation chain transfer provides polymer chains with an equal probability to grow in the case of RAFT polymerisation. Growing polymer radicals react with the thiocarbonyl group to generate a dormant unreactive radical species, which can then fragment to generate a new polymer radical. The RAFT mechanism is shown in Figure 1.14. The presence of the RAFT CTA reduces the effective concentration of propagating polymer radicals and therefore suppresses termination by either combination or disproportionation.

**Initiation****Reversible Chain Transfer****Reinitiation****Chain Equilibration****Termination**

**Figure 1.14.** RAFT mechanism as proposed by Rizzardo and co-workers.<sup>68-71</sup> [N.B. Z = Ph (dithiobenzoate), S-R (trithiocarbonate), N-R (dithiocarbamate) or O-R (xanthate)]

Initiation occurs via slow thermal decomposition as in FRP, with subsequent reaction with multiple monomer units producing polymer radicals,  $\text{P}_n^\bullet$ . However, in the case of RAFT polymerisation, the chain equilibrium occurs faster than the rate of propagation. When combined with the rapid fragmentation of the intermediate species, this leads to an equal probability of propagation for all polymer chains. Meanwhile, the relatively short lifetime of the polymer radicals leads to suppressed termination, which results in polymers with narrow MWDs ( $M_w/M_n$  typically between 1.10 and 1.30). Owing to each polymer chain being capped with a RAFT CTA and having equal probability of propagating, the  $M_n$  of the polymer increases linearly with monomer conversion. Therefore, final polymer  $\text{DP}_n$ s can be calculated using equation ( 10 )

$$\text{DP}_n = \frac{[\text{M}]}{[\text{CTA}]} \quad (10)$$

Initially, it was suggested that Z groups needed to be either aryl or alkyl in order to achieve effective RAFT polymerisation.<sup>68</sup> However, it was subsequently found that less activating CTAs (i.e. dithiocarbamates or xanthates) can effectively polymerise certain monomer classes.<sup>72-74</sup> In general, vinyl monomers can be split into two classes, more activated monomers (MAMs) and less activated monomers (LAMs). MAMs possess double bonds that are electron deficient, i.e. they are conjugated to a carbonyl, nitrile or aromatic groups. Some examples of MAMs are acrylates (e.g. acrylic acid or methyl acrylate), methacrylates (e.g. methyl methacrylate or glycerol monomethacrylate), acrylamides (e.g. *N,N*-dimethylacrylamide or *N*-isopropylacrylamide), methacrylamides (e.g. 2-hydroxypropyl methacrylamide), acrylonitrile and styrene. Conversely, LAMs are monomers with electron-rich double bonds, i.e. they are adjacent to electron-donating heteroatoms. Some examples of LAMs are vinyl acetate, *N*-vinylpyrrolidone and *N*-vinylformamide. In principle, well-controlled RAFT polymerisations are observed when dithiobenzoates or trithiocarbonates are employed to polymerise MAMs, whereas dithiocarbamates or xanthates must be used for LAMs. Some general guidelines for selecting the correct CTA for a specific monomer were published by Moad et al.<sup>71</sup> and are depicted in Figure 1.15.

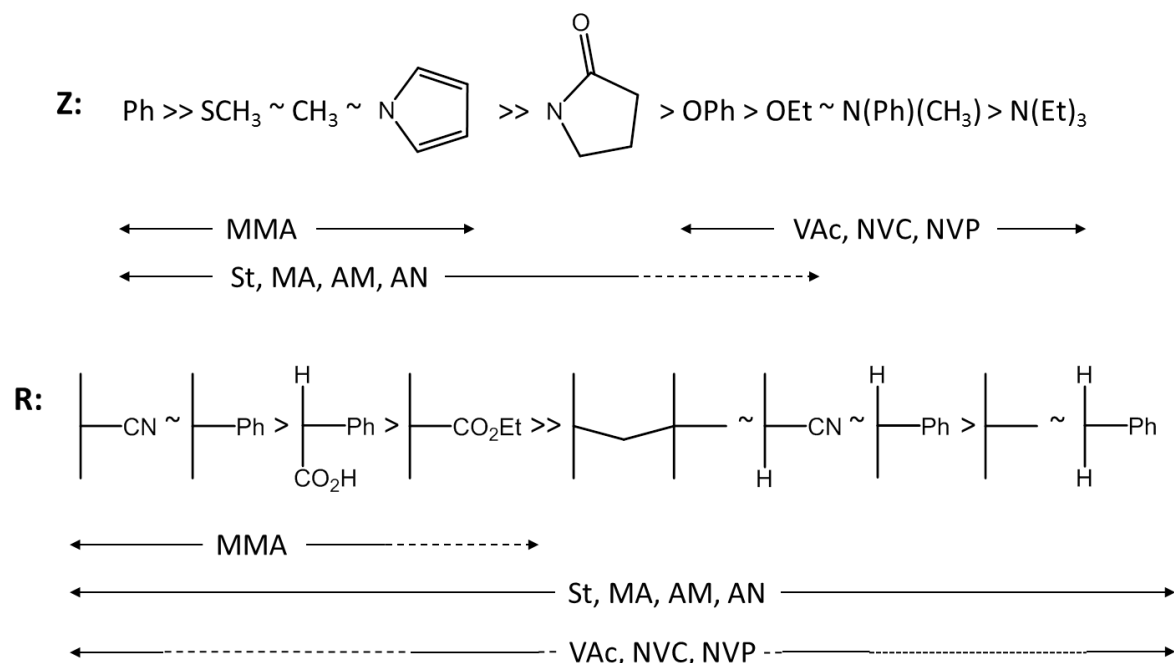


**Figure 1.15.** General guidelines for the selection of appropriate RAFT agents for a given monomer type. Solid lines indicate good control, while a dashed line indicates only partial control<sup>71</sup>

One of the most famous early examples of RAFT was by Mitsukami et al. who polymerised water-soluble monomers by RAFT aqueous solution polymerisation.<sup>75</sup> The authors utilised a 4-cyanopentanoic acid dithiobenzoate CTA to polymerise sodium 4-styrenesulfonate in water at 70 °C. Quantitative levels of conversion were achieved within 2 h at this temperature and the resulting polymer had a  $M_n$  of 16,900 g mol<sup>-1</sup> and an  $M_w/M_n$  of 1.17 as determined by aqueous GPC. The authors then chain extended this homopolymer with sodium 4-vinylbenzoate at 70 °C for 24 h. The final diblock copolymer had an  $M_n$  of 18,600 g mol<sup>-1</sup> and an  $M_w/M_n$  of 1.18. Finally, the polymers underwent reversible micellisation by means of a pH switch.

RAFT polymerisation is conceptually simple compared to other controlled polymerisations. Moreover, it can be performed in many protic solvents such as water or lower alcohols, displays excellent tolerance of many functional groups and can be performed over a wide range of temperature. Furthermore, RAFT polymerisation is the only form of CRP that is able to effectively polymerise LAMs and acidic monomers (without recourse to protecting group chemistry in the latter case).<sup>69, 76-77</sup> However, removal of oxygen is essential as oxygen is a well-known retarder. RAFT polymerisation formulations are essentially just FRP syntheses performed in the presence of a suitable CTA. This means there are just four components in a RAFT formulation: initiator, monomer, solvent and the RAFT CTA.<sup>69-71</sup>

### **Modification and Removal of RAFT End-Groups**

One of the major drawbacks of RAFT polymerisation is the inevitable presence of a malodorous and intrinsically coloured CTA, which becomes the end-group on the polymer chains. Thus, the facile removal or modification of this CTA species by post-polymerisation modification is of considerable interest.<sup>78-80</sup> In principle, this can be achieved using various reagents.<sup>79, 81-86</sup> A comprehensive review by Willcock and O'Reilly<sup>79</sup> summarises many well-established routes for the end-group modification of RAFT-synthesised polymers. One approach simply involves thermal elimination, whereby a monomer unit loses a hydrogen atom on the secondary carbon at elevated temperature in order to eliminate the end-group. This method yields a sulfur-free polymer, but the polymer chains need to be chemically stable at 120 to 200 °C in order to avoid thermal degradation. As expected, the critical temperature required for thermal elimination depends on both the polymer type and the nature of the RAFT end-group. For the latter parameter, the observed order of thermal stability is: dithiobenzoates > trithiocarbonates > xanthates.<sup>81-82</sup> Alternatively, RAFT end-groups can be readily removed



by reaction with various nucleophiles. The nucleophile attacks the thiocarbonyl and displaces the organosulfur unit to leave a terminal thiol group on the polymer chain. The reaction of nucleophiles with thiocarbonates was reported in 1990.<sup>84</sup> However, it is only relatively recently that this chemistry has been utilised to remove RAFT end-groups from polymer chains. Typical nucleophiles are amines and the residual thiol end-group can be further functionalised to give a range of products. Another method for end group removal is addition of a large excess of a radical-generating species such as an azo initiator. The radicals react with the thiocarbonyl group, causing displacement of polymer radicals. One benefit of this method is that the RAFT agent can sometimes be recovered for reuse.<sup>85</sup> Finally, Diels-Alder chemistry can be used to remove RAFT end-groups.<sup>87</sup> More specifically, the thiocarbonyl end-group can be reacted with a diene. This chemistry is driven by the electron-deficient nature of the thiocarbonyl group. Although it does not remove the RAFT end-group, this modification is often sufficient to remove the intrinsic colour associated with this species.<sup>86</sup> These end-group removal strategies are depicted below (Figure 1.16).<sup>83</sup>

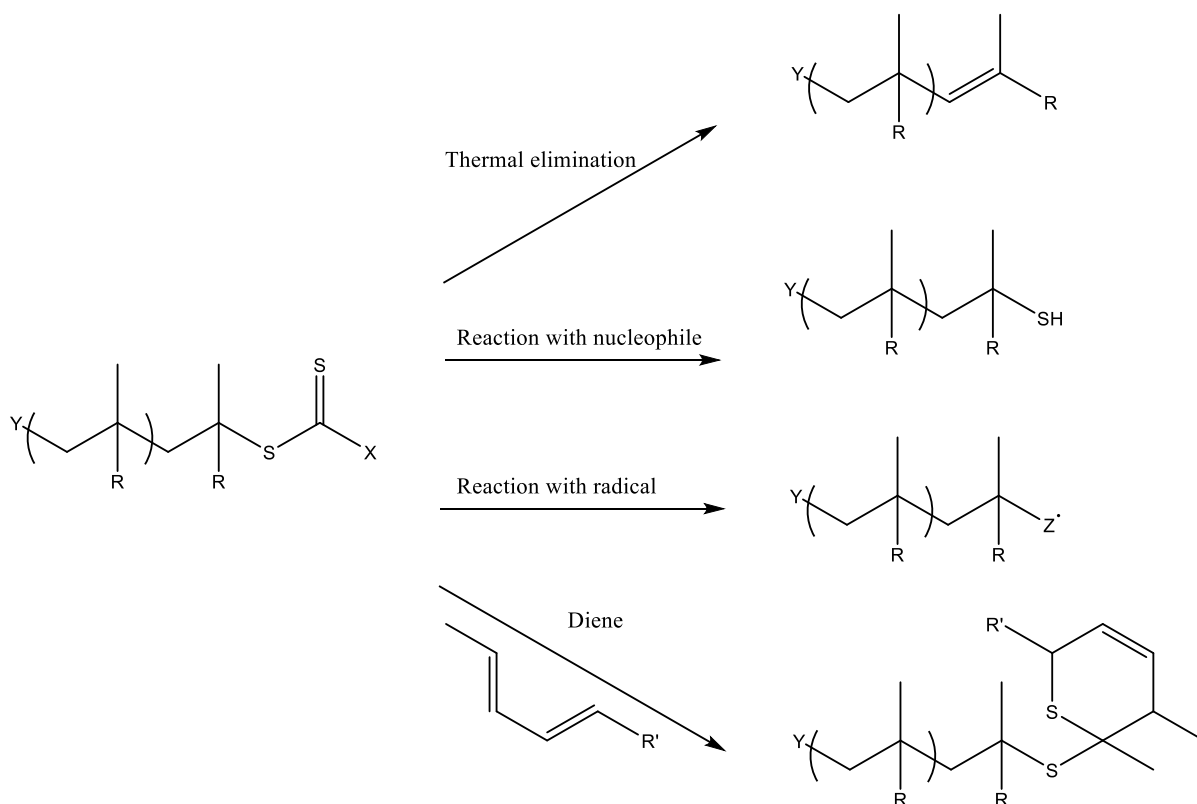


**Figure 1.16.** Summary of common RAFT end-group modification reactions.<sup>83</sup>

More recently, RAFT end-group removal has involved exploration of more environmentally-friendly approaches. For example, Pfukwa et al. have examined the use of hydrogen peroxide

for the post-polymerisation modification of RAFT-synthesised polymers.<sup>88</sup> Thus, RAFT homopolymerisation of either NVP or styrene was conducted in the bulk to afford PNVP with an  $M_n$  of around 2500 g mol<sup>-1</sup> and polystyrene (PS) with an  $M_n$  of around 1800 g mol<sup>-1</sup>. Each polymer was reacted with a twenty-fold excess of hydrogen peroxide based on RAFT end-groups at either 60 °C for 16 h (PNVP) or 80 °C for 6 h (PS), respectively. GPC analysis indicated only minimal changes in molecular weights and dispersities after end-group modification. The proposed mechanism is thermal decomposition of hydrogen peroxide to generate hydroxyl radicals, which then add to the CTA and eliminate the polymer radical. Given the large excess of peroxide reagent, this polymer radical then combines with a hydroxyl radical to give hydroxyl-terminated polymer chains. Evidence for the proposed hydroxyl chain-ends was provided by <sup>1</sup>H NMR and matrix assisted laser desorption/ionisation-time of flight mass spectrometry (MALDI-ToF-MS) analysis and a crosslinking reaction was performed using a trifunctional isocyanate.<sup>88</sup>

Of particular relevance to this thesis, Destarac and co-workers utilised ozone to remove the xanthate end-groups from polymer latexes in aqueous solution.<sup>89</sup> More specifically, *n*-butyl acrylate was polymerised by RAFT aqueous emulsion polymerisation using the commercially available xanthate CTA, rhodixan A1. The resulting low molecular weight latex dispersions ( $M_n = 1300$  and  $5300$  g mol<sup>-1</sup>,  $M_w/M_n = 1.72$  and  $1.55$  respectively) were treated with ozone using a custom-built rig that passed a stream of latex through an ozone-rich atmosphere. Progressive disappearance of the yellow colour associated with the RAFT end-groups was observed and quantified by using ultra-violet coupled GPC (UV GPC) at 290 nm, with full end-group modification being achieved within 1 h. The authors confirmed transformation of the xanthate moiety into a thiocarbonate using <sup>13</sup>C and <sup>1</sup>H NMRs and used this information to propose a mechanism for the reaction (see Figure 1.17).

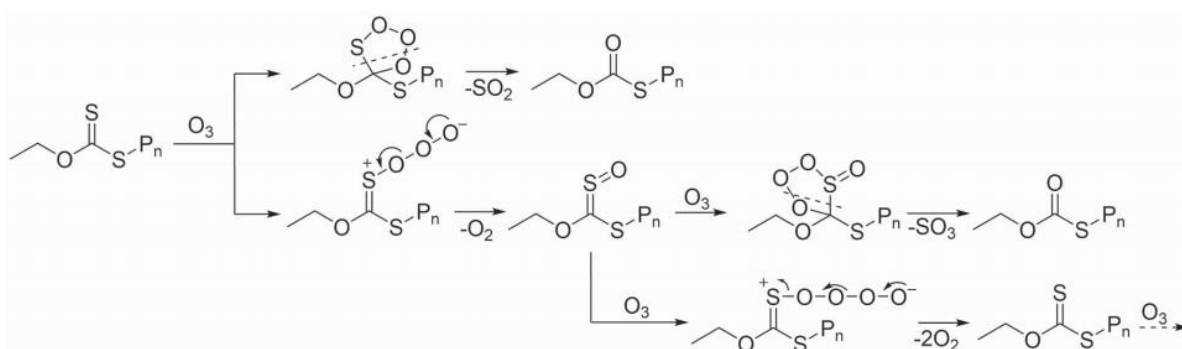


**Figure 1.17.** Proposed mechanism for the oxidation of xanthate end-groups with ozone.<sup>89</sup>

## **Polymer Brushes**

Polymer brushes are formed when a high density of polymer chains are grafted by one end of each chain to a solid substrate.<sup>90</sup> As a direct result of their high grafting density, the chains are forced to stretch out from the surface to adopt a low-entropy brush conformation as opposed to forming a typical random coil. In principle, such polymer brushes may be useful as adhesives, protein-resistant biosurfaces, chromatographic devices, chemical lubricants<sup>91</sup> and lubricious (low friction) surfaces.<sup>92</sup> This field has been well studied over the past fifteen years or so and many review articles have been published.<sup>90, 93-95</sup>

There are many different types of polymer brushes, including 1D brushes (bottle brushes) which are graft copolymers grown from a single polymer chain,<sup>96</sup> So-called 2D brushes are grown from a planar surface<sup>97</sup> while 3D polymer brushes are grown from the surface of colloidal nanoparticles.<sup>98</sup> Many brush synthesis protocols via various polymerisation techniques have been explored, including both covalent and non-covalent grafting, ‘grafting to’ and ‘grafting from’. However, in this Thesis will only focus on 2D polymer brushes grown from planar substrates by ARGET ATRP.

Of particular relevance to this work is a study of oil repellent poly(N-(dimethylamino)ethyl methacrylate) (PDMAEMA) brushes by Dunderdale et al.<sup>99</sup> These authors developed a brush synthesis protocol that is cheap, applicable to large-area substrates and relatively undemanding reaction conditions. More specifically, such methacrylic brushes can be grown in aqueous solution at ambient temperature without the need for rigorous oxygen removal and at monomer concentrations as low as 1 % w/v. This optimised route offers a cost reduction of almost three orders of magnitude and a reduction in toxic chemical usage by 99.9 %.

## **Self-Assembly of Amphiphiles**

Water is a unique naturally-occurring solvent that can dissolve many polar and ionic materials. The structure and physical properties of liquid water are dominated by its extensive network of hydrogen bonds. If a non-polar compound is placed in water, a ‘cage’ like structure is formed around the hydrophobic species. This rearrangement of water molecules is known as the ‘hydrophobic effect’ and this provides the driving force for the self-assembly of amphiphilic molecules in aqueous media.<sup>100</sup>

Micellar self-assembly was first postulated for amphiphiles by Schryver et al. in 1913.<sup>101</sup> Over the past century or so, this concept has become widely used to describe the behaviour of

surfactant molecules in aqueous solution. Surfactants are amphiphiles that generally contain a polar head group that interacts strongly with water and a non-polar highly hydrophobic tail. The hydrophobic effect (see above) causes the non-polar tails to cluster together in aqueous solution order to minimise disruption to the water structure. Relatively weak van der Waals attractive forces between these non-polar tails further stabilise the self-assembled micelles. The most common morphology for amphiphiles to adopt is spherical micelles.<sup>102</sup> However, other possible morphologies include worms (cylindrical micelles), vesicles or lamellae (i.e. either curved or planar bilayers). Electrostatics, van der Waals forces and hydrogen bonding each have an impact on the overall area occupied per head group ( $a$ ), the volume occupied by the hydrophobic tail group ( $V_c$ ) and hence the preferred morphology. The packing parameter ( $N_S$ ) was introduced by Israelachvili and co-workers for small molecule amphiphiles in 1976.<sup>102</sup> This purely geometric concept is useful for understanding micellar self-assembly and is based on the relative volume fractions of the solvophilic and solvophobic components of the surfactant. The packing parameter equation is shown below ( 11 ).<sup>103</sup>

$$N_S = \frac{V_c}{a * l_c} \quad ( 11 )$$

Here  $V_c$  is the volume occupied by the hydrophobic surfactant tail,  $l_c$  is the length of this tail and  $a$  is the equilibrium cross-sectional area of the head-group per molecule within the micelle aggregate. The numerical value of the packing parameter,  $N_s$ , indicates the preferred micelle morphology. If  $N_S \leq 1/3$ , this indicates that each surfactant molecule adopts a conical shape, which then self-assembles to form spherical micelles. For  $1/3 < N_S \leq 1/2$ , the surfactant molecules form a truncated cone (or frustum), which self-assembles to produce cylindrical micelles. Finally, if  $N_S > 1/2$  the amphiphile has an approximately cylindrical shape, which leads to the formation of curved bilayers (vesicles or polymersomes) or planar bilayers (lamellae).<sup>102, 104</sup>

Like surfactants, amphiphilic diblock copolymers can self-assemble when exposed to a solvent which is a good solvent for one block but a poor solvent for the other block. The latter structure-directing block drives aggregation to form a range of nanostructures, depending on the relative volume fraction of each block. The packing parameter concept can also be (more loosely)

applied to amphiphilic block copolymers (see Figure 1.18). However, in this case it is even more difficult to assign reliable experimental values for  $V_c$ ,  $l_c$  and  $a$ . Nevertheless, it is still a useful qualitative concept for explaining the evolution in copolymer morphology that is observed when varying the relative volume fractions of the solvophilic and solvophobic blocks.

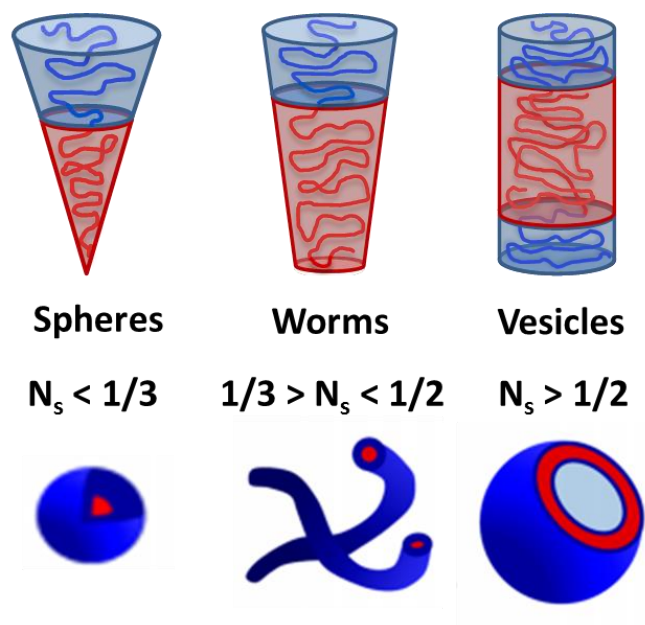


**Figure 1.18.** Schematic illustration of the three most common morphologies (and their characteristic packing parameter,  $N_s$ ) formed by amphiphilic diblock copolymers in aqueous solution.<sup>105</sup>

Until relatively recently, the micellar self-assembly of amphiphilic diblock copolymer chains has only been achieved by post-polymerisation techniques such as direct dissolution,<sup>106</sup> a solvent switch,<sup>107-108</sup> a pH switch<sup>109</sup> or thin film rehydration.<sup>110-111</sup> Each of these techniques is typically only utilised at rather low copolymer concentrations (typically  $< 1\%$  w/w solutions) and involves a laborious multistep process.<sup>112</sup> This makes industrial scale-up extremely problematic. However, the development of polymerisation-induced self-assembly (PISA) over the past decade enables the micellar self-assembly of block copolymers to be achieved at much higher copolymer concentrations (up to 50% w/w solids) *during the synthesis of copolymer chains*. This approach eliminates the need for post-polymerisation processing steps, and in some cases can even be conducted as a high-yielding one-pot synthesis starting from the constituent monomers.

### Polymerisation-Induced Self-Assembly (PISA)

Within the past decade or so, PISA has become widely recognised as a powerful route for the convenient synthesis of a broad range of block copolymer nano-objects at high copolymer concentration. In essence, PISA involves chain extension of a soluble polymer (known as a macro-CTA) with a second insoluble block in order to drive *in situ* self-assembly (see Figure 1.19). The main prerequisite for PISA is a (pseudo)-living polymerisation that enables high blocking efficiencies to be achieved.<sup>105, 113</sup> In principle, any (pseudo)-living polymerisation chemistry can be utilised. However, although spherical micelles have been produced by ATRP<sup>114-115</sup> and Telluride-mediated polymerisation (TERP),<sup>116-117</sup> it is mainly RAFT polymerisation and nitroxide-mediated polymerisation (NMP) that have been used to target higher order morphologies such as worms or vesicles. The PISA literature is now quite extensive, with many studies focusing on either water or lower alcohols as the continuous phase. In 2012 Charleux et al. published the first comprehensive review of the various advances in PISA using various CRP techniques.<sup>118</sup> More recently, Canning et al. summarised recent advances in RAFT-mediated PISA.<sup>119</sup> Copolymer morphologies that have been observed thus far include spheres,<sup>105</sup> worms/rods,<sup>105</sup> lumpy rods<sup>120</sup>, vesicles,<sup>105</sup> framboidal (raspberry-like) vesicles<sup>121</sup> and lamellae.<sup>122-123</sup>

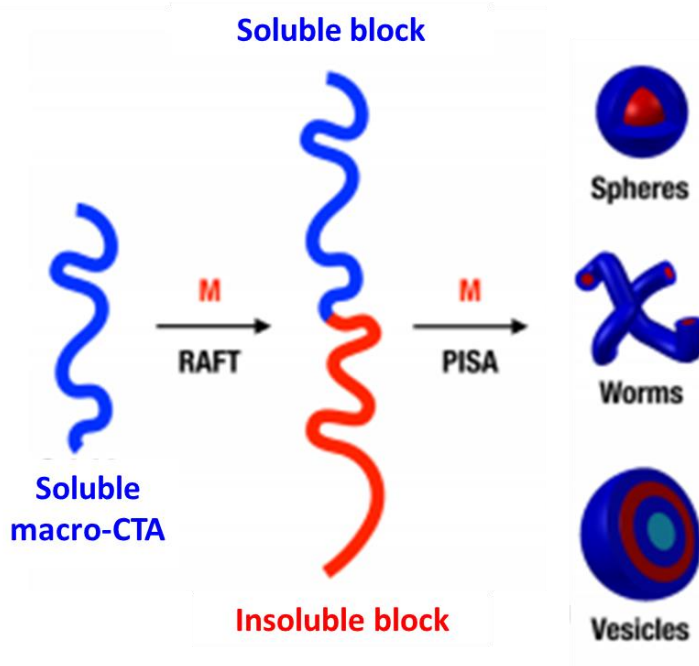


**Figure 1.19.** Schematic representation of the *in situ* formation of diblock copolymer nanoparticles by RAFT-mediated polymerisation-induced self-assembly (PISA)

One of the earliest examples of PISA was reported by Ferguson et al. in 2002.<sup>124</sup> This Australian team aimed to address various technical problems associated with RAFT aqueous emulsion polymerisation, including poor molecular weight control, substantially incomplete conversions and colloidal instability.<sup>125-126</sup> Acrylic acid (AA) was polymerised to a relatively low degree of polymerisation via RAFT solution polymerisation in water to afford poly(acrylic acid) (PAA). This macro-CTA was then chain-extended with various amounts of water-immiscible *n*-butyl acrylate (BA), which was added under monomer-starved conditions. This led to the formation of well-defined spherical nanoparticles with a mean diameter of approximately 60 nm. THF GPC studies confirmed the expected linear evolution of molecular weight against conversion (see Figure 1.20). However, only limited control over the molecular weight distribution was achieved, with  $M_w/M_n$  values approaching 1.50 at higher conversions. These spheres could be used as a seed for further reactions without requiring any additional stabiliser.

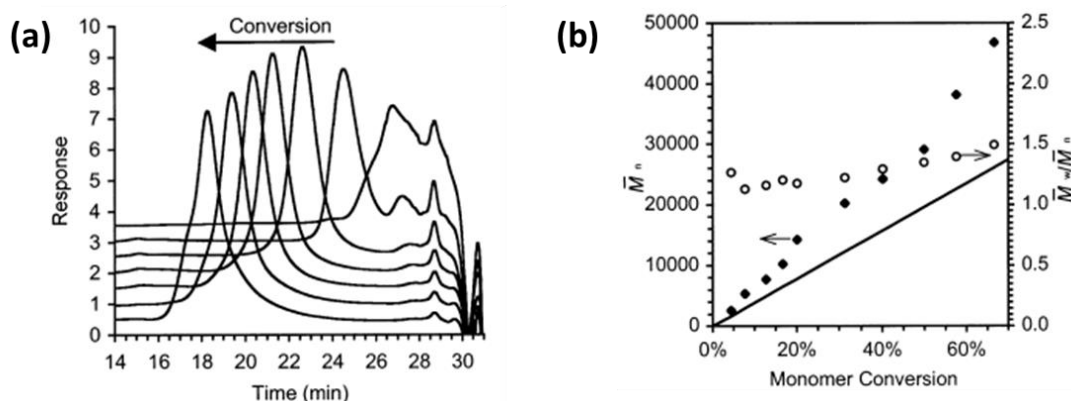


**Figure 1.20.** (a) THF GPC traces obtained for the chain extension of a poly(acrylic acid) macro-CTA with *n*-butyl acrylate. (b) Linear evolution in molecular weight (filled diamonds) and dispersity (open circles) against monomer conversion, where the solid line represents the theoretical molecular weight<sup>124</sup>

One important disadvantage of RAFT aqueous emulsion polymerisation is that it is difficult to access higher order morphologies, with kinetically-trapped spheres being the typical morphology in many cases.<sup>127-134</sup> For example, Cunningham et al. synthesised a series of poly(glycerol monomethacrylate)-poly(benzyl methacrylate) (PGMA-PBzMA) spheres via RAFT aqueous emulsion polymerisation of benzyl methacrylate.<sup>127</sup> These spheres could be prepared at up to 50 % w/w solids and were characterised by transmission electron microscopy (TEM) and dynamic light scattering (DLS), see Figure 1.21a. The mean sphere diameter increased linearly with the target degree of polymerisation of the PBzMA core-forming block

up to a maximum size of 200 nm for PGMA<sub>51</sub>-PBzMA<sub>1000</sub>. Selected spheres were shown to be effective oil-in-water Pickering emulsifiers for several oils. Furthermore, pH-modulated adsorption onto a phenylboronic acid-functionalised micropatterned planar substrate was demonstrated. Control experiments confirmed that this was facilitated by complexation between the phenylboronic acid surface groups and the pendent cis-diol units on the PGMA stabiliser chains (see Figure 1.21c).

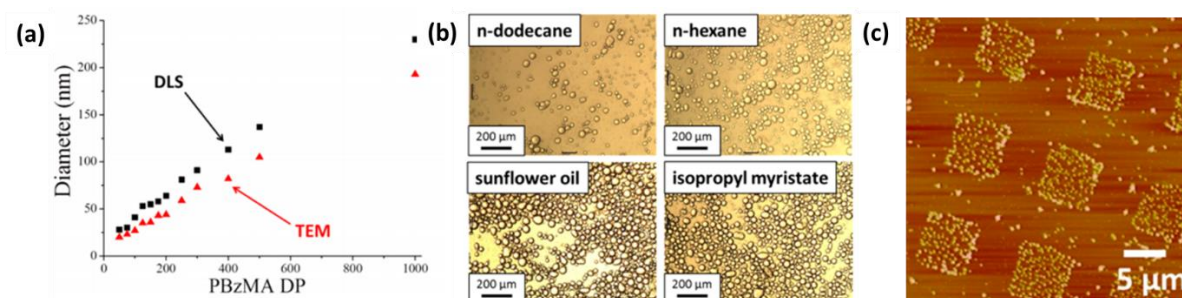


**Figure 1.21.** (a) DLS and TEM diameters determined for PGMA<sub>51</sub>-PBzMA<sub>x</sub> spheres against the target PBzMA DP. (b) Optical microscopy images obtained for PGMA<sub>51</sub>-PBzMA<sub>100</sub> stabilised Pickering emulsions. (c) AFM image illustrating the selective adsorption of PGMA<sub>51</sub>-PBzMA<sub>100</sub> spheres onto a micropatterned silicon wafer (squares contain chemically-bound phenylboronic acid groups).<sup>127</sup>

Davis and co-workers explored the synthesis of ultrahigh molecular weight polystyrene spheres ( $M_n > 10^6 \text{ g mol}^{-1}$ ) by RAFT aqueous emulsion polymerisation.<sup>133</sup> Initially, a series of P(PEGA-*stat*-HEAA) macro-CTAs was prepared via RAFT solution copolymerisation in DMSO, incorporating an equimolar amount of each comonomer. These macro-CTAs were each chain-extended with styrene to produce near-monodisperse spheres. Copolymer molecular weights of up to  $70 \text{ kg mol}^{-1}$  could be prepared at high conversion within 6 h at 80 °C with final dispersities of around 1.20 (see Figure 1.22). Higher styrene concentrations enabled copolymer molecular weights in excess of  $1 \times 10^6 \text{ g mol}^{-1}$  to be achieved, while maintaining  $M_w/M_n$  values below 1.40. Finally, the mean sphere volume increased linearly with molecular weight.



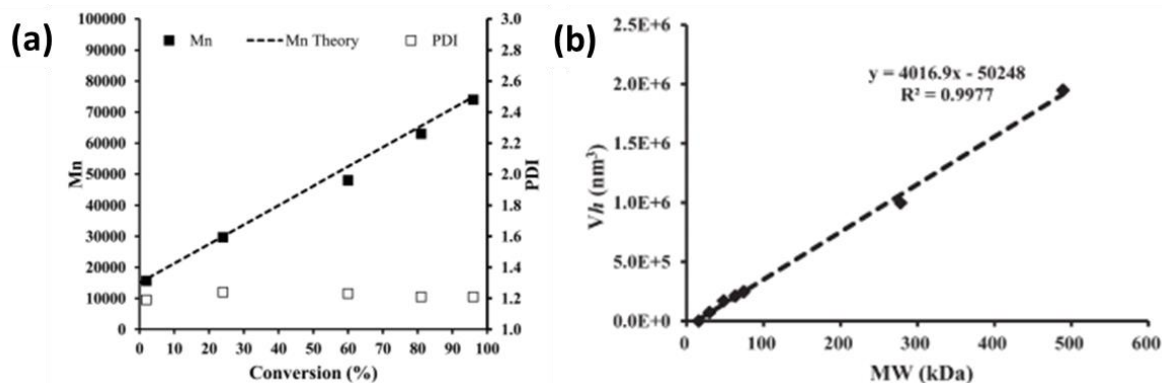


**Figure 1.22.** (a) Evolution of  $M_n$  and dispersity against conversion for the synthesis of P(PEGA-*stat*-HEAA)-PS diblock copolymer spheres via RAFT aqueous emulsion polymerisation. (b) Linear relationship between copolymer volume and molecular weight for a series of P(PEGA-*stat*-HEAA)-PS spheres.<sup>133</sup>

One of the first documented examples of non-spherical morphologies being obtained via PISA was by Wan et al. in 2009.<sup>135</sup> In this study, a trithiocarbonate-capped poly(4-vinylpyridine) macro-CTA was chain-extended with styrene in methanol via RAFT alcoholic dispersion polymerisation. A gradual evolution in copolymer morphology was observed when the styrene/AIBN molar ratio was increased from 5,000 to 50,000. The morphology of the particles was determined by TEM and field emission scanning electron microscopy (FESEM), and their respective sizes were measured by dynamic light scattering (DLS). Periodic sampling of the reaction solution indicated that ~12 nm diameter spheres were formed after 2 h, followed by an increase in sphere diameter up to 32 nm after 3 h. During the fourth hour, a morphological transition from spherical micelles to ‘rod-like’ (with the benefit of hindsight, ‘worm-like’ is probably a more accurate description) micelles was observed. The ‘rods’ gradually grew in length up to 12 h (see Figure 1.23). From this point until the end of the reaction, the cross-sectional diameter of the ‘rods’ progressively increased. According to the authors, such rods could be dried and then redispersed easily in methanol. While this successfully demonstrates the formation of non-spherical particles by PISA, optimisation of the monomer conversion is required (currently only 52 % conversion in 6 h at 80 °C)

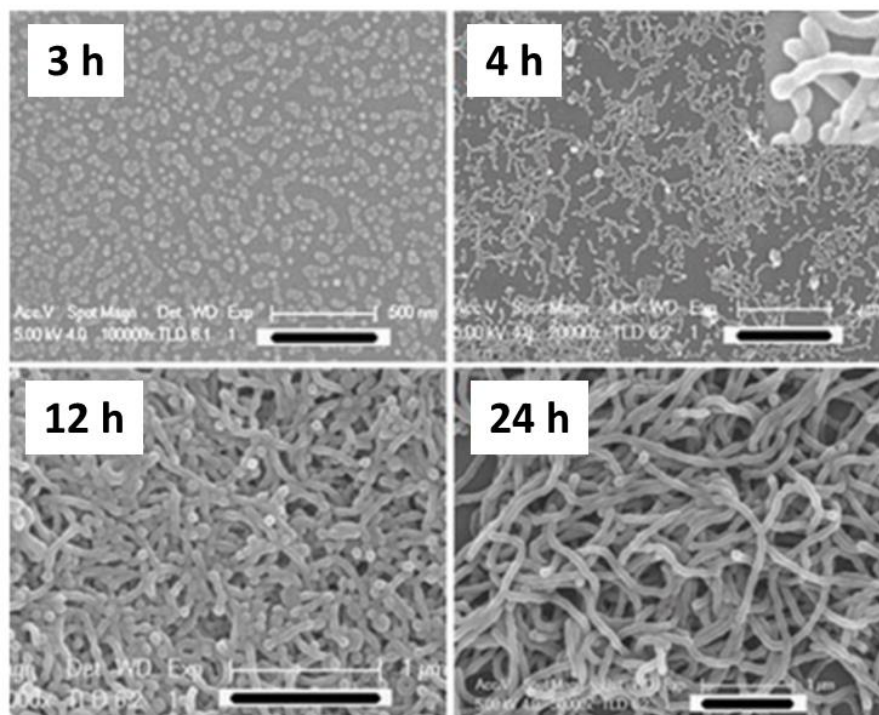


**Figure 1.23.** FESEM images showing the evolution in copolymer morphology over time.<sup>135</sup>

Since then, many copolymer morphologies have been reproducibly accessed via PISA. The Armes group has used RAFT aqueous dispersion polymerisation to design many types of diblock copolymer nano-objects with various morphologies. In particular, the commodity monomer HPMA has been widely explored as a weakly hydrophobic core-forming block owing to its aqueous solubility as a monomer. For example, Li and Armes chain-extended a PGMA macro-CTA using various amounts of HPMA monomer.<sup>137</sup> More specifically, a PGMA<sub>65</sub> macro-CTA was initially prepared in a water/dioxane mixture using 4-cyanopentanoic acid dithiobenzoate. When this precursor was chain-extended with 30 to 300 units of HPMA at 10 % w/w, well-defined spherical nanoparticles of 26 to 105 nm diameter were obtained, depending on the target DP<sub>n</sub> of the PHPMA core-forming block (see Figure 1.24). Interestingly, when the copolymer concentration was increased to 20 % w/w, large polydisperse vesicles were observed by TEM.

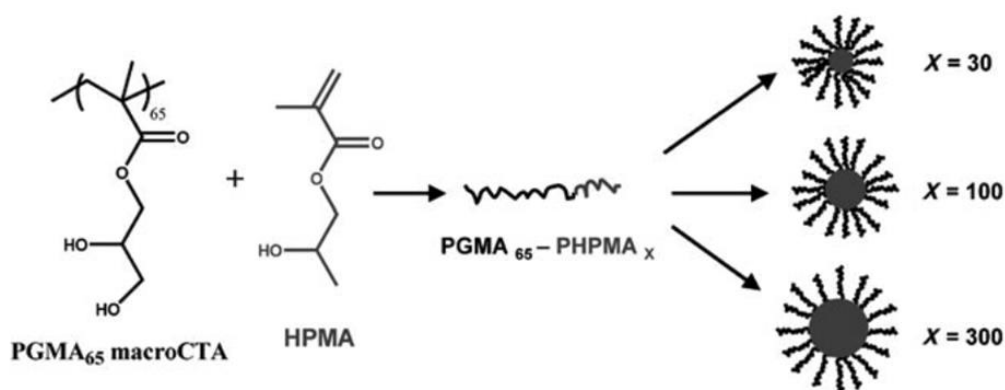


**Figure 1.24.** Schematic representation of the chain extension of a PGMA<sub>65</sub> macro-CTA with HPMA via RAFT aqueous dispersion polymerisation. The final particle size can be adjusted depending on the DP<sub>n</sub> of the PHPMA block (X).<sup>136</sup>

Subsequently, spheres, worms or vesicles have been obtained for various PHPMA-based diblock copolymer nanoparticles prepared via RAFT aqueous dispersion polymerisation.<sup>138</sup> Blanazs and co-workers explored the evolution in copolymer morphology that occurs during such aqueous PISA syntheses.<sup>29</sup> Initially, a well-defined PGMA<sub>45</sub> macro-CTA was synthesised by RAFT solution polymerisation in ethanol. By fixing the copolymer concentration at 10 % w/v, and systematically increasing the target PHPMA DP<sub>n</sub>, either spheres, worms or vesicles could be reproducibly obtained (see Figure 1.25).

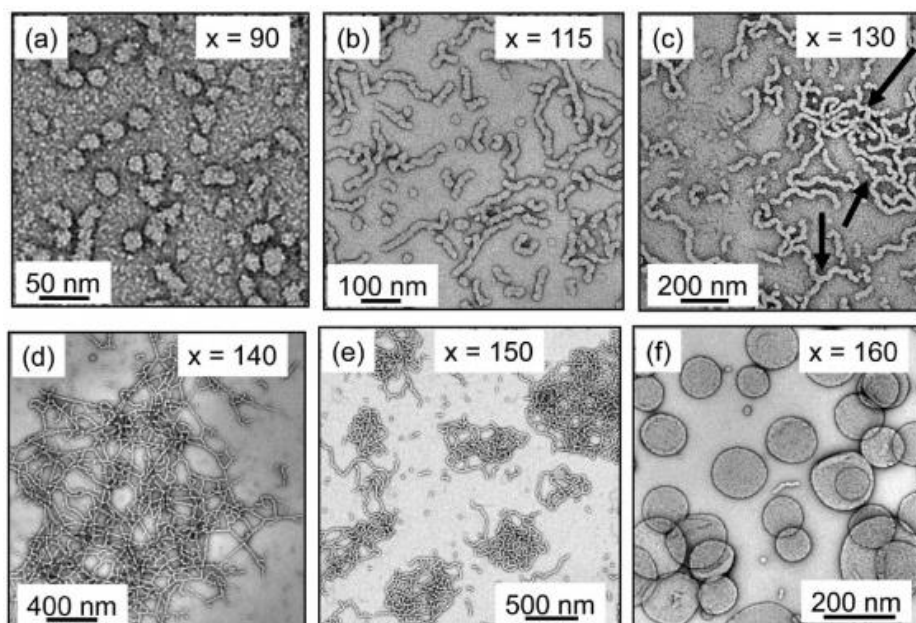


**Figure 1.25.** Representative TEM images of the final particle morphologies (at more than 99% conversion and 10 w/v %) observed for a series of six PGMA<sub>47</sub>-PHPMA<sub>x</sub> diblock copolymers, where x corresponds to (a) 90, (b) 115, (c) 130, (d) 140, (e) 150, and (f) 160.<sup>29</sup>

Blanazs and co-workers then continued to observe the evolution of worms into vesicles and identified some key structural intermediates. They targeted PGMA<sub>47</sub>-PHPMA<sub>200</sub> at 10 % solids via RAFT aqueous dispersion polymerisation. The reaction mixture was periodically sampled at various monomer conversions, as determined by <sup>1</sup>H NMR spectroscopy. TEM was used to characterise the evolution in copolymer morphology that occurred during the growth of the PHPMA block. The onset of micellar nucleation occurred at 46 % HPMa conversion and was accompanied by a five-fold increase in rate of polymerisation. The authors suggest that this rate acceleration is due to unreacted HPMa monomer diffusing into the newly-formed polymer spheres. These nascent spheres then underwent multiple 1D fusion events to form worms, and eventually pure vesicles were observed at high conversion. Interestingly, the transition from worms to vesicles proceeds via a series of transient intermediates, including branched worms, octopus-like and jellyfish-like structures (see Figure 1.26). The latter intermediate deserves particular mention as its hemi-vesicle appearance immediately suggests the opportunity for the *in situ* encapsulation of nanoparticles or other relevant payloads such as proteins.<sup>138</sup>

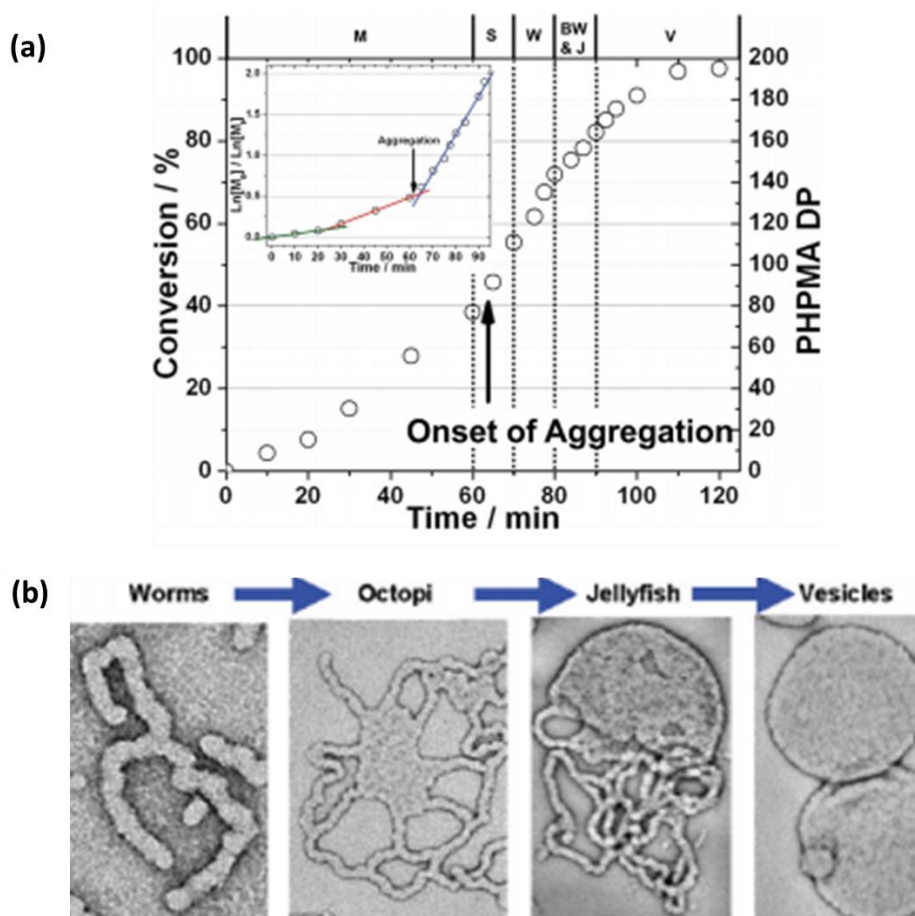


**Figure 1.26.** (a) <sup>1</sup>H NMR kinetic data obtained during the synthesis of PGMA<sub>47</sub>-PHPMA<sub>200</sub> diblock copolymer nano-objects via aqueous RAFT dispersion polymerisation. The five distinct regions

represent molecularly-dissolved chains (M), spheres (S), worms (W), branched worms (BW) and jellyfish (J), and vesicles (V). The inset shows a semi-logarithmic plot, indicating that a significant acceleration in the rate of polymerisation occurs immediately after micellar nucleation. (b) TEM images obtained during the synthesis of PGMA<sub>47</sub>-PHPMA<sub>200</sub>, showing the evolution in copolymer morphology from worms to vesicles.<sup>29</sup>

Later, Blanazs et al. explored the effect of polymerisation parameters on the final morphology of PGMA-PHPMA diblock copolymer nanoparticles.<sup>30</sup> These polymerisations were conducted at various copolymer concentrations while targeting differing degrees of polymerisation for the PHPMA block. This systematic approach produced well-defined spheres, worms or vesicles. The final copolymer morphology depended on the DP<sub>n</sub> of the PGMA stabiliser block, the DP<sub>n</sub> of the PHPMA core-forming block and the overall copolymer concentration. Phase diagrams in which the copolymer concentration is varied against the degree of polymerisation of the PHPMA block were constructed for three different PGMA macro-CTAs. This information is of vital importance when targeting specific copolymer morphologies using a particular macro-CTA (see Figure 1.27). For example, if the PGMA macro-CTA is too long (DP<sub>n</sub> = 112), then only kinetically-trapped can be obtained. If this macro-CTA is relatively short (DP<sub>n</sub> = 47), then either spheres, worms or vesicles can be obtained regardless of the copolymer concentration. On the other hand, if an intermediate PGMA DP<sub>n</sub> is utilised (DP<sub>n</sub> = 78), then a strong concentration dependence is observed for the final copolymer morphology, with higher concentrations favouring the formation of worms and vesicles.

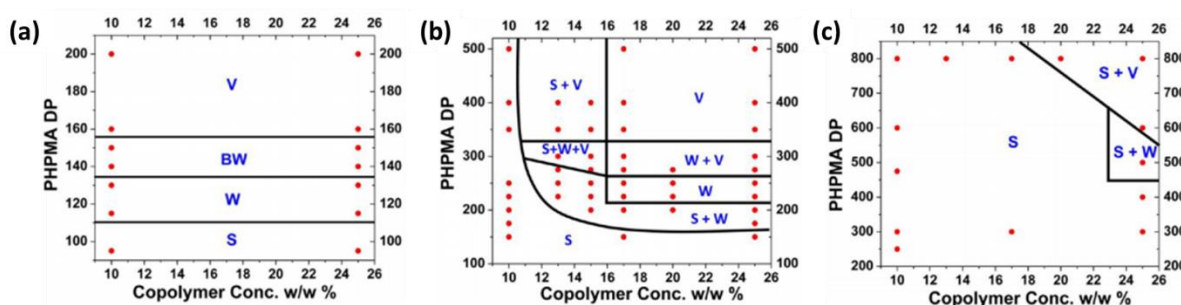


**Figure 1.27.** Phase diagrams constructed for PGMA-PHPMA diblock copolymer nano-objects by targeting various PHPMA DPs and copolymer concentrations where the mean DP of the PGMA macro-CTA is (a) 47, (b) 78 or (c) 112.<sup>30</sup>

Reproducible targeting of pure copolymer morphologies, particularly the relatively narrow worm phase, underpinned more detailed studies on such nanoparticles. Blanazs et al.

extensively explored PGMA-PHPMA worms.<sup>139</sup> Interestingly, these highly anisotropic nanoparticles form relatively soft, free-standing physical hydrogels at 10 % w/w solids and 21 °C. In addition, such highly hydroxylated diblock copolymers exhibit excellent biocompatibility. In principle, these worm gels might serve as ideal hydrogels for biomedical applications, including new 3D cell culture media. However, such hydrogels invariably require rigorous sterilisation. Blanz et al. found that PGMA<sub>54</sub>-PHPMA<sub>140</sub> worms underwent degelation on cooling to 4 °C as a result of a reversible worm-to-sphere morphological transition, as corroborated by TEM and small-angle x-ray scattering (SAXS) studies (see Figure 1.28). This behaviour proved to be fully reversible, which offered an opportunity to use ultrafiltration for convenient sterilisation. Thus, PGMA<sub>54</sub>-PHPMA<sub>140</sub> worms were cooled to 4 °C to form low-viscosity spherical nanoparticles of 20-30 nm diameter, which easily passed through a 0.45 µm filter. On the other hand, fluorescently-labelled micrometer-sized bacteria that had been deliberately added to the original worm gel were completely removed by this simple protocol. Then the cold spheres were returned to room temperature and a sterile worm gel was reformed.

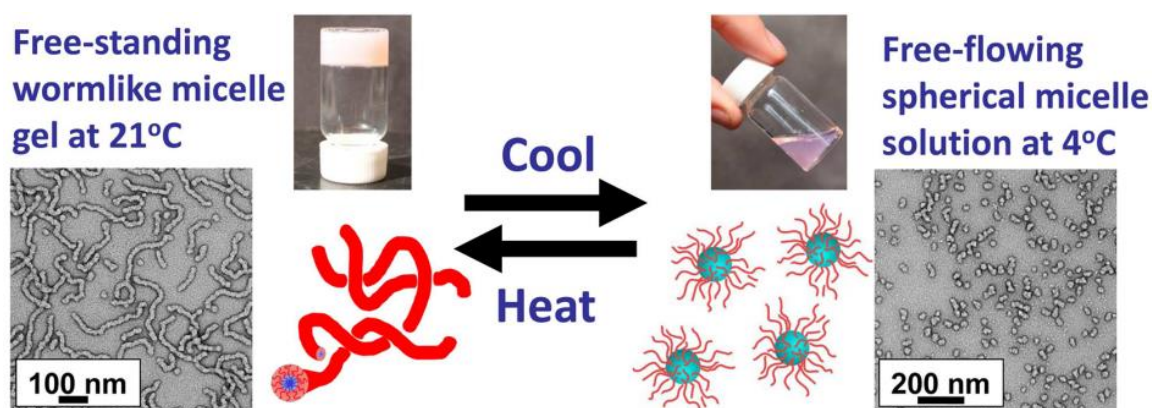


**Figure 1.28.** Thermoresponsive aqueous solution behavior of a 10 w/w % aqueous dispersion of PGMA<sub>54</sub>-PHPMA<sub>140</sub> diblock copolymer particles. A free-standing gel is formed at 21 °C, which becomes a free-flowing solution when cooled below 10 °C. TEM studies of grids prepared from a dilute aqueous dispersion of PGMA<sub>54</sub>-PHPMA<sub>140</sub> dried at either 21 or 4 °C provide strong evidence for a reversible worm-to-sphere transition.<sup>139</sup>

Potential biomedical applications for these worm gels was explored by Canton et al., who noted their structural and chemical similarity to naturally-occurring mucins (see Figure 1.29).<sup>78</sup> These worm gels proved to be highly biocompatible and were examined as 3D matrices for the storage of pluripotent human stem cells and embryos. Remarkably, cells stored within these gels

entered stasis and could be stored in this non-proliferative state for up to two weeks at 37 °C without the need for any passaging. Once removed from the worm gel, the cells began to proliferate again and little or no loss of pluripotency was observed. In addition, human embryos stored in such worm gels appear to enter diapause (i.e. delayed gestation) for up to 4 days after immersion.

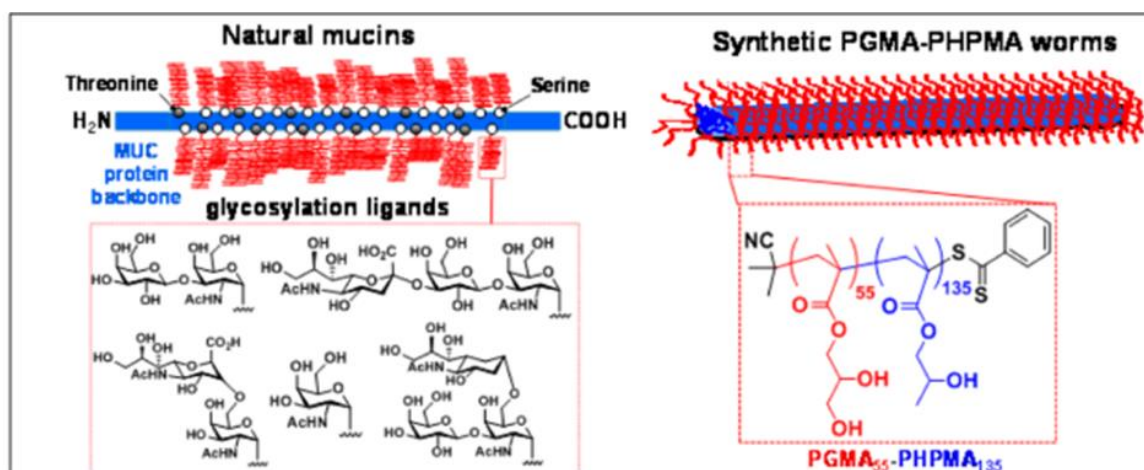


**Figure 1.29.** Schematic representation of the similar physical and chemical (hydroxyl-rich brush) structures of naturally-occurring mucin gels and PGMA<sub>55</sub>-PHPMA<sub>135</sub> worm gels.<sup>78</sup>

Being able to consistently target the worm phase using any given initial PGMA macro-CTA is clearly important. Warren et al. collated data based on various PISA syntheses of PGMA-PHPMA diblock copolymer nano-objects reported in the literature.<sup>140</sup> TEM studies were used to confirm the morphology and hence construct a master phase diagram (see Figure 1.30a). This systematic approach enables each copolymer morphology to be predicted from the mean  $DP_n$  of each block. This information was then used to target worms of various thickness (see red stars shown in Figure 1.30a). Shorter copolymer chains with the correct diblock composition formed thinner worms, as confirmed by TEM and SAXS studies. Interestingly, the  $DP_n$  of the PHPMA block significantly affected the dynamics and reversibility of the worm-sphere transition. On cooling to 2 °C, PGMA<sub>37</sub>-PHPMA<sub>80</sub> worms underwent a fully reversible worm-to-sphere and a sphere-to-unimer double transition within a relatively short time frame. However, these worms appeared to be unstable with respect to dilution. In contrast, PGMA<sub>54</sub>-PHPMA<sub>140</sub> worms only exhibited a reversible worm-to-sphere transition but remained intact on dilution. Finally, PGMA<sub>71</sub>-PHPMA<sub>200</sub> worms only underwent an *irreversible* worm-sphere transition on cooling (see Figure 1.30b).

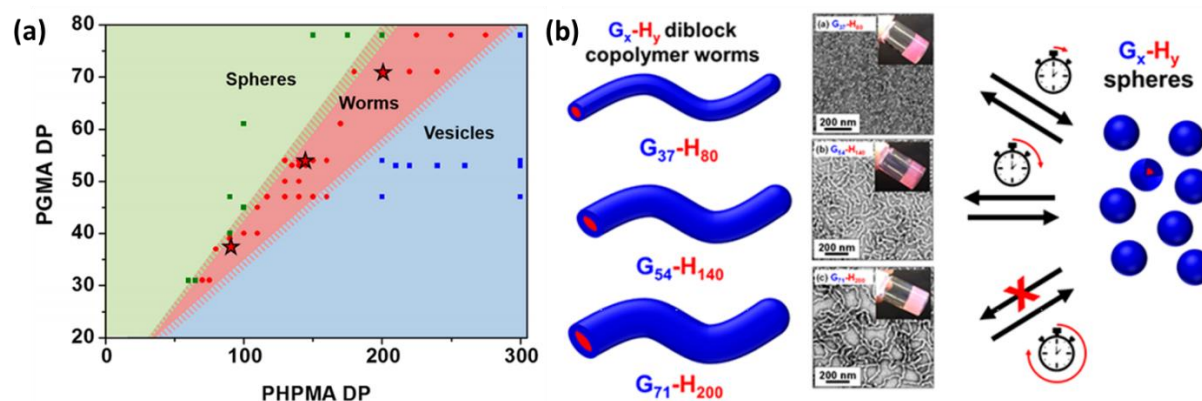


**Figure 1.30.** (a) Phase diagram constructed for PGMA<sub>x</sub>-PHPMA<sub>y</sub> diblock copolymer nano-objects to determine the precise copolymer composition for each morphological phase. Each point represents the copolymer morphology assigned on the basis of post-mortem TEM studies. Green squares indicate spheres, red circles indicate worms, and blue squares indicate vesicles. Shaded boundaries represent regions of uncertainty. All copolymer syntheses were conducted at 20% w/w solids except for those involving PGMA DPs below 47, which were conducted at 10% w/w solids. These can be included in this phase diagram because the copolymer morphologies produced using such short stabilizer blocks exhibit no concentration dependence. (b) The effect of the worm composition on the temperature dependant worm-sphere transition.<sup>140</sup>

PISA undoubtedly provides convenient access to a wide range of diblock copolymer nano-objects. Some of these nanoparticles offer unique properties that suggest potential biomedical applications. However, their RAFT end-groups confer unwanted colour and malodour. Given their known long-term hydrolytic instability,<sup>79</sup> these end-groups are also a potential source of toxic small molecule by-products that are likely to compromise biocompatibility. Clearly, it would be beneficial if such RAFT end-groups could be simply removed from the diblock copolymer nanoparticles at the end of the PISA synthesis.

### Aims of this PhD Project

The main objectives for this industrially-sponsored PhD project are three-fold. Firstly, there is commercial interest from the industrial sponsor (GEO) in developing a convenient, cost-effective and atom-efficient synthesis of high molecular weight ( $> 1 \times 10^5 \text{ g mol}^{-1}$ ) PGMA homopolymer. In principle, this can be achieved simply by FRP of GMA in either water or ethanol. However, in practice, this approach produces highly viscous solutions that require long reaction times, does not lead to full monomer conversion and can be susceptible to gelation owing to the dimethacrylate content ( $\sim 0.06 \text{ mol } \%$ ) present within GMA monomer. A potential



technical solution to these problems is to polymerise the water-insoluble precursor for GMA, isopropylidene glycerol methacrylate (IPGMA), in the form of insoluble PIPGMA latex particles by aqueous emulsion polymerisation. The kinetics of emulsion polymerisation are usually much faster than that of solution polymerisation, enabling significantly higher degrees of conversion to be achieved within comparable (or shorter) time scales. Such heterogeneous formulations also address the problem of high viscosity by producing a low-viscosity aqueous dispersion. In principle, the emulsion polymerisation of IPGMA can be performed via FRP using a suitable commercial surfactant to maintain colloidal stability. Alternatively, PIPGMA particles can be prepared via RAFT aqueous emulsion polymerisation, which can potentially provide much better control over the MWD by virtue of its pseudo-living character. Thus, a relatively short water-soluble PGMA macro-CTA could be chain-extended using water-immiscible IPGMA to produce PGMA-PIPGMA diblock copolymer nanoparticles. In each case, the initial surfactant-stabilised PIPGMA latex or sterically stabilised PGMA-PIPGMA nanoparticles can be treated with mineral acid to remove the acetone protecting group and convert the water-insoluble PIPGMA component into water-soluble PGMA chains. These two approaches will be critically compared in terms of cost, convenience, maximum solids concentration, viscosity, monomer conversion and the molecular weight distribution of the final high molecular weight PGMA chains to determine the most effective protocol.

Within the last five years or so, GEO has augmented their monomer palette by designing a new methacrylic monomer, GEO5MA. This hybrid monomer comprises a series of five EG units between the methacrylate backbone unit and the cis-diol end-group. Thus, it can be viewed as a hybrid structure that combines structural features found in GMA and oligo(ethylene glycol) methacrylate (OEGMA) (see Figure 1.31 for chemical structures). The physicochemical properties of GEO5MA and its corresponding homopolymer are yet to be explored, although the latter is expected to be water-soluble. Interestingly, there is good literature precedent to suggest that the terminal cis-diol group in GMA or GEO5MA could be readily converted into an aldehyde using a selective oxidant such as sodium periodate. However, preliminary data obtained by a former Armes group post-doc (Dr. N. J. Warren) suggests that, although this oxidative transformation can be achieved for PGMA, the resulting homopolymer was no longer water-soluble (and appears to be chemically cross-linked). Thus the same transformation will be applied to GEO5MA with the expectation that the OEG side-chain should ensure that water solubility is retained. If so, this would constitute a very rare example of a water-soluble

aldehydic monomer. In principle, this should in turn provide access to a wide range of aldehyde-functionalised water-soluble polymers, nanoparticles and polymer brushes.

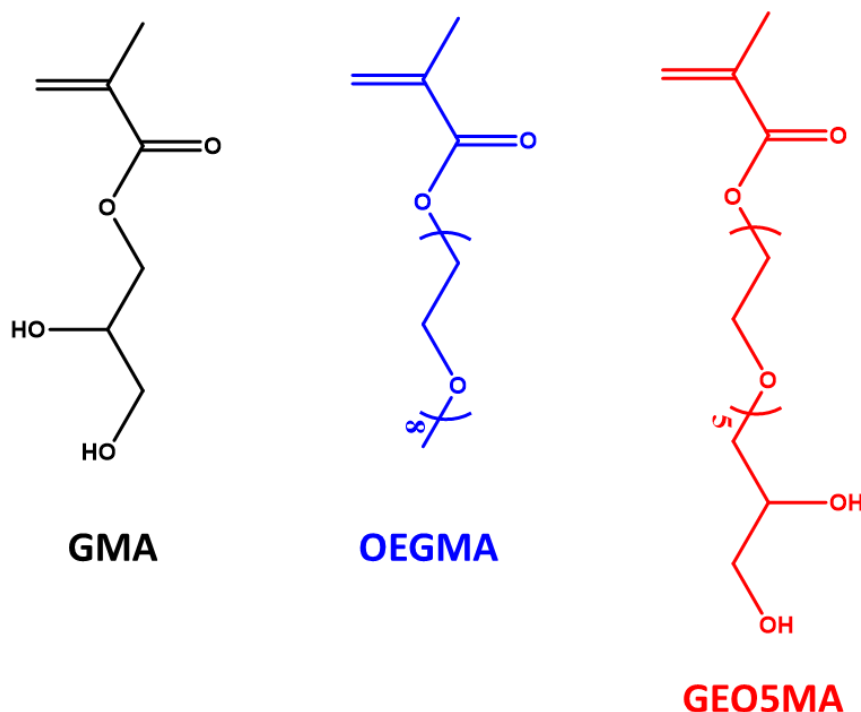


**Figure 1.31.** The chemical structures of GMA, OEGMA and GEO5MA

The final step of this project examines the efficient removal of RAFT end-groups directly from diblock copolymer nano-objects in order to eliminate the intrinsic colour and noxious odour associated with these organosulfur groups. Previous work within the Armes group has demonstrated that thermoresponsive PGMA-PHPMA worm gels are highly biocompatible, readily sterilisable and may have applications for the long-term storage of human stem cells. However, the RAFT end-groups should be ideally removed for such biomedical applications, preferably retaining the desirable physical properties of such hydrogels. In principle, this can be achieved by addition of a suitable nucleophile or a large excess of a radical initiator. Although RAFT end-groups can be removed from *soluble* polymer chains using such chemistry, this unfortunately leads to deterioration in the physical properties of the PGMA-PHPMA worm gels (e.g. a reduction in gel modulus). Herein we explore the use of hydrogen peroxide as a cost-effective reagent for the facile RAFT end-group removal from aqueous dispersions of PGMA-PHPMA diblock copolymer spheres, worms or vesicles.

---

**References**

1. Staudinger, H., Über Polymerisation. *Berichte der deutschen chemischen Gesellschaft (A and B Series)* **1920**, 53 (6), 1073-1085.
2. Carothers, W. H., Studies On Polymerization And Ring Formation. I. An Introduction To The General Theory Of Condensation Polymers. *Journal of the American Chemical Society* **1929**, 51 (8), 2548-2559.
3. Flory, P. J., *Principles of polymer chemistry*. Cornell University Press: Ithica, New York, 1953.
4. Cowie, J. M. G.; Arrighi, V., *Polymers: Chemistry and Physics of Modern Materials*. 3rd ed. Nelson Thornes: Cheltenham, 2007.
5. Odian, G., *Principles of Polymerization*. Wiley: Hoboken, NJ, 2004.
6. Matyjaszewski, K.; Gnanou, Y.; Leibler, L., *Macromolecular Engineering: Precise Synthesis, Material Properties, Applications*. Wiley: Hoboken, NJ, 2007; Vol. 1.
7. Braun, D.; Cherdron, H.; Rehahn, M.; Ritter, H.; Voit, B., *Polymer synthesis: theory and practice: fundamentals, methods, experiments*. 4th ed. Springer Science & Business Media: Heidelberg, 2012.
8. Nicholson, J. W., *The Chemistry of Polymers*. Royal Society of Chemistry: Cambridge, 2012.
9. Salamone, J. C., *Concise Polymeric Materials Encyclopedia*. 1st ed. CRC Press: Boca Raton, 1998.
10. Dawkins, J. V.; Neep, D. J.; Shaw, P. L., Non-aqueous polystyrene dispersions: steric stabilization by partially hydrolysed poly(vinyl alcohol) in methanolic media. *Polymer* **1994**, 35 (24), 5366-5368.
11. Baines, F. L.; Dionisio, S.; Billingham, N. C.; Armes, S. P., Use of Block Copolymer Stabilizers for the Dispersion Polymerization of Styrene in Alcoholic Media. *Macromolecules* **1996**, 29 (9), 3096-3102.
12. Winzor, C. L.; Mrázek, Z.; Winnik, M. A.; Croucher, M. D.; Riess, G., Stabilization of dispersion polymerization by poly(styrene-b-ethylene oxide) copolymers. *European Polymer Journal* **1994**, 30 (1), 121-128.
13. Dawkins, J. V.; Taylor, G., Nonaqueous poly(methyl methacrylate) dispersions: radical dispersion polymerization in the presence of AB block copolymers of polystyrene and poly(dimethyl siloxane). *Polymer* **1979**, 20 (5), 599-604.
14. Dawkins, J.; Shakir, S. In *Nonaqueous Polymer Colloids-Stabilization Of Poly (Vinyl Acetate) Particles With The Diblock Copolymer Poly (Styrene-Beta-[Ethylene-Co-*

*Propylene*]), Acs Symposium Series, Amer Chemical Soc 1155 16TH ST, NW, Washington, DC 20036: 1992; pp 432-444.

15. Christian, P.; Howdle, S. M.; Irvine, D. J., Dispersion Polymerization of Methyl Methacrylate in Supercritical Carbon Dioxide with a Monofunctional Pseudo-Graft Stabilizer. *Macromolecules* **2000**, *33* (2), 237-239.
16. Li, G.; Yates, M. Z.; Johnston, K. P.; Howdle, S. M., In-Situ Investigation on the Mechanism of Dispersion Polymerization in Supercritical Carbon Dioxide. *Macromolecules* **2000**, *33* (11), 4008-4014.
17. Hsiao, Y.-L.; Maury, E. E.; DeSimone, J. M.; Mawson, S.; Johnston, K. P., Dispersion Polymerization of Methyl Methacrylate Stabilized with Poly(1,1-dihydroperfluorooctyl acrylate) in Supercritical Carbon Dioxide. *Macromolecules* **1995**, *28* (24), 8159-8166.
18. DeSimone, J. M.; Maury, E. E.; Menciloglu, Y. Z.; McClain, J. B.; Romack, T. J.; Combes, J. R., Dispersion Polymerizations in Supercritical Carbon Dioxide. *Science*, **1994**, *265* (5170), 356-359.
19. Minami, H.; Kimura, A.; Kinoshita, K.; Okubo, M., Preparation of Poly(acrylic acid) Particles by Dispersion Polymerization In an Ionic Liquid. *Langmuir* **2010**, *26* (9), 6303-6307.
20. Armes, S. P.; Aldissi, M.; Idzorek, G. C.; Keaton, P. W.; Rowton, L. J.; Stradling, G. L.; Collopy, M. T.; McColl, D. B., Particle size distributions of polypyrrole colloids. *Journal of Colloid and Interface Science* **1991**, *141* (1), 119-126.
21. DeArmitt, C.; Armes, S. P., Colloidal dispersions of surfactant-stabilized polypyrrole particles. *Langmuir* **1993**, *9* (3), 652-654.
22. Armes, S. P.; Vincent, B., Dispersions of electrically conducting polypyrrole particles in aqueous media. *Chemical Communications* **1987**, (4), 288-290.
23. An, Z.; Shi, Q.; Tang, W.; Tsung, C.-K.; Hawker, C. J.; Stucky, G. D., Facile RAFT Precipitation Polymerization for the Microwave-Assisted Synthesis of Well-Defined, Double Hydrophilic Block Copolymers and Nanostructured Hydrogels. *Journal of the American Chemical Society* **2007**, *129* (46), 14493-14499.
24. An, Z.; Tang, W.; Hawker, C. J.; Stucky, G. D., One-Step Microwave Preparation of Well-Defined and Functionalized Polymeric Nanoparticles. *Journal of the American Chemical Society* **2006**, *128* (47), 15054-15055.
25. Delaittre, G.; Save, M.; Charleux, B., Nitroxide-Mediated Aqueous Dispersion Polymerization: From Water-Soluble Macroalkoxyamine to Thermosensitive Nanogels. *Macromolecular Rapid Communications* **2007**, *28* (15), 1528-1533.

- 
26. Gazon, C.; Rieger, J.; Sanson, N.; Charleux, B., Study of poly(N,N-diethylacrylamide) nanogel formation by aqueous dispersion polymerization of N,N-diethylacrylamide in the presence of poly(ethylene oxide)-b-poly(N,N-dimethylacrylamide) amphiphilic macromolecular RAFT agents. *Soft Matter* **2011**, 7 (7), 3482-3490.
27. Liu, G.; Qiu, Q.; An, Z., Development of thermosensitive copolymers of poly(2-methoxyethyl acrylate-co-poly(ethylene glycol) methyl ether acrylate) and their nanogels synthesized by RAFT dispersion polymerization in water. *Polymer Chemistry* **2012**, 3 (2), 504-513.
28. Liu, G.; Qiu, Q.; Shen, W.; An, Z., Aqueous Dispersion Polymerization of 2-Methoxyethyl Acrylate for the Synthesis of Biocompatible Nanoparticles Using a Hydrophilic RAFT Polymer and a Redox Initiator. *Macromolecules* **2011**, 44 (13), 5237-5245.
29. Blanazs, A.; Madsen, J.; Battaglia, G.; Ryan, A. J.; Armes, S. P., Mechanistic Insights for Block Copolymer Morphologies: How Do Worms Form Vesicles? *Journal of the American Chemical Society* **2011**, 133 (41), 16581-16587.
30. Blanazs, A.; Ryan, A. J.; Armes, S. P., Predictive Phase Diagrams for RAFT Aqueous Dispersion Polymerization: Effect of Block Copolymer Composition, Molecular Weight, and Copolymer Concentration. *Macromolecules* **2012**, 45 (12), 5099-5107.
31. Ali, A. M. I.; Pareek, P.; Sewell, L.; Schmid, A.; Fujii, S.; Armes, S. P.; Shirley, I. M., Synthesis of poly(2-hydroxypropyl methacrylate) latex particles via aqueous dispersion polymerization. *Soft Matter* **2007**, 3 (8), 1003-1013.
32. Shen, W.; Chang, Y.; Liu, G.; Wang, H.; Cao, A.; An, Z., Biocompatible, Antifouling, and Thermosensitive Core-Shell Nanogels Synthesized by RAFT Aqueous Dispersion Polymerization. *Macromolecules* **2011**, 44 (8), 2524-2530.
33. Hoffman F., Delbruch K., German Patent 250690, 1909.
34. Whitby, G. S.; Katz, M., Synthetic Rubber. *Industrial & Engineering Chemistry* **1933**, 25 (12), 1338-1348.
35. Ciesielski, A., *An introduction to rubber technology*, 1st ed. Redwood Books Limited: Trowbridge, 1999.
36. Qun, W.; Shoukuan, F.; Tongyin, Y., Emulsion polymerization. *Progress in Polymer Science* **1994**, 19 (4), 703-753.
37. Gilbert, R. G., *Emulsion polymerization: a mechanistic approach*. Academic Press: London, 1995.
38. Arshady, R., Suspension, emulsion, and dispersion polymerization: A methodological survey. *Colloid and Polymer Science* **1992**, 270 (8), 717-732.

39. Szwarc, M., 'Living' Polymers. *Nature* **1956**, 178 (4543), 1168-1169.
40. Szwarc, M.; Levy, M.; Milkovich, R., Polymerization Initiated By Electron Transfer To Monomer. A New Method Of Formation Of Block Polymers 1. *Journal of the American Chemical Society* **1956**, 78 (11), 2656-2657.
41. Stefan, M.; Mapolie, S.; Gabriela Britchi, A., Styrene-butadiene rubber synthesized by anionic polymerization. *Macromolecular Symposia*, **2001**; Vol. 165, p 55-62.
42. Hsieh, H.; Quirk, R. P., *Anionic Polymerization: Principles and Practical Applications*. CRC Press: Boca Raton, 1996.
43. Bodratti, A. M.; Sarkar, B.; Alexandridis, P. J. A., Adsorption of poly (ethylene oxide)-containing amphiphilic polymers on solid-liquid interfaces: Fundamentals and applications. *Adv Colloid Interface Sci*, **2017**, 244, 132-163.
44. Bodratti, A. M.; Wu, J.; Jahan, R.; Sarkar, B.; Tsianou, M.; Alexandridis, P. J.; Technology, Mono-and Di-valent Salts as Modifiers of PEO-PPO-PEO Block Copolymer Interactions with Silica Nanoparticles in Aqueous Dispersions. *Journal of Dispersion Science and Technology*, **2015**, 36 (12), 1806-1815.
45. Growney, D. J.; Mykhaylyk, O. O.; Derouineau, T.; Fielding, L. A.; Smith, A. J.; Aragrag, N.; Lamb, G. D.; Armes, S. P., Star Diblock Copolymer Concentration Dictates the Degree of Dispersion of Carbon Black Particles in Nonpolar Media: Bridging Flocculation versus Steric Stabilization. *Macromolecules* **2015**, 48 (11), 3691-3704.
46. Li, Y.; Tang, Y.; Narain, R.; Lewis, A. L.; Armes, S. P., Biomimetic Stimulus-Responsive Star Diblock Gelators. *Langmuir* **2005**, 21 (22), 9946-9954.
47. Growney, D. J.; Mykhaylyk, O. O.; Armes, S. P., Micellization and Adsorption Behavior of a Near-Monodisperse Polystyrene-Based Diblock Copolymer in Nonpolar Media. *Langmuir* **2014**, 30 (21), 6047-6056.
48. Shar, J. A.; Cosgrove, T.; Obey, T. M.; Warne, M. R.; Wedlock, D. J., Adsorption Studies of Diblock Copolymers at the Cyclohexane/Carbon Black Interface. *Langmuir* **1999**, 15 (22), 7688-7694.
49. Geoffrey, H.; Ralph, M., US Patent US3265765, 1966
50. Morton, M., Chapter 9 - Block Copolymers. In *Anionic Polymerization: Principles and Practice*, Morton, M., Ed. Academic Press: London, 1983; pp 179-220.
51. Matyjaszewski, K.; Patten, T. E.; Xia, J., Controlled/"living" radical polymerization. Kinetics of the homogeneous atom transfer radical polymerization of styrene. *Journal of the American Chemical Society* **1997**, 119 (4), 674-680.

52. Wang, J.-S.; Matyjaszewski, K., Controlled/"living" radical polymerization. Atom transfer radical polymerization in the presence of transition-metal complexes. *Journal of the American Chemical Society* **1995**, *117* (20), 5614-5615.
53. Kato, M.; Kamigaito, M.; Sawamoto, M.; Higashimura, T., Polymerization of Methyl Methacrylate with the Carbon Tetrachloride/Dichlorotris-(triphenylphosphine)ruthenium(II)/Methylaluminum Bis(2,6-di-tert-butylphenoxide) Initiating System: Possibility of Living Radical Polymerization. *Macromolecules* **1995**, *28* (5), 1721-1723.
54. Wang, J.-S.; Matyjaszewski, K., Controlled/"living" radical polymerization. Halogen atom transfer radical polymerization promoted by a Cu (I)/Cu (II) redox process. *Macromolecules* **1995**, *28* (23), 7901-7910.
55. Curran, D. P., The Design and Application of Free Radical Chain Reactions in Organic Synthesis. Part 2. *Synthesis* **1988**, *1988* (07), 489-513.
56. Trost, B. M.; Fleming, I., *Comprehensive Organic Synthesis: Selectivity, Strategy, and Efficiency in Modern Organic Chemistry*. Pergamon Press: Oxford, 1991.
57. Taylor, M. J. W.; Eckenhoff, W. T.; Pintauer, T., Copper-catalyzed atom transfer radical addition (ATRA) and cyclization (ATRC) reactions in the presence of environmentally benign ascorbic acid as a reducing agent. *Dalton Transactions* **2010**, *39* (47), 11475-11482.
58. Matyjaszewski, K., Atom Transfer Radical Polymerization (ATRP): Current Status and Future Perspectives. *Macromolecules* **2012**, *45* (10), 4015-4039.
59. Tang, W.; Matyjaszewski, K., Effects of Initiator Structure on Activation Rate Constants in ATRP. *Macromolecules* **2007**, *40* (6), 1858-1863.
60. Zerk, T. J.; Bernhardt, P. V., Redox-coupled structural changes in copper chemistry: Implications for atom transfer catalysis. *Coordination Chemistry Reviews* **2018**, *375*, 173-190.
61. Matyjaszewski, K.; Tsarevsky, N. V., Macromolecular Engineering by Atom Transfer Radical Polymerization. *Journal of the American Chemical Society* **2014**, *136* (18), 6513-6533.
62. Tang, W.; Matyjaszewski, K., Effect of Ligand Structure on Activation Rate Constants in ATRP. *Macromolecules* **2006**, *39* (15), 4953-4959.
63. Ayres, N., Atom Transfer Radical Polymerization: A Robust and Versatile Route for Polymer Synthesis. *Polymer Reviews* **2011**, *51* (2), 138-162.
64. Jeon, H. J.; Youk, J. H.; Ahn, S. H.; Choi, J. H.; Cho, K. S. J. M. R., Synthesis of high molecular weight 3-arm star PMMA by ARGET ATRP. *Macromolecular Research*, **2009**, *17* (4), 240-244.

65. Lyra, E. P.; Petzhold, C. L.; Lona, L. M. F., Tin(II) 2-ethylhexanoate and ascorbic acid as reducing agents in solution ARGET ATRP: A kinetic study approach by mathematical modeling and simulation. *Chemical Engineering Journal* **2019**, *364*, 186-200.
66. Jakubowski, W.; Min, K.; Matyjaszewski, K., Activators Regenerated by Electron Transfer for Atom Transfer Radical Polymerization of Styrene. *Macromolecules* **2006**, *39* (1), 39-45.
67. Ma, I. Y.; Lobb, E. J.; Billingham, N. C.; Armes, S. P.; Lewis, A. L.; Lloyd, A. W.; Salvage, J., Synthesis of Biocompatible Polymers. 1. Homopolymerization of 2-Methacryloyloxyethyl Phosphorylcholine via ATRP in Protic Solvents: An Optimization Study. *Macromolecules* **2002**, *35* (25), 9306-9314.
68. Chiefari, J.; Chong, Y. K.; Ercole, F.; Krstina, J.; Jeffery, J.; Le, T. P. T.; Mayadunne, R. T. A.; Meijs, G. F.; Moad, C. L.; Moad, G.; Rizzardo, E.; Thang, S. H., Living Free-Radical Polymerization by Reversible Addition–Fragmentation Chain Transfer: The RAFT Process. *Macromolecules* **1998**, *31* (16), 5559-5562.
69. Moad, G.; Rizzardo, E.; Thang, S. H., Living Radical Polymerization by the RAFT Process. *Australian Journal of Chemistry* **2005**, *58* (6), 379-410.
70. Moad, G.; Rizzardo, E.; Thang, S. H., Living Radical Polymerization by the RAFT Process – A Second Update. *Australian Journal of Chemistry* **2009**, *62* (11), 1402-1472.
71. Moad, G.; Rizzardo, E.; Thang, S. H., Living Radical Polymerization by the RAFT Process – A Third Update. *Australian Journal of Chemistry* **2012**, *65* (8), 985-1076.
72. Mayadunne, R. T. A.; Rizzardo, E.; Chiefari, J.; Chong, Y. K.; Moad, G.; Thang, S. H., Living Radical Polymerization with Reversible Addition–Fragmentation Chain Transfer (RAFT Polymerization) Using Dithiocarbamates as Chain Transfer Agents. *Macromolecules* **1999**, *32* (21), 6977-6980.
73. Destarac, M.; Charmot, D.; Franck, X.; Zard, S. Z., Dithiocarbamates as universal reversible addition-fragmentation chain transfer agents. *Macromolecular Rapid Communications* **2000**, *21* (15), 1035-1039.
74. Charmot, D.; Corpart, P.; Adam, H.; Zard, S. Z.; Biadatti, T.; Bouhadir, G., Controlled radical polymerization in dispersed media. *Macromolecular Symposia* **2000**, *150* (1), 23-32.
75. Mitsukami, Y.; Donovan, M. S.; Lowe, A. B.; McCormick, C. L., Water-Soluble Polymers. 81. Direct Synthesis of Hydrophilic Styrenic-Based Homopolymers and Block Copolymers in Aqueous Solution via RAFT. *Macromolecules* **2001**, *34* (7), 2248-2256.
76. Patten, T. E.; Matyjaszewski, K., Atom Transfer Radical Polymerization and the Synthesis of Polymeric Materials. *Advanced Materials* **1998**, *10* (12), 901-915.



77. J. Ashford, E.; Naldi, V.; O'Dell, R.; C. Billingham, N.; P. Armes, S., First example of the atom transfer radical polymerisation of an acidic monomer: direct synthesis of methacrylic acid copolymers in aqueous media. *Chemical Communications* **1999**, (14), 1285-1286.
78. Canton, I.; Warren, N. J.; Chahal, A.; Amps, K.; Wood, A.; Weightman, R.; Wang, E.; Moore, H.; Armes, S. P., Mucin-Inspired Thermoresponsive Synthetic Hydrogels Induce Stasis in Human Pluripotent Stem Cells and Human Embryos. *ACS Central Science* **2016**, 2 (2), 65-74.
79. Willcock, H.; O'Reilly, R. K., End group removal and modification of RAFT polymers. *Polymer Chemistry* **2010**, 1 (2), 149-157.
80. Moad, G.; Rizzardo, E.; Thang, S. H., End-functional polymers, thiocarbonylthio group removal/transformation and reversible addition–fragmentation–chain transfer (RAFT) polymerization. *Polymer International*, **2011**, 60 (1), 9-25.
81. Legge, T. M.; Slark, A. T.; Perrier, S., Thermal stability of reversible addition–fragmentation chain transfer/macromolecular architecture design by interchange of xanthates chain-transfer agents. *Journal of Polymer Science Part A: Polymer Chemistry* **2006**, 44 (24), 6980-6987.
82. Chong, B.; Moad, G.; Rizzardo, E.; Skidmore, M.; Thang, S. H., Thermolysis of RAFT-Synthesized Poly(Methyl Methacrylate). *Australian Journal of Chemistry* **2006**, 59 (10), 755-762.
83. Chong, Y. K.; Moad, G.; Rizzardo, E.; Thang, S. H., Thiocarbonylthio End Group Removal from RAFT-Synthesized Polymers by Radical-Induced Reduction. *Macromolecules* **2007**, 40 (13), 4446-4455.
84. Deletre, M.; Levesque, G., Kinetics and mechanism of polythioamidation in solution. 1. Reaction of mono- and bis(dithioester)s with excess amine. *Macromolecules* **1990**, 23 (22), 4733-4741.
85. Perrier, S.; Takolpuckdee, P.; Mars, C. A., Reversible addition-fragmentation chain transfer polymerization: End group modification for functionalized polymers and chain transfer agent recovery. *Macromolecules* **2005**, 38 (6), 2033-2036.
86. Nebhani, L.; Sinnwell, S.; Inglis, A. J.; Stenzel, M. H.; Barner-Kowollik, C.; Barner, L., Efficient Surface Modification of Divinylbenzene Microspheres via a Combination of RAFT and Hetero Diels-Alder Chemistry. *Macromolecular Rapid Communications* **2008**, 29 (17), 1431-1437.

- 
87. Sinnwell, S.; Inglis, A. J.; Davis, T. P.; Stenzel, M. H.; Barner-Kowollik, C., An atom-efficient conjugation approach to well-defined block copolymers using RAFT chemistry and hetero Diels–Alder cycloaddition. *Chemical Communications* **2008**, (17), 2052-2054.
88. Pfukwa, R.; Pound, G.; Klumperman, B., Facile End Group Modification Of Raft Made Polymers, By Radical Exchange With Hydrogen Peroxide. *Polymer Preprints* **2008**, 49 (2), 117-118.
89. Matioszek, D.; Dufils, P.-E.; Vinas, J.; Destarac, M., Selective and Quantitative Oxidation of Xanthate End-Groups of RAFT Poly(n-butyl acrylate) Latexes by Ozonolysis. *Macromolecular Rapid Communications* **2015**, 36 (14), 1354-1361.
90. Milner, S. T., Polymer Brushes., *Science*, **1991**, 251 (4996), 905-914.
91. Dahman, Y., Chapter 3 - Smart Nanomaterials, Dahman, Y, Kamil, A, Baena, D. In *Nanotechnology and Functional Materials for Engineers*, Dahman, Y., Ed. Elsevier: Amsterdam, 2017; pp 47-66.
92. Klein, J., Entropic interactions: neutral and end-functionalized chains in confined geometries. *Journal of Physics: Condensed Matter* **2000**, 12 (8A), A19-A27.
93. Halperin, A.; Tirrell, M.; Lodge, T. P., Tethered chains in polymer microstructures. In *Macromolecules: Synthesis, Order and Advanced Properties*, Springer Berlin Heidelberg: Berlin, Heidelberg, 1992; pp 31-71.
94. Binder, K., *Monte Carlo and molecular dynamics simulations in polymer science*. Oxford University Press: London, 1995.
95. Feng, C.; Huang, X., Polymer Brushes: Efficient Synthesis and Applications. *Accounts of Chemical Research* **2018**, 51 (9), 2314-2323.
96. Feng, C.; Li, Y.; Yang, D.; Hu, J.; Zhang, X.; Huang, X., Well-defined graft copolymers: from controlled synthesis to multipurpose applications. *Chemical Society Reviews* **2011**, 40 (3), 1282-1295.
97. Advincula R. C., Brittain W. J., Caster K. C., Ruhe J., Recent Advances in the Synthesis and Rearrangement of Block Copolymer Brushes. In *Polymer Brushes*. Wiley: Darmstadt, 2004
98. Ling, D.; Hackett, M. J.; Hyeon, T., Surface ligands in synthesis, modification, assembly and biomedical applications of nanoparticles. *Nano Today* **2014**, 9 (4), 457-477.
99. Dunderdale, G. J.; Urata, C.; Miranda, D. F.; Hozumi, A., Large-Scale and Environmentally Friendly Synthesis of pH-Responsive Oil-Repellent Polymer Brush Surfaces under Ambient Conditions. *ACS Applied Materials & Interfaces* **2014**, 6 (15), 11864-11868.

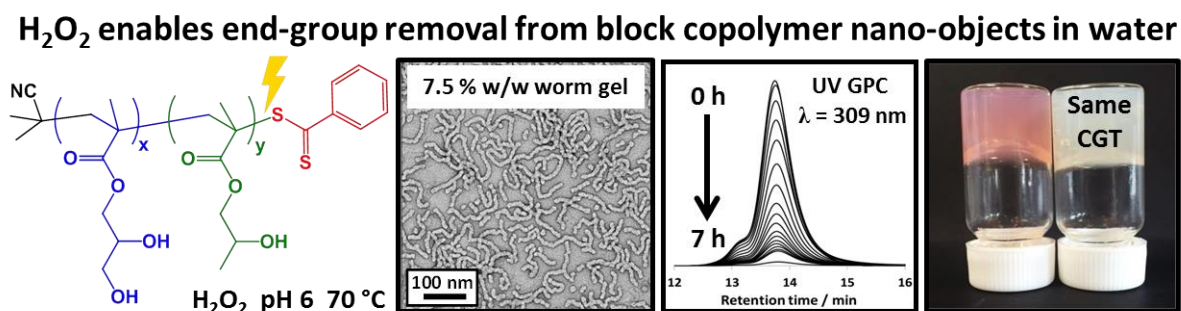
100. Aakeroy, C. B.; Seddon, K. R., The hydrogen bond and crystal engineering. *Chemical Society Reviews* **1993**, 22 (6), 397-407.
101. Schryver, S. B.; Ramsden, W.; Cross, C. F.; Schidrowitz, P.; Dreaper, W. P.; McBain, J. W.; Turner, T.; Worley, F. P.; Martin, C. J.; Bousfield, W. R.; Morse, H. N.; Henri, V.; Freundlich, H.; The, C.; Ostwald, W.; Chapman, C.; Senter, G., Discussion. *Transactions of the Faraday Society* **1913**, 9 (0), 93-107.
102. Israelachvili, J. N., *Intermolecular and Surface Forces: Revised Third Edition*. Elsevier Science: Waltham, MA, 2011.
103. Blanazs, A.; Armes, S. P.; Ryan, A. J., Self-Assembled Block Copolymer Aggregates: From Micelles to Vesicles and their Biological Applications. *Macromolecular Rapid Communications* **2009**, 30 (4-5), 267-277.
104. Chu, Z.; Dreiss, C. A.; Feng, Y., Smart wormlike micelles. *Chemical Society Reviews* **2013**, 42 (17), 7174-7203.
105. Warren, N. J.; Armes, S. P., Polymerization-Induced Self-Assembly of Block Copolymer Nano-objects via RAFT Aqueous Dispersion Polymerization. *Journal of the American Chemical Society* **2014**, 136 (29), 10174-10185.
106. Won, Y.-Y.; Davis, H. T.; Bates, F. S., Giant Wormlike Rubber Micelles. *Science* **1999**, 283 (5404), 960-963.
107. Bellomo, E. G.; Wyrsta, M. D.; Pakstis, L.; Pochan, D. J.; Deming, T. J., Stimuli-responsive polypeptide vesicles by conformation-specific assembly. *Nature Materials* **2004**, 3, 244.
108. Cui, H.; Chen, Z.; Zhong, S.; Wooley, K. L.; Pochan, D. J., Block Copolymer Assembly via Kinetic Control. *Science* **2007**, 317 (5838), 647-650.
109. Du, J.; Tang, Y.; Lewis, A. L.; Armes, S. P., pH-Sensitive Vesicles Based on a Biocompatible Zwitterionic Diblock Copolymer. *Journal of the American Chemical Society* **2005**, 127 (51), 17982-17983.
110. Arifin, D. R.; Palmer, A. F., Polymersome Encapsulated Hemoglobin: A Novel Type of Oxygen Carrier. *Biomacromolecules* **2005**, 6 (4), 2172-2181.
111. Ghoroghchian, P. P.; Frail, P. R.; Susumu, K.; Blessington, D.; Brannan, A. K.; Bates, F. S.; Chance, B.; Hammer, D. A.; Therien, M. J., Near-infrared-emissive polymersomes: Self-assembled soft matter for in vivo optical imaging. *Proceedings of the National Academy of Sciences of the United States of America*, **2005**, 102 (8), 2922-2927.
112. Hayward, R. C.; Pochan, D. J., Tailored Assemblies of Block Copolymers in Solution: It Is All about the Process. *Macromolecules* **2010**, 43 (8), 3577-3584.

- 
113. Zhou, W.; Qu, Q.; Xu, Y.; An, Z., Aqueous Polymerization-Induced Self-Assembly for the Synthesis of Ketone-Functionalized Nano-Objects with Low Polydispersity. *ACS Macro Letters* **2015**, *4* (5), 495-499.
114. Kim, K. H.; Kim, J.; Jo, W. H., Preparation of hydrogel nanoparticles by atom transfer radical polymerization of N-isopropylacrylamide in aqueous media using PEG macro-initiator. *Polymer* **2005**, *46* (9), 2836-2840.
115. Sugihara, S.; Sugihara, K.; Armes, S. P.; Ahmad, H.; Lewis, A. L., Synthesis of Biomimetic Poly(2-(methacryloyloxy)ethyl phosphorylcholine) Nanolatexes via Atom Transfer Radical Dispersion Polymerization in Alcohol/Water Mixtures. *Macromolecules* **2010**, *43* (15), 6321-6329.
116. Okubo, M.; Sugihara, Y.; Kitayama, Y.; Kagawa, Y.; Minami, H., Emulsifier-Free, Organotellurium-Mediated Living Radical Emulsion Polymerization of Butyl Acrylate. *Macromolecules* **2009**, *42* (6), 1979-1984.
117. Kitayama, Y.; Moribe, H.; Kishida, K.; Okubo, M., Emulsifier-free, organotellurium-mediated living radical emulsion polymerization (emulsion TERP) of methyl methacrylate with dimethyl ditelluride as the catalyst. *Polymer Chemistry* **2012**, *3* (6), 1555-1559.
118. Charleux, B.; Delaittre, G.; Rieger, J.; D'Agosto, F., Polymerization-Induced Self-Assembly: From Soluble Macromolecules to Block Copolymer Nano-Objects in One Step. *Macromolecules* **2012**, *45* (17), 6753-6765.
119. Canning, S. L.; Smith, G. N.; Armes, S. P., A Critical Appraisal of RAFT-Mediated Polymerization-Induced Self-Assembly. *Macromolecules* **2016**, *49* (6), 1985-2001.
120. Sugihara, S.; Armes, S. P.; Blanazs, A.; Lewis, A. L., Non-spherical morphologies from cross-linked biomimetic diblock copolymers using RAFT aqueous dispersion polymerization. *Soft Matter* **2011**, *7* (22), 10787-10793.
121. Mable, C. J.; Warren, N. J.; Thompson, K. L.; Mykhaylyk, O. O.; Armes, S. P., Framboidal ABC triblock copolymer vesicles: a new class of efficient Pickering emulsifier. *Chemical Science* **2015**, *6* (11), 6179-6188.
122. Higuchi, T.; Yabu, H.; Onoue, S.; Kunitake, T.; Shimomura, M., Preparation of lamella-structured block-copolymer particles and their irreversible lamella-disorder phase transition. *Colloids and Surfaces A: Physicochemical and Engineering Aspects* **2008**, *313–314*, 87-90.
123. Yang, P.; Ratcliffe, L. P. D.; Armes, S. P., Efficient Synthesis of Poly(methacrylic acid)-block-Poly(styrene-alt-N-phenylmaleimide) Diblock Copolymer Lamellae Using RAFT Dispersion Polymerization. *Macromolecules* **2013**, *46* (21), 8545-8556.

124. Ferguson, C. J.; Hughes, R. J.; Pham, B. T. T.; Hawzett, B. S.; Gilbert, R. G.; Serelis, A. K.; Such, C. H., Effective ab Initio Emulsion Polymerization under RAFT Control. *Macromolecules* **2002**, *35* (25), 9243-9245.
125. Monteiro, M. J.; Hodgson, M.; De Brouwer, H., The influence of RAFT on the rates and molecular weight distributions of styrene in seeded emulsion polymerizations. *Journal of Polymer Science Part A: Polymer Chemistry* **2000**, *38* (21), 3864-3874.
126. Prescott, S. W.; Ballard, M. J.; Rizzardo, E.; Gilbert, R. G., RAFT in Emulsion Polymerization: What Makes it Different? *Australian Journal of Chemistry* **2002**, *55* (7), 415-424.
127. Cunningham, V. J.; Alswieleh, A. M.; Thompson, K. L.; Williams, M.; Leggett, G. J.; Armes, S. P.; Musa, O. M., Poly(glycerol monomethacrylate)–Poly(benzyl methacrylate) Diblock Copolymer Nanoparticles via RAFT Emulsion Polymerization: Synthesis, Characterization, and Interfacial Activity. *Macromolecules* **2014**, *47* (16), 5613-5623.
128. Chaduc, I.; Girod, M.; Antoine, R.; Charleux, B.; D'Agosto, F.; Lansalot, M., Batch Emulsion Polymerization Mediated by Poly(methacrylic acid) MacroRAFT Agents: One-Pot Synthesis of Self-Stabilized Particles. *Macromolecules* **2012**, *45* (15), 5881-5893.
129. Zhang, X.; Boissé, S.; Zhang, W.; Beaunier, P.; D'Agosto, F.; Rieger, J.; Charleux, B., Well-Defined Amphiphilic Block Copolymers and Nano-objects Formed in Situ via RAFT-Mediated Aqueous Emulsion Polymerization. *Macromolecules* **2011**, *44* (11), 4149-4158.
130. Rieger, J.; Osterwinter, G.; Bui, C.; Stoffelbach, F.; Charleux, B., Surfactant-Free Controlled/Living Radical Emulsion (Co)polymerization of n-Butyl Acrylate and Methyl Methacrylate via RAFT Using Amphiphilic Poly(ethylene oxide)-Based Trithiocarbonate Chain Transfer Agents. *Macromolecules* **2009**, *42* (15), 5518-5525.
131. Rieger, J.; Zhang, W.; Stoffelbach, F.; Charleux, B., Surfactant-Free RAFT Emulsion Polymerization Using Poly(N,N-dimethylacrylamide) Trithiocarbonate Macromolecular Chain Transfer Agents. *Macromolecules* **2010**, *43* (15), 6302-6310.
132. Chenal, M.; Bouteiller, L.; Rieger, J., Ab initio RAFT emulsion polymerization of butyl acrylate mediated by poly(acrylic acid) trithiocarbonate. *Polymer Chemistry* **2013**, *4* (3), 752-762.
133. Truong, N. P.; Dussert, M. V.; Whittaker, M. R.; Quinn, J. F.; Davis, T. P., Rapid synthesis of ultrahigh molecular weight and low polydispersity polystyrene diblock copolymers by RAFT-mediated emulsion polymerization. *Polymer Chemistry* **2015**, *6* (20), 3865-3874.

134. St Thomas, C.; Guerrero-Santos, R.; D'Agosto, F., Alkoxyamine-functionalized latex nanoparticles through RAFT polymerization-induced self-assembly in water. *Polymer Chemistry* **2015**, *6* (30), 5405-5413.
135. Wan, W.-M.; Hong, C.-Y.; Pan, C.-Y., One-pot synthesis of nanomaterials via RAFT polymerization induced self-assembly and morphology transition. *Chemical Communications* **2009**, (39), 5883-5885.
136. Li, Y.; Armes, S. P., RAFT Synthesis of Sterically Stabilized Methacrylic Nanolatexes and Vesicles by Aqueous Dispersion Polymerization. *Angewandte Chemie International Edition*, **2010**, *49* (24), 4042-4046.
137. Sugihara, S.; Blanazs, A.; Armes, S. P.; Ryan, A. J.; Lewis, A. L., Aqueous Dispersion Polymerization: A New Paradigm for in Situ Block Copolymer Self-Assembly in Concentrated Solution. *Journal of the American Chemical Society* **2011**, *133* (39), 15707-15713.
138. Mable, C. J.; Gibson, R. R.; Prevost, S.; McKenzie, B. E.; Mykhaylyk, O. O.; Armes, S. P., Loading of Silica Nanoparticles in Block Copolymer Vesicles during Polymerization-Induced Self-Assembly: Encapsulation Efficiency and Thermally Triggered Release. *Journal of the American Chemical Society* **2015**, *137* (51), 16098-16108.
139. Blanazs, A.; Verber, R.; Mykhaylyk, O. O.; Ryan, A. J.; Heath, J. Z.; Douglas, C. W. I.; Armes, S. P., Sterilizable Gels from Thermoresponsive Block Copolymer Worms. *Journal of the American Chemical Society* **2012**, *134* (23), 9741-9748.
140. Warren, N. J.; Derry, M. J.; Mykhaylyk, O. O.; Lovett, J. R.; Ratcliffe, L. P. D.; Ladmiral, V.; Blanazs, A.; Fielding, L. A.; Armes, S. P., Critical Dependence of Molecular Weight on Thermoresponsive Behavior of Diblock Copolymer Worm Gels in Aqueous Solution. *Macromolecules* **2018**, *51* (21), 8357-8371.

## Chapter 2 - H<sub>2</sub>O<sub>2</sub> enables convenient removal of RAFT end-groups from block copolymer nano-objects prepared via polymerisation-induced self-assembly in water



The work carried out in this chapter was at least 80 % completed by C. P. Jesson

The rest of the work was completed by C. M. Pearce, H. Simon, A. Werner and N. J. Warren

## Introduction

Over the past two decades reversible addition-fragmentation chain transfer (RAFT) polymerisation<sup>1-4</sup> has become a well-established route for the synthesis of a wide range of controlled-structure functional copolymers for various potential applications.<sup>5-10</sup> RAFT polymerisation enables good control over target molecular weight, molecular weight distribution and copolymer architecture, while also providing access to a wide range of specific end-groups.<sup>11-18</sup> The recent development of polymerisation-induced self-assembly (PISA) has been based largely on RAFT-mediated polymerisation conducted in heterogeneous media.<sup>19-26</sup> PISA has enabled the rational design of a wide range of bespoke block copolymer nanoparticles (e.g. spheres, worms, vesicles, framboidal vesicles, platelets etc.)<sup>27-30</sup> and certain formulations appear to be promising for potential biomedical applications. For example, poly(glycerol monomethacrylate)-poly(2-hydroxypropyl methacrylate) diblock copolymer worm gels are readily sterilisable via cold ultrafiltration and induce stasis in human embryonic stem cells.<sup>31</sup> Closely-related disulfide-functional worm gels are sufficiently robust to enable 3D cell culture for extended periods in plastic matrices.<sup>32</sup> Targeting diblock copolymer vesicles via PISA has enabled encapsulation (and, in some cases, the subsequent release) of various model payloads such as fluorescently-labelled water-soluble polymers, silica nanoparticles or globular proteins, which augurs well for drug delivery applications.<sup>12,33,34</sup>

In the context of potential biomedical and cosmetics applications, one of the main drawbacks of RAFT-synthesised (co)polymers is the colour, malodour and possible toxicity conferred by the sulfur-based end-groups, whether they be dithioesters, trithiocarbonates or xanthates,<sup>4</sup> RAFT end-group cleavage via hydrolysis<sup>35,36</sup> (or other chemistries) results in the formation of low molecular weight by-products that may be preferentially internalised within mammalian cells, apparently without inducing toxicity in at least some cases.<sup>37</sup>

In practice, such problems are often circumvented by pre-emptive removal of the RAFT end-group under controlled conditions. Not surprisingly, this approach works rather better for acrylic (or styrenic) polymers compared to more sterically-congested methacrylic polymers.<sup>38,39</sup> Numerous chemistries have been employed, such as aminolysis using either primary amines or hydrazine;<sup>40</sup> ozonolysis,<sup>41</sup> bond cleavage using radicals derived from addition of excess initiator,<sup>42-44</sup> thermolysis<sup>45,46</sup> or, more recently, light-mediated removal.<sup>47</sup> However, as far as we are aware, there is only one literature report of using H<sub>2</sub>O<sub>2</sub> for removing



RAFT end-groups and this brief study was restricted to the derivatisation of *soluble* poly(*N*-vinyl pyrrolidone) chains in aqueous solution at 80 °C.<sup>48</sup> A radical mechanism was proposed, whereby hydroxyl radicals generated at elevated temperature replaced each RAFT end-group with a terminal alcohol.

Herein we revisit the use of H<sub>2</sub>O<sub>2</sub> as a means of removing RAFT end-groups from various examples of *methacrylic diblock copolymer nanoparticles* in aqueous solution. In this context, the non-ionic nature and relatively low molecular weight of H<sub>2</sub>O<sub>2</sub> might be expected to offer a significant advantage in terms of its faster ingress within the nanoparticle interior. Moreover, it is emphasised that H<sub>2</sub>O<sub>2</sub> is relatively cheap and produces only water and oxygen as by-products. It is perhaps also noteworthy that relatively few RAFT end-group derivatisation studies have focused on methacrylic copolymers, rather than the more reactive acrylic or styrenic copolymers.

## Experimental

### *Materials*

Glycerol monomethacrylate (GMA, 99.8%), 2-hydroxypropyl methacrylate (HPMA, 99.3%) and benzyl methacrylate (BzMA, 99.2%) were donated by GEO Specialty Chemicals (Hythe, UK) and used without further purification. The synthetic route used to obtain HPMA results in the production of two isomeric forms.<sup>49</sup> The isomeric composition was confirmed by <sup>1</sup>H NMR spectroscopy. The 'HPMA' monomer actually contained 75 mol % HPMA, with the remainder being its closely related isomer, 2-hydroxyisopropyl methacrylate [HIPMA].

4,4'-Azobis(4-cyanopentanoic acid) (ACVA, 99%) and dichloromethane were purchased from Sigma-Aldrich (UK) and were used as received. 2-Cyano-2-propyldithiobenzoate (CPDB) was purchased from Strem Chemicals Ltd. (Cambridge, UK) and was used as received. 4-Cyano-4-(2-phenylethanesulfanylthiocarbonyl)sulfanylpentanoic acid (PETTC) RAFT agent was synthesised as previously reported.<sup>50</sup> For the sake of brevity, the acronyms DB and TTC are used to denote dithiobenzoate and trithiocarbonate end-groups for the various copolymers prepared in this study. Deuterated DMF and methanol were purchased from Goss Scientific Instruments Ltd. (Crewe, UK). All other solvents were purchased from Fisher Scientific (Loughborough, UK) and used as received. Deionised water was used for all experiments.

*Protocol for the synthesis of PGMA macro-CTAs*

Synthesis of a dithiobenzoate functionalised poly(glycerol monomethacrylate) PGMA<sub>52</sub> chain transfer agent is representative of all dithiobenzoate functionalised macro-CTAs and was prepared as follows. GMA monomer (25.0 g, 156.1 mmol) and CPDB RAFT agent (0.864 g, 3.9 mmol; target degree of polymerisation, DP = 40) were weighed into a 100 mL round-bottomed flask and purged under N<sub>2</sub> for 30 min. ACVA initiator (218.6 mg, 0.78 mmol; CTA/ACVA molar ratio = 5.0) and anhydrous ethanol (49.6 mL; previously purged with N<sub>2</sub> for 30 min) were then added, and the resulting red solution was degassed for a further 10 min. The flask was subsequently sealed and immersed into an oil bath set at 70 °C. After 100 min, the GMA polymerisation was quenched by exposing to air, immersing in liquid nitrogen for 30 seconds, followed by dilution with methanol (100 mL). A final GMA conversion of 78 % was determined by <sup>1</sup>H NMR analysis. The methanolic PGMA solution was precipitated into a ten-fold excess of dichloromethane. After filtration, the crude PGMA precipitate was washed with dichloromethane, dissolved in water and residual dichloromethane was evaporated under reduced pressure. The resulting aqueous solution was freeze-dried overnight to yield a pink powder. <sup>1</sup>H NMR analysis indicated a number-average degree of polymerisation of 52 for this PGMA-DB macro-CTA (M<sub>n</sub> = 13,600, M<sub>w</sub>/M<sub>n</sub> = 1.19, see Figure 2.1). This suggests a CTA efficiency of around 60 %.

Synthesis of a trithiocarbonate-functionalised PGMA<sub>52</sub> macro-CTA was performed using PETTC RAFT agent (target degree of polymerisation, DP = 55) instead of CPDB via the same general protocol as that described above. A final GMA conversion of 70% was determined by <sup>1</sup>H NMR analysis. The crude copolymer was purified via precipitation from methanol into excess dichloromethane to yield a yellow powder. <sup>1</sup>H NMR analysis indicated a number-average degree of polymerisation of 52 for this PGMA-TTC macro-CTA (M<sub>n</sub> = 13,700, M<sub>w</sub>/M<sub>n</sub> = 1.26, see Figure 2.1). This suggests a CTA efficiency of around 74 %.

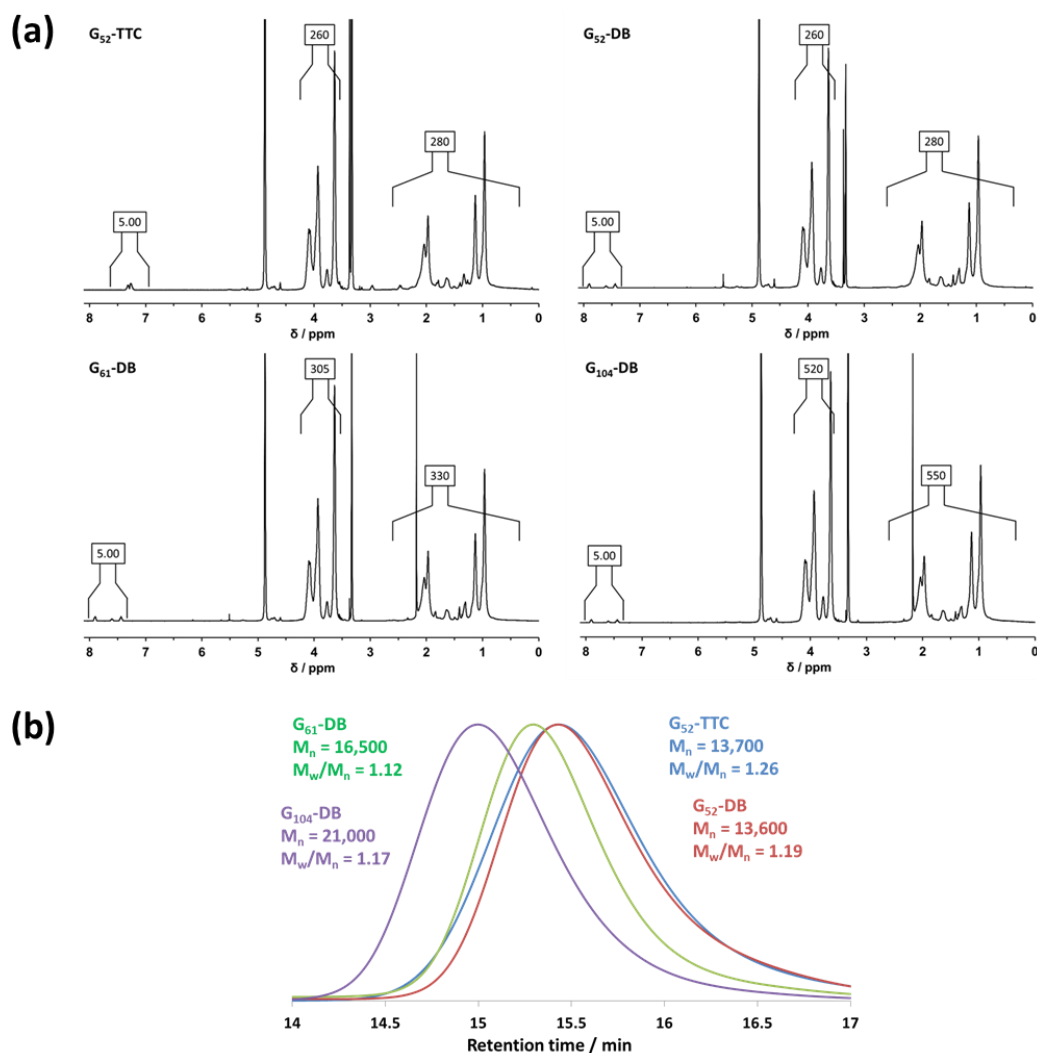


**Figure 2.1.** (a) Integrated <sup>1</sup>H NMR spectra and (b) DMF GPC chromatograms for G<sub>52</sub>-TTC, G<sub>52</sub>-DB, G<sub>61</sub>-DB and G<sub>104</sub>-DB macro-CTAs

### Synthesis of PGMA<sub>104</sub>-PHPMA<sub>y</sub> diblock copolymer spheres

These diblock copolymer nanoparticles were prepared via RAFT aqueous dispersion polymerisation, as reported by Blanazs et al.<sup>51</sup> As a typical example, PGMA<sub>104</sub>-PHPMA<sub>600</sub> spheres were synthesised as follows. PGMA<sub>104</sub>-DB macro-CTA (0.332 g, 19.7 μmol), HPMA monomer (1.70 g, 11.8 mmol; target DP = 600) and ACVA initiator (1.84 mg, 6.55 μmol; macro-CTA/ACVA molar ratio = 3.0) were weighed into a 50 mL round-bottomed flask and dissolved in deionised water (18.3 mL). The resulting solution was purged under N<sub>2</sub> for 30 min before being sealed and immersed in an oil bath at 70 °C for 5 h. The HPMA polymerisation was quenched by exposure to air. A final HPMA conversion of more than 99 % was determined

by <sup>1</sup>H NMR analysis. These copolymer spheres were characterised by DMF GPC without further purification and used directly for RAFT end-group removal experiments ( $M_n = 79,100$ ,  $M_w/M_n = 1.24$ , see Figure 2.2).

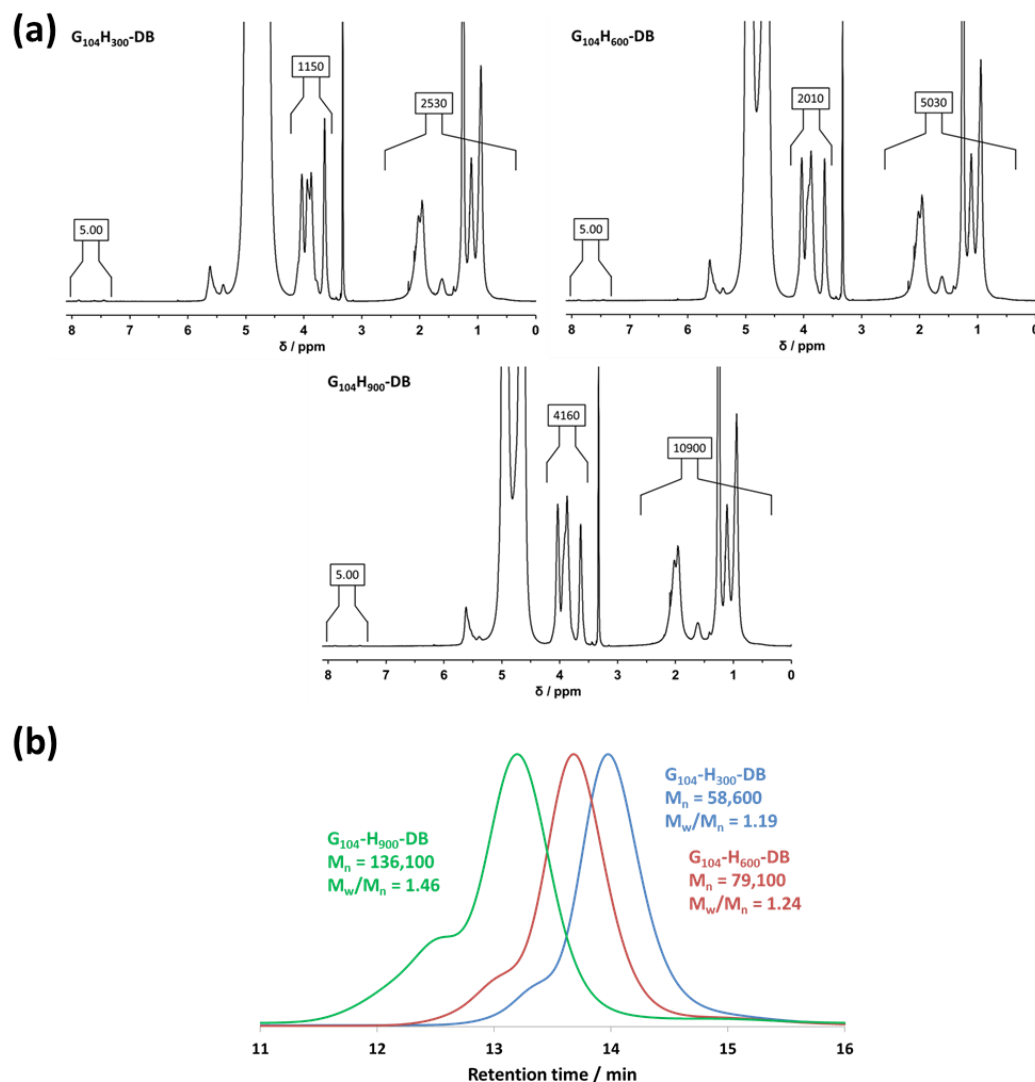


**Figure 2.2.** (a) Integrated <sup>1</sup>H NMR spectra and (b) DMF GPC chromatograms for G<sub>104</sub>-H<sub>X</sub> (X = 300, 600, 900) diblock copolymer spheres

#### *Synthesis of PGMA<sub>52</sub>-PHPMA<sub>135</sub> diblock copolymer worms*

These diblock copolymer nanoparticles were prepared via RAFT aqueous dispersion polymerisation, as reported by Blanz et al.<sup>51</sup> A typical protocol used for the PISA synthesis of PGMA<sub>52</sub>-PHPMA<sub>135</sub> worms was as follows. PGMA<sub>52</sub> macro-CTA (3.60 g, 0.395 mmol) and HPMA monomer (7.70 g, 53.5 mmol; target DP = 135) were weighed into a 25 mL round-

bottomed flask and purged with N<sub>2</sub> for 20 min. ACVA was added (28.3 mg, 0.101 mmol, CTA/ACVA molar ratio = 5.0) and purged with N<sub>2</sub> for a further 5 min. Deionised water (46.1 mL, producing a 20.0% w/w aqueous solution) that had been previously purged with N<sub>2</sub> for 30 min was then added and the solution was degassed for a further 5 min prior to immersion in an oil bath set at 70 °C. This reaction solution was stirred for 3 h before the polymerisation was quenched by exposure to air. These copolymer worms were characterised by DMF GPC without further purification and used directly for RAFT end-group removal experiments ( $M_n = 35,600$ ,  $M_w/M_n = 1.12$ , see Figure 2.3).

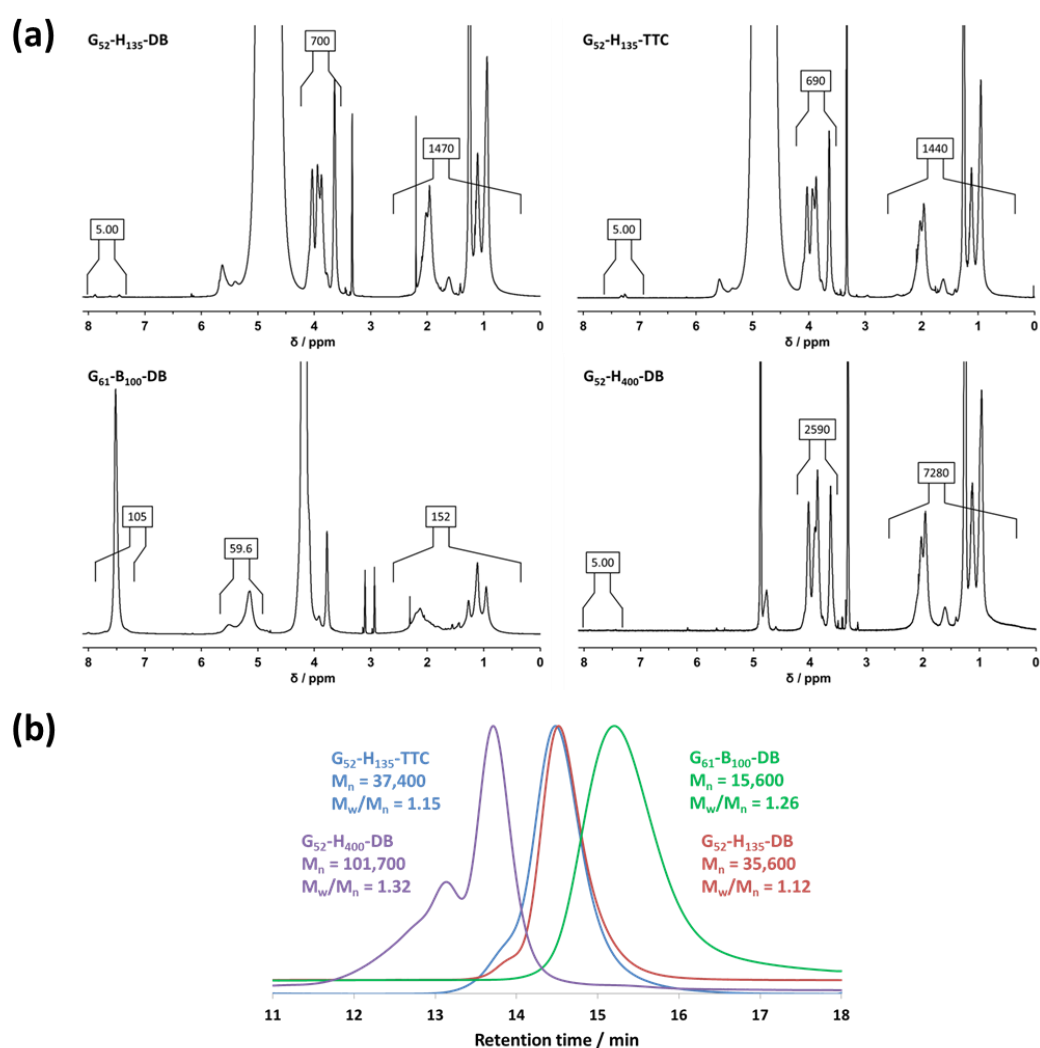


**Figure 2.3.** (a) Integrated <sup>1</sup>H NMR spectra and (b) DMF GPC chromatograms for G<sub>52</sub>-H<sub>135</sub>-TTC and G<sub>52</sub>-H<sub>135</sub>-DB worms, G<sub>61</sub>-B<sub>100</sub> spheres and G<sub>52</sub>-H<sub>400</sub> vesicles

#### *Synthesis of PGMA<sub>52</sub>-PHPMA<sub>400</sub> diblock copolymer vesicles*

These diblock copolymer nanoparticles were prepared via RAFT aqueous dispersion polymerisation, as reported by Blanz et al.<sup>51</sup> PGMA<sub>52</sub>-DB macro-CTA (0.133 g, 15.6 μmol), HPMA monomer (0.90 g, 6.2 mmol; target DP = 400) and ACVA initiator (1.46 mg, 5.20 μmol, CTA/ACVA molar ratio = 3.0) were weighed into a 25 mL round-bottomed flask and dissolved in deionised water (9.31 mL). The resulting solution was purged under N<sub>2</sub> for 30 min before being sealed and immersed in an oil bath at 70 °C for 4 h. The HPMA polymerisation was quenched by exposure to air and a final HPMA conversion of more than 99 % was determined by <sup>1</sup>H NMR analysis. These copolymer vesicles were characterised without further purification and used directly for RAFT end-group removal experiments (M<sub>n</sub> = 101,700, M<sub>w</sub>/M<sub>n</sub> = 1.32, see Figure 2.3).

#### *Synthesis of PGMA<sub>61</sub>-PBzMA<sub>100</sub> diblock copolymer spheres*

These diblock copolymer nanoparticles were prepared via RAFT aqueous emulsion polymerisation, as reported by Cunningham et al.<sup>52</sup> PGMA<sub>61</sub>-DB macro-CTA (0.368 g, 36.9 μmol), BzMA monomer (0.65 g, 3.69 mmol; target DP = 100) and ACVA initiator (3.45 mg, 12.3 μmol; macro-CTA/ACVA molar ratio = 3.0) were weighed into a 25 mL round-bottomed flask and dissolved in deionised water (9.19 mL). The resulting solution was purged under N<sub>2</sub> for 30 min before being sealed and immersed in an oil bath at 70 °C for 4 h. The BzMA polymerisation was quenched by exposure to air and a final BzMA conversion of more than 99 % was determined by <sup>1</sup>H NMR analysis. These copolymer spheres were characterised without further purification and used directly for RAFT end-group removal experiments (M<sub>n</sub> = 15,600, M<sub>w</sub>/M<sub>n</sub> = 1.26, see Figure 2.3).

#### *H<sub>2</sub>O<sub>2</sub> protocol for cleavage of RAFT end-groups*

The dithiobenzoate end-groups on PGMA<sub>104</sub>-PHPMA<sub>600</sub> spheres were cleaved as follows: A 10 % w/w copolymer dispersion (3.0 mL) was diluted to 7.5 % w/w by addition of deionised water (1.0 mL). H<sub>2</sub>O<sub>2</sub> (1.48 μL, 14.5 μmol; H<sub>2</sub>O<sub>2</sub>/CTA molar ratio = 5.0) was added to this dispersion as a 30 % w/w aqueous solution. The resulting reaction solution was immersed in an oil bath at 70 °C and left exposed to air. The intrinsic pink colouration disappeared after around 7 h as judged by visual inspection. The trithiocarbonate end-groups on PGMA<sub>52</sub>-

PHPMA<sub>135</sub> worms were cleaved using the same protocol. Visual inspection indicated that the initial yellow colouration almost completely disappeared after 8 h. Preliminary experiments were conducted at pH 6, but subsequent more detailed studies were conducted at pH 3-4, with these lower values arising from the presence of the carboxylic acid-functionalised ACVA initiator and RAFT CTA (PETTC).

### *Characterisation Techniques*

*NMR Spectroscopy.* All <sup>1</sup>H NMR spectra were recorded in either deuterated methanol (for the PGMA macro-CTAs and PGMA-PHPMA diblock copolymers) or deuterated DMF (for the PGMA-PBzMA diblock copolymers) using a 400 MHz Bruker Avance-400 spectrometer (64 scans averaged per spectrum).

*Gel Permeation Chromatography (GPC).* Copolymer molecular weights and polydispersities were determined using an Agilent 1260 Infinity GPC system equipped with both refractive index and UV-visible detectors. Two Agilent PL gel 5 μm Mixed-C columns and a guard column were connected in series and maintained at 60°C. HPLC-grade DMF containing 10 mM LiBr was used as eluent and the flow rate was set at 1.0 mL min<sup>-1</sup>. DMSO was used as a flow-rate marker. The refractive index detector was used for calculation of molecular weights and polydispersities by calibration using a series of ten near-monodisperse poly(methyl methacrylate) standards (with M<sub>n</sub> values ranging from 625 to 618,000 g mol<sup>-1</sup>). UV GPC chromatograms were obtained simultaneously by detection at a fixed wavelength of 309 nm which corresponds to the absorption maximum assigned to the dithiobenzoate or trithiocarbonate RAFT end-groups.

*UV-visible absorption spectroscopy.* Absorption spectra were recorded between 200 and 800 nm using a Shimadzu UV-1800 spectrophotometer. For kinetic studies, 0.10 mL aliquots were diluted ten-fold by addition of methanol (0.90 mL). Measurements were also conducted on purified freeze-dried copolymers after redispersing in water at either 0.25 mg mL<sup>-1</sup> or 5 mg mL<sup>-1</sup> in order to observe absorption maxima at 309 nm and 550 nm, respectively.

*Transmission Electron Microscopy (TEM).* Copolymer dispersions were diluted fifty-fold at 20°C to generate 0.20% w/w dispersions. Copper/palladium TEM grids (Agar Scientific, UK) were coated in-house to produce a thin film of amorphous carbon. These grids were then treated with a plasma glow discharge for 30 seconds to create a hydrophilic surface. Each aqueous diblock copolymer dispersion (12 µL; 0.20% w/w) was placed on a freshly-treated grid for 1 min and then blotted with filter paper to remove excess solution. To stain the deposited nanoparticles, an aqueous solution of uranyl formate (9 µL; 0.75% w/w) was placed on the sample-loaded grid via micropipet for 20 s and then carefully blotted to remove excess stain. Each grid was then carefully dried using a vacuum hose. Imaging was performed using a FEI Tecnai Spirit TEM instrument equipped with a Gatan 1kMS600CW CCD camera operating at 120 kV.

*Oscillatory Rheology experiments* An AR-G2 rheometer equipped with a variable temperature Peltier plate, a 40 ml 2° aluminium cone and a solvent trap was used for all experiments. Temperature sweeps were conducted at an angular frequency of 1.0 rad s<sup>-1</sup> and a constant strain of 1.0 %. The temperature was increased by 1.0 °C between each measurement, allowing an equilibration time of 2 min in each case. A solvent trap was required to prevent evaporation of water over the time scale of these experiments.

## **Results and Discussion**

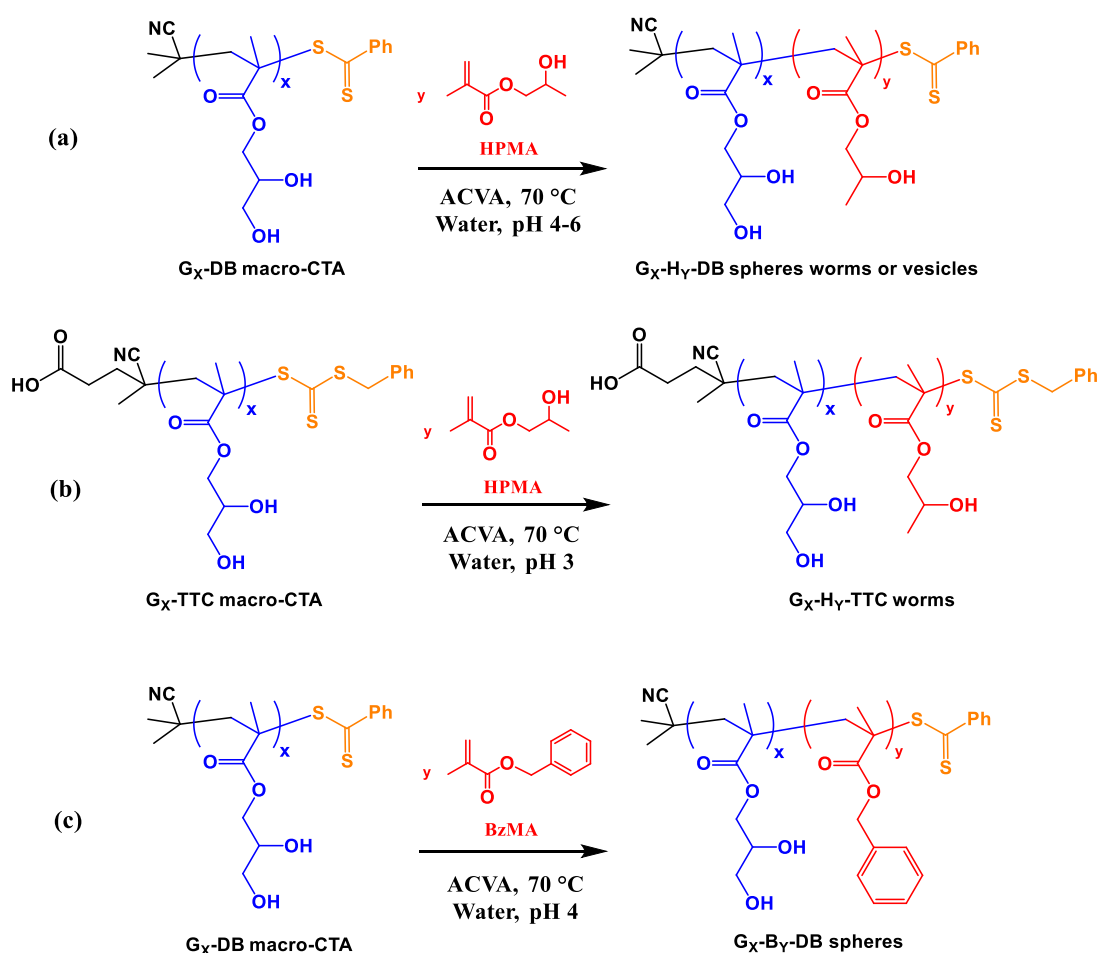
A series of PISA-synthesised diblock copolymer nano-objects were examined in this study. These nano-objects were carefully selected in order to enable various comparisons to be made. In particular we wished to explore: (i) the effect of varying the particle diameter for a series of spherical nanoparticles; (ii) the effect of copolymer morphology (i.e. spheres vs. worms vs. vesicles); (iii) the extent to which the hydrophobic character of the core-forming block retarded ingress of the H<sub>2</sub>O<sub>2</sub> reagent; (iv) whether trithiocarbonate end-groups (TTC) could be removed as readily as dithiobenzoate end-groups (DB) from otherwise identical nano-objects. For the sake of brevity, the three PGMA, PHPMA and PBzMA blocks investigated in this study are abbreviated to G, H and B in all of the Figures and Tables, with the number-average degrees of polymerisation (DP<sub>n</sub>) of each block being indicated in subscript.

Recently, we have designed a range of thermoresponsive PGMA-PHPMA worm gels for various biomedical applications, including highly biocompatible 3D cell culture matrices<sup>32,53</sup>



induction of stasis in human stem cell colonies<sup>31</sup> and the cryopreservation of red blood cells.<sup>54</sup> For such biomaterials, the removal of RAFT end-groups is likely to be important for FDA approval, so in our initial experiments we focused on one such system.

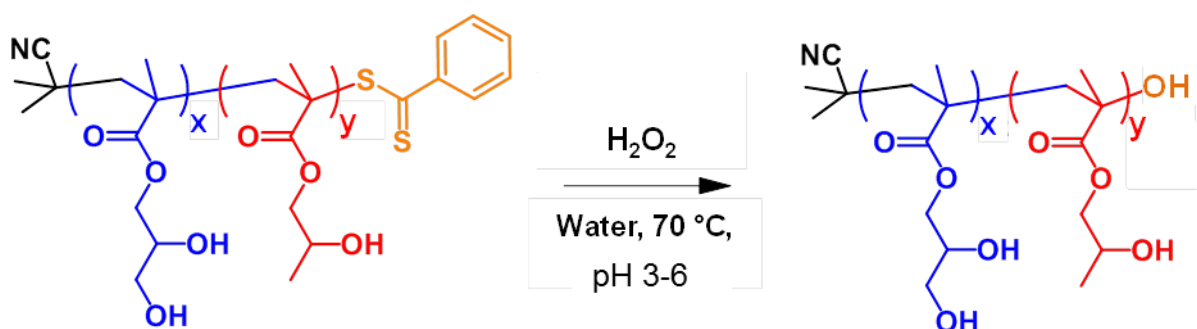
For the preparation of the PGMA-PHPMA-DB worm gel examined in this study, HPMA was polymerised using a well-defined PGMA<sub>52</sub>-DB macro-CTA (see Figure 2.1 for the characterisation of this macro-CTA) to almost full conversion (> 99 %, see Scheme 2.1a), as indicated by the disappearance of the vinyl proton signals at 5.5 and 6.2 ppm. According to <sup>1</sup>H NMR spectroscopy, the mean diblock copolymer composition was calculated to be PGMA<sub>52</sub>-PHPMA<sub>135</sub>. DMF GPC analysis (refractive index detector) indicated that this diblock copolymer had an M<sub>n</sub> of 35,600 g mol<sup>-1</sup> and an M<sub>w</sub>/M<sub>n</sub> of 1.12.



**Scheme 2.1.** Reaction schemes for (a) the synthesis of a G<sub>x</sub>-H<sub>y</sub>-DB diblock copolymer via RAFT aqueous dispersion polymerisation, (b) the synthesis of a G<sub>x</sub>-H<sub>y</sub>-TTC diblock copolymer via RAFT aqueous dispersion polymerisation, (c) the synthesis of a G<sub>x</sub>-B<sub>y</sub>-DB diblock copolymer via RAFT emulsion dispersion polymerisation.

Chapter 2 - H<sub>2</sub>O<sub>2</sub> enables convenient removal of RAFT end-groups from block copolymer nano-objects prepared via polymerisation-induced self-assembly in water

Initial attempts to cleave RAFT end-groups involved treating a 7.5 % w/w PGMA<sub>52</sub>-PHPMA<sub>135</sub>-DB worm gel with various amounts of H<sub>2</sub>O<sub>2</sub> in the presence of air at 70 °C (see Scheme 2.2). In each case, UV-visible absorption spectra were recorded after diluting the aqueous dispersion ten-fold with methanol to produce 9:1 methanol/water solutions. Normalised absorbance vs. time plots (see Figure 2.4) indicated that more than 90 % of dithiobenzoate end-groups could be removed using a H<sub>2</sub>O<sub>2</sub>/dithiobenzoate molar ratio of either 5.0 or 10.0. Lower molar ratios required rather long reaction times, whereas higher molar ratios led to the evolution of a high molecular weight shoulder in the GPC chromatogram (see Figure 2.5) and also produced subtle differences in the copolymer worm rheology (see Figure 2.6). On the basis of these preliminary experiments, a H<sub>2</sub>O<sub>2</sub>/dithiobenzoate molar ratio of 5.0 was selected for more detailed studies.



**Scheme 2.2.** Proposed reaction scheme for the removal of dithiobenzoate end-groups from PGMA<sub>x</sub>-PHPMA<sub>y</sub> diblock copolymer nano-objects using H<sub>2</sub>O<sub>2</sub> in water.

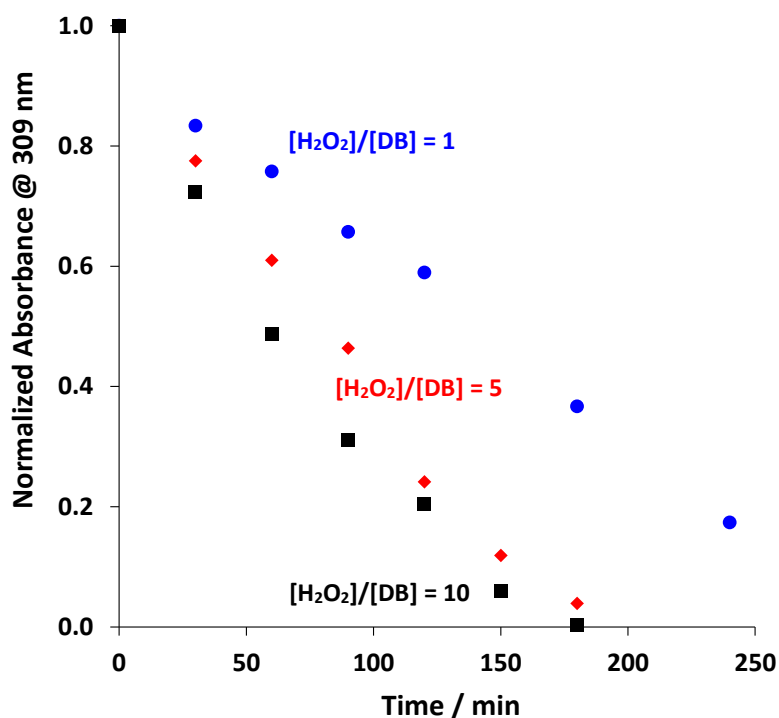


**Figure 2.4.** Normalised absorbance plots obtained using UV spectroscopy for the rate of removal of dithiobenzoate (DB) end-groups from 7.5% w/w aqueous dispersions of poly(glycerol monomethacrylate)-poly(2-hydroxypropyl methacrylate) (G<sub>52</sub>-H<sub>135</sub>-DB) worms. These data sets were obtained by monitoring the progressive attenuation of the UV absorption ( $\lambda_{\text{max}} = 309 \text{ nm}$ ) using the stated H<sub>2</sub>O<sub>2</sub>/DB molar ratios at 70 °C and pH 4-6.

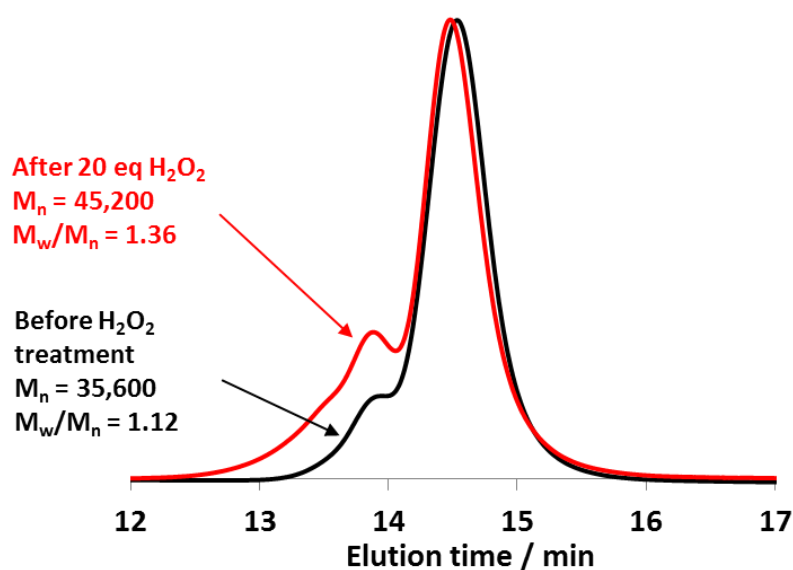


**Figure 2.5.** DMF GPC traces recorded for G<sub>52</sub>-H<sub>135</sub>-DB before (black) and after (red) H<sub>2</sub>O<sub>2</sub> treatment. Conditions: H<sub>2</sub>O<sub>2</sub>/dithiobenzoate molar ratio = 20 for 3 h at 70 °C.

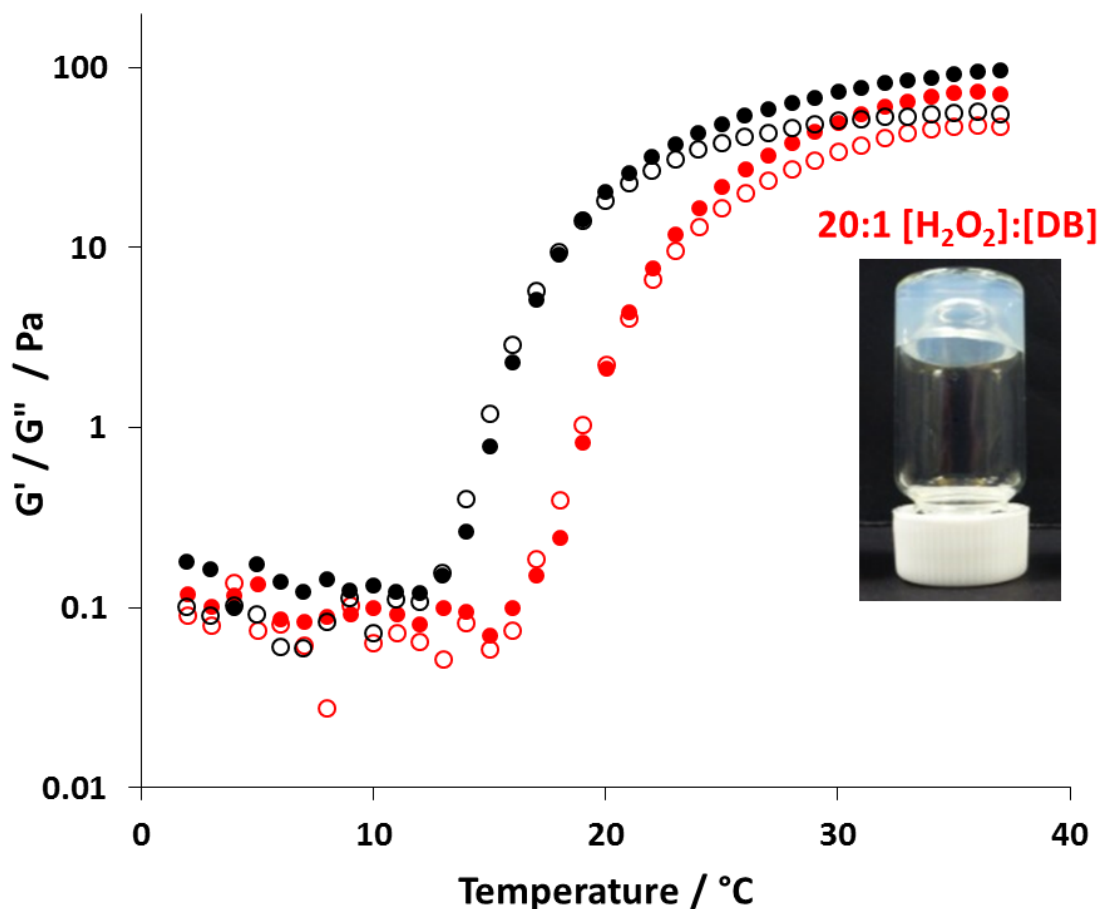


**Figure 2.6.** Gel storage modulus ( $G'$ , closed symbols) and loss modulus ( $G''$ , open symbols) vs. temperature plots obtained for a  $G_{52}$ - $H_{135}$ -DB worm gel before (black) and after (red) treatment with  $\text{H}_2\text{O}_2$ . Conditions: [ $\text{H}_2\text{O}_2$ ]/[DB] = 20 for 3 h at 70  $^{\circ}\text{C}$ . Note that a weaker worm gel is obtained after  $\text{H}_2\text{O}_2$  treatment ( $G' = 71$  Pa, vs.  $G' = 96$  Pa originally) and the critical gelation temperature (CGT) is raised from 19  $^{\circ}\text{C}$  to 21  $^{\circ}\text{C}$ .

End-group removal from a 7.5 % w/w aqueous dispersion of  $\text{PGMA}_{52}$ - $\text{PHPMA}_{135}$ -DB worms using a  $\text{H}_2\text{O}_2$ /dithiobenzoate molar ratio of 5.0 was repeated on a gram scale to enable full characterisation. Visual inspection indicated almost complete removal of the initial pink colouration, producing a white dispersion after 2 h at 70  $^{\circ}\text{C}$ . After purification by dialysis,  $^1\text{H}$  NMR studies indicated disappearance of the aromatic signals at 7.5 – 8.0 ppm assigned to the dithiobenzoate group (see Figure 2.4a), suggesting successful end-group removal. Comparison of the remaining integrated copolymer signals suggests little effect on the overall copolymer composition. DMF GPC chromatograms obtained for  $\text{PGMA}_{52}$ - $\text{PHPMA}_{135}$  before and after

H<sub>2</sub>O<sub>2</sub> treatment are similar, although a high molecular weight shoulder becomes slightly more prominent (see Figure 2.7b). However, there are only minimal change in  $M_n$  (from 35,600 g mol<sup>-1</sup> to 35,700 g mol<sup>-1</sup>) and  $M_w/M_n$  (from 1.12 to 1.16), suggesting little change in the molecular weight distribution of this copolymer.

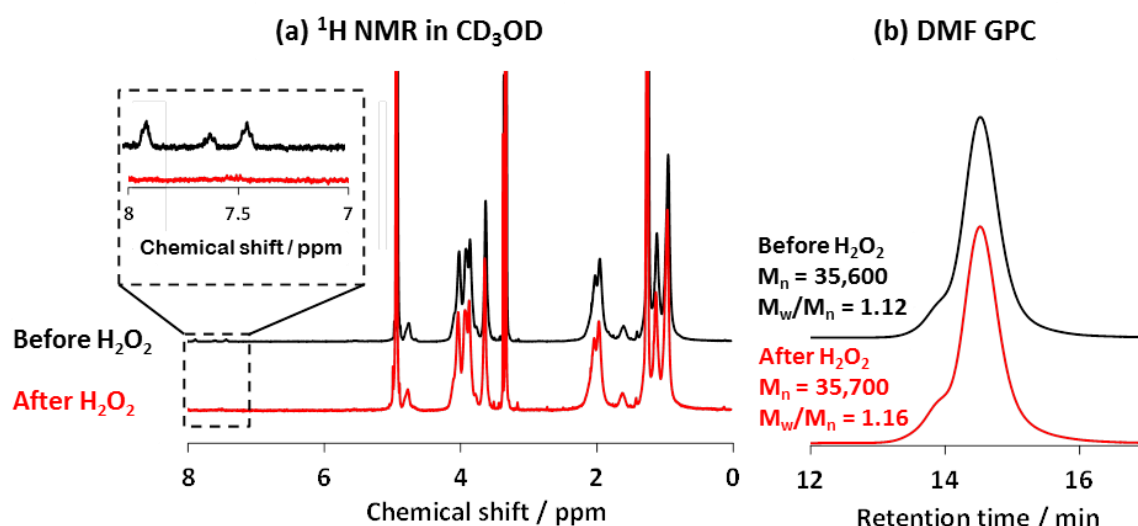


**Figure 2.7.** (a) <sup>1</sup>H NMR spectra recorded before and after removal of the dithiobenzoate (DB) end-group from a 7.5 % w/w G<sub>52</sub>-H<sub>135</sub> diblock copolymer aqueous dispersion by exposure to H<sub>2</sub>O<sub>2</sub> for 160 min in water (pH 4-6, 70 °C) using a [H<sub>2</sub>O<sub>2</sub>]/[DB] molar ratio of 5.0; a refractive index detector was used to obtain molecular weight data (vs. poly(methyl methacrylate) standards).

A white powder was produced on freeze-drying the purified copolymer, which was dissolved in methanol and analysed by UV-visible spectroscopy in order to assess the extent of end-group removal (see Figure 2.8a). Methanol is a good solvent for both PGMA and PHPMA blocks, therefore this protocol leads to molecular dissolution of the copolymer chains and hence minimises light scattering effects on the spectra. Dithiobenzoate end-groups exhibit a characteristic absorbance at 309 nm, which is clearly visible in the original PGMA<sub>52</sub>-PHPMA<sub>135</sub> copolymer spectrum. However, H<sub>2</sub>O<sub>2</sub> treatment of the aqueous copolymer dispersion (H<sub>2</sub>O<sub>2</sub>/dithiobenzoate molar ratio = 5.0; 70 °C for 160 min) leads to almost complete disappearance of this 309 nm peak. However, a relatively weak new absorption appears at approximately 270 nm, which prevents the absorbance at 309 nm falling to zero. The origin of this new spectral feature is currently unclear and probably warrants further studies. Similar observations are made in the corresponding visible region of the same spectrum (Figure 2.8b): the much weaker absorption located at around 509 nm almost completely disappears. This is

consistent with the digital images shown in Figure 2.8c, which confirm the complete removal of the pink colouration from the freeze-dried copolymer powder. Moreover, a tube inversion test indicated that thermo-reversible degelation can still be induced on cooling a reconstituted H<sub>2</sub>O<sub>2</sub>-treated copolymer worm gel from 37 °C to 4 °C. These observations were confirmed using variable temperature oscillatory rheology studies (Figure 2.9). Moreover, such gel rheology data are almost identical to the data set obtained for the original worm gel prior to H<sub>2</sub>O<sub>2</sub> treatment. In particular, there is almost no change in the gel modulus, G', at 37 °C or in the critical gelation temperature (CGT) for this worm gel.

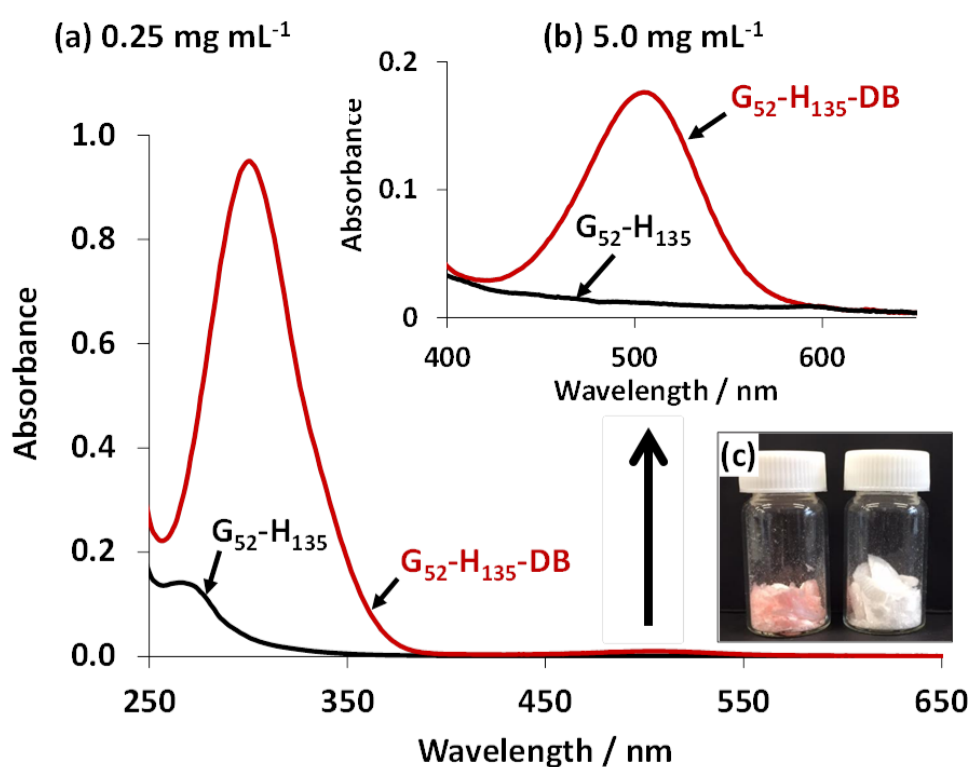


**Figure 2.8.** (a) UV-visible absorption spectra recorded for 0.25 mg mL<sup>-1</sup> G<sub>52</sub>-H<sub>135</sub> diblock copolymer solutions in methanol before and after dithiobenzoate end-group removal ([H<sub>2</sub>O<sub>2</sub>]/[DB] = 5.0, 70 °C, 160 min). (b) Visible absorption spectra obtained for the same copolymers at 5.0 mg mL<sup>-1</sup> in methanol indicating the disappearance of the relatively weak absorption band at approximately 500 nm (which corresponds to the intrinsic pink colour conferred by the RAFT chain-end). (c) Digital image showing the freeze-dried G<sub>52</sub>-H<sub>135</sub> copolymer before and after dithiobenzoate end- group removal.

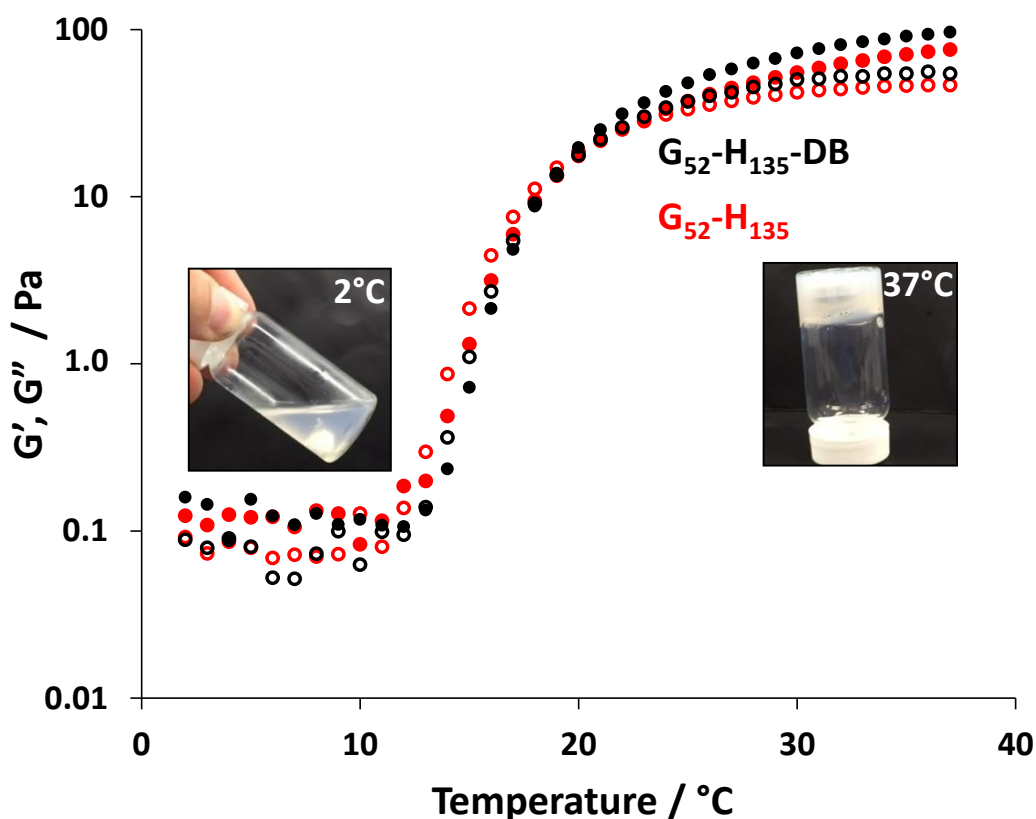


**Figure 2.9.** Temperature-dependent oscillatory rheology studies on a 10 % w/w  $G_{52}$ - $H_{135}$  worm gel before ( $G_{52}$ - $H_{135}$ -DB) and after ( $G_{52}$ - $H_{135}$ ) treatment with H<sub>2</sub>O<sub>2</sub> to remove the dithiobenzoate chain-ends. The freeze-dried powder was redispersed in cold 150 mM PBS at 2 °C. Inset digital images show a 10 % w/w dispersion of the reconstituted  $G_{52}$ - $H_{135}$  copolymer after end-group removal as a free flowing liquid at 2 °C and a free-standing gel at 37 °C.

The kinetics of dithiobenzoate end-group removal at 70 °C from H<sub>2</sub>O<sub>2</sub>-treated PGMA<sub>104</sub>-PHPMA<sub>300</sub>-DB spheres was conducted by extracting a series of aliquots from the 7.5 % w/w copolymer dispersion after various time periods and subsequently diluting ten-fold with methanol (to produce a 9:1 methanol/water solution) prior to analysis by UV-visible spectroscopy at 20 °C. As expected, gradual attenuation in the 309 nm absorption band was initially observed (see Figure 2.10a). However, apparently no further reduction occurred after approximately 6 h. Inspecting the evolution in UV spectra more closely, this artefact appears to be the result of an additional spectral feature at 270 nm, which is associated with the formation of unknown low molecular weight degradation products. In order to circumvent this problem, further end-group removal studies were conducted using UV GPC analysis. By

setting the UV detector to a fixed wavelength of 309 nm, it was possible to monitor the extent of end-group removal for copolymer chains bearing either a dithiobenzoate or a trithiocarbonate end-group. The decisive advantage of this approach is that fractionation of the copolymer chains from the small molecule impurities occurs in the GPC column prior to analysis. Thus there is no longer any interference from the small molecule impurities absorbing at shorter wavelengths, which aids quantification. For this particular data set, an overall 96 % reduction in the original UV signal was observed within 8 h (see Figure 2.10b). At this point, we examined whether full end-group removal could be achieved given a sufficiently long reaction time. Thus the H<sub>2</sub>O<sub>2</sub> treatment was extended from 8 h to 24 h at 70 °C, which led to an overall reduction in the original UV GPC signal of 98 % (see Figure 2.11).

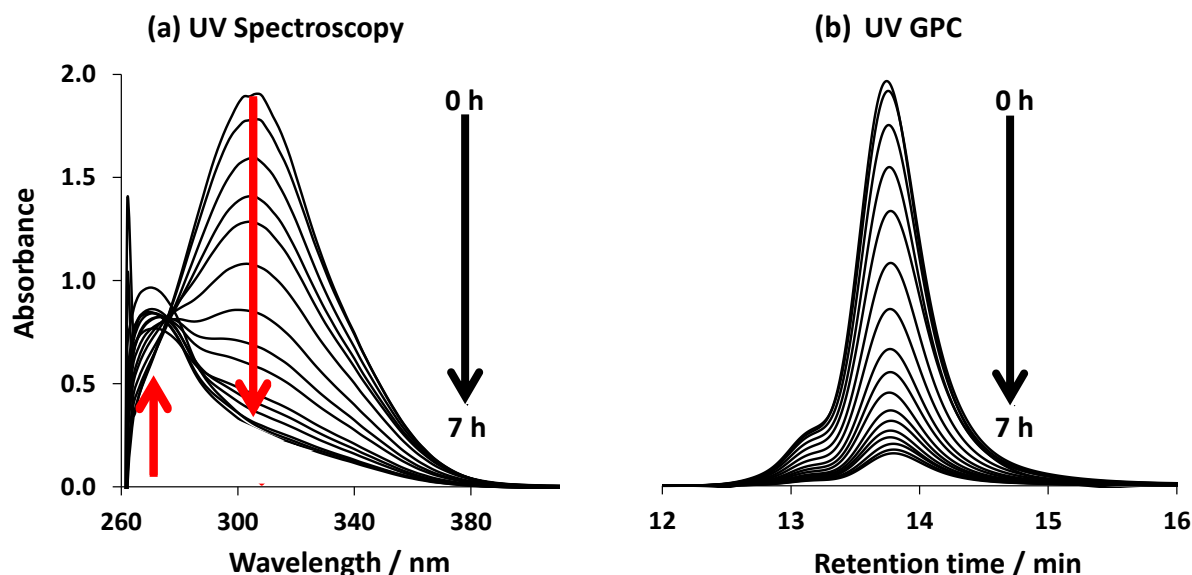


**Figure 2.10.** (a) UV spectra and (b) UV GPC chromatograms (recorded at a  $\lambda_{\text{max}}$  of 309 nm) obtained during kinetic studies of the removal of dithiobenzoate end-groups from a 7.5 % w/w G<sub>104</sub>-H<sub>300</sub> aqueous dispersion using a H<sub>2</sub>O<sub>2</sub>/dithiobenzoate molar ratio of 5.0 at 70 °C in water (pH 3-4). All GPC samples were diluted to 7.5 mg mL<sup>-1</sup> prior to analysis.



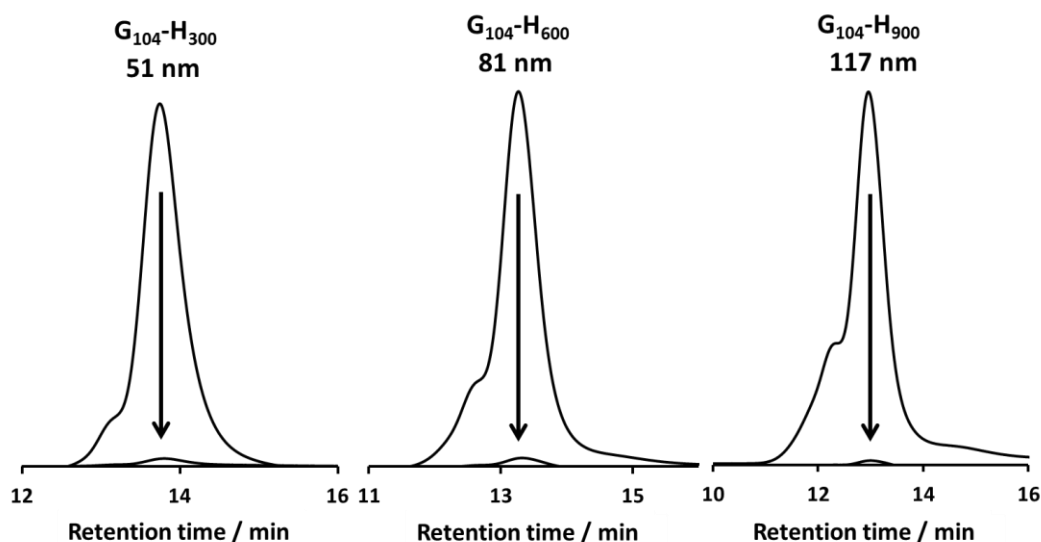


**Figure 2.11.** DMF GPC chromatograms (UV detector) of G<sub>104</sub>-H<sub>X</sub>-DB spheres before end-group removal and after H<sub>2</sub>O<sub>2</sub> treatment for 24 h (see arrows) using a H<sub>2</sub>O<sub>2</sub>/dithiobenzoate molar ratio of 5.0 at 70 °C. In each case at least 98 % of the original end-groups are removed.

Applying this optimised analytical protocol to the PGMA<sub>52</sub>-PHPMA<sub>135</sub>-DB worms (see Figure 2.9) indicated a 95 % reduction in RAFT end-group concentration within 2.5 h at 70 °C. Moreover, the rate of end-group removal achieved for this aqueous dispersion of copolymer worms was comparable to that achieved for a *water-soluble* dithiobenzoate PGMA<sub>52</sub>-DB homopolymer precursor under the same conditions (i.e. same molar concentration of dithiobenzoate groups) (see Figure 2.12). This indicates that the H<sub>2</sub>O<sub>2</sub> reagent can readily access the dithiobenzoate end-groups within the weakly hydrophobic PHPMA cores, which is consistent with the partially hydrated nature of these core-forming chains.<sup>53</sup> Essentially the same PGMA<sub>52</sub>-PHPMA<sub>135</sub>-TTC diblock copolymer worms ( $M_n = 37,400 \text{ gmol}^{-1}$ ,  $M_w/M_n = 1.15$ ) were also prepared at 10% w/w solids using PETTC (see Scheme 2.1b), which is a well-known trithiocarbonate-based RAFT agent.<sup>55</sup> On dilution, the resulting 7.5% w/w copolymer worm dispersion was also treated with H<sub>2</sub>O<sub>2</sub> under identical conditions as those utilised for the dithiobenzoate-functionalised copolymer worms. However, the kinetic data obtained by monitoring the UV GPC signal at 309 nm suggest that trithiocarbonate cleavage proceeded significantly more slowly than dithiobenzoate cleavage, with only around 89% end-group removal being achieved within 7 h at 70 °C (see Figure 2.12). This was not unexpected given that trithiocarbonates are known to exhibit greater hydrolytic stability compared to dithiobenzoates.<sup>35</sup> The effect of varying the nature of the core-forming chains on the extent of

end-group removal was also investigated by replacing the PHPMA block with the more hydrophobic PBzMA block. More specifically, a dithiobenzoate-based PGMA<sub>61</sub>-DB macro-CTA (see Figure 2.1 for characterisation of this macro-CTA) was used to prepare PGMA<sub>61</sub>-PBzMA<sub>100</sub>-DB spheres via RAFT aqueous emulsion polymerisation (see Scheme 2.1c) according to a protocol recently reported by Cunningham et al.<sup>52</sup> This diblock composition was selected so that the mean diameter of these spheres was approximately 25 nm, which is comparable to the mean width of the dithiobenzoate-based PGMA<sub>52</sub>-PHPMA<sub>135</sub> worms (as estimated by TEM studies). On treating these PGMA<sub>61</sub>-PBzMA<sub>100</sub>-DB spheres with H<sub>2</sub>O<sub>2</sub> the rate of end-group removal was found to be very slow, with 57 % of end-groups remaining after 8 h as judged by UV GPC (see Figure 2.12). This suggests that, despite its non-ionic nature and relatively low molecular weight, diffusion of the H<sub>2</sub>O<sub>2</sub> reagent into the PBzMA cores is severely retarded compared to PHPMA cores.

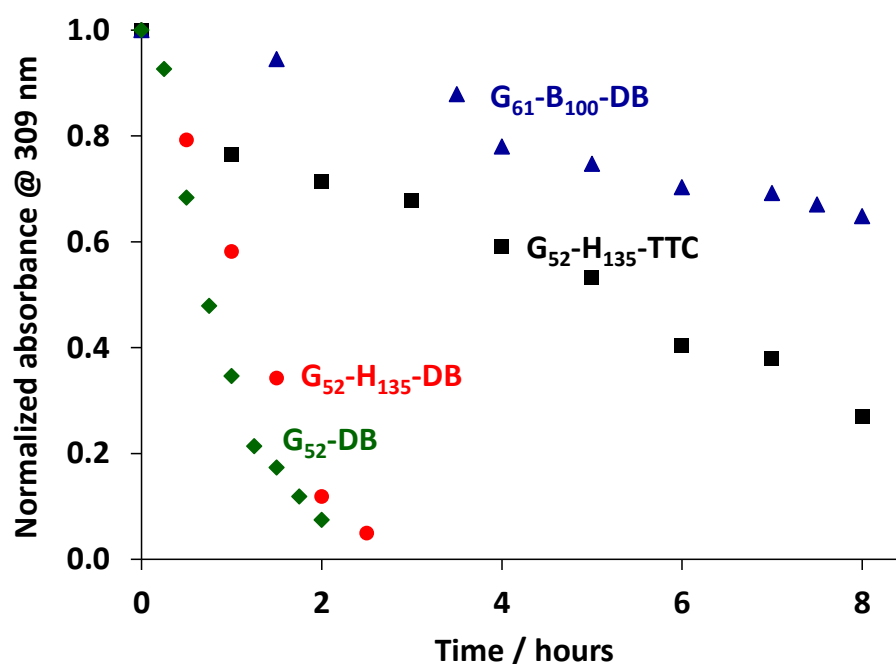


**Figure 2.12.** Kinetic plots for the rate of removal of dithiobenzoate or trithiocarbonate end-groups using a [H<sub>2</sub>O<sub>2</sub>]:[end-group] molar ratio of 5.0 at 70 °C and pH 3-4. (a) 7.5 % w/w dithiobenzoate-terminated poly(glycerol monomethacrylate)-poly(benzyl methacrylate) (G<sub>61</sub>-B<sub>100</sub>) spheres of 24 nm diameter; (b) 7.5 % w/w trithiocarbonate-terminated poly(glycerol monomethacrylate)-poly(2-hydroxypropyl methacrylate) worms (G<sub>52</sub>-H<sub>135</sub>-TTC); (c) 7.5 % w/w dithiobenzoate-terminated poly(glycerol monomethacrylate)-poly(2-hydroxypropyl methacrylate) worms (G<sub>52</sub>-H<sub>135</sub>-DB); (d) 2.3 % w/w (equimolar to G<sub>52</sub>-H<sub>135</sub>-DB) dithiobenzoate-terminated molecularly-dissolved poly(glycerol monomethacrylate) chains (G<sub>52</sub>-DB).

In a related series of experiments, three examples of PGMA<sub>104</sub>-PHPMA<sub>x</sub>-DB spheres (where x = 300, 600 or 900, which correspond to mean DLS hydrodynamic diameters of 54 nm, 81 nm and 117 nm respectively) were also subjected to H<sub>2</sub>O<sub>2</sub> treatment followed by UV GPC analysis (see Figure 2.13). The purpose of these experiments was to examine whether particle size had any effect on the rate of end-group removal. Normally, slower H<sub>2</sub>O<sub>2</sub> ingress might be expected for larger particles, but if the PHPMA cores are relatively hydrated then in principle there might be no physical barrier to the diffusion of this reagent.

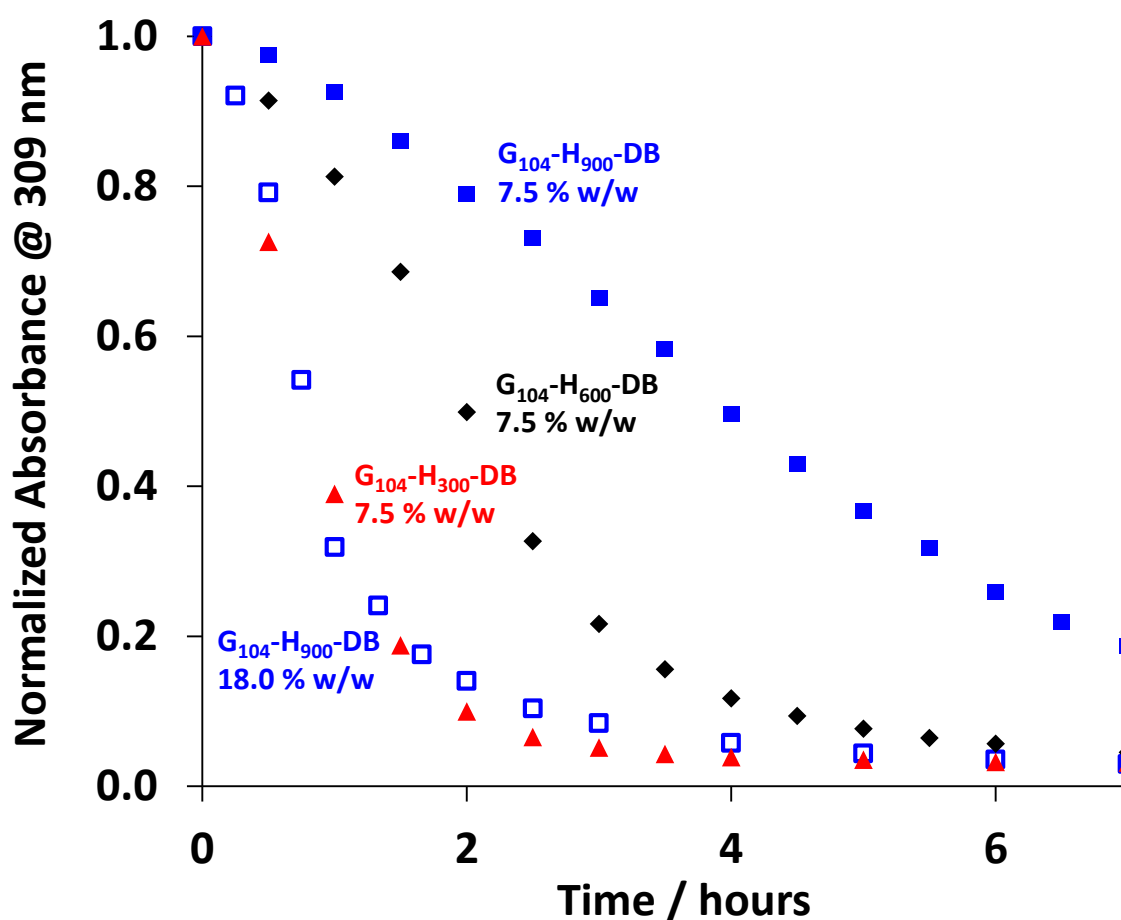


**Figure 2.13.** Kinetic plots for the rate of removal of dithiobenzoate end-groups from poly(glycerol monomethacrylate)-poly(2-hydroxypropyl methacrylate) (G<sub>104</sub>-H<sub>y</sub>) aqueous dispersions as judged by UV GPC analysis ( $\lambda_{\text{max}} = 309$  nm) using a [H<sub>2</sub>O<sub>2</sub>]:[end-group] molar ratio of 5.0 at 70 °C and pH 3-4. (a) 7.5 % w/w G<sub>104</sub>-H<sub>300</sub> spheres of 51 nm diameter; (b) 7.5 % w/w G<sub>104</sub>-H<sub>600</sub> spheres of 81 nm diameter; (c) 7.5 % w/w G<sub>104</sub>-H<sub>900</sub> spheres of 117 nm diameter; (d) 18.0 % w/w G<sub>104</sub>-H<sub>900</sub> spheres of 117 nm diameter.

H<sub>2</sub>O<sub>2</sub> treatment (using a H<sub>2</sub>O<sub>2</sub>/dithiobenzoate molar ratio = 5.0 at 70 °C) of these PGMA<sub>104</sub>-PHPMA<sub>300-900</sub>-DB spheres at a fixed 7.5% w/w copolymer concentration led to a significant reduction in the rate of end-group removal with increasing PHPMA DP (see Figure 2.13). At first sight, this suggests a slower rate of H<sub>2</sub>O<sub>2</sub> ingress into the larger spheres. However, targeting a higher DP at the same fixed copolymer concentration inevitably means a lower concentration of dithiobenzoate end-groups. Comparing the rate of end-group cleavage for PGMA<sub>104</sub>-PHPMA<sub>300</sub> spheres at 7.5% w/w with that for PGMA<sub>104</sub>-PHPMA<sub>900</sub> spheres at 18.0% w/w (i.e., at the same *molar* concentration of dithiobenzoate end-groups) indicates essentially no difference in kinetics (see Figure 2.13). This confirms that the partially hydrated PHPMA cores of this series of spheres present no diffusional barrier to H<sub>2</sub>O<sub>2</sub> ingress, at least for the particle size range investigated herein.

Finally, 10% w/w aqueous dispersions of PGMA<sub>104</sub>-PHPMA<sub>600</sub>-DB spheres, PGMA<sub>52</sub>-PHPMA<sub>135</sub>-DB worms and PGMA<sub>58</sub>-PHPMA<sub>400</sub>-DB vesicles were each subjected to H<sub>2</sub>O<sub>2</sub> treatment (H<sub>2</sub>O<sub>2</sub>/dithiobenzoate molar ratio = 5.0; 70 °C for 3 h). In each case a high degree of decolourisation was observed, indicating almost complete cleavage of the dithiobenzoate end-groups (see digital images shown in Figure 2.14). Moreover, it is perhaps worth emphasising that, if any loss of RAFT end-groups did occur during such PISA syntheses, then the relatively low levels (2-5% in most cases) of residual RAFT end-groups determined by UV GPC analysis actually represent *upper limit* values. TEM studies confirmed that this derivatisation protocol produced no discernible effect on the copolymer morphology, with comparable images being obtained before and after H<sub>2</sub>O<sub>2</sub> treatment in each case (Figure 2.14).

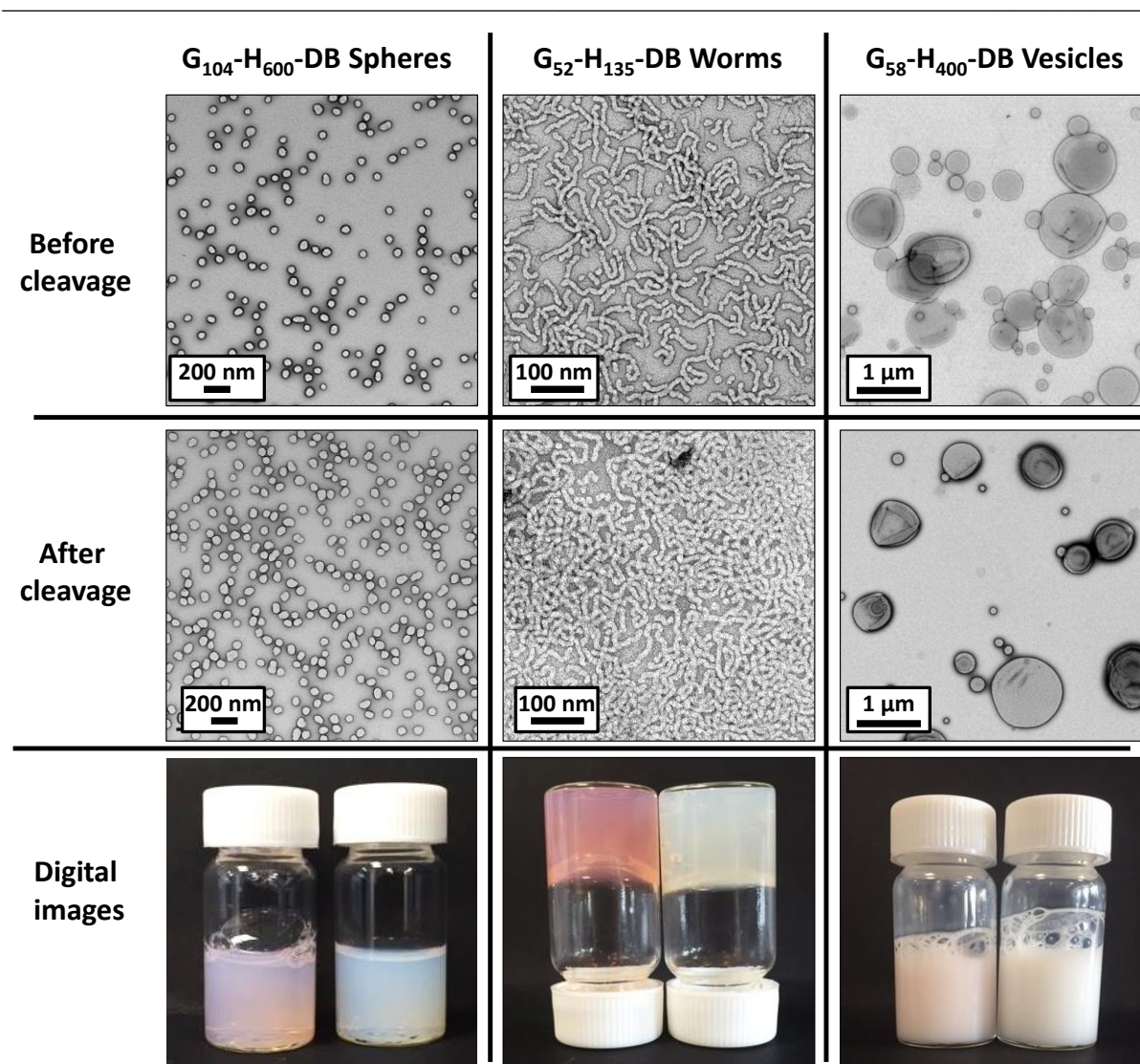


**Figure 2.14.** TEM and digital images recorded for 10 % w/w aqueous copolymer dispersions of G<sub>104</sub>-H<sub>600</sub> spheres, G<sub>52</sub>-H<sub>135</sub> worms and G<sub>58</sub>-H<sub>400</sub> vesicles before and after treatment using H<sub>2</sub>O<sub>2</sub> at a [H<sub>2</sub>O<sub>2</sub>]/[DB] molar ratio of 5.0 for 3 h at 70 °C and pH 3-4.

Moreover, DMF GPC analysis (using a refractive index detector) indicated only minimal changes (often within experimental error) in the  $M_n$  values obtained for each of the seven H<sub>2</sub>O<sub>2</sub>-treated diblock copolymers examined in this study and also a PGMA<sub>52</sub>-DB macro-CTA control (see Table 2.1 and also Figure 2.15). The  $M_w/M_n$  values are typically slightly higher after derivatisation, but overall the extent of chemical degradation appears to be very modest. Longer reaction times of up to 7 h also led to no discernible change in the GPC chromatograms recorded for PGMA<sub>104</sub>-PHPMA<sub>300-900</sub>-DB spheres (see Figure 2.16).

**Table 2.1.** Summary of molecular weight data obtained using DMF GPC (refractive index detector; vs. poly(methyl methacrylate) calibration standards) before and after H<sub>2</sub>O<sub>2</sub> treatment for the series of diblock copolymer nano-objects used in this study.

Copolymer composition	Copolymer morphology	M <sub>n</sub> / g mol <sup>-1</sup>		M <sub>w</sub> /M <sub>n</sub>	
		Before	After	Before	After
G <sub>52</sub> -DB	Dissolved chains	15,700	15,500	1.18	1.19
G <sub>52</sub> -H <sub>135</sub> -DB	Worms	35,600	35,700	1.12	1.16
G <sub>52</sub> -H <sub>135</sub> -TTC	Worms	37,400	34,900	1.15	1.20
G <sub>61</sub> -B <sub>100</sub> -DB	Spheres	15,600	16,800	1.26	1.29
G <sub>104</sub> -H <sub>300</sub> -DB	Spheres	58,600	56,600	1.19	1.24
G <sub>104</sub> -H <sub>600</sub> -DB	Spheres	79,100	74,300	1.24	1.28
G <sub>104</sub> -H <sub>900</sub> -DB	Spheres	136,100	129,500	1.46	1.46
G <sub>52</sub> -H <sub>400</sub> -DB	Vesicles	101,700	106,300	1.32	1.40

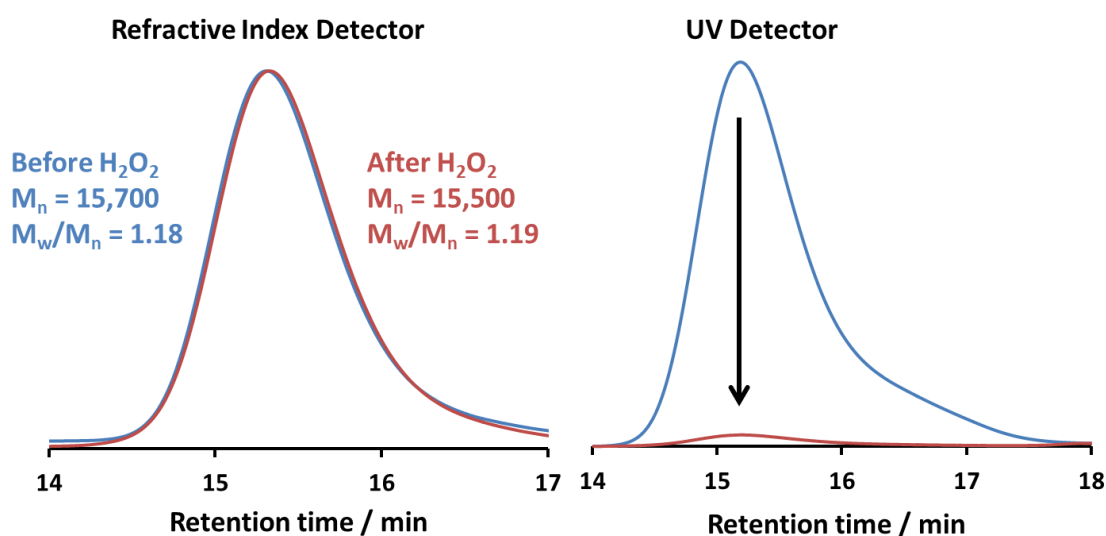


**Figure 2.15.** GPC chromatograms recorded for the G<sub>52</sub>-DB macro-CTA before (blue traces) and after (red traces) end-group removal via H<sub>2</sub>O<sub>2</sub> treatment using a H<sub>2</sub>O<sub>2</sub>/dithiobenzoate molar ratio of 5.0 at 70 °C: (a) minimal change in the molecular weight distribution as judged using a refractive index detector and (b) 97 % disappearance in the 309 nm signal associated with the RAFT end-group using the UV detector.

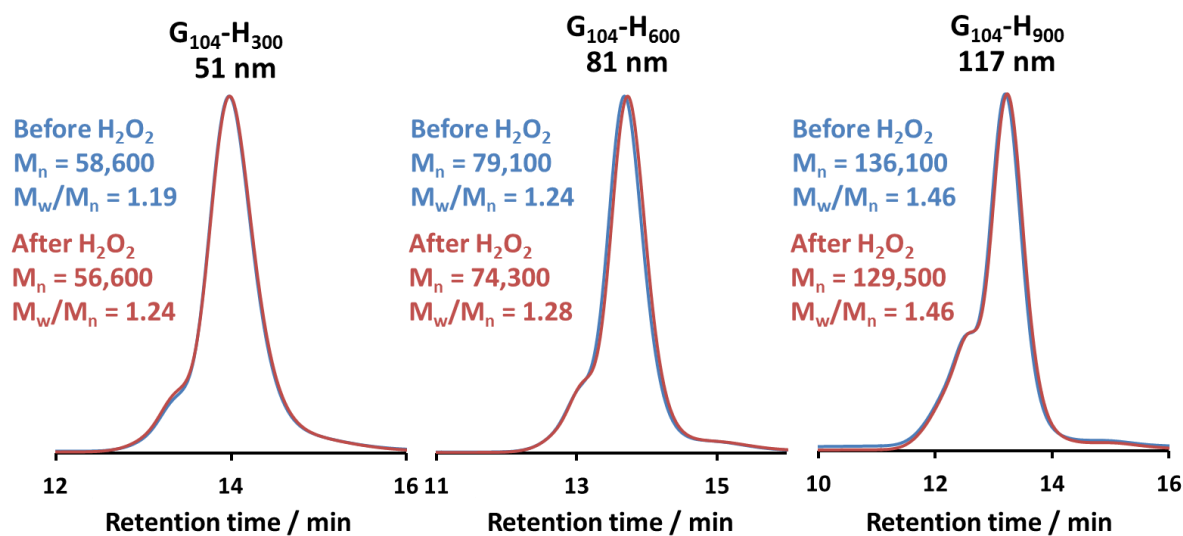


**Figure 2.16.** DMF GPC chromatograms (refractive index detector) of G<sub>104</sub>-H<sub>X</sub>-DB spheres before end-group removal and after H<sub>2</sub>O<sub>2</sub> treatment for 7 h using a H<sub>2</sub>O<sub>2</sub>/dithiobenzoate molar ratio of 5.0 at 70 °C. Note that there is minimal change in the molecular weight distributions under these optimised end-group removal conditions.

Although a hydroxyl radical mechanism was proposed by Pfukwa et al.<sup>48</sup>, the following observations indicate that an *oxidation* mechanism may be more likely, at least under the end-group cleavage conditions described herein. Two identical batches of the same dithiobenzoate-functionalised PGMA<sub>52</sub>-PHPMA<sub>135</sub> copolymer were subjected to end-group removal using H<sub>2</sub>O<sub>2</sub> (H<sub>2</sub>O<sub>2</sub>/dithiobenzoate molar ratio = 5.0; 7.5 % w/w copolymer dispersion; 70 °C). One batch was degassed for 30 min using N<sub>2</sub> prior to end-group removal, with UV-visible spectroscopy studies indicating that dithiobenzoate cleavage was complete within about 240 min. In contrast, the second batch was not degassed and remained exposed to air during the H<sub>2</sub>O<sub>2</sub> reaction. In this case, dithiobenzoate cleavage was complete within 150 min (see Figure 2.17). This rate acceleration in the presence of oxygen is consistent with an oxidative mechanism. Moreover, oxygen is a well-known retarder of radical-based reactions (e.g. free radical polymerisations or RAFT polymerisations). In summary, we suggest that H<sub>2</sub>O<sub>2</sub>-mediated end-group removal may proceed via an oxidative mechanism, rather than a radical mechanism. Further studies are required to establish the precise nature of the end-groups that are formed after H<sub>2</sub>O<sub>2</sub> treatment, although Pfukwa et al.<sup>48</sup> present some indirect evidence that terminal hydroxyl groups may be formed, at least in the case of poly(*N*-vinylpyrrolidone) prepared using a xanthate-based RAFT agent.

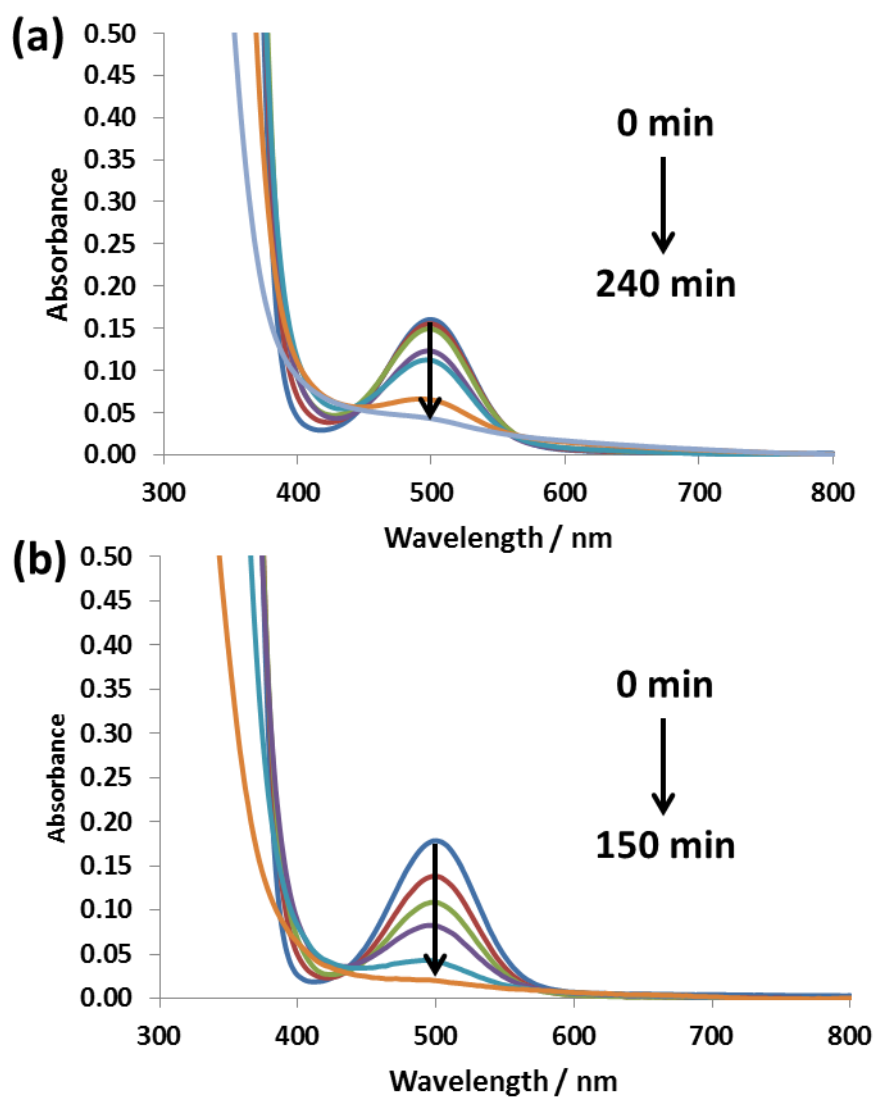


**Figure 2.17.** UV-Visible spectra showing the kinetics of RAFT end-group removal at 70 °C for (a) a G<sub>52</sub>H<sub>135</sub> worm gel after degassing for 30 min under N<sub>2</sub> prior to treatment with H<sub>2</sub>O<sub>2</sub> and (b) a G<sub>52</sub>H<sub>135</sub> worm gel that was exposed to air during H<sub>2</sub>O<sub>2</sub> treatment. Conditions: 7.5% w/w copolymer, [H<sub>2</sub>O<sub>2</sub>]/[DB] molar ratio = 5.0. Note that spectra were recorded at 30 min intervals in each case.



### Conclusions

H<sub>2</sub>O<sub>2</sub> can be utilised as a relatively cheap reagent for the convenient and efficient removal of dithiobenzoate end-groups from PGMA<sub>x</sub>-PHPMA<sub>y</sub> diblock copolymer nano-objects in concentrated aqueous solution. The original spherical, worm-like or vesicular copolymer morphologies are retained after this chemical derivatisation and UV GPC analysis indicates that approximately 96 % of dithiobenzoate end-groups can be removed within 8 h at 70 °C when using a H<sub>2</sub>O<sub>2</sub>/dithiobenzoate molar ratio of 5.0. Moreover, H<sub>2</sub>O<sub>2</sub> treatment of a series of PGMA<sub>104</sub>-PHPMA<sub>x</sub>-DB spheres indicates that the rate of end-group removal was both independent of particle size and comparable to that observed for a water-soluble PGMA<sub>52</sub>-DB homopolymer under the same conditions. This suggests that the highly hydrated nature of the weakly hydrophobic PHPMA core-forming chains does not inhibit H<sub>2</sub>O<sub>2</sub> diffusion.

Oscillatory rheology studies confirm that removal of dithiobenzoate end-groups does not adversely affect the thermoresponsive gelation behavior exhibited by PGMA<sub>52</sub>-PHPMA<sub>135</sub> worms in aqueous solution. However, end-group removal is much less effective for dithiobenzoate-functionalised PGMA<sub>61</sub>-PBzMA<sub>100</sub> spheres, with less than 40 % of these RAFT chain-ends being cleaved within 8 h at 70 °C using the same H<sub>2</sub>O<sub>2</sub>/dithiobenzoate molar ratio. This marked difference simply reflects the retarded diffusion of the H<sub>2</sub>O<sub>2</sub> reagent into the relatively dehydrated hydrophobic PBzMA cores. It is also clear from this study that trithiocarbonate end-groups are significantly more resistant to H<sub>2</sub>O<sub>2</sub> cleavage than dithiobenzoate end-groups under the same conditions. Finally, it is emphasised that UV GPC analysis in DMF is much more useful than UV-visible spectroscopy analysis of aqueous dispersions for monitoring the rate of RAFT end-group removal. This is because the former technique separates the copolymer chains from small molecule impurities prior to analysis, which eliminates spectral interference from the latter species.

## References

1. Chiefari, J.; Chong, Y. K.; Ercole, F.; Krstina, J.; Jeffery, J.; Le, T. P. T.; Mayadunne, R. T. A.; Meijs, G. F.; Moad, C. L.; Moad, G.; Rizzardo, E.; Thang, S. H. Living free-radical polymerisation by reversible addition-fragmentation chain transfer: The RAFT process. *Macromolecules* **1998**, *31*, 5559.
2. Moad, G.; Rizzardo, E.; Thang, S. H. Living Radical Polymerisation by the RAFT Process. *Australian Journal of Chemistry*, **2005**, *58*, 379.
3. Moad, G.; Rizzardo, E.; Thang, S. H. Living Radical Polymerisation by the RAFT Process - A Second Update. *Australian Journal of Chemistry*, **2009**, *62*, 1402.
4. Moad, G.; Rizzardo, E.; Thang, S. H. Living Radical Polymerisation by the RAFT Process - A Third Update. *Australian Journal of Chemistry*, **2012**, *65*, 985.
5. Fairbanks, B. D.; Gunatillake, P. A.; Meagher, L. Biomedical applications of polymers derived by reversible addition - fragmentation chain-transfer (RAFT). *Advanced Drug Delivery Reviews* **2015**, *91*, 141.
6. Price, D.; Mosier, P. E.; Vilardo, J. S.; Baum, M.; US Patent US8507422B2: 2013.
7. Loiseau, J.; Doerr, N.; Suau, J. M.; Egraz, J. B.; Llauro, M. F.; Ladaviere, C. Synthesis and characterisation of poly(acrylic acid) produced by RAFT polymerisation. Application as a very efficient dispersant of CaCO<sub>3</sub>, kaolin, and TiO<sub>2</sub>. *Macromolecules* **2003**, *36*, 3066.
8. Moad, G.; Chen, M.; Haussler, M.; Postma, A.; Rizzardo, E.; Thang, S. H. Functional polymers for optoelectronic applications by RAFT polymerisation. *Polymer Chemistry* **2011**, *2*, 492.
9. Boyer, C.; Bulmus, V.; Davis, T. P.; Ladmiral, V.; Liu, J. Q.; Perrier, S. Bioapplications of RAFT Polymerisation. *Chemical Reviews* **2009**, *109*, 5402.
10. Boyer, C.; Stenzel, M. H.; Davis, T. P. Building Nanostructures Using RAFT Polymerisation. *Journal of Polymer Science Part a-Polymer Chemistry* **2011**, *49*, 551.
11. Perrier, S.; Takolpuckdee, P. Macromolecular design via reversible addition-fragmentation chain transfer (RAFT)/Xanthates (MADIX) polymerisation. *Journal of Polymer Science Part a-Polymer Chemistry* **2005**, *43*, 5347.
12. Tan, J.; Sun, H.; Yu, M.; Sumerlin, B. S.; Zhang, L. Photo-PISA: Shedding Light on Polymerisation-Induced Self-Assembly. *ACS Macro Letters* **2015**, *4*, 1249.

13. Li, M.; De, P.; Gondi, S. R.; Sumerlin, B. S. End group transformations of RAFT-generated polymers with bismaleimides: Functional telechelics and modular block copolymers. *Journal of Polymer Science Part a-Polymer Chemistry* **2008**, *46*, 5093.
14. Beija, M.; Marty, J. D.; Destarac, M. RAFT/MADIX polymers for the preparation of polymer/inorganic nanohybrids. *Progress in Polymer Science* **2011**, *36*, 845.
15. Gody, G.; Zetterlund, P. B.; Perrier, S.; Harrisson, S. The limits of precision monomer placement in chain growth polymerisation. *Nature Communications* **2016**, *7*, 8.
16. Gody, G.; Roberts, D. A.; Maschmeyer, T.; Perrier, S. A New Methodology for Assessing Macromolecular Click Reactions and Its Application to Amine–Tertiary Isocyanate Coupling for Polymer Ligation. *Journal of the American Chemical Society* **2016**, *138*, 4061.
17. Kolomanska, J.; Johnston, P.; Gregori, A.; Dominguez, I. F.; Egelhaaf, H. J.; Perrier, S.; Rivaton, A.; Dagron-Lartigau, C.; Topham, P. D. Design, synthesis and thermal behaviour of a series of well-defined clickable and triggerable sulfonate polymers. *RSC Advances* **2015**, *5*, 66554.
18. Moskowitz, J. D.; Abel, B. A.; McCormick, C. L.; Wiggins, J. S. High Molecular Weight and Low Dispersity Polyacrylonitrile by Low Temperature RAFT Polymerisation. *Journal of Polymer Science Part a-Polymer Chemistry* **2016**, *54*, 553.
19. Ferguson, C. J.; Hughes, R. J.; Nguyen, D.; Pham, B. T. T.; Gilbert, R. G.; Serelis, A. K.; Such, C. H.; Hawket, B. S. Ab Initio Emulsion Polymerisation by RAFT-Controlled Self-Assembly. *Macromolecules* **2005**, *38*, 2191.
20. Zhang, X.; Boisson, F.; Colombani, O.; Chassenieux, C.; Charleux, B. Synthesis of Amphiphilic Poly(acrylic acid)-b-poly(n-butyl acrylate-co-acrylic acid) Block Copolymers with Various Microstructures via RAFT Polymerisation in Water/Ethanol Heterogeneous Media. *Macromolecules* **2014**, *47*, 51.
21. Jia, Z.; Bobrin, V. A.; Truong, N. P.; Gillard, M.; Monteiro, M. J. Multifunctional Nanoworms and Nanorods through a One-Step Aqueous Dispersion Polymerisation. *Journal of the American Chemical Society* **2014**, *136*, 5824.
22. Hatton, F. L.; Ruda, M.; Lansalot, M.; D'Agosto, F.; Malmstrom, E.; Carlmark, A. Xyloglucan-Functional Latex Particles via RAFT-Mediated Emulsion Polymerisation for the Biomimetic Modification of Cellulose. *Biomacromolecules* **2016**, *17*, 1414.

23. De la Haye, J. L.; Zhang, X. W.; Chaduc, I.; Brunel, F.; Lansalot, M.; D'Agosto, F. The Effect of Hydrophile Topology in RAFT-Mediated Polymerisation-Induced Self-Assembly. *Angewandte Chemie - International Edition* **2016**, *55*, 3739.
24. Poon, C. K.; Tang, O.; Chen, X.-M.; Pham, B. T. T.; Gody, G.; Pollock, C. A.; Hawsett, B. S.; Perrier, S. Preparation of Inert Polystyrene Latex Particles as MicroRNA Delivery Vectors by Surfactant-Free RAFT Emulsion Polymerisation. *Biomacromolecules* **2016**, *17*, 965.
25. Huynh, V. T.; Nguyen, D.; Such, C. H.; Hawsett, B. S. Polymer coating of graphene oxide via reversible addition–fragmentation chain transfer mediated emulsion polymerisation. *Journal of Polymer Science Part A: Polymer Chemistry* **2015**, *53*, 1413.
26. Pham, B. T. T.; Such, C. H.; Hawsett, B. S. Synthesis of polymeric janus nanoparticles and their application in surfactant-free emulsion polymerisations. *Polymer Chemistry* **2015**, *6*, 426.
27. Charleux, B.; Delaittre, G.; Rieger, J.; D'Agosto, F. Polymerisation-Induced Self-Assembly: From Soluble Macromolecules to Block Copolymer Nano-Objects in One Step. *Macromolecules* **2012**, *45*, 6753.
28. Warren, N. J.; Armes, S. P. Polymerisation-Induced Self-Assembly of Block Copolymer Nano-objects via RAFT Aqueous Dispersion Polymerisation. *Journal of the American Chemical Society* **2014**, *136*, 10174.
29. Canning, S. L.; Smith, G. N.; Armes, S. P. A Critical Appraisal of RAFT-Mediated Polymerisation-Induced Self-Assembly. *Macromolecules* **2016**, *49*, 1985.
30. Mable, C. J.; Warren, N. J.; Thompson, K. L.; Mykhaylyk, O. O.; Armes, S. P. Framboidal ABC triblock copolymer vesicles: a new class of efficient Pickering emulsifier. *Chemical Science* **2015**, *6*, 6179.
31. Canton, I.; Warren, N. J.; Chahal, A.; Amps, K.; Wood, A.; Weightman, R.; Wang, E.; Moore, H.; Armes, S. P. Mucin-Inspired Thermoresponsive Synthetic Hydrogels Induce Stasis in Human Pluripotent Stem Cells and Human Embryos. *ACS Central Science* **2016**, *2*, 65.
32. Simon, K. A.; Warren, N. J.; Mosadegh, B.; Mohammady, M. R.; Whitesides, G. M.; Armes, S. P. Disulfide-Based Diblock Copolymer Worm Gels: A Wholly-Synthetic

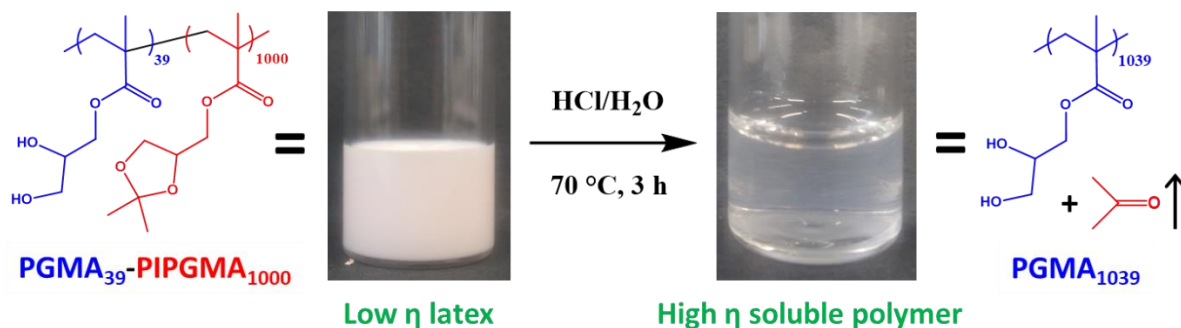
- Thermoreversible 3D Matrix for Sheet-Based Cultures. *Biomacromolecules* **2015**, *16*, 3952.
33. Warren, N. J.; Mykhaylyk, O. O.; Mahmood, D.; Ryan, A. J.; Armes, S. P. RAFT Aqueous Dispersion Polymerisation Yields Poly(ethylene glycol)-Based Diblock Copolymer Nano-Objects with Predictable Single Phase Morphologies. *Journal of the American Chemical Society* **2014**, *136*, 1023.
34. Mable, C. J.; Gibson, R. R.; Prevost, S.; McKenzie, B. E.; Mykhaylyk, O. O.; Armes, S. P. Loading of Silica Nanoparticles in Block Copolymer Vesicles during Polymerisation-Induced Self-Assembly: Encapsulation Efficiency and Thermally Triggered Release. *Journal of the American Chemical Society* **2015**, *137*, 16098.
35. Thomas, D. B.; Convertine, A. J.; Hester, R. D.; Lowe, A. B.; McCormick, C. L. Hydrolytic Susceptibility of Dithioester Chain Transfer Agents and Implications in Aqueous RAFT Polymerisations. *Macromolecules* **2004**, *37*, 1735.
36. Mertoglu, M.; Laschewsky, A.; Skrabania, K.; Wieland, C. New Water Soluble Agents for Reversible Addition–Fragmentation Chain Transfer Polymerisation and Their Application in Aqueous Solutions. *Macromolecules* **2005**, *38*, 3601.
37. Pissuwan, D.; Boyer, C.; Gunasekaran, K.; Davis, T. P.; Bulmus, V. In Vitro Cytotoxicity of RAFT Polymers. *Biomacromolecules* **2010**, *11*, 412.
38. Moad, G.; Rizzardo, E.; Thang, S. H. End-functional polymers, thiocarbonylthio group removal/transformation and reversible addition-fragmentation-chain transfer (RAFT) polymerisation. *Polymer International* **2011**, *60*, 9.
39. Willcock, H.; O'Reilly, R. K. End group removal and modification of RAFT polymers. *Polymer Chemistry* **2010**, *1*, 149.
40. Shen, W.; Qiu, Q.; Wang, Y.; Miao, M.; Li, B.; Zhang, T.; Cao, A.; An, Z. Hydrazine as a Nucleophile and Antioxidant for Fast Aminolysis of RAFT Polymers in Air. *Macromolecular Rapid Communications* **2010**, *31*, 1444.
41. Matioszek, D.; Dufils, P.-E.; Vinas, J.; Destarac, M. Selective and Quantitative Oxidation of Xanthate End-Groups of RAFT Poly(n-butyl acrylate) Latexes by Ozonolysis. *Macromolecular Rapid Communications* **2015**, *36*, 1354.
42. Chong, Y. K.; Moad, G.; Rizzardo, E.; Thang, S. H. Thiocarbonylthio End Group Removal from RAFT-Synthesised Polymers by Radical-Induced Reduction. *Macromolecules* **2007**, *40*, 4446.

43. Michl, T. D.; Locock, K. E. S.; Stevens, N. E.; Hayball, J. D.; Vasilev, K.; Postma, A.; Qu, Y.; Traven, A.; Haeussler, M.; Meagher, L.; Griesser, H. J. RAFT-derived antimicrobial polymethacrylates: elucidating the impact of end-groups on activity and cytotoxicity. *Polymer Chemistry* **2014**, *5*, 5813.
44. Chen, M.; Moad, G.; Rizzardo, E. Thiocarbonylthio End Group Removal from RAFT-Synthesised Polymers by a Radical-Induced Process. *Journal of Polymer Science Part a-Polymer Chemistry* **2009**, *47*, 6704.
45. Legge, T. M.; Slark, A. T.; Perrier, S. Thermal stability of reversible addition–fragmentation chain transfer/macromolecular architecture design by interchange of xanthates chain-transfer agents. *J. Polym. Sci., Part A: Polym. Chem.* **2006**, *44*, 6980.
46. Postma, A.; Davis, T. P.; Moad, G.; O'Shea, M. S. Thermolysis of RAFT-Synthesised Polymers. A Convenient Method for Trithiocarbonate Group Elimination. *Macromolecules* **2005**, *38*, 5371.
47. Mattson, K. M.; Pester, C. W.; Gutekunst, W. R.; Hsueh, A. T.; Discekici, E. H.; Luo, Y.; Schmidt, B. V. K. J.; McGrath, A. J.; Clark, P. G.; Hawker, C. J. Metal-Free Removal of Polymer Chain Ends Using Light. *Macromolecules* **2016**, *49*, 8162.
48. Pfukwa, R.; Pound, G.; Klumperman, B. POLY 407-Facile end group modification of RAFT made polymers, by radical exchange with hydrogen peroxide. *Abstracts of Papers - American Chemical Society* **2008**, *236*, 1.
49. Save, M.; Weaver, J. V. M.; Armes, S. P.; McKenna, P. Atom Transfer Radical Polymerisation of Hydroxy-Functional Methacrylates at Ambient Temperature: Comparison of Glycerol Monomethacrylate with 2-Hydroxypropyl Methacrylate. *Macromolecules* **2002**, *35*, 1152.
50. Jones, E. R.; Semsarilar, M.; Blanazs, A.; Armes, S. P. Efficient Synthesis of Amine-Functional Diblock Copolymer Nanoparticles via RAFT Dispersion Polymerisation of Benzyl Methacrylate in Alcoholic Media. *Macromolecules* **2012**, *45*, 5091.
51. Blanazs, A.; Ryan, A. J.; Armes, S. P. Predictive Phase Diagrams for RAFT Aqueous Dispersion Polymerisation: Effect of Block Copolymer Composition, Molecular Weight, and Copolymer Concentration. *Macromolecules* **2012**, *45*, 5099.
52. Cunningham, V. J.; Alswieleh, A. M.; Thompson, K. L.; Williams, M.; Leggett, G. J.; Armes, S. P.; Musa, O. M. Poly(glycerol monomethacrylate)–Poly(benzyl

- methacrylate) Diblock Copolymer Nanoparticles via RAFT Emulsion Polymerisation: Synthesis, Characterisation, and Interfacial Activity. *Macromolecules* **2014**, *47*, 5613.
53. Blanazs, A.; Verber, R.; Mykhaylyk, O. O.; Ryan, A. J.; Heath, J. Z.; Douglas, C. W. I.; Armes, S. P. Sterilisable Gels from Thermoresponsive Block Copolymer Worms. *Journal of the American Chemical Society* **2012**, *134*, 9741.
54. Mitchell, D. E.; Lovett, J. R.; Armes, S. P.; Gibson, M. I. Combining Biomimetic Block Copolymer Worms with an Ice-Inhibiting Polymer for the Solvent-Free Cryopreservation of Red Blood Cells. *Angewandte Chemie International Edition* **2016**, *55*, 2801.
55. Lovett, J. R.; Warren, N. J.; Ratcliffe, L. P. D.; Kocik, M. K.; Armes, S. P. pH-Responsive Non-Ionic Diblock Copolymers: Ionization of Carboxylic Acid End-Groups Induces an Order–Order Morphological Transition. *Angewandte Chemie International Edition* **2015**, *54*, 1279.

# Chapter 3 - Synthesis of high molecular weight poly(glycerol monomethacrylate) via RAFT emulsion polymerisation of isopropylidene glycerol methacrylate

High molecular weight water-soluble polymer by RAFT aqueous emulsion polymerization



The work carried out in this chapter was 100 % completed by C. P. Jesson



## Introduction

Water-soluble polymers can be used for a wide range of commercial applications, including as flocculants in brewing<sup>1</sup> for dewatering in paper manufacture<sup>2-4</sup> or for municipal water purification.<sup>5-7</sup> High molecular weight ( $> 10^5$  g mol<sup>-1</sup>) polymers are particularly efficient and include non-ionic, anionic or cationic polyacrylamides,<sup>7-9</sup> poly(ethylene oxide) (PEO)<sup>10</sup> and poly(diallyldimethylammonium) chloride (PDADMAC).<sup>11</sup> Such polymers induce aggregation via a bridging flocculation mechanism.<sup>12-14</sup> Water-soluble polymers are also widely employed as viscosity modifiers.<sup>15-17</sup> For example, PEO<sup>18</sup> and poly(acrylic acid) (PAA)<sup>19</sup> are commonly used as thickening agents in cosmetics, while polyurethanes (PU)<sup>20</sup> or poly(vinyl alcohol) (PVA) are utilised in paint formulations.<sup>21</sup> In such applications polymers often confer the additional benefit of acting as steric stabilisers for other parts of the formulation e.g. oil droplets or pigments.<sup>22</sup>

Poly(glycerol monomethacrylate) (PGMA) is another water-soluble polymer which is highly biocompatible and non-fouling and has been utilised for the manufacture of soft contact lenses,<sup>23-25</sup> GMA is a relatively expensive specialty monomer. In principle, it can be obtained via hydrolysis of a cheap commodity monomer, glycidyl methacrylate, in aqueous solution,<sup>26</sup> but in practice it is actually prepared via a protected precursor, isopropylidenglycerol methacrylate.<sup>27</sup> In the field of biomaterials, GMA-based copolymers have been used to prepare hydrogels that act as corneal substitutes,<sup>28</sup> for the design of amphiphilic networks that serve as suitable substrates for dermal fibroblasts<sup>29-31</sup> and grown in the form of a brush from tissue culture polystyrene in order to improve cell adhesion.<sup>32</sup> Canton et al. demonstrated that human stem cell colonies enter stasis within 16 h of their immersion within PGMA-based block copolymer worm gels.<sup>33</sup> In addition, the cis-diol moiety of PGMA has been utilised for metal binding to magnetite<sup>34</sup> and other iron-based materials.<sup>35</sup> Recently, Deng et al. reported that 4-aminophenylboronic acid can bind to PGMA-based block copolymer vesicles in alkaline aqueous solution and hence induces various morphological order-order transitions.<sup>36</sup>

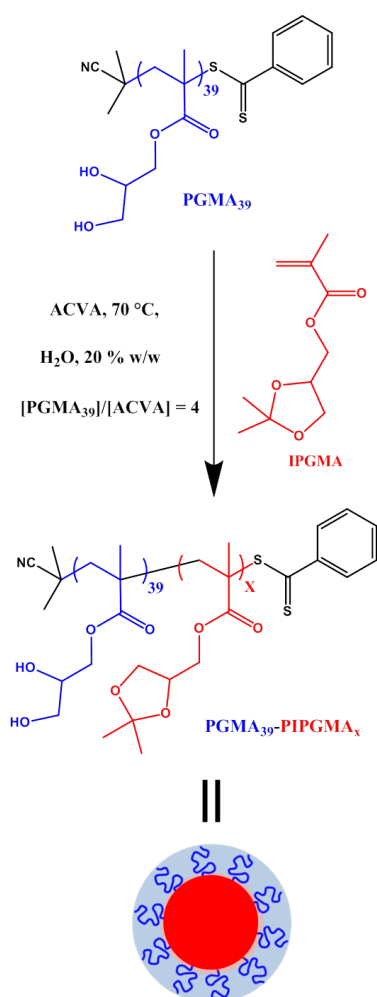
Polymerisation-induced self-assembly (PISA) is a well-recognised versatile platform technology for the efficient synthesis of a wide range of block copolymer nano-objects.<sup>37-44</sup> PISA formulations based on RAFT aqueous emulsion polymerisation involve chain-extending a water-soluble precursor polymer with a water-immiscible monomer to produce an amphiphilic diblock copolymer *in situ*.<sup>45-56</sup> This drives self-assembly to produce sterically-

stabilised nanoparticles. In principle, the copolymer morphology should simply depend on the relative volume fractions of each block, with more asymmetric blocks forming either worms or vesicles.<sup>38,47,57-60</sup> However, in many cases only kinetically-trapped spheres are accessible.<sup>45,61-67</sup> This approach offers a method of synthesising high molecular weight polymers in a low viscosity form, however the resulting copolymers are inherently insoluble in the reaction medium.

Destarac and co-workers recently reported the synthesis of high molecular weight water-soluble polymers via the RAFT *solution* polymerisation of acrylamide.<sup>68</sup>  $M_n$  values of more than  $10^6$  g mol<sup>-1</sup> with relatively narrow molecular weight distributions (typically  $M_w/M_n < 1.30$ ) were achieved reproducibly at 10 °C by utilising high monomer concentrations and a relatively low initiator concentration. However, the final reaction solutions were relatively viscous. Cunningham et al.<sup>69</sup> offered a potential technical solution to this problem by utilising RAFT aqueous dispersion polymerisation to prepare a high molecular weight water-soluble polymer above its lower critical solution temperature (LCST). Thus a PGMA macromolecular chain transfer agent (macro-CTA) was chain-extended with *N*-(2-(methacryloyloxy)ethyl)pyrrolidone (NMEP) at 70 °C to yield a low-viscosity dispersion of partially hydrated spherical PGMA-PNMEP nanoparticles. PNMEP exhibits an LCST of around 55 °C. Thus, cooling such aqueous dispersions induced particle dissolution to produce molecularly-dissolved copolymer chains at 20 °C, with a concomitant significant increase in solution viscosity. Although not a true homopolymer, the number-average degree of polymerisation ( $DP_n$ ) of the PNMEP could be systematically varied from 1000 up to 4500, which substantially exceeded that of the PGMA stabiliser block ( $DP_n = 51$ ). Moreover, DMF GPC analysis indicated relatively low dispersities ( $M_w/M_n < 1.50$ ) and high NMEP conversions (> 98 %) could be achieved for such PISA formulations. However, literature examples of the preparation of high molecular weight water-soluble *homopolymers* in low-viscosity form using wholly aqueous formulations are rather rare.<sup>70,71</sup>

Herein a new strategy for the synthesis of high molecular weight PGMA of relatively narrow molecular weight distribution is examined. More specifically, a water-soluble PGMA stabiliser is chain-extended with isopropylidenglycerol methacrylate (IPGMA) using RAFT aqueous emulsion polymerisation at pH 4 to produce amphiphilic PGMA-PIPGMA diblock copolymers in the form of sterically-stabilised nanoparticles, see Scheme 3.1. Optimisation of this PISA formulation enables  $DP_n$  values of up to 1000 to be achieved at relatively high monomer

conversions. Subsequently, the hydrophobic PIPGMA block can be deprotected to afford a water-soluble PGMA homopolymer via selective hydrolysis at low pH. This approach bears some similarity to that employed by Zentel and co-workers, who copolymerised IPGMA to form pH-responsive nanoparticles that undergo dissociation on addition of acid.<sup>72</sup> In this context, it is also worth noting a recent report by Rimmer and co-workers, who prepared polystyrene-poly(isopropylidenglycerol methacrylate) core-shell latexes via conventional aqueous emulsion polymerisation.<sup>73</sup> Subsequent deprotection of the methacrylic residues in the shell at low pH led to PGMA-stabilised PS latexes that proved to be highly resistant to protein fouling.



**Scheme 3.1.** Synthesis of PGMA-PIPGMA (G<sub>39</sub>-I<sub>x</sub>) diblock copolymer nanoparticles via RAFT aqueous emulsion polymerisation of isopropylidenglycerol methacrylate (IPGMA) at 70 °C using a PGMA chain transfer agent as a steric stabiliser.

## Experimental

### *Materials*

Glycerol monomethacrylate (GMA, 99.8%), and isopropylidenglycerol methacrylate (IPGMA, 97.8%) were donated by GEO Specialty Chemicals (Hythe, UK) and used without further purification. 4,4'-Azobis(4-cyanopentanoic acid) (ACVA, 99%) and dichloromethane were purchased from Sigma-Aldrich (UK) and were used as received. 2-Cyano-2-propyldithiobenzoate (CPDB) was purchased from Strem Chemicals Ltd. (Cambridge, UK) and was used as received. Deuterated DMF and methanol were purchased from Goss Scientific Instruments Ltd. (Crewe, UK). All other solvents were purchased from Fisher Scientific (Loughborough, UK) and used as received. Deionised water was used for all experiments.

### *Protocol for the synthesis of PGMA macro-CTAs*

A PGMA<sub>39</sub> (or G<sub>39</sub>) macromolecular chain transfer agent (macro-CTA) was synthesised as follows: CPDB RAFT agent (0.829 g, 3.70 mmol) and GMA monomer (30.0 g, 187.3 mmol) were weighed into a 100 mL round-bottomed flask and purged under N<sub>2</sub> for 30 min. ACVA initiator (210 mg, 0.75 mmol; CTA/ACVA molar ratio = 5.0) and anhydrous ethanol (46.6 mL; previously purged with N<sub>2</sub> for 30 min) were then added, and the resulting red solution was degassed for a further 10 min. The flask was subsequently sealed and immersed into an oil bath set at 70 °C. After 100 min, the GMA polymerisation was quenched by opening to air, immersing the flask in liquid nitrogen for 30 seconds and dilution with methanol (100 mL). A final GMA conversion of 69 % was determined by <sup>1</sup>H NMR analysis by comparing the integrated monomer vinyl signals at 6.1-6.2 ppm to oxymethylene signals adjacent to the methacrylic ester groups of polymerised GMA residues at 3.8-4.3 ppm (see Figure 3.1). The methanolic solution was precipitated into a ten-fold excess of dichloromethane. After filtering and washing with dichloromethane, the crude polymer was dissolved in water and the residual dichloromethane was evaporated under vacuum. The resulting aqueous solution was freeze-dried overnight to yield a pink powder. <sup>1</sup>H NMR analysis indicated a mean degree of polymerisation of 39 ± 1, by comparing the integrated aromatic protons assigned to the RAFT CTA end-group at 7.3-8.0 ppm to that of the polymerised GMA repeat units at 3.8-4.3 ppm (see Figure 3.1), for this purified PGMA macro-CTA. DMF GPC analysis confirmed that this GMA homopolymerisation was well-controlled ( $M_n = 11,100 \text{ g mol}^{-1}$ ,  $M_w/M_n = 1.13$ ).

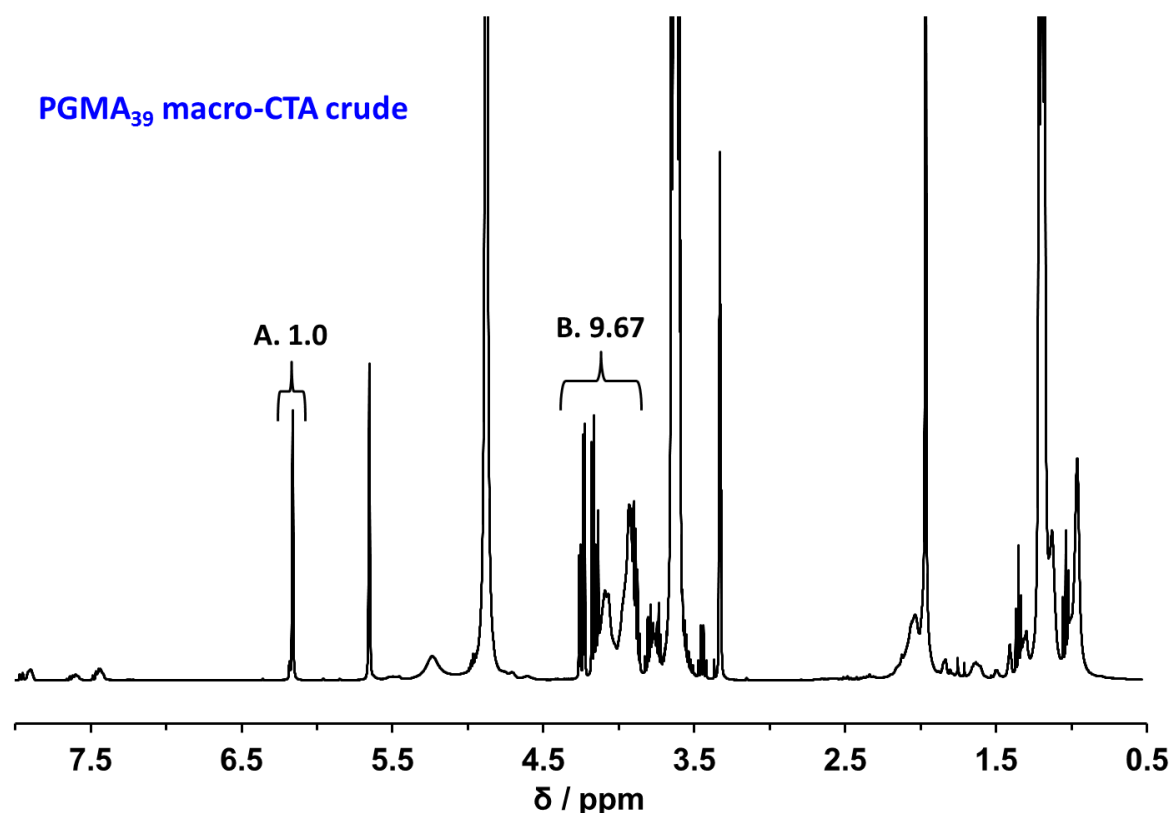


**Figure 3.1.**  $^1\text{H}$  NMR spectrum ( $\text{d}_4$ -methanol) recorded for a crude  $\text{PGMA}_{39}$  macro-CTA. The GMA conversion can be calculated by comparing the integrated signals A and B while accounting for the number of protons associated with each signal.

*Preparation of  $\text{PGMA}_{39}$ - $\text{PIPGMA}_X$  nanoparticles via RAFT aqueous emulsion polymerisation*  
 $\text{PGMA}_{39}$ - $\text{PIPGMA}_{1000}$  ( $\text{G}_{39}$ - $\text{I}_{1000}$ ) was synthesised as follows:  $\text{PGMA}_{39}$  macro-CTA (0.026 g, 4.00  $\mu\text{mol}$ ), IPGMA monomer (0.80 g, 3.99 mmol) and ACVA initiator (0.28 mg, 1.00  $\mu\text{mol}$ ) were weighed into a 10 mL round-bottomed flask and dissolved in deionised water (3.30 mL). The resulting solution was purged under  $\text{N}_2$  for 30 min before being sealed and immersed in an oil bath at 70  $^\circ\text{C}$  for 5 h. The polymerisation was quenched by exposure to air and cooling to 20  $^\circ\text{C}$ . A final IPGMA conversion of > 97 % was determined by  $^1\text{H}$  NMR analysis by comparing the integrated monomer vinyl signals at 6.2 – 6.3 ppm to that of the six methyl protons assigned to the acetal group of the polymerised IPGMA residues at 1.5 – 1.7 ppm (see Figure 3.2). These  $\text{PGMA}_{39}$ - $\text{PIPGMA}_{1000}$  spherical nanoparticles were used without further purification.

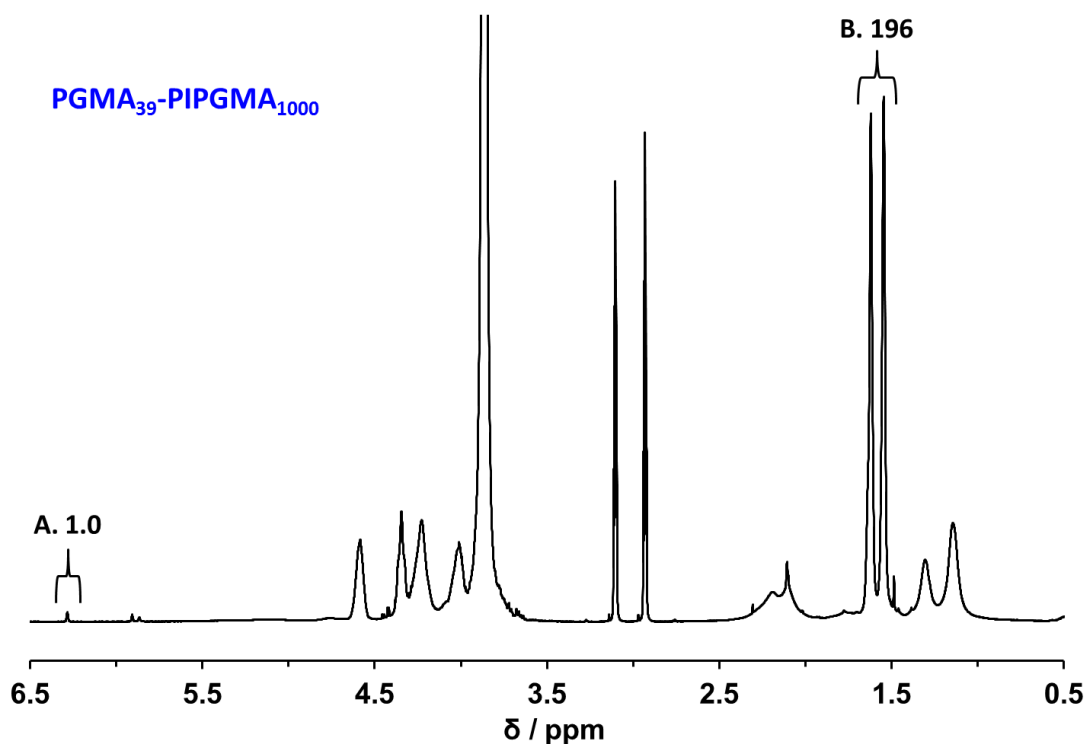


**Figure 3.2.**  $^1\text{H}$  NMR spectrum ( $d_7$ -DMF) recorded for a  $\text{PGMA}_{39}$ - $\text{PIPGMA}_{1000}$  diblock copolymer. The IPGMA conversion can be calculated by comparing the integrated signals A and B while accounting for the number of protons associated with each signal.

*Deprotection of  $\text{PGMA}_{39}$ - $\text{PIPGMA}_{1000}$  nanoparticles to afford water-soluble  $\text{PGMA}_{1039}$*

A 20 % w/w aqueous dispersion of  $\text{PGMA}_{39}$ - $\text{PIPGMA}_{1000}$  diblock copolymer spheres (4.0 mL; initial pH 3) was transferred into a 10 mL round-bottomed flask and adjusted to pH 1 by addition of concentrated HCl. The resulting acidic solution was immersed in an oil bath at 70 °C for 3 h.  $^1\text{H}$  NMR analysis indicated that 99 % of the IPGMA residues were converted into GMA residues, yielding a 16 % w/w aqueous acidic solution of water-soluble  $\text{PGMA}_{1039}$  homopolymer.

*One-pot protocol to afford water-soluble  $\text{PGMA}_{1039}$  via RAFT aqueous emulsion polymerisation of IPGMA followed by acid hydrolysis*

$\text{PGMA}_{39}$  macro-CTA (0.026 g, 4.00  $\mu\text{mol}$ ), IPGMA monomer (0.80 g, 3.99 mmol) and ACVA initiator (0.28 mg, 1.00  $\mu\text{mol}$ ) were weighed into a 10 mL round-bottomed flask and dissolved in deionised water (3.30 mL). The resulting solution was purged under  $\text{N}_2$  for 30 min before being sealed and immersed in an oil bath at 70 °C for 6 h. A final IPGMA conversion of > 99 % was determined by  $^1\text{H}$  NMR analysis. The polymerisation was quenched by exposure to air.

The solution was adjusted to pH 1 by addition of concentrated HCl. The resulting acidic solution was maintained at 70 °C for 3 h. <sup>1</sup>H NMR analysis indicated that 99 % of the IPGMA residues were converted into GMA residues, yielding a 16 % w/w aqueous acidic solution of water-soluble PGMA<sub>1039</sub> homopolymer.

*RAFT aqueous solution polymerisation of GMA*

CPDB RAFT agent (11 mg, 5.00 μmol) and GMA monomer (0.80 g, 5.00 mmol) were weighed into a 10 mL round-bottomed flask and purged under N<sub>2</sub> for 30 min. ACVA initiator (0.35 mg, 1.25 μmol; CTA/ACVA molar ratio = 4.0) and dissolved in deionised water (3.21 mL) The resulting solution was purged under N<sub>2</sub> for 30 min before being sealed and immersed in an oil bath at 70 °C for 5 h. The polymerisation was quenched by exposure to air and cooling to 20 °C. A final GMA conversion of more than 97 % was determined by <sup>1</sup>H NMR analysis.

*NMR Spectroscopy.* All <sup>1</sup>H NMR spectra were recorded in either deuterated methanol (for the PGMA macro-CTAs) or deuterated DMF (for the PGMA-PIPGMA diblock copolymers and for monitoring the acid-catalysed deprotection of the PGMA-PIPGMA diblock precursor to afford PGMA homopolymer) using a 400 MHz Bruker Avance-400 spectrometer (64 scans averaged per spectrum).

*Gel Permeation Chromatography (GPC).* Copolymer molecular weights and dispersities were determined using an Agilent 1260 Infinity GPC system equipped with both refractive index and UV-visible detectors. Two Agilent PL gel 5 μm Mixed-C columns and a guard column were connected in series and maintained at 60°C. HPLC-grade DMF containing 10 mM LiBr was used as eluent and the flow rate was set at 1.0 mL min<sup>-1</sup>. DMSO was used as a flow-rate marker. The refractive index detector was used for calculation of molecular weights and dispersities by calibration using a series of ten near-monodisperse poly(methyl methacrylate) standards (with M<sub>n</sub> values ranging from 625 to 618,000 g mol<sup>-1</sup>). UV GPC chromatograms were obtained simultaneously by detection at a fixed wavelength of 309 nm which corresponds to the absorption maximum for the dithiobenzoate RAFT end-groups.

*Transmission Electron Microscopy (TEM).* Copolymer dispersions were diluted fifty-fold at 20°C to generate 0.20% w/w dispersions. Copper/palladium TEM grids (Agar Scientific, UK) were coated in-house to produce a thin film of amorphous carbon. These grids were then treated with a plasma glow discharge for 30 seconds to create a hydrophilic surface. Each aqueous diblock copolymer dispersion (12 µL; 0.20% w/w) was placed on a freshly-treated grid for 1 min and then blotted with filter paper to remove excess solution. To stain the deposited nanoparticles, an aqueous solution of uranyl formate (9 µL; 0.75% w/w) was placed on the sample-loaded grid via micropipet for 20 s and then carefully blotted to remove excess stain. Each grid was then carefully dried using a vacuum hose. Imaging was performed using a FEI Tecnai Spirit TEM instrument equipped with a Gatan 1kMS600CW CCD camera operating at 120 kV.

*Oscillatory Rheology experiments* An AR-G2 rheometer equipped with a variable temperature Peltier plate, a 40 ml 2° aluminium cone and a solvent trap was used for all experiments. Temperature sweeps were conducted at an angular frequency of 1.0 rad s<sup>-1</sup> and a constant strain of 1.0 %. The temperature was increased by 1.0 °C between each measurement, allowing an equilibration time of 2 min in each case. A solvent trap was required to prevent evaporation of water on the time scale of these experiments.

*Dynamic light scattering (DLS).* Measurements were conducted at 25 °C using a Malvern Instruments Zetasizer Nano series instrument equipped with a 4 mW He–Ne laser ( $\lambda = 633$  nm) and an avalanche photodiode detector. Scattered light was detected at 173°. Copolymer dispersions were diluted to 0.10% w/w. Intensity-average hydrodynamic diameters were averaged over three runs and calculated via the Stokes–Einstein equation.

## **Results and Discussion**

The goal of this research was to synthesise high molecular weight PGMA homopolymer in aqueous solution via deprotection of PGMA-PIPGMA diblock copolymer nanoparticles, thus circumventing the problem of high solution viscosity usually associated with an aqueous solution polymerisation route.<sup>68</sup> Moreover, given that an emulsion polymerisation protocol was employed to prepare the intermediate sterically-stabilised nanoparticles, a significantly faster



rate of polymerisation was anticipated compared to that obtained via aqueous solution polymerisation owing to the well-known effect of compartmentalisation, which leads to a significant reduction in the rate of termination and hence allows access to high molecular weight polymer chains.<sup>74,75</sup>

### Optimisation of PGMA-PIPGMA diblock copolymer synthesis

First, a well-defined PGMA macro-CTA ( $M_n = 11\ 100$ ;  $M_w/M_n = 1.13$ ) was prepared at 70 °C in ethanol using CPDB as the RAFT CTA. In principle, a trithiocarbonate-based RAFT agent should also be suitable for the RAFT emulsion polymerisation of IPGMA. However, a dithiobenzoate-based CTA was chosen based on the well-controlled RAFT emulsion polymerisations obtained for other water-immiscible monomers such as benzyl methacrylate or 2,2,2-trifluoroethyl methacrylate.<sup>61,76</sup> The  $DP_n$  of this water-soluble homopolymer was determined to be 39 by  $^1H$  NMR spectroscopy (see Figure 3.3).

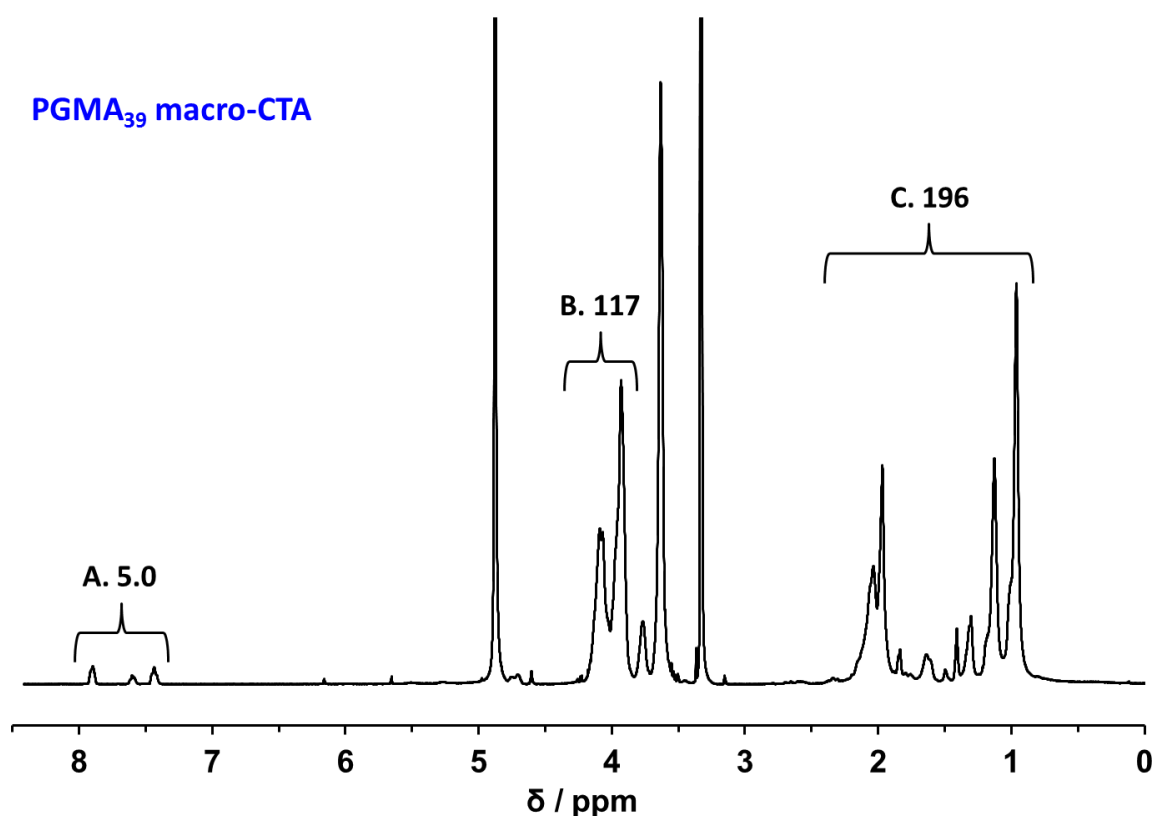


**Figure 3.3.**  $^1H$  NMR spectrum ( $d_4$ -methanol) recorded for a PGMA<sub>39</sub> macro-CTA synthesised by RAFT solution polymerisation of GMA in ethanol at 70 °C. The  $DP_n$  for this polymer can be calculated by comparing the integrated signal A with that of either B or C while accounting for the number of protons associated with each signal.

Subsequently, this PGMA<sub>39</sub> precursor was chain-extended *via* RAFT emulsion polymerisation of IPGMA at 20 % w/w solids. Like the majority of RAFT aqueous emulsion polymerisation formulations, only spherical nanoparticles were obtained using this protocol.<sup>40,61,62</sup> In the context of the present study, this kinetically-trapped morphology is an advantage because it ensures that a relatively low dispersion viscosity is maintained during such syntheses. In each case, high monomer conversions (> 97%) were determined by <sup>1</sup>H NMR spectroscopy, as judged by the disappearance of the vinyl proton signals at 5.9 and 6.2 ppm. In addition, DMF GPC analysis indicated low dispersities (typically  $M_w/M_n < 1.29$ , see Figure 3.4), while DLS studies confirmed the formation of near-monodisperse spheres (polydispersities typically below 0.10). Thus good control was achieved over both the molecular weight distribution and the particle size distribution during such heterogeneous polymerisations.

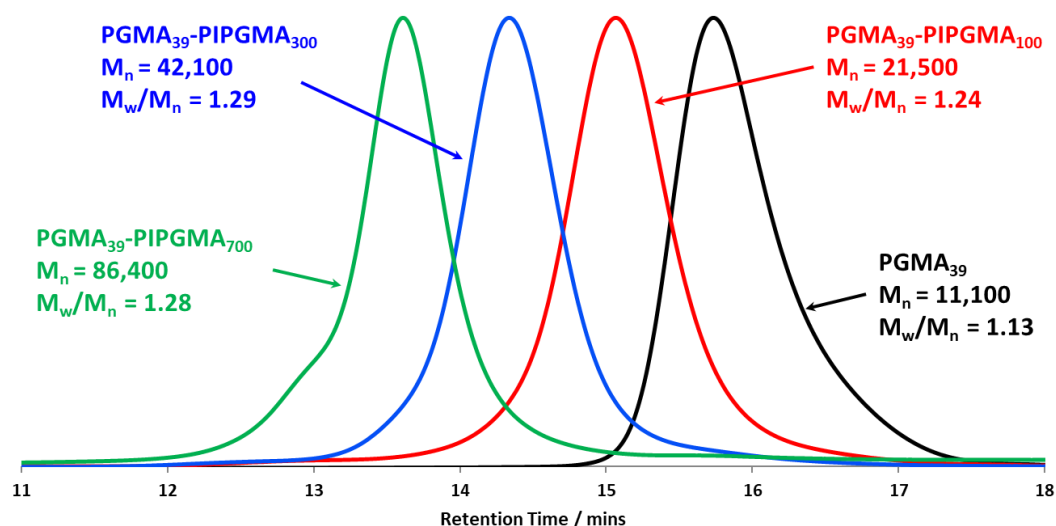


**Figure 3.4.** Some representative DMF GPC for RAFT aqueous emulsion polymerisation of IPGMA from a PGMA<sub>39</sub> macro-CTA showing good blocking efficiency and good control. Conditions: 20 % w/w solids; ACVA initiator; macro-CTA/ACVA molar ratio = 4.0.

The kinetics for the RAFT emulsion polymerisation of IPGMA were monitored when targeting a final diblock composition of PGMA<sub>39</sub>-PIPGMA<sub>1000</sub> by extracting aliquots from the reaction solution at regular time intervals. After quenching the polymerisation via dilution and cooling, these samples were analysed in turn by <sup>1</sup>H NMR, DLS and DMF GPC (see Figures 3.5a, 3.5b and 3.5c, respectively. Further DLS data is available in the appendix Figure 7.. <sup>1</sup>H NMR spectra recorded at various reaction times (and hence monomer conversions) are shown in Figure 3.6).

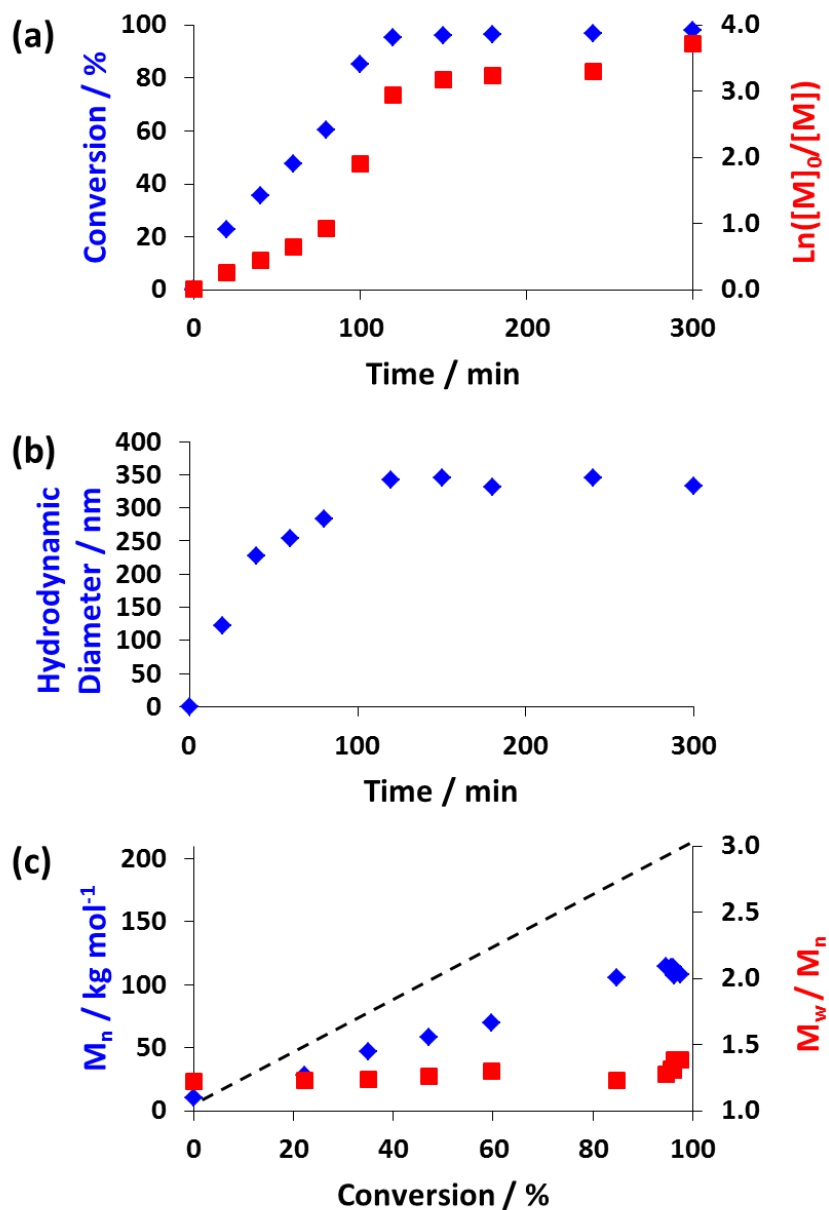


**Figure 3.5.** Analysis of aliquots extracted during the PISA synthesis of PGMA<sub>39</sub>-PIPGMA<sub>1000</sub> via RAFT emulsion polymerisation of IPGMA at 70 °C showing: (a) conversion vs. time curve and the corresponding semi-logarithmic plot against time as determined by <sup>1</sup>H NMR spectroscopy, (b) evolution of intensity-average DLS diameter against time and (c) evolution of  $M_n$  and  $M_w/M_n$  against conversion determined by DMF GPC using a series of near-monodisperse poly(methyl methacrylate) calibration standards. The theoretical  $M_n$  is shown by a dashed line. Conditions: 20 % w/w solids; ACVA initiator; macro-CTA/ACVA molar ratio = 4.0.

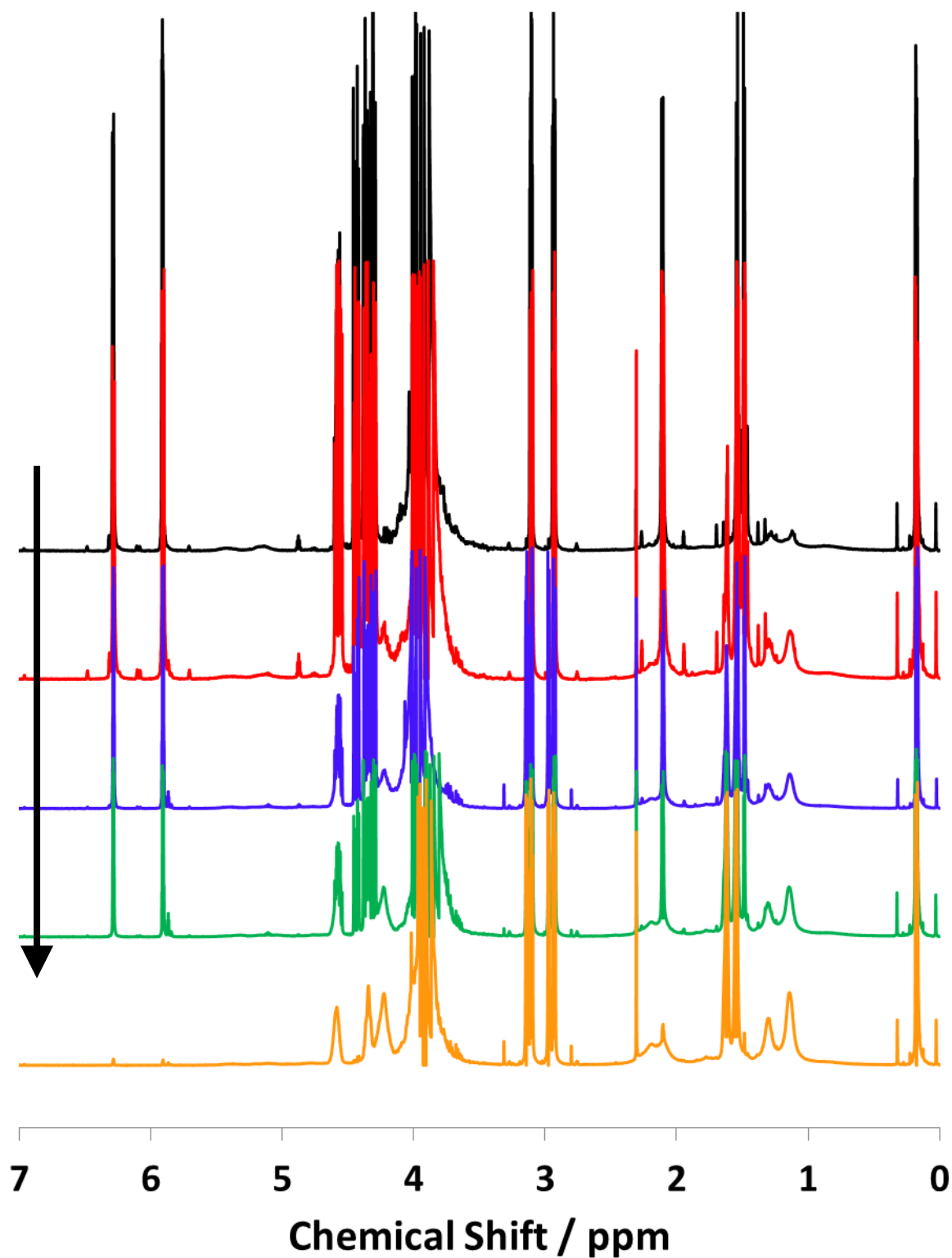


**Figure 3.6.** Overlaid <sup>1</sup>H NMR spectra showing the evolution of the RAFT emulsion polymerisation of IPGMA when targeting PGMA<sub>39</sub>-PIPGMA<sub>1000</sub>. The arrow indicates progression in time from 0 to 300 min.

<sup>1</sup>H NMR studies confirmed that more than 95 % conversion was achieved within 2 h at 70 °C. DMF GPC analysis indicated the linear evolution of molecular weight with conversion expected for a well-controlled RAFT polymerisation, with relatively low dispersities ( $M_w/M_n < 1.40$ ) being maintained throughout the reaction. Somewhat broader molecular weight distributions are observed above 90 % conversion, as judged by the significant increase in dispersity (from  $M_w/M_n \sim 1.23$  up to  $M_w/M_n \sim 1.38$ ). This is attributed to chain transfer to polymer, which becomes more likely under monomer-starved conditions. Close inspection of the semi-logarithmic plot revealed a significant rate acceleration between 90 and 120 min. In the case of RAFT dispersion polymerisation formulations, such data have been interpreted in terms of the onset of micellar nucleation.<sup>77-81</sup> However, the concomitant DLS studies indicate the presence of (presumably) monomer-swollen nanoparticles of around 120 nm in the reaction solution after just 20 min (DLS attenuator = 4; this corresponds to the time at which the first aliquot was extracted). Such early nucleation is not atypical for RAFT emulsion polymerisation syntheses.<sup>61,82</sup> For the present formulation it is also physically realistic, because the monomer conversion observed after 20 min is approximately 22 %, which corresponds to a  $DP_n$  of 220 for the hydrophobic PIPGMA block. Between 80 and 100 min there is a discernible increase in the rate of IPGMA polymerisation. There are only a few literature examples of PISA formulations exhibiting faster polymerisation kinetics *after* the onset of micellar nucleation.<sup>80,83,84</sup> This unusual behavior is not fully understood but it is worth emphasising that we have seen such behavior in both aqueous and non-aqueous PISA systems.

In a second set of experiments, a series of PGMA<sub>39</sub>-PIPGMAX diblock copolymers were prepared by targeting PIPGMA DPs ranging between 100 and 2000 whilst maintaining an overall solids concentration of 20 % w/w. Given that the PGMA macro-CTA/initiator molar ratio was fixed at 4, this means that lower initiator concentrations are utilised when targeting higher DPs. This leads to progressively slower RAFT polymerisations and at some point the radical flux becomes so low that the final monomer conversion becomes rather irreproducible for such formulations.<sup>69</sup> Indeed, high IPGMA conversions (at least 97%) could be achieved when targeting DPs up to 1000, with narrow molecular weight distributions being maintained (see Table 3.1). However, a substantially lower conversion (42%) was obtained when targeting a DP of 2000. For an intermediate target DP of 1500, a final IPGMA conversion of 95% was achieved in one particular synthesis, but several attempts to repeat this result were unsuccessful (Table 3.1 contains details of the best results achieved for this PISA formulation, which is on

the cusp of irreproducibility owing to the relatively low initiator concentration). Thus high conversions could only be reproducibly achieved when targeting a DP of 1000. In this case, the  $M_w/M_n$  determined for the final PIPGMA homopolymer was 1.20, which indicates relatively good RAFT control.<sup>85-87</sup>

**Table 3.1.** Summary of monomer conversion, molecular weight and intensity-average particle diameter data obtained using  $^1\text{H}$  NMR spectroscopy, DMF GPC (refractive index detector; poly(methyl methacrylate) standards) and dynamic light scattering (DLS) respectively for a series of  $\text{PGMA}_{39}\text{-PIPGMA}_x$  ( $\text{G}_{39}\text{-I}_x$ ) diblock copolymer nanoparticles prepared at 20 % w/w solids via RAFT aqueous emulsion polymerisation of IPGMA at 70 °C.

Sample Number	Target Composition	Conversion (%)	GPC $M_n$ / $\text{g mol}^{-1}$	$M_w/M_n$	Diameter / nm
1	$\text{G}_{39}$	69	11 100	1.13	N/A
2	$\text{G}_{39}\text{-I}_{100}$	99	21 500	1.24	42
3	$\text{G}_{39}\text{-I}_{200}$	99	30 500	1.26	66
4	$\text{G}_{39}\text{-I}_{300}$	99	42 100	1.29	98
5	$\text{G}_{39}\text{-I}_{400}$	99	51 800	1.23	132
6	$\text{G}_{39}\text{-I}_{500}$	99	61 500	1.21	163
7	$\text{G}_{39}\text{-I}_{600}$	99	71 900	1.22	207
8	$\text{G}_{39}\text{-I}_{700}$	98	86 400	1.28	247
9	$\text{G}_{39}\text{-I}_{800}$	97	90 000	1.28	297
10	$\text{G}_{39}\text{-I}_{900}$	97	99 200	1.22	315
11	$\text{G}_{39}\text{-I}_{1000}$	97	125 000	1.20	363
12*	$\text{G}_{39}\text{-I}_{1500}$	95	159 500	1.32	717
13	$\text{G}_{39}\text{-I}_{2000}$	42	96 200	1.16	1172

\* Attempts to reproduce this formulation led to significantly lower monomer conversions.

DMF GPC analysis of the first eleven samples shown in Table 3.1 revealed a linear evolution in  $M_n$  with increasing PIPGMA block DP (see Figure 3.7a), which is similar to that previously observed for the RAFT aqueous dispersion polymerisation of NMEP.<sup>69</sup> Moreover, DLS studies indicated a linear correlation between the intensity-average diameter and PIPGMA DP for this

series of spherical nanoparticles, see Figure 3.7b (for more detailed DLS data, see appendix Figure 7.2). For each sample, the DLS PDI was  $< 0.1$  and the correlogram showed good monodispersity. Cunningham et al. also reported a monotonic increase in particle size with core-forming block DP<sub>n</sub> for the synthesis of PGMA-PBzMA diblock copolymer nanoparticles prepared via RAFT emulsion polymerisation. However, the mean hydrodynamic sphere diameters obtained in this earlier work were much smaller than those observed in the current study for similar core-forming block DPs.<sup>61</sup> Unlike the PNMEP-core particles reported by Cunningham et al.,<sup>69</sup> it seems unlikely that the PIPGMA-core particles are appreciably hydrated. However, we cannot rule out the possibility that some degree of deprotection of the IPGMA residues occurs *in situ* during the RAFT aqueous emulsion polymerisation. If this were the case, it would introduce hydrophilic GMA units within the core-forming block, which could lead to some degree of particle swelling.

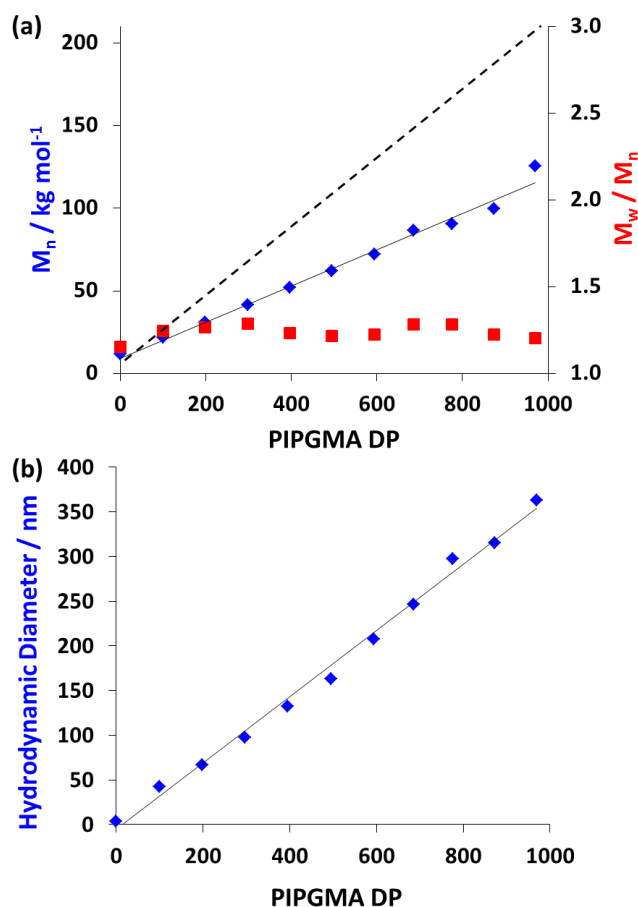


**Figure 3.7.** (a) Evolution of  $M_n$  and  $M_w/M_n$  with PIPGMA DP, where the theoretical  $M_n$  is shown by a dashed line and (b) correlation between intensity-average DLS diameter against

PIPGMA DP for a series of PGMA<sub>39</sub>-PIPGMA<sub>X</sub> spherical nanoparticles prepared via RAFT aqueous emulsion polymerisation of IPGMA at 70 °C (see Table 3.1).

Transmission electron microscopy images obtained for the PGMA<sub>39</sub>-PIPGMA<sub>1000</sub> diblock copolymer nanoparticles (see entry 11 Table 3.1) are shown in Figure 3.8. This confirms the well-defined spherical morphology for such nanoparticles.

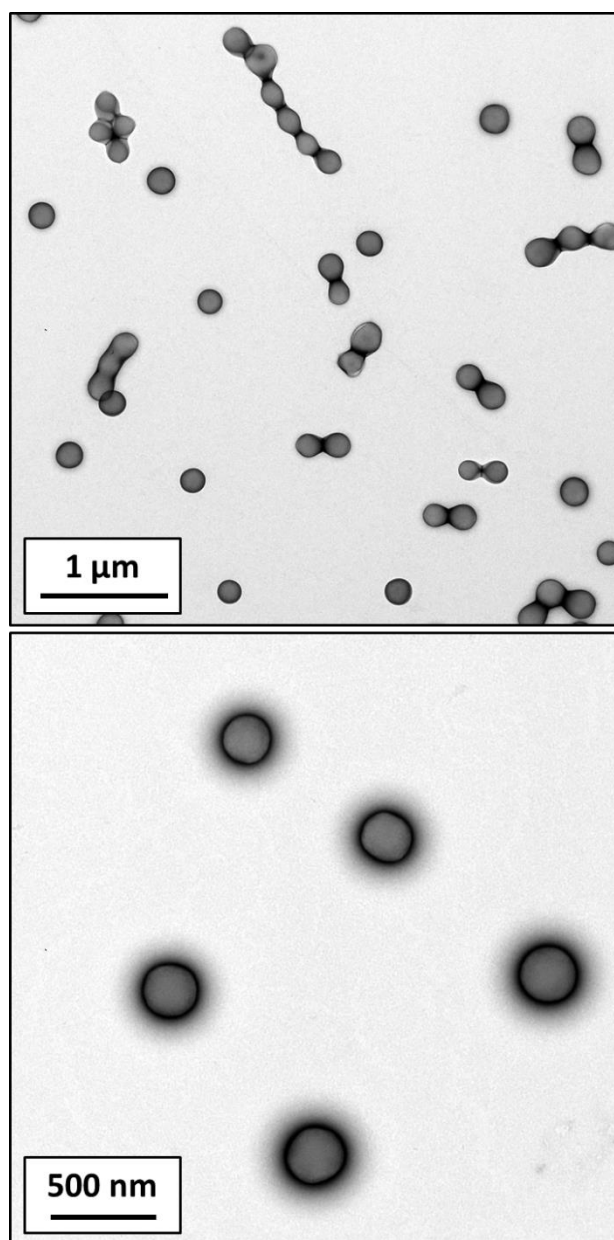


**Figure 3.8.** Representative TEM images obtained for the PGMA<sub>39</sub>-PIPGMA<sub>1000</sub> diblock copolymer nanoparticles.



### **Systematic variation of the copolymer concentration**

PIPGMA DP<sub>n</sub>s of 1000, 1500 and 2000 were targeted in turn at 30 % w/w solids using PGMA<sub>39</sub> as the steric stabiliser block. However, such formulations only led to the formation of thick pastes, rather than free-flowing colloidal dispersions. Similar results were obtained at 25 % w/w solids. Empirically, it was found that free-flowing dispersions could only be obtained at 20 % w/w copolymer concentration when targeting PIPGMA DP<sub>n</sub>s of 1000. Attempts to confer greater steric stabilisation by utilising a PGMA<sub>63</sub> macro-CTA at 20% w/w solids also proved to be unsuccessful when targeting DPs of 1500 or 2000; free-flowing dispersions were obtained under such conditions but conversions proved to be substantially incomplete. Using a low-temperature initiator (2,2'-azobis[2-(2-imidazolin-2-yl)propane]dihydrochloride; VA-044) at 50 °C combined with this longer stabiliser block enabled a final conversion of 84 % to be achieved when targeting a DP<sub>n</sub> of 2000. DMF GPC analysis of this PGMA<sub>39</sub>-PIPGMA<sub>1680</sub> copolymer indicated an M<sub>n</sub> of 203,000 but a relatively broad molecular weight distribution was obtained (M<sub>w</sub>/M<sub>n</sub> = 1.65), which suggests significant loss of RAFT control under such conditions. In summary, the optimal conditions for the RAFT aqueous emulsion polymerisation of IPGMA at 70 °C involves using the PGMA<sub>39</sub> macro-CTA at 20% w/w solids. This formulation reproducibly affords a final conversion of at least 97 % within 2 h when targeting a DP of 1000, which produces an apparent M<sub>n</sub> of around 125 000 g mol<sup>-1</sup> and an M<sub>w</sub>/M<sub>n</sub> of 1.20-1.37 (e.g. see entry 11 in Table 3.1).

### **Deprotection of PGMA-PIPGMA spheres**

It is well-known that acetal protecting groups are readily removed on addition of aqueous acid.<sup>88</sup> Indeed, the industrial manufacture of GMA monomer is achieved via acid-catalysed deprotection of IPGMA<sup>27</sup> and Hoogveen et al. reported the preparation of PGMA-based diblock copolymers from PIPGMA-based precursors via acid hydrolysis at ambient temperature for 72 h.<sup>89</sup> Very recently, Russell and co-workers reported the deprotection of IPGMA residues in a series of polystyrene-PIPGMA (PS-PIPGMA) diblock copolymers using HCl in 1,4-dioxane.<sup>90</sup> Of particular relevance to the present study, a similar strategy was recently utilised by Rimmer and co-workers for the synthesis of sterically-stabilised PS-PGMA latexes from precursor core-shell PS-PIPGMA particles.<sup>73</sup> In this case, acid hydrolysis was conducted in aqueous solution at approximately pH 1 for 4-8 h at 60 °C, but no kinetic studies of the extent of deprotection were reported.

Initial deprotection experiments involved adjusting the solution pH of a 20% w/w aqueous dispersion of PGMA<sub>39</sub>-PIPGMA<sub>1000</sub> nanoparticles to pH 1 via addition of HCl. This acidified turbid dispersion was then stirred for several days at 20 °C but there was no discernible change in its appearance. In principle, successful deprotection of the acetal groups on the hydrophobic PIPGMA block should result in nanoparticle dissolution to form a transparent solution, because the resulting PGMA homopolymer is water-soluble. This transformation was subsequently achieved for the same copolymer formulation by heating to 70 °C at pH 1. It is perhaps worth noting that the volatile acetone by-product (b.p. 56 °C) is removed from the reaction solution at this temperature, which helps to drive the reaction towards completion. The extent of acetal deprotection under such conditions was monitored by extracting aliquots from the reaction dispersion/solution at pre-determined time intervals for analysis by <sup>1</sup>H NMR spectroscopy (in d<sub>7</sub>-DMF), DMF GPC and DLS (see Figures 3.9 and 3.10).

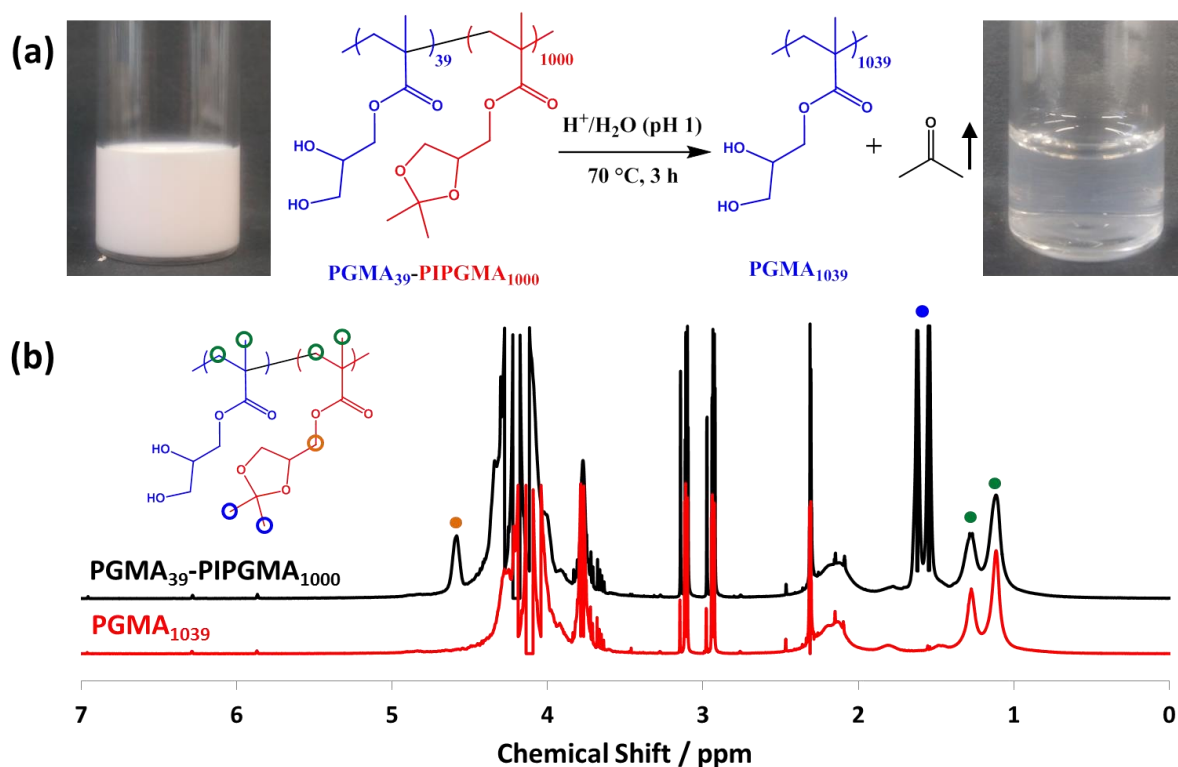


**Figure 3.9.** (a) Reaction scheme for the acid-catalysed deprotection of PGMA<sub>39</sub>-PIPGMA<sub>1000</sub> nanoparticles at 70 °C to afford water-soluble PGMA<sub>1039</sub> chains after 3 h at pH 1. (b) <sup>1</sup>H NMR spectra in d<sub>7</sub>-DMF recorded for the initial PGMA<sub>39</sub>-PIPGMA<sub>1000</sub> nanoparticles and the final water-soluble PGMA<sub>1039</sub> product obtained as a result of this acid-catalysed deprotection.

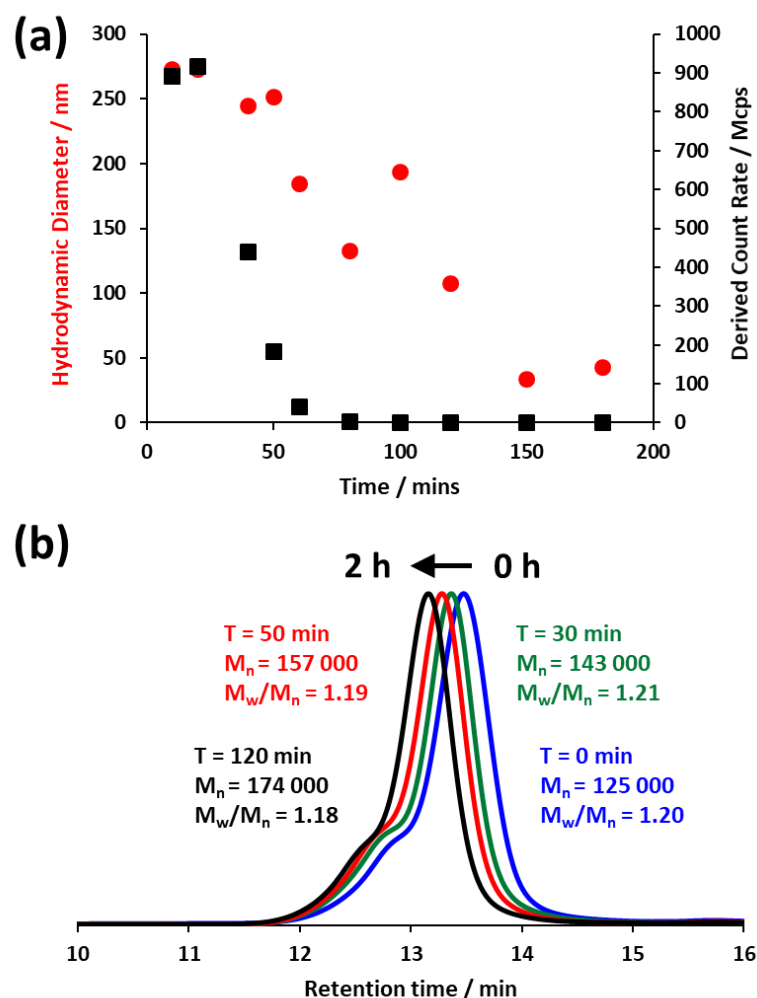


**Figure 3.10.** (a) Gradual reduction in particle size and derived count rate observed during the deprotection of PGMA<sub>39</sub>-PIPGMA<sub>1000</sub> nanoparticles under the conditions described in Figure 4. (b) DMF GPC curves indicating the apparent increase in  $M_n$  and reduction in  $M_w/M_n$  during the acid-catalysed deprotection of PGMA<sub>39</sub>-PIPGMA<sub>1000</sub>.

The disappearance of the pendent methyl proton signals assigned to the IPGMA residues at 1.55 and 1.62 ppm relative to the methacrylic copolymer backbone proton signals at 0.93-1.43 ppm in the <sup>1</sup>H NMR spectra allowed the extent of hydrolysis to be determined during the course of the acetal deprotection reaction. This analysis confirmed that more than 98 % of the acetal groups were removed within 2 h at 70 °C. As expected, the initially turbid dispersion gradually became less opaque and eventually became transparent as water-soluble GMA-rich copolymer chains (and ultimately PGMA homopolymer) were formed towards the end of the reaction. Surprisingly, DMF GPC analysis of the initial PGMA<sub>39</sub>-PIPGMA<sub>1000</sub> diblock copolymer, intermediate copolymers and final PGMA<sub>1039</sub> homopolymer indicated an apparent *increase* in

$M_n$  during acid deprotection. This is clearly an experimental artifact, because the GMA repeat unit ( $160 \text{ g mol}^{-1}$ ) is less massive than the IPGMA repeat unit ( $200 \text{ g mol}^{-1}$ ). Presumably, DMF is a significantly better solvent for the PGMA chains (which hence occupy a larger hydrodynamic volume) than for the PIPGMA chains. It is perhaps also noteworthy that the molecular weight distribution remains essentially unchanged after deprotection, which confirms that no chain scission or cross-linking of the (co)polymer chains occurred under the hydrolysis conditions. Finally, DLS enabled the nanoparticle dissolution process to be conveniently monitored. The initial intensity-average diameter of 270 nm was reduced to just 30 nm within 150 min at 70 °C, while the scattered light intensity (or derived count rate) was reduced by more than two orders of magnitude over this time period. Moreover, the DLS polydispersities exceeded 0.50 after 120 min, which approximately corresponds to the time at which a significant reduction in solution turbidity is observed. Clearly, the size data shown here are rather noisy compared to the scattered light intensity (derived count rate), which most likely indicates the formation of transient, weakly scattering hydrogen-bonded complexes in aqueous solution. Overall, these observations are consistent with complete dissolution of the PGMA<sub>39</sub>-PIP<sub>1000</sub> diblock copolymer nanoparticles to afford molecularly-dissolved PGMA<sub>1039</sub> homopolymer chains.

Deprotection of the IPGMA residues was also examined under milder conditions. A 20 % w/w aqueous dispersion of PGMA<sub>39</sub>-PIP<sub>1000</sub> nanoparticles was adjusted to pH 2 using HCl and heated to 70 °C. As expected, the rate of acid hydrolysis was significantly slower but nevertheless 93 % deprotection was achieved within 10 h (see Figure 3.11). This presents a facile deprotection method for such polymers where the reaction conditions can be made less harsh, albeit at the expense of longer reaction times.

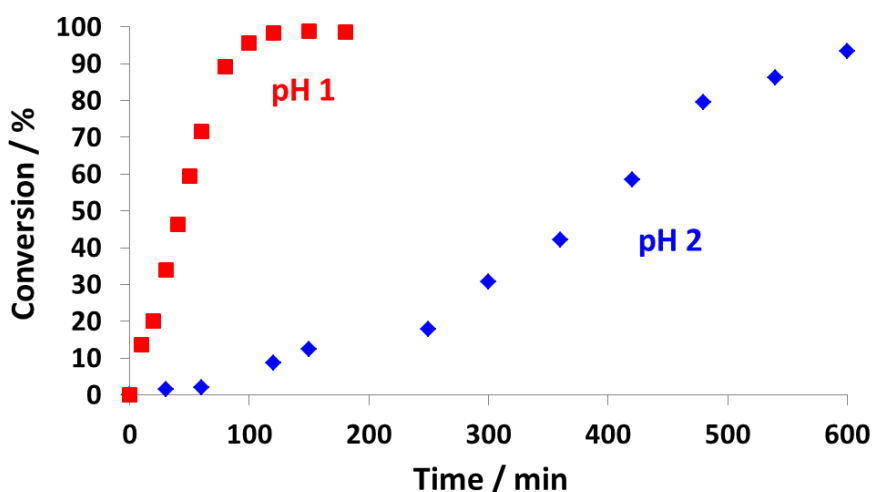


**Figure 3.11.** Conversion against time curves determined for the acid hydrolysis of a 20% w/w aqueous dispersion of PGMA<sub>39</sub>-PIPGMA<sub>1000</sub> nanoparticles at 70 °C by <sup>1</sup>H NMR spectroscopy: (a) at pH 1 (red squares) and pH 2 (blue diamonds).

### One-pot polymerisation and deprotection protocol

Given that the RAFT aqueous emulsion polymerisation and subsequent acid hydrolysis are both performed in aqueous solution at 70 °C, the feasibility of developing a convenient one-pot polymerisation and deprotection route to high molecular weight PGMA homopolymers was examined, as outlined in Figure 3.12. Thus, IPGMA was polymerised using the same PGMA<sub>39</sub> macro-CTA targeting a DP<sub>n</sub> of 1000 for the PIPGMA. After 6 h, an aliquot of the resulting turbid dispersion was extracted for analysis by <sup>1</sup>H NMR, and DLS. The former technique indicated more than 99% conversion and the latter suggested the presence of relatively uniform nanoparticles (338 nm, polydispersity = 0.053). DMF GPC analysis indicated an M<sub>n</sub> of 128,000 and an M<sub>w</sub>/M<sub>n</sub> of 1.37, which indicates a somewhat broader molecular weight distribution than that reported in Table 3.1 (see entry 11) but still suggests reasonable RAFT control. This hot 20 % w/w aqueous dispersion was then exposed to air and immediately adjusted to pH 1 using HCl. The reaction temperature was maintained at 70 °C for a further 3 h before taking an aliquot from the resulting transparent solution for analysis. <sup>1</sup>H NMR spectroscopy indicated more than 99 % acetal deprotection, while both DLS studies and visual inspection confirmed loss of the original nanoparticles (see Figure 3.9, 3.10 and Figure 3.12, respectively). Finally, DMF GPC analysis of the final water-soluble PGMA<sub>1039</sub> homopolymer obtained after an overall reaction time of 9 h at 70 °C had an M<sub>n</sub> of 154 000 and an M<sub>w</sub>/M<sub>n</sub> of 1.42.

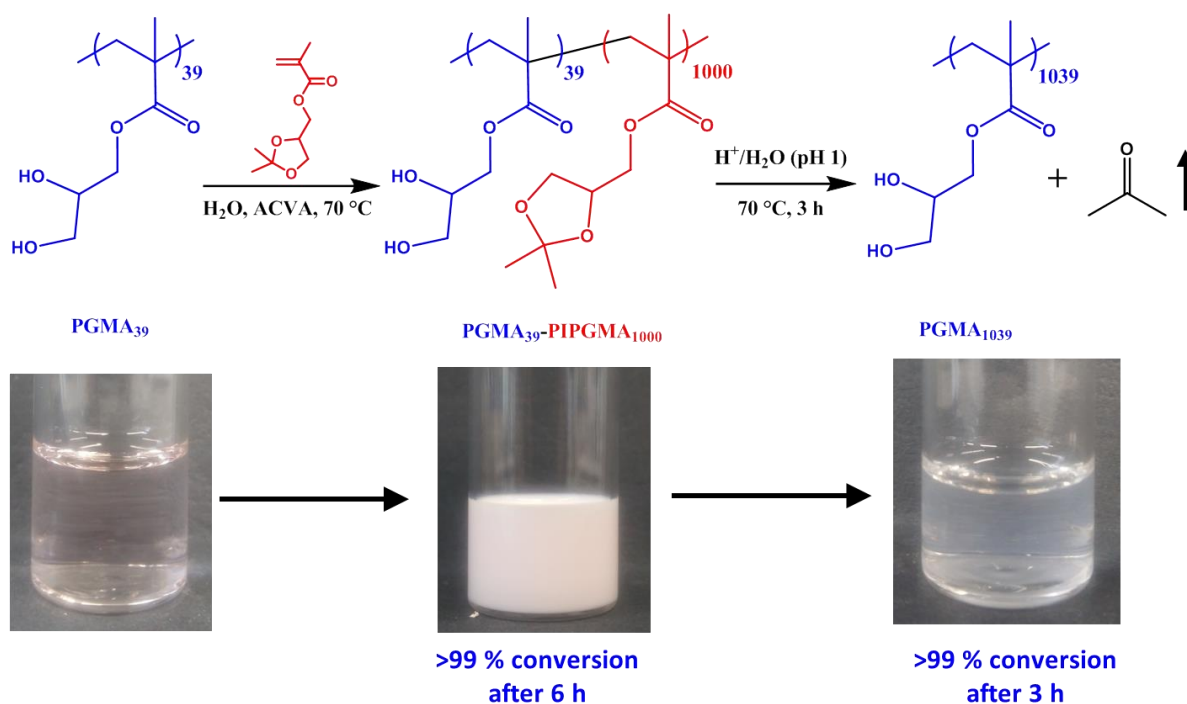


**Figure 3.12.** A one-pot wholly aqueous synthetic protocol for the preparation of high molecular weight PGMA starting from a PGMA<sub>39</sub> macro-CTA at 20% w/w solids. First, RAFT aqueous emulsion polymerisation of IPGMA is conducted at 70 °C to produce PGMA<sub>39</sub>-PIP-GMA<sub>1000</sub> nanoparticles at pH 4 and then acid hydrolysis of the IPGMA residues is conducted at the same temperature at pH 1. The latter deprotection reaction leads to nanoparticle dissolution and the formation of a transparent aqueous solution comprising water-soluble PGMA<sub>1039</sub> chains.

#### Advantages over conventional solution polymerisation

As described above, a wholly aqueous two-step one-pot synthetic route to high molecular weight water-soluble PGMA has been developed. At this point, it is pertinent to ask whether this strategy offers any useful advantage(s) over the RAFT aqueous solution polymerisation of GMA. Thus, the RAFT aqueous solution polymerisation of GMA was conducted using the same GMA concentration (16 % w/w solids) as that achieved after acid hydrolysis of the PGMA<sub>39</sub>-PIP-GMA<sub>1000</sub> nanoparticles. To circumvent its limited water solubility, the CPDB RAFT agent was first dissolved in GMA monomer prior to addition of water and ACVA to make up the initial reaction solution. Aliquots were periodically taken for <sup>1</sup>H NMR and DMF GPC analysis to determine the kinetics of GMA polymerisation and hence enable a direct comparison to be made with the overall time scale required for the two-step one-pot protocol utilising the precursor PGMA<sub>39</sub>-PIP-GMA<sub>1000</sub> nanoparticles (see Figure 3.13).

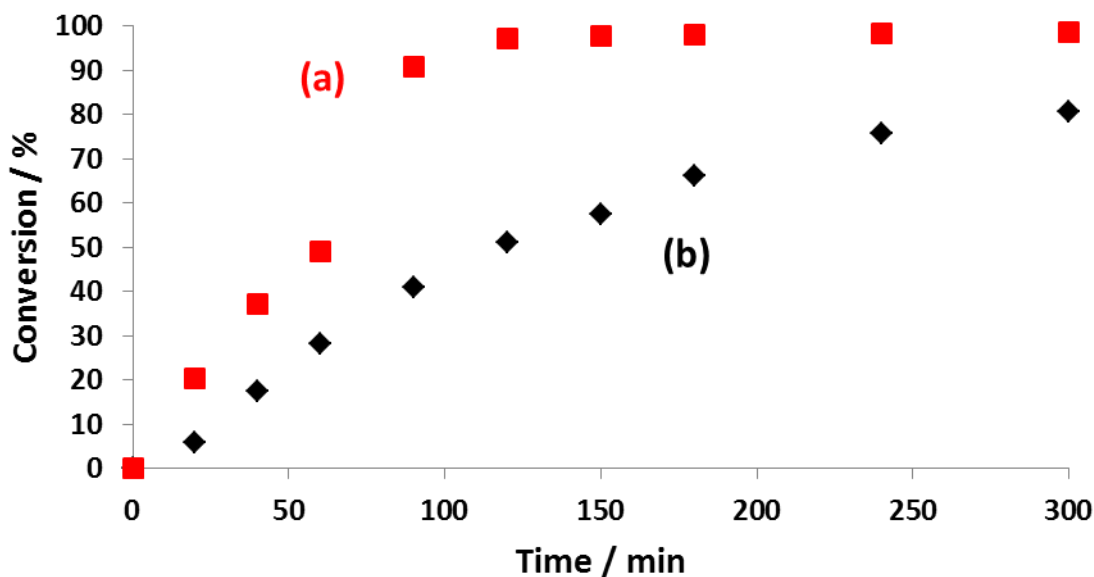


**Figure 3.13.** Conversion vs. time plots obtained for (a) PGMA<sub>39</sub>-PIPGMA<sub>1000</sub> nanoparticles prepared by RAFT aqueous emulsion polymerisation of IPGMA (red squares) and (b) PGMA<sub>1000</sub> prepared via RAFT aqueous solution polymerisation of GMA (black diamonds). Both syntheses were conducted at 70 °C using identical molar concentrations of monomer (either IPGMA or GMA); this corresponds to 16 % w/w solids for the PGMA<sub>1000</sub> chains and 20% w/w solids for the PGMA<sub>39</sub>-PIPGMA<sub>1000</sub>. The loss of the acetone protecting group during acid hydrolysis of the IPGMA residues in the latter synthesis accounts for the difference in solids content.

The RAFT solution polymerisation of GMA (targeting PGMA<sub>1000</sub>) proceeded to 81 % conversion within 5 h at 70 °C, whereas the RAFT emulsion polymerisation of IPGMA (targeting PGMA<sub>39</sub>-PIPGMA<sub>1000</sub>) attained 97 % conversion within 2 h at the same temperature. It is well-known that emulsion polymerisations typically proceed significantly faster than the equivalent solution polymerisation.<sup>80,91</sup> This rate acceleration is attributed to compartmentalisation, which reduces the instantaneous number of propagating polymer radicals per growing nanoparticle and hence lowers the rate of termination relative to that of propagation.<sup>74,75</sup> This homopolymer had an  $M_w/M_n$  of 1.27 at 81 % conversion (see Figure 3.14), which is somewhat higher than that achieved for the final PGMA<sub>1039</sub> homopolymer obtained via the RAFT aqueous emulsion polymerisation of IPGMA ( $M_w/M_n = 1.20$  at 97 % conversion).

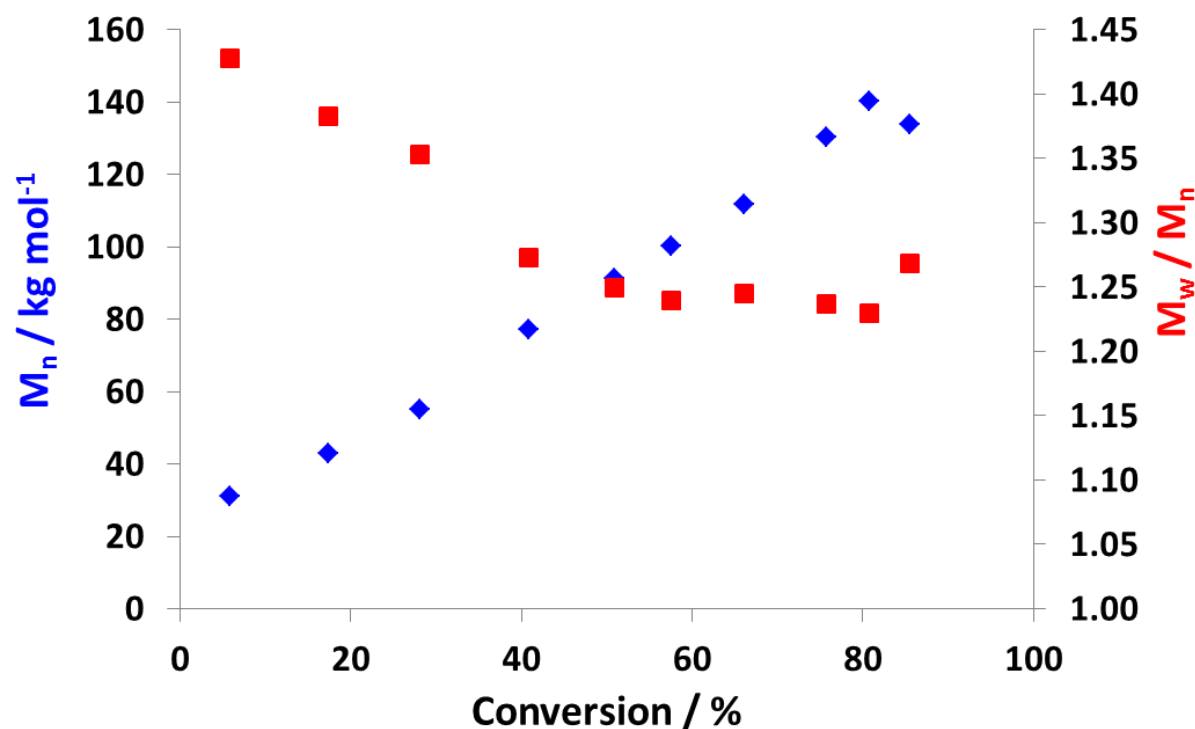


**Figure 3.14.** Evolution of  $M_n$  and  $M_w/M_n$  with monomer conversion as determined by DMF GPC for the RAFT aqueous solution homopolymerisation of GMA at 70 °C when targeting a PGMA DP of 1000 at 16% w/w solids.

Importantly, the overall time scale required for the synthesis of PGMA<sub>1039</sub> chains using the two-step one-pot synthesis protocol is significantly shorter than that required for the RAFT aqueous solution polymerisation of GMA. Assuming that first-order rate kinetics holds for this solution polymerisation (which is the best case scenario), a further 5.5 h at 70 °C would be required to achieve 97 % conversion. Thus it is clear that significantly higher final monomer conversions can be achieved using the former route within shorter overall reaction times.

Finally, rheological studies were performed to compare the viscosity of the aqueous solution of PGMA<sub>1000</sub> to that of the aqueous dispersion of PGMA<sub>39</sub>-PIPGMA<sub>1000</sub> nanoparticles. In addition, the final water-soluble PGMA<sub>1039</sub> homopolymer obtained after acid hydrolysis of the PGMA<sub>39</sub>-PIPGMA<sub>1000</sub> nanoparticles was also examined (see Figure 3.15).



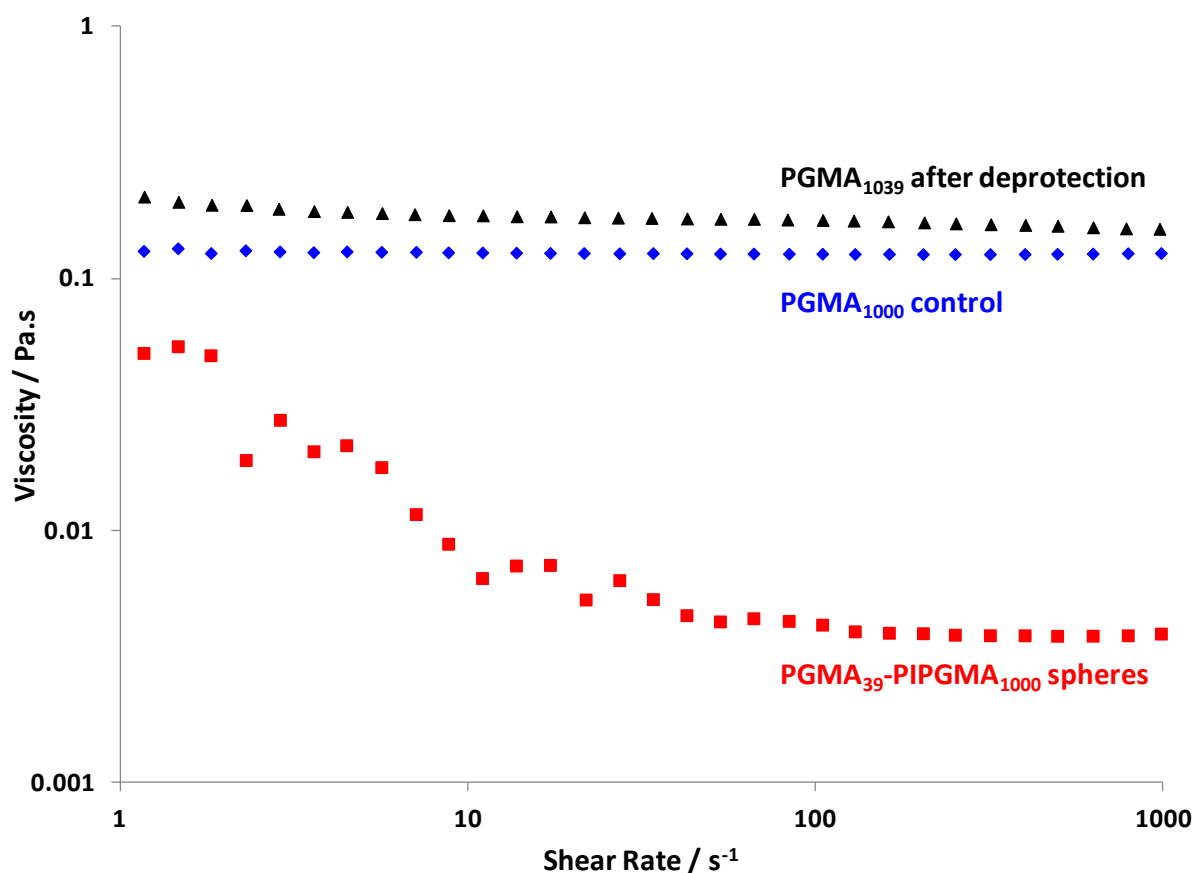


**Figure 3.15.** Viscosity vs. shear rate curves obtained for: (a) a 16% w/w aqueous solution of PGMA<sub>1000</sub> prepared via RAFT solution polymerisation of GMA (blue diamonds); (b) a 20% w/w aqueous dispersion of PGMA<sub>39</sub>-PIPGMA<sub>1000</sub> nanoparticles prepared via RAFT emulsion polymerisation of IPGMA (red squares); (c) a 16% w/w aqueous solution of PGMA<sub>1039</sub> obtained after acid hydrolysis of a 20% w/w aqueous dispersion of PGMA<sub>39</sub>-PIPGMA<sub>1000</sub> nanoparticles (black triangles). Rheological measurements were performed at 20 °C and the differing solids concentrations correspond to approximately equimolar polymer concentrations.

The 20 % w/w aqueous dispersion of PGMA<sub>39</sub>-PIPGMA<sub>1000</sub> nanoparticles exhibits a significantly lower viscosity than either of the two PGMA homopolymer solutions across the entire range of shear rates investigated ( $10^1$ - $10^3$  s<sup>-1</sup>). Interestingly, an approximately Newtonian response is displayed by both these water-soluble homopolymers under these conditions, whereas shear-thinning behaviour might have been expected.<sup>92,93</sup> This could be simply because the range of shear rates examined in the present study is too narrow. Alternatively, it may indicate extensive inter-chain interactions (e.g. hydrogen bonding). In addition, the upturn observed at low shear rates for the PGMA<sub>39</sub>-PIPGMA<sub>1000</sub> dispersion suggests weakly interacting nanoparticles. In summary, the one-pot synthesis of high molecular weight water-

soluble PGMA via precursor PGMA-PIPGMA nanoparticles can be conducted with faster kinetics, higher final monomer conversions and lower viscosities than those achieved during the RAFT aqueous solution polymerisation of GMA. This provides a further example of the advantages offered by PISA formulations compared to conventional polymer syntheses conducted in homogeneous solution.

### Conclusions

RAFT emulsion polymerisation of IPGMA at 70 °C affords well-defined PGMA<sub>39</sub>-PIPGMA<sub>x</sub> diblock copolymer spherical nanoparticles at 20% w/w solids. High final monomer conversions (at least 97%) could be reproducibly obtained when targeting PIPGMA block DPs up to 1000. A monotonic increase in both  $M_n$  and mean particle diameter was observed up to this critical value, with relatively low dispersities ( $M_w/M_n < 1.29$ ) being maintained. However, irreproducible results were obtained when targeting DPs of 1500 or 2000, so a target DP of 1000 appears to represent an upper limit, at least for this specific PISA formulation. Acid hydrolysis of the aqueous *dispersion* of PGMA<sub>39</sub>-PIPGMA<sub>1000</sub> nanoparticles at 70 °C converts almost all (> 98%) of the hydrophobic IPGMA residues into hydrophilic GMA residues within 2 h at pH 1. This leads to nanoparticle dissolution and the formation of an aqueous *solution* of PGMA<sub>1039</sub> homopolymer.

Furthermore, an optimised one-pot protocol was developed whereby a highly viscous aqueous solution of PGMA<sub>1039</sub> can be prepared at 20 % w/w solids within 9 h via the PGMA<sub>39</sub>-PIPGMA<sub>1000</sub> nanoparticles, which act as a low-viscosity precursor. Importantly, the relatively fast kinetics achieved during the RAFT emulsion polymerisation of IPGMA means that the overall time scale for this one-pot synthesis is significantly shorter than that required for the synthesis of PGMA<sub>1039</sub> via RAFT aqueous solution polymerisation, despite the requirement for post-polymerisation deprotection of the IPGMA residues. Moreover, the viscosity of an aqueous dispersion of PGMA<sub>39</sub>-PIPGMA<sub>1000</sub> nanoparticles at 20 % w/w solids is significantly lower than that of PGMA<sub>1000</sub> prepared via RAFT aqueous solution polymerisation. In summary, we report a new wholly aqueous synthetic route to relatively high molecular weight PGMA via RAFT aqueous emulsion polymerisation that offers significant advantages in terms of both overall kinetics and lower viscosity compared to the RAFT aqueous solution polymerisation of GMA.

## References

1. Ginovart, M.; López, D.; Giró, A.; Silbert, M. Flocculation in brewing yeasts: a computer simulation study. *Biosystems* **2006**, *83*, 51.
2. Zhang, D.; Thundat, T.; Narain, R. Flocculation and Dewatering of Mature Fine Tailings Using Temperature-Responsive Cationic Polymers, *Langmuir* **2017**, *33*, 5900
3. Mori, T.; Tsubaki, J.; O'Shea, J. P.; Franks, G. V. Hydrostatic pressure measurement for evaluation of particle dispersion and flocculation in slurries containing temperature responsive polymers, *Chemical Engineering Science* **2013**, *85*, 38.
4. Ng, W. S.; Sonsie, R.; Forbes, E.; Franks, G. V. Flocculation/flotation of hematite fines with anionic temperature-responsive polymer acting as a selective flocculant and collector. *Minerals Engineering* **2015**, *77*, 64.
5. Brostow, W.; Hagg Loblund, H.; Pal, S.; Singh, R. Polymeric flocculants for wastewater and industrial effluent treatment *Journal of Materials Education* **2009**, *31*, 157.
6. Gregory, J. In *Chemistry and Technology of Water-Soluble Polymers*; Finch, C. A., Ed.; Springer US: Boston, MA, 1983, p 307.
7. Lee, C. S.; Robinson, J.; Chong, M. F. A review on application of flocculants in wastewater treatment. *Process Safety and Environmental Protection* **2014**, *92*, 489.
8. Pal, S.; Das, R.; Ghorai, S. In *Cellulose-Based Graft Copolymers*; CRC Press: Boca Raton, 2015, p 301.
9. Sakohara, S.; Nishikawa, K. Compaction of TiO<sub>2</sub> suspension utilizing hydrophilic/hydrophobic transition of cationic thermosensitive polymers. *Journal of Colloid Interface Science* **2004**, *278*, 304.
10. Abdallah/Qasaimh, M. R.; Bani Hani, F.; Dawagreh, A. M. Neutral polyethylene oxide with a cofactor recommended for particle flocculation. *Brazilian Journal of Chemical Engineering* **2011**, *28*, 467.
11. Oveissi, F.; Sitter, T.; Fatehi, P. PDADMAC as a flocculant for lignosulfonate of NSSC pulping process. *Biotechnology Progress* **2016**, *32*, 686.
12. Napper, D. H. *Polymeric stabilisation of colloidal dispersions*; Academic Press Incorporated: London, New York, 1983.
13. Fellows, C. M.; Doherty, W. O. S. Insights into Bridging Flocculation. *Macromolecular Symposia* **2005**, *231*, 1.

14. Hogg, R. Bridging Flocculation by Polymers. *KONA Powder and Particle Journal* **2013**, *30*, 3.
15. Schulz, D. N.; Glass, J. E. *Polymers as Rheology Modifiers*; American Chemical Society, 1991; Vol. 462.
16. Miller, D.; Löffler, M. Rheological effects with a hydrophobically modified polymer. *Colloids and Surfaces A: Physicochemical and Engineering Aspects* **2006**, *288*, 165.
17. Arai, N. Structural analysis of telechelic polymer solution using dissipative particle dynamics simulations. *Molecular Simulation* **2015**, *41*, 996.
18. Ma, S. X.; Cooper, S. L. Shear Thickening in Aqueous Solutions of Hydrocarbon End-Capped Poly(ethylene oxide). *Macromolecules* **2001**, *34*, 3294.
19. Glass, J. E. *Polymers in Aqueous Media*; American Chemical Society, 1989; Vol. 223.
20. Du, Z.; Ren, B.; Chang, X.; Dong, R.; Peng, J.; Tong, Z. Aggregation and Rheology of an Azobenzene-Functionalized Hydrophobically Modified Ethoxylated Urethane in Aqueous Solution. *Macromolecules* **2016**, *49*, 4978.
21. Glass, J. E. The role played by water-soluble polymers in paint performance. Part II: Chemical modeling studies. *Journal of the Oil and Colour Chemists' Association* **1976**, *59*, 86.
22. Farrokhpay, S. A review of polymeric dispersant stabilisation of titania pigment. *Advances in Colloid and Interface Science* **2009**, *151*, 24.
23. Bothe, H.; Tretter, M.; Hagemann, P. US Patent US20140178595A1, **2015**.
24. Kim, J.; Liu, O.; Agresti, J.; Nguyen, A. T. US Patent US9714897B2, **2016**
25. Holland, T. V.; Chang, F.; Haken, U.; Weinschenk, J. I. US Patent US9315669B2, **2016**.
26. Ratcliffe, L. P. D.; Ryan, A. J.; Armes, S. P. From a Water-Immiscible Monomer to Block Copolymer Nano-Objects via a One-Pot RAFT Aqueous Dispersion Polymerization Formulation. *Macromolecules* **2013**, *46*, 769.
27. Save, M.; Weaver, J. V. M.; Armes, S. P.; McKenna, P. Atom Transfer Radical Polymerization of Hydroxy-Functional Methacrylates at Ambient Temperature: Comparison of Glycerol Monomethacrylate with 2-Hydroxypropyl Methacrylate. *Macromolecules* **2002**, *35*, 1152.

28. Hassan, E.; Deshpande, P.; Claeysens, F.; Rimmer, S.; MacNeil, S. Amine functional hydrogels as selective substrates for corneal epithelialization. *Acta Biomaterialia* **2014**, *10*, 3029.
29. Haigh, R.; Rimmer, S.; Fullwood, N. J. Synthesis and properties of amphiphilic networks. 1: the effect of hydration and polymer composition on the adhesion of immunoglobulin-G to poly(laurylmethacrylate-stat-glycerolmonomethacrylate-stat-ethylene-glycol-dimethacrylate) networks. *Biomaterials* **2000**, *21*, 735.
30. Rimmer, S.; German, M. J.; Maughan, J.; Sun, Y.; Fullwood, N.; Ebdon, J.; MacNeil, S. Synthesis and properties of amphiphilic networks 3: preparation and characterization of block conetworks of poly(butyl methacrylate-block-(2,3 propandiol-1-methacrylate-stat-ethandiol dimethacrylate)). *Biomaterials* **2005**, *26*, 2219.
31. Haigh, R.; Fullwood, N.; Rimmer, S. Synthesis and properties of amphiphilic networks 2: a differential scanning calorimetric study of poly(dodecyl methacrylate-stat-2,3 propandiol-1-methacrylate-stat-ethandiol dimethacrylate) networks and adhesion and spreading of dermal fibroblasts on these materials. *Biomaterials* **2002**, *23*, 3509.
32. Patrucco, E.; Ouasti, S.; Vo, C. D.; De Leonardis, P.; Pollicino, A.; Armes, S. P.; Scandola, M.; Tirelli, N. Surface-Initiated ATRP Modification of Tissue Culture Substrates: Poly(glycerol monomethacrylate) as an Antifouling Surface. *Biomacromolecules* **2009**, *10*, 3130.
33. Canton, I.; Warren, N. J.; Chahal, A.; Amps, K.; Wood, A.; Weightman, R.; Wang, E.; Moore, H.; Armes, S. P. Mucin-Inspired Thermoresponsive Synthetic Hydrogels Induce Stasis in Human Pluripotent Stem Cells and Human Embryos. *ACS Central Science* **2016**, *2*, 65.
34. Yuan, J. J.; Armes, S. P.; Takabayashi, Y.; Prassides, K.; Leite, C. A. P.; Galembeck, F.; Lewis, A. L. Synthesis of Biocompatible Poly[2-(methacryloyloxy)ethyl phosphorylcholine]-Coated Magnetite Nanoparticles. *Langmuir* **2006**, *22*, 10989.
35. You, D. G.; Saravanakumar, G.; Son, S.; Han, H. S.; Heo, R.; Kim, K.; Kwon, I. C.; Lee, J. Y.; Park, J. H. Dextran sulfate-coated superparamagnetic iron oxide nanoparticles as a contrast agent for atherosclerosis imaging. *Carbohydrate Polymers* **2014**, *101*, 1225.
36. Deng, R.; Derry, M. J.; Mable, C. J.; Ning, Y.; Armes, S. P. Using Dynamic Covalent Chemistry To Drive Morphological Transitions: Controlled Release of Encapsulated

- Nanoparticles from Block Copolymer Vesicles. *Journal of the American Chemical Society* **2017**, *139*, 7616.
37. Canning, S. L.; Smith, G. N.; Armes, S. P. A Critical Appraisal of RAFT-Mediated Polymerization-Induced Self-Assembly. *Macromolecules* **2016**, *49*, 1985.
38. Warren, N. J.; Armes, S. P. Polymerization-Induced Self-Assembly of Block Copolymer Nano-objects via RAFT Aqueous Dispersion Polymerization. *Journal of the American Chemical Society* **2014**, *136*, 10174.
39. Derry, M. J.; Fielding, L. A.; Armes, S. P. Polymerization-induced self-assembly of block copolymer nanoparticles via RAFT non-aqueous dispersion polymerization. *Progress in Polymer Science* **2016**, *52*, 1.
40. Charleux, B.; Delaittre, G.; Rieger, J.; D'Agosto, F. Polymerization-Induced Self-Assembly: From Soluble Macromolecules to Block Copolymer Nano-Objects in One Step. *Macromolecules* **2012**, *45*, 6753.
41. Cunningham, M. F. Controlled/living radical polymerization in aqueous dispersed systems. *Progress in Polymer Science* **2008**, *33*, 365.
42. Rieger, J. Guidelines for the Synthesis of Block Copolymer Particles of Various Morphologies by RAFT Dispersion Polymerization. *Macromolecular Rapid Communications* **2015**, *36*, 1458.
43. Zetterlund, P. B.; Thickett, S. C.; Perrier, S.; Bourgeat-Lami, E.; Lansalot, M. Controlled/Living Radical Polymerization in Dispersed Systems: An Update. *Chemical Reviews* **2015**, *115*, 9745.
44. Lansalot, M.; Rieger, J.; D'Agosto, F. In *Macromolecular Self-assembly*; John Wiley & Sons, Inc.: Hoboken, New Jersey, 2016, p 33.
45. Rieger, J.; Zhang, W.; Stoffelbach, F.; Charleux, B. Surfactant-Free RAFT Emulsion Polymerization Using Poly(N,N-dimethylacrylamide) Trithiocarbonate Macromolecular Chain Transfer Agents. *Macromolecules* **2010**, *43*, 6302.
46. Truong, N. P.; Quinn, J. F.; Anastasaki, A.; Rolland, M.; Vu, M. N.; Haddleton, D. M.; Whittaker, M. R.; Davis, T. P. Surfactant-free RAFT emulsion polymerization using a novel biocompatible thermoresponsive polymer. *Polymer Chemistry* **2017**, *8*, 1353.
47. Zhang, W.; D'Agosto, F.; Dugas, P.-Y.; Rieger, J.; Charleux, B. RAFT-mediated one-pot aqueous emulsion polymerization of methyl methacrylate in presence of

- poly(methacrylic acid-co-poly(ethylene oxide) methacrylate) trithiocarbonate macromolecular chain transfer agent. *Polymer* **2013**, *54*, 2011.
48. Ferguson, C. J.; Hughes, R. J.; Pham, B. T. T.; Hawkett, B. S.; Gilbert, R. G.; Serelis, A. K.; Such, C. H. Effective ab Initio Emulsion Polymerization under RAFT Control. *Macromolecules* **2002**, *35*, 9243.
49. Binauld, S.; Delafresnaye, L.; Charleux, B.; D'Agosto, F.; Lansalot, M. Emulsion Polymerization of Vinyl Acetate in the Presence of Different Hydrophilic Polymers Obtained by RAFT/MADIX. *Macromolecules* **2014**, *47*, 3461.
50. Etchenausia, L.; Khoukh, A.; Deniau Lejeune, E.; Save, M. RAFT/MADIX emulsion copolymerization of vinyl acetate and N-vinylcaprolactam: towards waterborne physically crosslinked thermoresponsive particles. *Polymer Chemistry*, **2017**, *8*, 2244.
51. Poon, C. K.; Tang, O.; Chen, X.-M.; Kim, B.; Hartlieb, M.; Pollock, C. A.; Hawkett, B. S.; Perrier, S. Fluorescent Labeling and Biodistribution of Latex Nanoparticles Formed by Surfactant-Free RAFT Emulsion Polymerization. *Macromolecular Bioscience* **2017**, *17*, 1600366.
52. Byard, S. J.; Williams, M.; McKenzie, B. E.; Blanazs, A.; Armes, S. P. Preparation and Cross-Linking of All-Acrylamide Diblock Copolymer Nano-Objects via Polymerization-Induced Self-Assembly in Aqueous Solution. *Macromolecules* **2017**, *50*, 1482.
53. Canning, S. L.; Cunningham, V. J.; Ratcliffe, L. P. D.; Armes, S. P. Phenyl acrylate is a versatile monomer for the synthesis of acrylic diblock copolymer nano-objects via polymerization-induced self-assembly. *Polymer Chemistry*, **2017**, *8*, 4811.
54. Wright, D. B.; Touve, M. A.; Adamiak, L.; Gianneschi, N. C. ROMPISA: Ring-Opening Metathesis Polymerization-Induced Self-Assembly. *ACS Macro Letters*, **2017**, *6*, 925.
55. Lesage de la Haye, J.; Zhang, X.; Chaduc, I.; Brunel, F.; Lansalot, M.; D'Agosto, F. The Effect of Hydrophile Topology in RAFT-Mediated Polymerization-Induced Self-Assembly. *Angewandte Chemie* **2016**, *128*, 3803.
56. Tan, J.; Liu, D.; Bai, Y.; Huang, C.; Li, X.; He, J.; Xu, Q.; Zhang, L. Enzyme-Assisted Photoinitiated Polymerization-Induced Self-Assembly: An Oxygen-Tolerant Method for Preparing Block Copolymer Nano-Objects in Open Vessels and Multiwell Plates. *Macromolecules* **2017**, *50*, 5798.

57. Zhang, W.; D'Agosto, F.; Boyron, O.; Rieger, J.; Charleux, B. Toward a Better Understanding of the Parameters that Lead to the Formation of Nonspherical Polystyrene Particles via RAFT-Mediated One-Pot Aqueous Emulsion Polymerization. *Macromolecules* **2012**, *45*, 4075.
58. Boissé, S.; Rieger, J.; Pembouong, G.; Beaunier, P.; Charleux, B. Influence of the stirring speed and CaCl<sub>2</sub> concentration on the nano-object morphologies obtained via RAFT-mediated aqueous emulsion polymerization in the presence of a water-soluble macroRAFT agent. *Journal of Polymer Science Part A: Polymer Chemistry*, **2011**, *49*, 3346.
59. Boisse, S.; Rieger, J.; Belal, K.; Di-Cicco, A.; Beaunier, P.; Li, M.-H.; Charleux, B. Amphiphilic block copolymer nano-fibers via RAFT-mediated polymerization in aqueous dispersed system. *Chemical Communications* **2010**, *46*, 1950.
60. Zhang, X.; Boissé, S.; Zhang, W.; Beaunier, P.; D'Agosto, F.; Rieger, J.; Charleux, B. Well-Defined Amphiphilic Block Copolymers and Nano-objects Formed in Situ via RAFT-Mediated Aqueous Emulsion Polymerization. *Macromolecules* **2011**, *44*, 4149.
61. Cunningham, V. J.; Alswieleh, A. M.; Thompson, K. L.; Williams, M.; Leggett, G. J.; Armes, S. P.; Musa, O. M. Poly(glycerol monomethacrylate)–Poly(benzyl methacrylate) Diblock Copolymer Nanoparticles via RAFT Emulsion Polymerization: Synthesis, Characterization, and Interfacial Activity. *Macromolecules* **2014**, *47*, 5613.
62. Truong, N. P.; Dussert, M. V.; Whittaker, M. R.; Quinn, J. F.; Davis, T. P. Rapid synthesis of ultrahigh molecular weight and low polydispersity polystyrene diblock copolymers by RAFT-mediated emulsion polymerization. *Polymer Chemistry*, **2015**, *6*, 3865.
63. Chaduc, I.; Girod, M.; Antoine, R.; Charleux, B.; D'Agosto, F.; Lansalot, M. Batch Emulsion Polymerization Mediated by Poly(methacrylic acid) MacroRAFT Agents: One-Pot Synthesis of Self-Stabilized Particles. *Macromolecules* **2012**, *45*, 5881.
64. Chaduc, I.; Crepet, A.; Boyron, O.; Charleux, B.; D'Agosto, F.; Lansalot, M. Effect of the pH on the RAFT Polymerization of Acrylic Acid in Water. Application to the Synthesis of Poly(acrylic acid)-Stabilized Polystyrene Particles by RAFT Emulsion Polymerization. *Macromolecules* **2013**, *46*, 6013.



65. Manguian, M.; Save, M.; Charleux, B. Batch Emulsion Polymerization of Styrene Stabilized by a Hydrophilic Macro-RAFT Agent. *Macromolecular Rapid Communications* **2006**, *27*, 399.
66. Fréal-Saison, S.; Save, M.; Bui, C.; Charleux, B.; Magnet, S. Emulsifier-Free Controlled Free-Radical Emulsion Polymerization of Styrene via RAFT Using Dibenzyltrithiocarbonate as a Chain Transfer Agent and Acrylic Acid as an Ionogenic Comonomer: Batch and Spontaneous Phase Inversion Processes. *Macromolecules* **2006**, *39*, 8632.
67. Chaduc, I.; Reynaud, E.; Dumas, L.; Albertin, L.; D'Agosto, F.; Lansalot, M. From well-defined poly(N-acryloylmorpholine)-stabilized nanospheres to uniform mannuronan- and guluronan-decorated nanoparticles by RAFT polymerization-induced self-assembly. *Polymer*, **2016**, *106*, 218.
68. Read, E.; Guinaudeau, A.; James Wilson, D.; Cadix, A.; Violleau, F.; Destarac, M. Low temperature RAFT/MADIX gel polymerisation: access to controlled ultra-high molar mass polyacrylamides. *Polymer Chemistry*, **2014**, *5*, 2202.
69. Cunningham, V. J.; Derry, M. J.; Fielding, L. A.; Musa, O. M.; Armes, S. P. RAFT Aqueous Dispersion Polymerization of N-(2-(Methacryloyloxy)ethyl)pyrrolidone: A Convenient Low Viscosity Route to High Molecular Weight Water-Soluble Copolymers. *Macromolecules* **2016**, *49*, 4520.
70. Cho, M. S.; Yoon, K. J.; Song, B. K. Dispersion polymerization of acrylamide in aqueous solution of ammonium sulfate: Synthesis and characterization. *Journal of Applied Polymer Science* **2002**, *83*, 1397.
71. Anderson, D. R.; Frisque, A. J. US Patent US3624019A, 1971
72. Scherer, M.; Kappel, C.; Mohr, N.; Fischer, K.; Heller, P.; Forst, R.; Depoix, F.; Bros, M.; Zentel, R. Functionalization of Active Ester-Based Polymersomes for Enhanced Cell Uptake and Stimuli-Responsive Cargo Release. *Biomacromolecules* **2016**, *17*, 3305.
73. McKenzie, A.; Hoskins, R.; Swift, T.; Grant, C.; Rimmer, S. Core (Polystyrene)–Shell [Poly(glycerol monomethacrylate)] Particles. *ACS Applied Materials & Interfaces* **2017**, *9*, 7577.
74. Smith, W. V.; Ewart, R. H. Kinetics of Emulsion Polymerization. *The Journal of Chemical Physics* **1948**, *16*, 592.

75. Harkins, W. D. A General Theory of the Mechanism of Emulsion Polymerization. *Journal of the American Chemical Society* **1947**, *69*, 1428.
76. Akpinar, B.; Fielding, L. A.; Cunningham, V. J.; Ning, Y.; Mykhaylyk, O. O.; Fowler, P. W.; Armes, S. P. Determining the Effective Density and Stabilizer Layer Thickness of Sterically Stabilized Nanoparticles. *Macromolecules* **2016**, *49*, 5160.
77. Blanazs, A.; Madsen, J.; Battaglia, G.; Ryan, A. J.; Armes, S. P. Mechanistic Insights for Block Copolymer Morphologies: How Do Worms Form Vesicles? *Journal of the American Chemical Society* **2011**, *133*, 16581.
78. Derry, M. J.; Fielding, L. A.; Warren, N. J.; Mable, C. J.; Smith, A. J.; Mykhaylyk, O. O.; Armes, S. P. In situ small-angle X-ray scattering studies of sterically-stabilized diblock copolymer nanoparticles formed during polymerization-induced self-assembly in non-polar media. *Chemical Science* **2016**, *7*, 5078.
79. Semsarilar, M.; Ladmiral, V.; Blanazs, A.; Armes, S. P. Anionic Polyelectrolyte-Stabilized Nanoparticles via RAFT Aqueous Dispersion Polymerization. *Langmuir* **2012**, *28*, 914.
80. Jones, E. R.; Semsarilar, M.; Wyman, P.; Boerakker, M.; Armes, S. P. Addition of water to an alcoholic RAFT PISA formulation leads to faster kinetics but limits the evolution of copolymer morphology. *Polymer Chemistry* **2016**, *7*, 851.
81. Chaduc, I.; Zhang, W.; Rieger, J.; Lansalot, M.; D'Agosto, F.; Charleux, B. Amphiphilic Block Copolymers from a Direct and One-pot RAFT Synthesis in Water. *Macromolecular Rapid Communications* **2011**, *32*, 1270.
82. Hatton, F. L.; Lovett, J. R.; Armes, S. P. Synthesis of well-defined epoxy-functional spherical nanoparticles by RAFT aqueous emulsion polymerization. *Polymer Chemistry* **2017**, *8*, 4856.
83. Lopez-Oliva, A. P.; Warren, N. J.; Rajkumar, A.; Mykhaylyk, O. O.; Derry, M. J.; Doncom, K. E. B.; Rymaruk, M. J.; Armes, S. P. Polydimethylsiloxane-Based Diblock Copolymer Nano-objects Prepared in Nonpolar Media via RAFT-Mediated Polymerization-Induced Self-Assembly. *Macromolecules* **2015**, *48*, 3547.
84. Cunningham, V. J.; Ning, Y.; Armes, S. P.; Musa, O. M. Poly(N-2-(methacryloyloxy)ethyl pyrrolidone)-poly(benzyl methacrylate) diblock copolymer nano-objects via RAFT alcoholic dispersion polymerisation in ethanol. *Polymer* **2016**, *106*, 189.

85. Moad, G.; Rizzardo, E.; Thang, S. H. Living Radical Polymerization by the RAFT Process – A Third Update. *Australian Journal of Chemistry* **2012**, *65*, 985.
86. Moad, G.; Rizzardo, E.; Thang, S. H. Living Radical Polymerization by the RAFT Process. *Australian Journal of Chemistry* **2005**, *58*, 379.
87. Moad, G.; Rizzardo, E.; Thang, S. H. Living Radical Polymerization by the RAFT Process – A Second Update. *Australian Journal of Chemistry* **2009**, *62*, 1402.
88. Clayden, J.; Greeves, N.; Warren, S. G. *Organic chemistry*; Oxford University Press: Oxford; New York, 2012.
89. Hoogeveen, N. G.; Stuart, M. A. C.; Fler, G. J.; Frank, W.; Arnold, M. Novel water-soluble block copolymers of dimethylaminoethyl methacrylate and dihydroxypropyl methacrylate. *Macromolecular Chemistry and Physics* **1996**, *197*, 2553.
90. Yu, D. M.; Mapas, J. K. D.; Kim, H.; Choi, J.; Ribbe, A. E.; Rzayev, J.; Russell, T. P. Evaluation of the Interaction Parameter for Poly(solketal methacrylate)-block-polystyrene Copolymers. *Macromolecules* **2018**, *51*, 1031–1040.
91. Odian, G. *Principles of Polymerisation, 4th ed.*; Wiley: Hoboken, NJ, 2004
92. Ryder, J. F.; Yeomans, J. M. Shear thinning in dilute polymer solutions. *The Journal of Chemical Physics* **2006**, *125*, 194906.
93. Bird, R. B.; Armstrong, R. C.; Hassager, O. *Dynamics of polymeric liquids. Vol. 1, 2nd Ed. : Fluid mechanics*; John Wiley and Sons Inc., New York, 1987.

**Chapter Four - Synthesis of high molecular weight poly(glycerol monomethacrylate) via conventional aqueous emulsion polymerisation of isopropylidenglycerol methacrylate**

The work carried out in this chapter was 100 % completed by C. P. Jesson

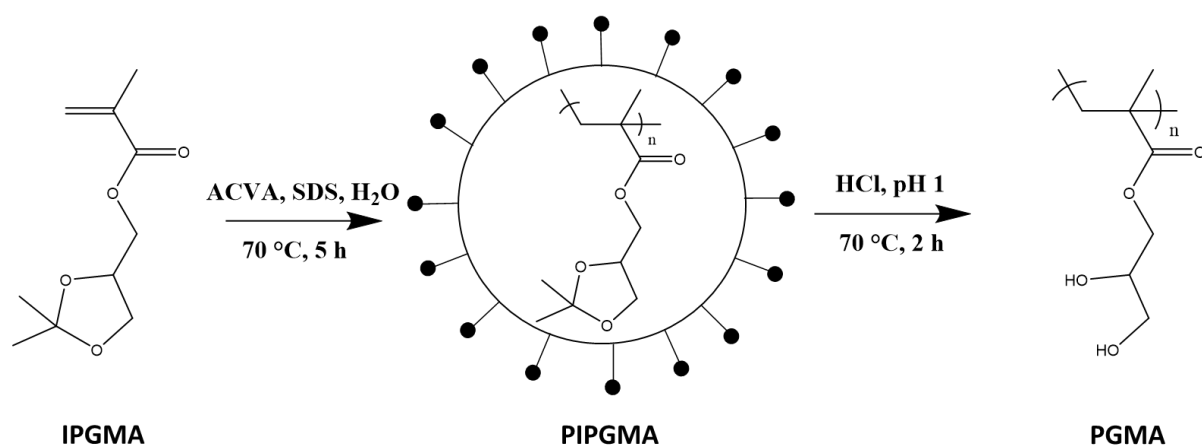
## Introduction

One of GEO's potential customers has expressed an interest in high molecular weight PGMA for use in the form of an aqueous proprietary cleaning formulation. Unfortunately, it is not possible for GEO to simply homopolymerise low diester content GMA derived from the acidic deprotection of IPGMA because this route infringes on an existing patent.<sup>1</sup> Previously, GEO has circumvented this problem by manufacturing GMA by the same route, but polymerising this monomer in aqueous solution. This alternative route produced an aqueous solution of PGMA that met the customer's requirements but nevertheless suffers from inherent limitations associated with the polymerisation conditions. More specifically, the aqueous solution polymerisation of GMA via conventional free radical polymerisation is relatively slow and hence suffers from significant residual monomer: up to 5% GMA remains unreacted after 5 h at 70 °C, with < 1 % levels typically requiring significantly longer reaction times of up to 24 h. In addition, GMA polymerisations conducted above 10% w/w solids result in extremely viscous solutions that are relatively difficult to handle when manufacturing on the multi-kilo scale. Perhaps most importantly, this route still requires acid hydrolysis of IPGMA to afford GMA, with this deprotection reaction being conducted for approximately 48 h at 20 °C to minimise side reactions (e.g. diester formation).<sup>1</sup> If high molecular weight PGMA is targeted, then minimising the diester content of the GMA precursor is essential, otherwise intermolecular cross-linking occurs to produce insoluble material. Unfortunately, this deprotection step represents a severe manufacturing bottleneck which means that GMA is much more expensive than IPGMA (see later).

Given the above technical problems, we sought to develop a new, preferably more cost-effective, synthetic route to high molecular weight PGMA. In Chapter 3, the RAFT aqueous emulsion polymerisation of IPGMA is outlined.<sup>2</sup> Importantly, the resulting PIPGMA latex particles can be readily converted into water-soluble PGMA chains via acid hydrolysis. Moreover, a one-pot protocol was developed that enabled relatively low-dispersity PGMA<sub>1000</sub> ( $M_w/M_n \sim 1.42$ ) to be conveniently prepared within 8 h at 70 °C. However, given the intrinsic colour, relatively high cost and malodour associated with RAFT agents it is unlikely that RAFT polymerisation chemistry would be considered acceptable for the intended cleaning formulation application. Bearing such limitations in mind, the aqueous emulsion polymerisation of IPGMA using conventional free radical polymerisation is explored in the present Chapter. If successful, the resulting PIPGMA latex particles could be converted on

demand into water-soluble PGMA without requiring the synthesis of the relatively expensive GMA monomer. Moreover, using conventional aqueous emulsion polymerisation confers important additional benefits such as a much faster rate of polymerisation than solution polymerisation, significantly lower levels of residual monomer and convenient access to high molecular weight polymer.<sup>3-6</sup> Furthermore, such heterogeneous polymerisations afford low-viscosity dispersions, which can be readily handled at scale prior to deprotection via acid hydrolysis. When performed on a multi-tonne scale, a monomer-starved protocol is typically used when conducting aqueous emulsion polymerisations.<sup>3,7</sup> This approach provides optimal control over the reaction exotherm and enables the efficient dissipation of excess heat. Moreover, such syntheses can be performed at up to 50% w/w solids, which would constitute a significant improvement on the 10% w/w concentration currently used by GEO for the free radical aqueous solution polymerisation of GMA (see above).

Thus, the aqueous emulsion polymerisation of IPGMA via conventional free radical chemistry was explored during a six-month placement at GEO. This formulation involved the use of sodium dodecyl sulfate (SDS) as an anionic surfactant, ACVA as a water-soluble free radical initiator, IPGMA and water (see Scheme 4.1).



**Scheme 4.1.** Synthesis of high molecular weight PGMA by (i) the aqueous emulsion polymerisation of IPGMA using an ACVA azo initiator at 70 °C to produce surfactant-stabilised PIPGMA latex, followed by (ii) acidic hydrolysis of the acetal residues using HCl at the same temperature, which leads to dissolution of the intermediate PIPGMA latex particles.

## **Experimental**

### *Materials*

Glycerol monomethacrylate (GMA, 99.8 %), and isopropylidenglycerol methacrylate (IPGMA, 97.8 %) were donated by GEO Specialty Chemicals (Hythe, UK) and used without further purification. 4,4'-Azobis(4-cyanopentanoic acid) (ACVA, 99 %) and sodium dodecyl sulfate (SDS, 98 %) were purchased from Sigma-Aldrich (UK) and used as received. Deuterated DMF and methanol were purchased from Goss Scientific Instruments Ltd. (Crewe, UK). All other solvents were purchased from Fisher Scientific (Loughborough, UK) and used as received. Deionised water was used for all experiments.

### *Aqueous emulsion polymerisation of IPGMA at pH 3.5 (native solution pH)*

A 500 mL round-bottomed flask was charged with IPGMA (5.00 g), deionised water (100.0 g), SDS (0.500 g) and 4,4'-azobis(4-cyanopentanoic acid) (ACVA; 50.0 mg). This reaction solution was deoxygenated using a N<sub>2</sub> gas sparge for 30 min while immersed in an ice bath. The flask was transferred to a 70°C oil bath and stirred under N<sub>2</sub> for 24 h. Then the flask was allowed to cool to room temperature and exposed to air to quench the polymerisation. This protocol afforded a transparent, viscous solution.

### *Aqueous emulsion polymerisation of IPGMA at pH 6-7*

A 500 mL round-bottomed flask was charged with IPGMA (5.00 g), deionised water (100.0 g), SDS (0.500 g) and 4,4'-azobis(4-cyanopentanoic acid) (ACVA; 50.0 mg). This reaction solution was adjusted to pH 7 by addition of 1 M NaOH prior to deoxygenation using a N<sub>2</sub> gas sparge for 30 min while immersed in an ice bath. The flask was transferred to an oil bath set at 70°C and stirred under N<sub>2</sub> for 24 h. Then the flask was allowed to cool to room temperature and the aqueous dispersion was exposed to air to quench the polymerisation. This protocol afforded a milky-white dispersion.

### *Acid hydrolysis of PIPGMA latexes to afford water-soluble PGMA chains*

The above-prepared PIPGMA aqueous dispersion (20.0 g) was adjusted to pH 1 by adding concentrated HCl. A condenser was added to the flask, which was then submerged in an oil bath set at 70 °C. The clear viscous liquid obtained after 2 h was allowed to cool to room temperature. Solution pH, gravimetry (for solids content) and viscosity measurements were performed at GEO, while samples were further analysed at Sheffield University using <sup>1</sup>H NMR spectroscopy, DMF GPC and DLS (see Table 4.2).

*Monomer-starved aqueous emulsion polymerisation of IPGMA*

SDS (9.375 g), ACVA (3.75 g), deionised water (656.25 g) and 1 M NaOH (approx 7.5 mL) were added to a multi-neck 2L round-bottomed flask and the resulting alkaline aqueous surfactant solution was sparged with nitrogen gas for 30 min, with care being taken to avoid excessive foaming. In a separate flask, IPGMA (90.0 g) was sparged with nitrogen gas for 30 min. Then, a 100 mL syringe was carefully degassed with nitrogen and used to carefully withdraw the degassed IPGMA, without introducing oxygen. This syringe was placed into a syringe pump unit, which was then connected to the 2L reaction flask. The reaction solution in this flask was heated to 70 °C and IPGMA was added via syringe at a constant rate of 28 mL per hour over a 3 h period. Once all the IPGMA (84 mL) had been added, the polymerisation was maintained at 70 °C for a further 2 h to give a total reaction time of 5 h. After this period, the polymerisation was quenched by exposing the hot reaction solution to air before allowing it to cool to 20 °C.

*Kinetic studies of the batch polymerisation of IPGMA*

A 100 mL round-bottomed flask was charged with IPGMA (9.00 g), SDS (0.9375 g), ACVA (0.375 g) and deionised water (65.6 g). The resulting aqueous emulsion was adjusted to pH 7 by adding 1 M NaOH (approx 0.75 mL) and degassed via nitrogen sparge for 30 min. The nitrogen sparge was changed to headspace and an aliquot (approx 1.0 mL) was withdrawn to represent the initial solution. The flask was submerged into an oil bath set at 70 °C and further aliquots were withdrawn by syringe at 20 min intervals. These extracted samples were analysed by <sup>1</sup>H NMR spectroscopy to determine the monomer conversion, by DLS to monitor the *in situ* particle growth and by DMF GPC to examine the evolution in molecular weight. After 5 h, the polymerisation was quenched by exposing the hot reaction solution to air before allowing it to cool to 20 °C.



*Effect of varying the ACVA initiator concentration during the monomer-starved aqueous emulsion polymerisation of IPGMA*

The above protocol for the monomer-starved aqueous emulsion polymerisation of IPGMA was repeated varying amounts of ACVA (0.1875 to 3.75 g, corresponding to ACVA concentrations of 0.024 % to 0.5 % w/w).

*Effect of varying the SDS concentration during the monomer-starved aqueous emulsion polymerisation of IPGMA*

The above protocol for the monomer-starved aqueous emulsion polymerisation of IPGMA was repeated using a fixed mass of ACVA (0.1875 g, corresponding to a constant ACVA concentration of 0.024 % w/w) and varying amounts of SDS (0.4688 to 9.375 g), which correspond to SDS concentrations of 0.06 % to 1.2 % w/w.

*Characterisation Techniques*

*NMR Spectroscopy.* All  $^1\text{H}$  NMR spectra were recorded in either deuterated methanol (for PGMA) or deuterated DMF (for PIPGMA) using a 400 MHz Bruker Avance-400 spectrometer (64 scans averaged per spectrum).

*Gel Permeation Chromatography (GPC).* Polymer molecular weights and dispersities were determined using an Agilent 1260 Infinity GPC system equipped with both refractive index and UV-visible detectors. Two Agilent PL gel 5  $\mu\text{m}$  Mixed-C columns and a guard column were connected in series and maintained at 60 °C. HPLC-grade DMF containing 10 mM LiBr was used as an eluent and the flow rate was set at 1.0 mL min<sup>-1</sup> with DMSO being used as a flow-rate marker. The refractive index detector was used for calculation of molecular weights and dispersities using a series of ten near-monodisperse poly(methyl methacrylate) calibration standards (with  $M_n$  values ranging from 625 to 2,200,000 g mol<sup>-1</sup>).

*Transmission Electron Microscopy (TEM).* As-prepared aqueous PIPGMA dispersions were diluted at 20 °C to generate 0.20 % w/w dispersions. Copper/palladium TEM grids (Agar Scientific, UK) were coated in-house to produce a thin film of amorphous carbon. These grids were then treated with a plasma glow discharge for 30 seconds to create a hydrophilic surface. Each aqueous dispersion (12  $\mu\text{L}$ ; 0.20 % w/w) was placed on a freshly-treated grid for 1 min and then blotted with filter paper to remove excess solution. To stain the deposited latex particles, an aqueous solution of uranyl formate (9  $\mu\text{L}$ ; 0.75% w/w) was placed on the sample-loaded grid via micropipette for 20 s and then carefully blotted to remove excess stain. Each

grid was then carefully dried using a vacuum hose. Imaging was performed using a FEI Tecnai Spirit TEM instrument equipped with a Gatan 1kMS600CW CCD camera operating at 120 kV.

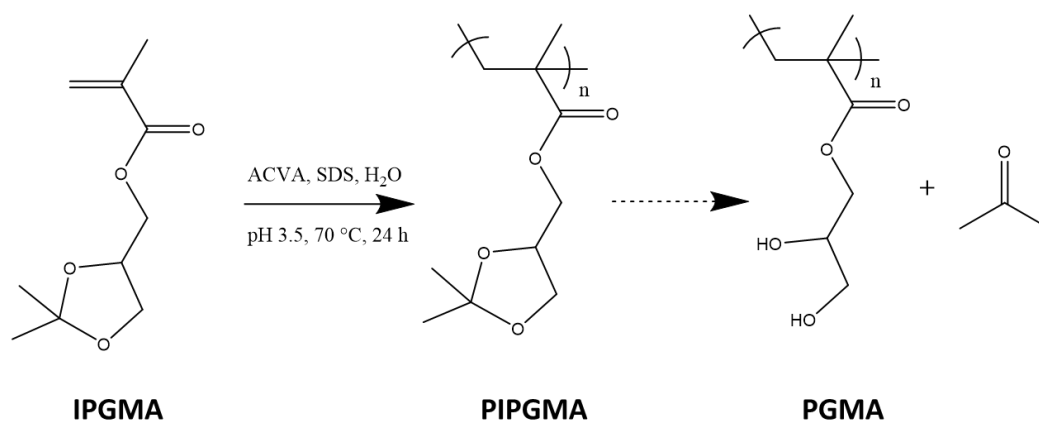
*Gravimetry.* Aqueous dispersions of PIPGMA latex particles (approx. 2.0 g) were placed in vials and allowed to dry at 60 °C within a Heraeus Instruments Vacutherm Oven coupled with a Vacuubrand Hybrid Vacuum Pump at a pressure of less than 50 mmHg. Samples were dried to constant weight prior to calculating monomer conversions.

*Viscosity.* Viscosities were determined using internally-calibrated U-tube viscometers immersed in a water/monoethylene glycol (MEG) bath at 25 °C. Each solution viscosity was an average of three independent measurements.

*Solution pH.* This was determined by immersing a calibrated Metrohm 744 pH meter directly into the aqueous polymer solution.

## **Results and Discussion**

Interestingly, performing the aqueous emulsion polymerisation of IPGMA at pH 3.5 and 10 % w/w unexpectedly afforded a transparent, viscous solution, as opposed to the milky-white low-viscosity latex dispersion that had been expected based on the data reported in Chapter 3. This is because the ACVA initiator ensured that the resulting solution was sufficiently acidic (pH 3.5) that *in situ* deprotection of the initially-formed water-insoluble PIPGMA chains occurred over 24 h at 70 °C to afford high molecular weight water-soluble PGMA chains (see scheme 4.2.). These experiments were also performed at varying solids concentrations and the results are summarised below (see entries 1-4 in Table 4.1). For the sake of comparison, PGMA was also produced via aqueous solution polymerisation of GMA using the same ACVA initiator at 70 °C for 5 h using the in-house protocol developed by GEO (see entries 5-8).



**Scheme 4.2.** Synthesis of high molecular weight PGMA by the aqueous emulsion polymerisation of IPGMA with *in situ* acidic hydrolysis of the acetal residues at 70 °C for 24 h at pH 3.5.

**Table 4.1.** Summary of the effect of varying the monomer concentration on the final monomer conversion, solution viscosity and molecular weight data obtained for two series of PGMA homopolymers produced by either the aqueous emulsion polymerisation of IPGMA with tandem deprotection of the resulting PIPGMA (entries 1-4) or the aqueous solution polymerisation of GMA (entries 5-8). Solution polymerisations were conducted for 5 h at 70 °C, whereas emulsion polymerisations were run for 24 h at the same temperature.

Entry	Concentration / %	Emulsion/Solution	Final pH	Conversion (Gravimetry) / %	Viscosity @ 25 °C / CSt	NMR Conversion / %	$M_n / g\ mol^{-1}$	$M_w / M_n$
1	5	Emulsion	3.9	108	208.9	100	585,000	4.89
2	10	Emulsion	3.7	102	1128	100	242,000	10.87
3	15	Emulsion	3.7	99	10691	100	Not Soluble	
4	20	Emulsion	3.7	79	too high	100	Not Soluble	
5	5	Solution	3.7	92*	12.0	97	220,000	3.61
6	10	Solution	3.6	100	148.6	100	228,000	5.14
7	15	Solution	3.4	108	1308	100	315,000	4.49
8	20	Solution	3.2	87	too high	100	239,000	5.28

\* This experiment was conducted for a shorter reaction time of 4 h at 70 °C.

Each final aqueous solution obtained from the heterogeneous polymerisations had a similar pH of around 3.7 - 3.9, as a result of the weakly acidic ACVA initiator. All polymerisations proceeded to high monomer conversions as judged by <sup>1</sup>H NMR spectroscopy and gravimetry, with the latter technique suffering from random errors as high as 8 %. Significantly higher viscosities were obtained for syntheses conducted at higher polymer concentrations. In general, the water-soluble PGMA chains obtained via aqueous emulsion polymerisation of IPGMA

with tandem deprotection of the PIPGMA residues exhibited higher viscosities than those produced via the aqueous solution polymerisation of GMA. This is not unexpected given that emulsion polymerisation usually favours the generation of higher molecular weight chains.<sup>3,4</sup> <sup>1</sup>H NMR studies conducted in d<sub>7</sub>-DMF confirmed that well-defined PGMA chains with no detectable IPGMA repeat units could be obtained via aqueous emulsion polymerisation of IPGMA (Figure 4.1).

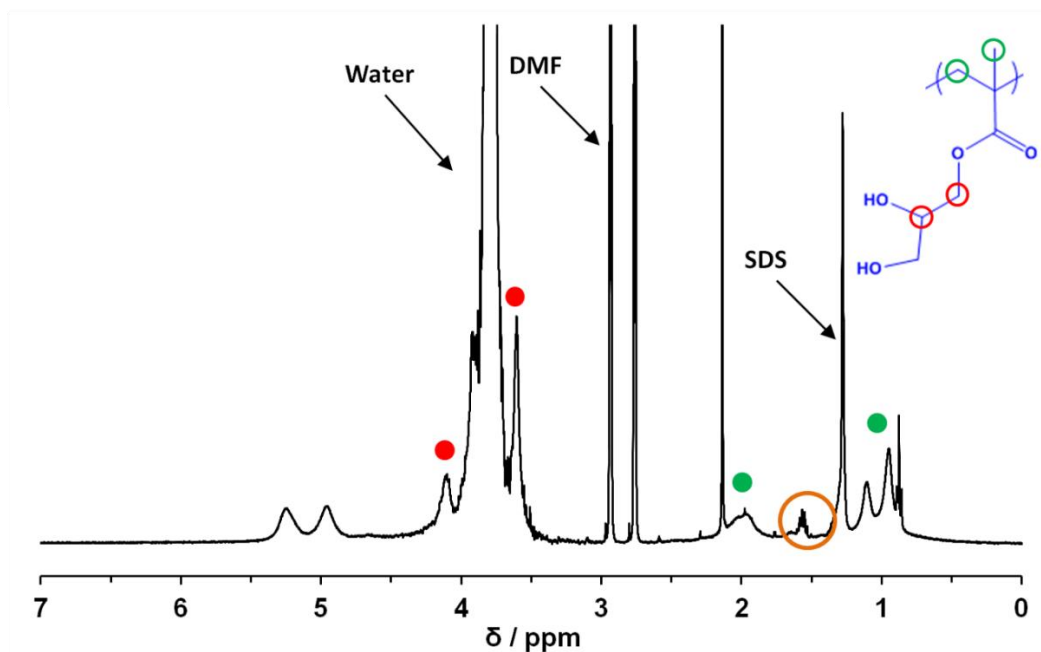


**Figure 4.1.** <sup>1</sup>H NMR spectrum recorded in d<sub>7</sub>-DMF for the product obtained after the aqueous emulsion polymerisation of IPGMA followed by *in situ* acidic hydrolysis of the resulting PIPGMA chains. There is little or no evidence for any IPGMA signals in this spectrum (these signals come at 1.6 ppm – orange circle), suggesting a very high degree of acid hydrolysis and hence the formation of PGMA homopolymer.

DMF GPC studies indicated  $M_n$  values of around 250,000 g mol<sup>-1</sup> and  $M_w$  values in excess of 1,000,000 g mol<sup>-1</sup>. According to GEO, nominal  $M_w$  values should exceed 100,000 g mol<sup>-1</sup> for the intended cleaning formulation application, so these data fulfil this specification. However, visual inspection of the final aqueous solution indicated the presence of a gel fraction for all PGMA homopolymers obtained via the aqueous emulsion polymerisation of IPGMA. Interestingly, this gelation problem was also observed for PGMA homopolymers prepared at higher concentrations (> 10 % w/w solids) via aqueous solution polymerisation when using the GEO in-house protocol. This method presents a highly convenient route to high molecular

weight PGMA but suffers from an extensive reaction time (24 h) and the presence of a gel fraction.

In order to reduce the long reaction times and simultaneously minimise the gel fraction, these aqueous emulsion polymerisation syntheses were repeated with the solution pH being adjusted to 7 by addition of 0.1 M NaOH prior to polymerisation. In such experiments, polymerisations were stirred for only 5 h at 70 °C before quenching, followed by acid hydrolysis at pH 1 for 2 h at the same temperature. A summary of the solution pH, gravimetry and viscosity measurements performed at GEO and <sup>1</sup>H NMR, DMF GPC and DLS analyses conducted at U. Sheffield is shown in Table 4.2 below.

**Table 4.2.** Effect of varying the IPGMA concentration on the final monomer conversion, solution viscosity, molecular weight and particle size data obtained for various PIPGMA latexes produced by free radical emulsion polymerisation of IPGMA (after deprotection of the resulting PIPGMA, where appropriate). Entries 1, 3, 5 and 7 correspond to the aqueous emulsion polymerisation of IPGMA conducted at approximately pH 7 for 5 h at 70 °C. Entries 2, 4, 6 and 8 correspond to the same PIPGMA latexes after their deprotection at pH 1 for 2.5 h at 70 °C to afford water-soluble PGMA chains. Entry 9 is a control experiment involving the aqueous solution polymerisation of GMA at 70 °C for 5 h at around neutral pH.

Entry	Concentration / %	Initial pH	Final pH	Conversion (Gravimetry) / %	Viscosity @ 25 °C / CSt	NMR Conversion / %	M <sub>n</sub> / g mol <sup>-1</sup>	M <sub>w</sub> / M <sub>n</sub>	DLS Diameter / nm	DLS PDI
1	5	7.0	7.1	90	1.078	100	721,000	3.21	83.5	0.04
2	5	1.0			47.1	100	994,000	3.54		
3	10	7.1	6.5	91	1.258	100	987,000	3.63	90.2	0.03
4	10	1.1			794	100	1,600,000	2.96		
5	15	7.0	7.0	90	1.342	Insoluble	717,000	5.26	103.8	0.08
6	15	1.1			Very High	Insoluble	830,000	5.21		
7	20	7.0	5.7	81	1.593	Insoluble	835,000	4.91	105.0	0.07
8	20	1.2			Gel	Insoluble	938,000	5.61		
9	5	7.3	5.4	87	7.099	97	216,000	3.81		

All polymerisations proceeded to high monomer conversions as judged by <sup>1</sup>H NMR spectroscopy (see Figure 4.3) and gravimetry. The resulting milky-white PIPGMA latex dispersions exhibited relatively low viscosities but highly viscous transparent solutions were obtained after acidic deprotection of the IPGMA residues. <sup>1</sup>H NMR studies confirmed that there was no residual IPGMA content for entries 5-8, which suggests the formation of well-defined PGMA chains.

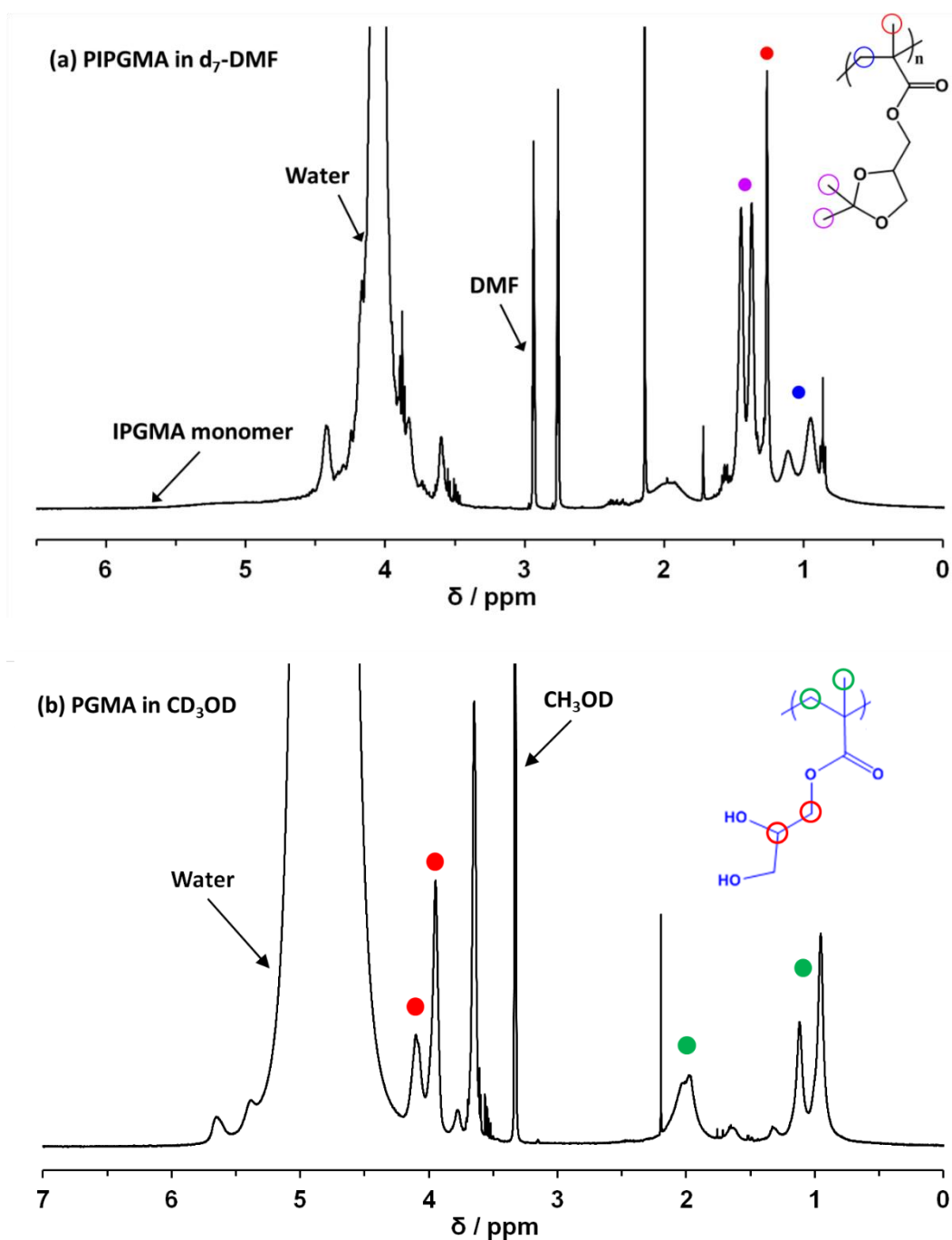


**Figure 4.3.**  $^1H$  NMR spectra showing (a) PIPGMA chains obtained at very high IPGMA conversion after the conventional aqueous emulsion polymerisation of IPGMA at pH 7 (no detectable IPGMA monomer signals at 5.7 and 6.2 ppm) and (b) the water-soluble PGMA obtained after acidic hydrolysis of the PIPGMA latex, showing little or no remaining IPGMA residues.

DMF GPC studies indicated  $M_n$  values of around  $800,000 \text{ g mol}^{-1}$  and  $M_w$  values in excess of  $2,000,000 \text{ g mol}^{-1}$ . The unexpected *increase* in these  $M_n$  values after deprotection is the result of a GPC artefact, as discussed in Chapter 3. However,  $M_w/M_n$  values remained similar after deprotection, indicating preservation of the original molecular weight distribution. Visual inspection confirmed that all polymerisations - either directly or after deprotection - afforded transparent, homogeneous solutions. These results (particularly the molecular weight data and the lack of a gel fraction) are superior to those obtained using the one-pot ‘emulsion polymerisation with tandem deprotection’ protocol conducted at pH 3.5 and may well warrant further scale-up studies in due course.

The two-step ‘aqueous emulsion polymerisation followed by acid hydrolysis’ synthesis (see entry 3 in Table 4.2) and the aqueous solution polymerisation of GMA (control reaction; see entry 6 in Table 4.1) were repeated on a 1.5 kg scale and analysed in the same way as the earlier corresponding syntheses performed on a smaller scale. The results obtained for these additional experiments are summarised in Table 4.3.

**Table 4.3.** Summary of the analysis of PGMA homopolymers produced by (i) the aqueous emulsion polymerisation of IPGMA conducted for 5 h at  $70 \text{ }^\circ\text{C}$  with subsequent acid hydrolysis performed for 2 h at  $70 \text{ }^\circ\text{C}$  (entries 1-3) and (ii) the aqueous solution polymerisation of GMA conducted at approximately pH 2 for 5 h at  $70 \text{ }^\circ\text{C}$  (entry 4). The ACVA initiator concentrations are 1: 2: 4 relative to entry 4 for entries 1-3, respectively. Viscosities were determined for the final deprotected water-soluble PGMA chains, whereas  $M_n$  and  $M_w/M_n$  values were determined for the PIPGMA precursor.

Entry	Concentration / %	Initial pH	Final pH	Conversion (Gravimetry) / %	Viscosity @ $25 \text{ }^\circ\text{C}$ / CSt	NMR Conversion / %	$M_n / \text{g mol}^{-1}$	$M_w / M_n$
1	12.5	7.0			Hazy Gel	> 99	516,000	8.41
2	12.5	7.1			Hazy Gel	> 99	1,170,000	3.73
3	12.5	6.8	4.3	133	Very High			
4	10	acidic	7.4	73	44.79	98	205,000	5.86

The PGMA homopolymer produced by the aqueous solution polymerisation route (entry 4 in Table 4.3) afforded a clear, slightly orange solution with very similar physical properties to the corresponding homopolymer prepared on a smaller scale (see entry 9 in Table 4.2). The scaled-up aqueous emulsion polymerisation of IPGMA (entry 1) gave a very high monomer conversion but a relatively broad molecular weight distribution ( $M_n = 516,000 \text{ g mol}^{-1}$ ;  $M_w/M_n = 8.41$  for the precursor PIPGMA latexes). Unfortunately, deprotection of this PIPGMA precursor yielded a rather hazy viscous gel. This is consistent with the relatively high  $M_w$  ( $> 4$

million) but may also indicate some degree of cross-linking. In order to reduce the molecular weight and viscosity of this polymer, the synthesis was repeated using twice the original initiator concentration (see entry 2 in Table 4.3). In principle, this adjustment should reduce the polymer molecular weight and hence lower the solution viscosity. However, DMF GPC analysis indicated a similarly high  $M_w$  value and acid hydrolysis again afforded a hazy gel. This synthetic protocol was then conducted using an initiator concentration four times higher than that used originally (entry 3). In this latter case, deprotection of the IPGMA residues was conducted under somewhat milder conditions (pH 1, 20 °C for 90 h). The final PGMA homopolymer produced using this modified method was less hazy and had a lower solution viscosity but still remained difficult to handle and dilute in aqueous solution.

An alternative method for reducing molecular weight of polymers during synthesis is to utilise monomer-starved conditions.<sup>3, 7</sup> The lower instantaneous concentration of the IPGMA monomer leads to an overall reduction in the polymer molecular weight.<sup>8</sup> A series of scaled-up syntheses of the aqueous emulsion polymerisation of IPGMA were conducted by feeding this monomer into the reaction flask at various rates of addition. Table 4.4 summarises the data obtained for this series of experiments.

**Table 4.4.** Summary of the effect of varying the rate of monomer addition during the aqueous emulsion polymerisation of IPGMA under monomer-starved conditions (and subsequent deprotection of the resulting PIPGMA latexes to afford water-soluble PGMA homopolymers). Entries 1, 3, 5, 7 and 9 indicate characterisation data obtained for the intermediate PIPGMA latexes, whereas entries 2, 4, 5, 8 and 10 indicate characterisation data obtained for the final PGMA homopolymer after subsequent acid hydrolysis. Each IPGMA polymerisation was run for 5 h at 70 °C (including the monomer addition time). All deprotection reactions were run at approximately pH 1 for 2 h at 70 °C.

Entry	Concentration / %	Addition Rate / mL / h	Addition Over / h	Final pH	Conversion (Gravimetry) / %	Viscosity @ 25 °C / CSt	NMR Conversion / %	$M_n$ / $g\ mol^{-1}$	$M_w$ / $M_n$	DLS Diameter / nm	DLS PDI
1	12.5	21	4.0	6.4	100	1.6	>99	144,000	4.1	45.5	0.21
2	10			1.1		39.55	>99	245,000	3.41		
3	12.5	28	3.0	4.8	95	3.93	>99	232,000	3.12	49.6	0.15
4	10			1.1		47.93	>99	312,000	3.07		
5	12.5	42	2.0	4.7	98	4.59	>99	982,000	1.98	49.9	0.13
6	10			1.1		1208	>99	1,440,000	1.93		
7	12.5	56	1.5	4.8	104	4.14	>99	328,000	3.02	56.1	0.13
8	10			1.0		132.2	>99	409,000	3.28		
9	12.5	84	1.0	4.8	102	4.69	>99	489,000	2.9	66.0	0.19
10	10			1.1		349.8	>99	768,000	2.43		



In principle, a faster rate of monomer addition should produce longer polymer chains and hence increase the solution viscosity. Indeed, quadrupling the rate of addition from 21 mL h<sup>-1</sup> to 84 mL h<sup>-1</sup> results in an increase in both molecular weight as judged by DMF GPC and in solution viscosity for the final water-soluble PGMA homopolymer (from 39.6 CSt to 350 CSt). One notable exception to this is the polymer produced with an addition rate of 42 mLh<sup>-1</sup>. This polymer has an extremely high molecular weight and low dispersity (see Figure 4.4). This particular experiment warrants further investigation to see if it can be replicated.

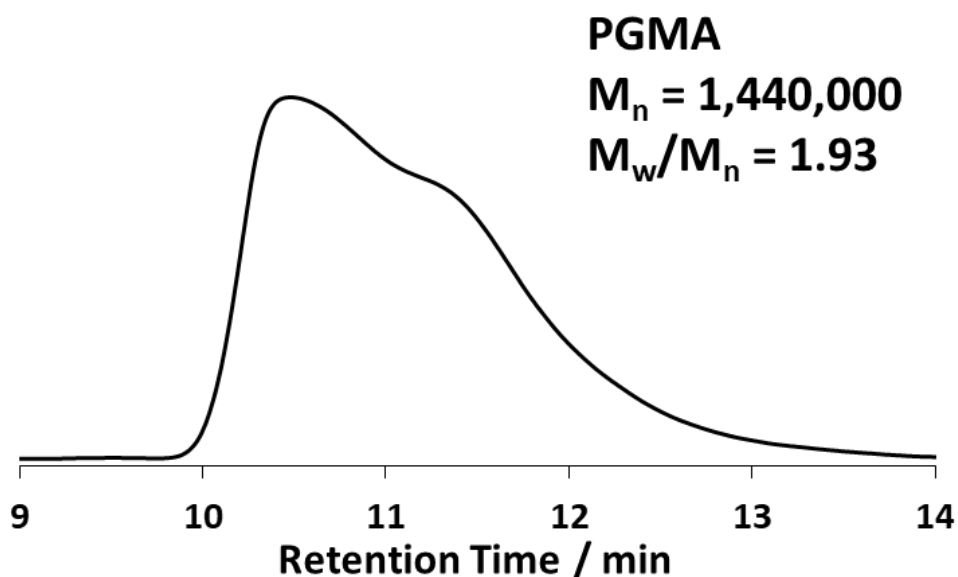


**Figure 4.4.** DMF GPC trace of a PGMA homopolymer produced after the monomer-starved aqueous emulsion polymerisation of IPGMA (42 mL h<sup>-1</sup>, pH 7, 70 °C, 5 h) and subsequent acid hydrolysis of the resulting PIPGMA latex (pH 1, 70 °C, 2 h).

Thus, this provides a convenient means of controlling the polymer molecular weight in such heterogeneous polymerisations. It is also noteworthy that larger PIPGMA latexes are obtained when using higher rates of monomer addition (see Figure 4.5). Importantly, very high IPGMA conversion was achieved for each polymerisation at 70 °C, even for (post-addition) reaction times as short as 1 h. This is consistent with classical studies of the kinetics of aqueous emulsion polymerisation.<sup>5, 7, 9</sup>

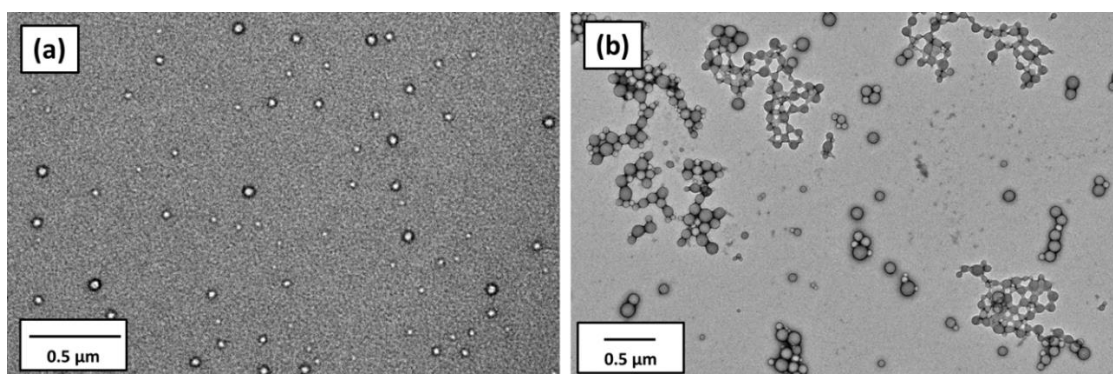


**Figure 4.5.** TEM images of PIPGMA latexes produced by the monomer-starved aqueous emulsion polymerisation of IPGMA. Conditions: (a) Table 4.4 entry 7, 12.5 % solids, 70 °C, 5 h, 56 mL h<sup>-1</sup> (b) Table 4.4 entry 9, 12.5 % solids, 70 °C, 5 h, 84 mL h<sup>-1</sup>

Determining polymerisation kinetics for such reactions is important to determine reaction time-scales. However, monitoring the rate of polymerisation under such monomer-starved polymerisations is complicated by the constant addition of fresh monomer. Therefore, to examine the kinetics of such reactions, the batch emulsion polymerisation of IPGMA was performed at 70 °C, and small aliquots (1 mL) were periodically withdrawn at various time points. The resulting monomer conversion vs. time curve and evolution in DLS particle size over time curve are shown in Figure 4.6.

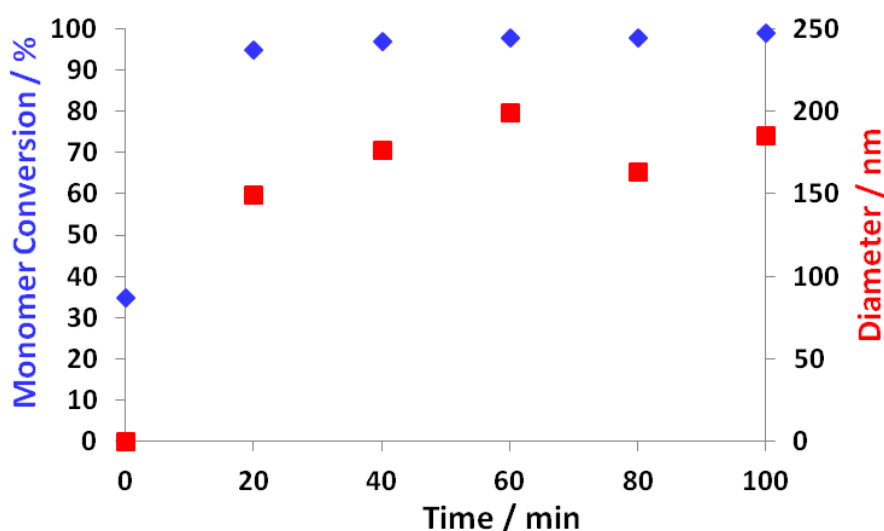


**Figure 4.6.** Monomer conversion vs. time curve (as judged by <sup>1</sup>H NMR spectroscopy) and the evolution of intensity-average particle diameter over time (as judged by DLS) for the batch aqueous emulsion polymerisation of IPGMA at 70 °C. Conditions: Initial pH 7, 12.5% solids.

As expected, the polymerisation of IPGMA under such conditions is extremely rapid, with more than 95 % conversion being achieved within 20 min and more than 99 % conversion within 1 h. Indeed, this polymerisation proceeds at such a fast rate that 35 % conversion was achieved within the short time period required to extract the first aliquot. Such fast kinetics provide some scope to reduce the relatively high initiator concentration utilised in this experiment, which will in turn lead to a higher polymer molecular weight. Of course, varying the rate of monomer addition may be important to compensate for any reduction in initiator concentration.

A series of experiments were performed whereby the IPGMA monomer was added over a 3 h period at a rate of 56 mL h<sup>-1</sup>. The initiator concentration was systematically reduced while keeping the quantities of all other reactants constant. The results are summarised in Table 4.5.

**Table 4.5.** Summary of the final monomer conversions, solution viscosities, molecular weight distribution data and DLS particle size distributions (for both the initial PIPGMA latexes and the corresponding water-soluble PGMA homopolymers obtained via acid hydrolysis) obtained for the aqueous emulsion polymerisation of IPGMA performed under monomer-starved conditions at a rate of IPGMA addition of 56 mL h<sup>-1</sup> for 1.5 h while varying the ACVA initiator concentration. All IPGMA polymerisations were run for 5 h at 70 °C (including the monomer addition time) and the ACVA concentration used for entry 1 was 0.50 % w/w. Acid hydrolyses were performed over 2 h at 70 °C.

Entry	Concentration / %	Relative ACVA Amount / %	Final pH	Conversion (Gravimetry) / %	Viscosity @ 25 °C / Cst	NMR Conversion / %	M <sub>n</sub> / g mol <sup>-1</sup>	M <sub>w</sub> / M <sub>n</sub>	DLS Diameter / nm	DLS PDI
1	12.5	100	4.8	104	4.14	>99	328,000	3.02	56.1	0.13
2	10		1.0		132.2	>99	409,000	3.28		
3	12.5	50	4.8	104	4.62	>99	184,000	4.15	151	0.16
4	10		1.4		65.95	>99	230,000	3.94		
5	12.5	25	6.5	107	1.71	>99	260,000	3.71	69.0	0.17
6	10		1.1		143.1	>99	382,000	3.47		
7	12.5	10	7.0	105	1.65	>99	482,000	3.20	98.2	0.18
8	10		1.0		547.7	>99	666,000	2.93		
9	12.5	5	7.2	108	1.66	>99	746,000	2.71	76.1	0.16
10	10		1.0		1588	>99	Insoluble			

Despite the reduction in initiator concentration, all IPGMA polymerisations proceeded to very high conversion within 5 h as judged by <sup>1</sup>H NMR spectroscopy and gravimetry. However, reducing the initiator concentration increases the molecular weight of the PIPGMA precursor and hence the solution viscosity of the final PGMA aqueous solution. Fortunately, this can be offset (if desired) by lowering the rate of monomer addition (see Table 4.4). One additional

benefit is the reduction in colour achieved when reducing the initiator concentration to 5 % of the original amount (or 0.024 % w/w). Based on this data set, the initiator concentration was kept constant at 0.024 % w/w and the SDS surfactant concentration was optimised. The results are summarised in Table 4.6.

**Table 4.6.** Summary of the final monomer conversions, solution viscosities, molecular weight distribution data and DLS intensity-average diameters and polydispersities (for both the initial PIPGMA latex dispersions and the corresponding water-soluble PGMA homopolymers obtained via acid hydrolysis) achieved for the aqueous emulsion polymerisation of IPGMA performed under monomer-starved conditions at a rate of IPGMA addition of 56 mL h<sup>-1</sup> for 1.5 h while varying the SDS surfactant concentration. All IPGMA polymerisations were run at 70 °C for a total of 5 h (including the monomer addition time) and the SDS concentration used for entry 1 was 1.2 % w/w. All deprotection reactions were performed over 2 h at 70 °C.

Entry	Concentration / %	Relative SDS Amount / %	Final pH	Conversion (Gravimetry) / %	Viscosity @ 25 °C / CSt	NMR Conversion / %	M <sub>n</sub> / g mol <sup>-1</sup>	M <sub>w</sub> / M <sub>n</sub>	DLS Diameter / nm	DLS PDI
1	12.5	100	7.2	108	1.66	>99	746,000	2.71	76.1	0.16
2	10		1.0		1588	>99	Insoluble			
3	12.5	50	7.0	96	1.47	>99	648,000	3.70	47.7	0.13
4	10		1.0		1188	>99	1,640,000	2.28		
5	12.5	25	6.9	105	1.31	>99	Insoluble		108	0.05
6	10		0.8		2296	>99	Insoluble			
7	12.5	10	7.0	100	1.3	>99	Insoluble		101	0.04
8	10		1.0		2361	>99	Insoluble			
9	12.5	5	7.1	105	1.28	>99	Insoluble		133	0.04
10	10		1.0		2085	>99	Insoluble			

Adjusting the surfactant concentration appears to have little effect on either the IPGMA monomer conversion or the aqueous solution viscosity of the final PGMA homopolymer. However, the aqueous dispersions of PIPGMA latex became distinctly more turbid when using less surfactant, which suggests a significant increase in particle size. DLS analysis confirms that there is indeed a systematic increase in particle size on lowering the SDS concentration, as expected (see Figure 4.7). Similar observations have been reported in the literature.<sup>10</sup> Given that the colloidal stability of such latexes was not compromised under such conditions, the lowest surfactant concentration (0.06 % w/w) was used for the final set of experiments.

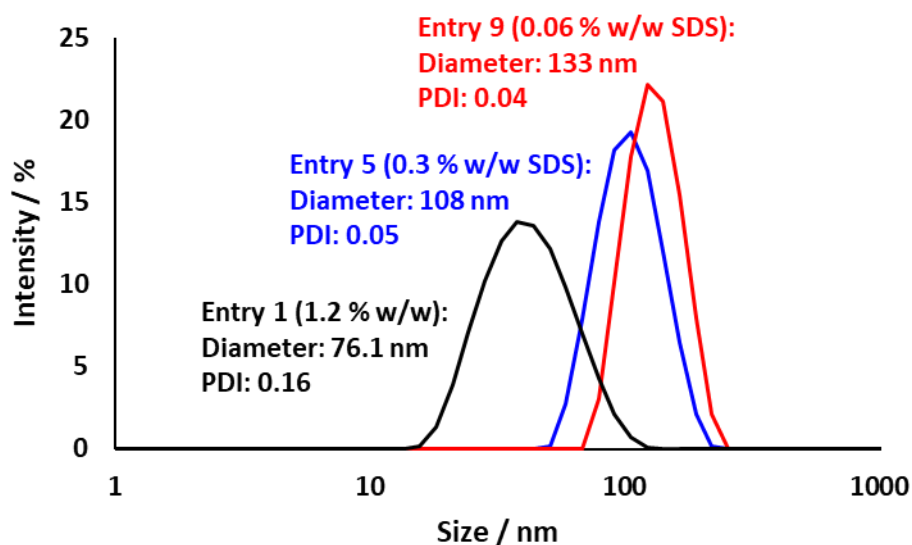


**Figure 4.7.** DLS particle size distributions obtained for the aqueous emulsion polymerisation of IPGMA at 70 °C performed using SDS concentrations ranging from 0.06 % w/w to 1.2 % w/w. Conditions: Initial pH 7, 12.5 % solids.

It is well-known in the literature that emulsion polymerisations can be performed at up to 50 % solids, especially when conducted under monomer-starved conditions.<sup>5, 11-12</sup> If this is the case, it is worth investigating whether the resulting low-viscosity intermediate latexes can be subsequently diluted prior to deprotection via acid hydrolysis to produce final PGMA homopolymers with similar physical properties (i.e. solution viscosity and molecular weight). To examine this possibility, aqueous dispersions of PIPGMA latex were prepared at 12.5, 21.5, 35.4 and 50 % w/w solids using a constant total monomer addition time of 1.5 h. These aqueous dispersions were subsequently diluted before deprotection via acid hydrolysis and the results are summarised in Table 4.7.

**Table 4.7.** Summary of the final monomer conversions, solution viscosities and DLS particle size distributions (for both the initial four PIPGMA latex dispersions and the three corresponding water-soluble PGMA homopolymers obtained via acid hydrolysis) achieved for the aqueous emulsion polymerisation of IPGMA performed under monomer-starved conditions with total IPGMA addition over 1.5 h while varying the IPGMA concentration. All IPGMA polymerisations were run at 70 °C for a total of 5 h (including the monomer addition time) and all deprotection reactions were performed over 2 h at 70 °C. In all cases, the ACVA and SDS concentrations were 0.024 % w/w and 0.06 % w/w, respectively.

Entry	Concentration / %	Initial Latex Concentration / %	Final pH	Conversion (Gravimetry) / %	Viscosity @ 25 °C / CSt	NMR Conversion / %	DLS Diameter / nm	DLS PDI
1	12.5	12.5	7.1	105	1.28	>99	133	0.04
2	10	12.5	1.0		2085	>99		
3	21.5	21.5	6.8	105	1.80	>99	185	0.01
4	17.2	21.5	1.1		Gel	>99		
5	10	21.5	1.0		12500	>99		
6	35.4	35.4	6.7	103	5.05	>99	176	0.02
7	50	50	6.8	103	156.7	>99	161	0.07

Firstly, high monomer conversions were obtained in all cases as judged by gravimetry. Low-viscosity, milky-white homogeneous dispersions were obtained at up to 35.4 % w/w, which appeared to be very similar in appearance to the PIPGMA latexes prepared at lower concentrations. However, this emulsion polymerisation formulation began to show signs of failure when conducted at 50 % w/w solids. More specifically, an insoluble ‘skin’ formed on the top of the polymerising mixture. Thus this concentration appears to represent an upper limit for the aqueous emulsion polymerisation of IPGMA, although it is possible that more efficient stirring might eliminate ‘skin’ formation. For all other emulsion polymerisation syntheses, the PIPGMA latex viscosity remained relatively low. In contrast, the aqueous solution polymerisation of GMA performed at the equivalent polymer concentration invariably resulted in gelation. Acid hydrolysis of the 21.5 % w/w PIPGMA latex was conducted at its initial concentration and also after dilution to 12.5 % w/w. Accounting for the reduction in mass arising from the loss of the acetone protecting group, these experiments should afford final PGMA homopolymer solutions of 17.2 and 10 % w/w, respectively. While deprotection of the 12.5 % w/w latex afforded a significantly lower aqueous solution viscosity than that of the 21.5 % w/w latex (which formed a gel), it was still much higher than the solution viscosity obtained

when deprotecting the latex prepared directly at 12.5% w/w (see entry 1 in Table 4.7). Bearing in mind the high viscosity of this product, the planned deprotection reactions for the 35.4% and 50 % latexes were aborted. In order to increase the final solids concentration while maintaining a constant total monomer addition time, the rate of monomer addition had to be increased. It seems likely that this increase in the rate of monomer addition is responsible for the higher solution viscosity observed for the final PGMA homopolymer. In order to examine this hypothesis, the aqueous emulsion polymerisation of IPGMA should be performed at 50 % w/w solids using a rate of monomer addition of 56 mL h<sup>-1</sup> for a total reaction time of 6 h. However, such additional experiments are beyond the scope of the current study.

### Conclusions

In summary, the aqueous emulsion polymerisation of IPGMA proceeds to high conversion within 24 h at 70 °C using an ACVA initiator and SDS as an anionic surfactant pH 6-7. This protocol affords relatively small latex particles with an intensity-average diameter of 83 - 105 nm, as judged by DLS studies.. Subsequent acidification of such latex dispersions leads to *in situ* acid hydrolysis on heating (pH 1, 70 °C for 2 h) to afford an aqueous transparent viscous solution of water-soluble PGMA. DMF GPC analysis confirms the formation of relatively polydisperse high molecular weight polymer chains ( $M_n = 700,000$  to  $1,000,000$  gmol<sup>-1</sup>;  $M_w/M_n = 3.2$  to  $5.6$ ), while <sup>1</sup>H NMR spectroscopy studies indicate very high levels of acetone deprotection (> 99 %). However, visual inspection of such formulations indicated a significant gel fraction in many cases. It is also noteworthy that if the initial aqueous emulsion is not neutralised using NaOH, the weakly acidic ACVA initiator leads to a native solution of pH 3.5. Perhaps surprisingly, this is sufficient to cause deprotection of the IPGMA residues to occur during the emulsion polymerisation at 70 °C. Thus the product obtained under such acidic conditions is the desired high molecular weight water-soluble PGMA chains in the form of a transparent, highly viscous aqueous solution, rather than a milky-white dispersion of the intermediate PIPGMA latex particles. Unfortunately, the current protocol for this reaction requires a very long reaction time (24 h) and gives rise to some inhomogeneity in the final homopolymer solution. However, this highly convenient one-pot synthesis still warrants further investigation.

Using a monomer-starved protocol eliminated the problem of gel formation and also afforded somewhat better control over the molecular weight distribution. For example, under optimised

conditions it was possible to obtain an  $M_n$  value in excess of one million with an  $M_w/M_n$  below 2.0 (see entry 6 in Table 4.4). However, the reproducibility of such syntheses remains to be established.

Preliminary experiments suggest that systematic reduction of the initiator concentration leads to higher molecular weight polymers (and hence a corresponding increase in solution viscosity) but with relatively little effect on the mean latex diameter. On the other hand, reducing the rate of monomer addition produced significantly lower molecular weight PGMA chains.

As expected, lowering the surfactant concentration by a factor of twenty led to the formation of larger latex particles. However, this parameter appears to have minimal effect on the molecular weight of the final PGMA homopolymer.

According to GEO scientists, the manufacture of IPGMA is an order of magnitude cheaper than that of GMA. Thus, aqueous emulsion polymerisation of the former monomer represents a highly attractive, atom-efficient, one-pot synthetic route to high molecular weight PGMA homopolymer at up to 20% w/w solids. In principle, this new formulation offers substantial advantages in terms of overall cost, handling and throughput compared to the aqueous solution polymerisation of GMA protocol that is currently performed by GEO.

### **Future Work**

One interesting question for the one-pot synthetic protocol performed at pH 3.5 is whether deprotection occurs during or after the IPGMA polymerisation. To address this question, IPGMA could be dispersed as a 10 % SDS-stabilised aqueous emulsion in the absence of any ACVA initiator. This emulsion could be adjusted to pH 3.5 and then heated to 70 °C. Periodic sampling of this emulsion should establish the rate of conversion of IPGMA to GMA and hence indicate whether this deprotection occurs on the same time scale as the IPGMA polymerisation, which is essentially complete within 1 h (albeit at pH 7).

Performing the emulsion polymerisation of IPGMA under monomer-starved conditions avoids the undesirable gel fraction associated with the early batch polymerisation syntheses. It would be interesting to examine whether the same approach could be applied to the one-pot synthesis of PGMA from IPGMA at pH 3.5.

Further optimisation of the aqueous emulsion polymerisation of IPGMA is desirable in terms of the initiator and surfactant concentrations, solution pH, polymerisation temperature and also the rate of monomer addition. The final polymer properties are most likely influenced by each



of these parameters, so identifying an appropriate compromise is important. Moreover, it would be important to establish reproducibility once suitable optimal conditions have been identified. Only at this point should scale-up syntheses be explored.

Adjusting the SDS concentration employed for the aqueous emulsion polymerisation of IPGMA offers a convenient means of targeting polymer latexes of varying mean particle diameter. In view of this particle size control, it would be interesting to examine the effect of particle size on the rate of acid hydrolysis. If acid hydrolysis proceeds via surface erosion, then smaller latex particles (with a higher specific surface area per unit mass) should be converted into water-soluble PGMA chains more quickly. On the other hand, if mineral acid diffuses freely within the precursor latex particles, then perhaps the rate of acid hydrolysis should be more or less independent of the initial latex dimensions.

In principle, the aqueous emulsion polymerisation of IPGMA can be conducted at up to 50% w/w solids while maintaining a relatively low dispersion viscosity at around neutral pH. Subsequently, such concentrated dispersions can be diluted to ~10 % w/w prior to acid hydrolysis to afford aqueous solutions of high molecular weight PGMA as desired. However, further experiments need to be conducted under monomer-starved conditions to establish the effective upper limit solids for this formulation. The resulting PGMA chains should be analysed by DMF GPC to ensure that more intensive reaction concentrations do not adversely affect their molecular weight distribution (and hence their solution viscosity) or lead to larger gel fractions.

If such high molecular weight PGMA homopolymers were to be used in cleaning formulations, there is a potential opportunity to replace the SDS surfactant with whatever ionic or non-ionic surfactants are used in the commercial cleaning formulation itself. This should ensure that the polymer synthesis was fully compatible with this commercial product. In principle, the IPGMA polymerisation (and its subsequent deprotection) could become an initial step when producing such cleaning formulations.

## References

1. McKenna, P.; Smallridge, M.; Matthews, M.; Roberts, S.; US Patent US20100249352A1, 2010.
2. Jesson, C. P.; Cunningham, V. J.; Smallridge, M. J.; Armes, S. P., Synthesis of High Molecular Weight Poly(glycerol monomethacrylate) via RAFT Emulsion Polymerization of Isopropylidenglycerol Methacrylate. *Macromolecules* **2018**, *51* (9), 3221-3232.
3. Antonietti, M.; Tauer, K., 90 Years of Polymer Latexes and Heterophase Polymerization: More vital than ever. *Macromolecular Chemistry and Physics* **2003**, *204* (2), 207-219.
4. Gilbert, R. G., *Emulsion polymerization: a mechanistic approach*. Academic Press: London, 1995.
5. Smith, W. V.; Ewart, R. H., Kinetics of Emulsion Polymerization. *The Journal of Chemical Physics* **1948**, *16* (6), 592-599.
6. Arshady, R., Suspension, emulsion, and dispersion polymerization: A methodological survey. *Colloid and Polymer Science* **1992**, *270* (8), 717-732.
7. Lovell, P. A.; El-Aasser, M. S., *Emulsion Polymerization and Emulsion Polymers*. Wiley: Hoboken, NJ, 1997.
8. Matyjaszewski, K.; Gnanou, Y.; Leibler, L., *Macromolecular Engineering: Precise Synthesis, Material Properties, Applications*. Wiley: 2007; Vol. 1.
9. Harkins, W. D., A General Theory of the Mechanism of Emulsion Polymerization I. *Journal of the American Chemical Society* **1947**, *69* (6), 1428-1444.
10. Dupin, D.; Fujii, S.; Armes, S. P.; Reeve, P.; Baxter, S. M., Efficient Synthesis of Sterically Stabilized pH-Responsive Microgels of Controllable Particle Diameter by Emulsion Polymerization. *Langmuir* **2006**, *22* (7), 3381-3387.
11. Odian, G., *Principles of Polymerization*. Wiley: Hoboken, NJ, 2004.
12. Ruckenstein, E., Concentrated emulsion polymerization. In *Polymer Synthesis/Polymer Catalysis*, Springer Berlin Heidelberg: Berlin, Heidelberg, 1997; pp 1-58.

# **Chapter Five – Synthesis and characterisation of aldehyde-functional homopolymers, block copolymers and brushes**

The work carried out in this chapter was at least 90 % completed by C. P. Jesson

The rest of the work in this chapter was carried out by Dr. N. J. Warren

## Introduction

Aldehydes are highly versatile functional groups that can react with various reagents. Some common examples are reduction of aldehydes to give primary alcohols, oxidation of aldehydes to give carboxylic acids, nucleophilic attack, Schiff-base reactions with amines to give imines or reactions with cis-diols to give (hemi)acetals.<sup>1-2</sup>

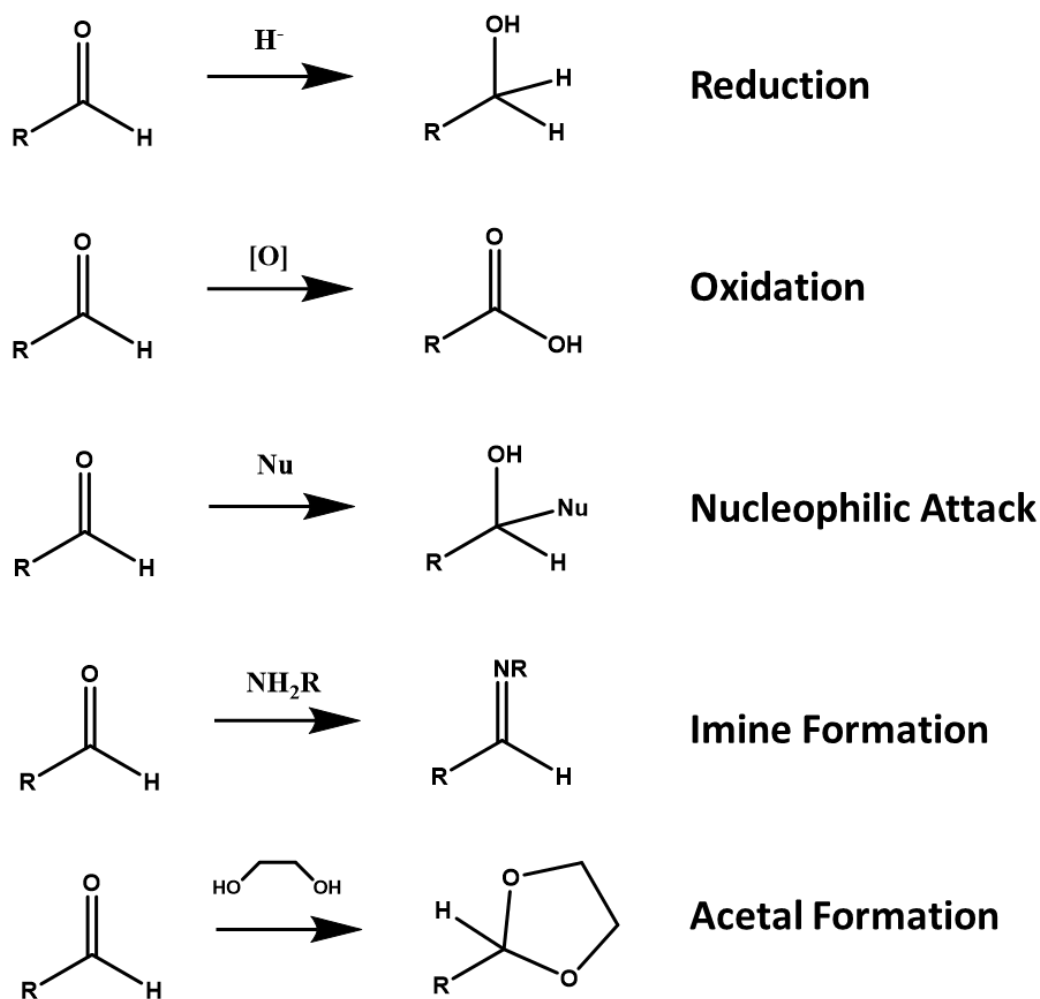


**Figure 5.1.** Examples of common reactions of aldehydes<sup>1-2</sup>

Given this chemical diversity, the design of aldehyde-functional polymers should be of significant interest. Indeed, there are many examples of hydrophobic aldehydic vinyl monomers, but examples of water-soluble aldehyde-functional monomers are rather rare. There is good literature precedent to suggest that the terminal cis-diol group in water-miscible monomers such as GMA could be readily converted into an aldehyde using a selective oxidant

such as sodium periodate.<sup>3</sup> Preliminary data obtained by a former Armes group post-doc (Dr. N. J. Warren) indicated that this oxidative transformation could be achieved for PGMA but the resulting homopolymer was no longer water-soluble (and appeared to be chemically cross-linked). In this context, it is well known that monomers containing oligo(ethylene glycol) (OEG) side-chains such as OEGMA are water-soluble. Within the last five years or so, GEO has augmented their monomer palette by designing a new methacrylic monomer, GEO5MA. This hybrid monomer comprises (on average) five EG units separating the methacrylate backbone unit from the cis-diol end-group. Thus, GEO5MA combines the structural features found in GMA and OEGMA (see Figure 5.2 for the chemical structures of these three monomers). The physicochemical properties of GEO5MA and its corresponding homopolymer are as yet unexplored, although the latter is expected to be water-soluble. Moreover, the additional OEG side-chain may enable the same periodate transformation to be applied to GEO5MA with retention of its water solubility (unlike GMA). If this hypothesis is correct, this would constitute a rare example of a water-soluble aldehydic vinyl monomer. In principle, this could provide access to a wide range of aldehyde-functionalised water-soluble polymers, block copolymer nanoparticles and polymer brushes.

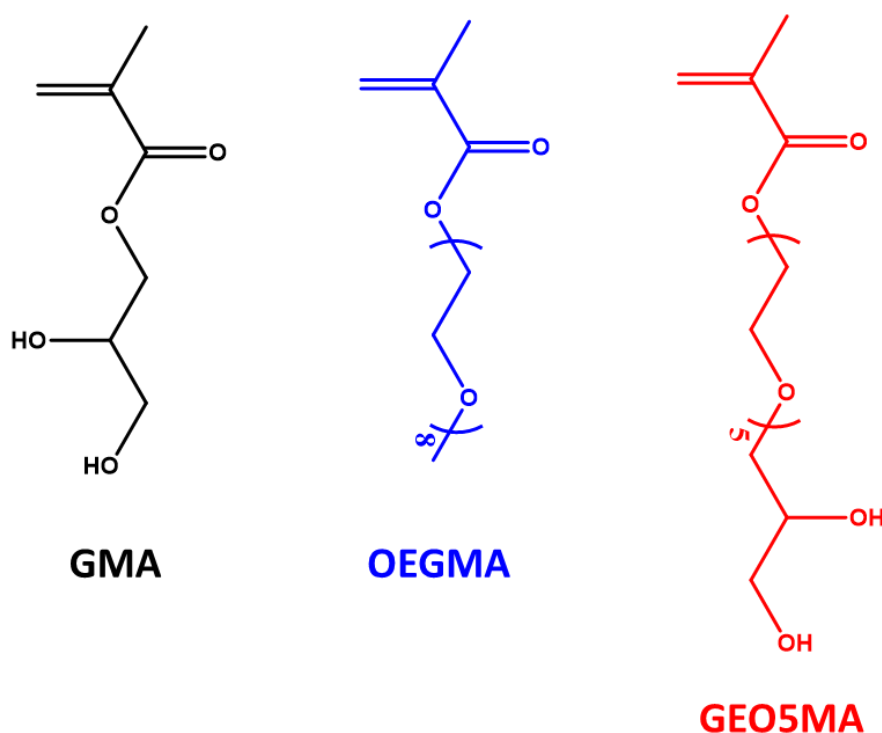


**Figure 5.2.** Chemical structures for three GEO monomers: GMA, OEGMA and GEO5MA.

Thus, the synthesis of GEO5MA was conducted on a kilo scale during a six-month internship at GEO Specialty Chemicals. This monomer was then polymerised by RAFT solution polymerisation before exploring the effect of sodium periodate on the corresponding homopolymer. Preliminary periodate oxidation studies were also conducted on the GEO5MA-based products.

## **Experimental**

### *Materials*

Glycerol monomethacrylate (GMA, 99.8 %), methyl methacrylate (MMA), isopropylidene glycerol pentaethylene glycol ether (IPG+5EO), 4-methoxyphenol (MEHQ) and titanate catalyst were provided by GEO Specialty Chemicals (Hythe, UK) and were used without further purification. 4,4'-Azobis(4-cyanopentanoic acid) (ACVA, 99 %), sodium periodate (NaIO<sub>4</sub>), hydrochloric acid (HCl), ascorbic acid, hydrogen peroxide solution (H<sub>2</sub>O<sub>2</sub>, 30 %), (3-aminopropyl)triethoxysilane (ATPES, 99 %),  $\alpha$ -bromoisobutyryl bromide (BiBB, 98%), Copper (II) Chloride (Cu(II)Cl<sub>2</sub>, 99.9 %), 2, 2'-Bipyridine (bpy, 99 %) and ascorbic acid were purchased from Sigma-Aldrich (UK) and were used as received. Deuterated DMF and methanol were purchased from Goss Scientific Instruments Ltd. (Crewe, UK). All other solvents and Decon90 were purchased from Fisher Scientific (Loughborough, UK) and were used as received. Silicon wafers were purchased from Pi-Kem. Deionised water was used for all experiments.

### *Transesterification of IPG + 5EO*

A 5 L transesterification rig was charged with isopropylidene glycerol pentaethylene glycol ether (IPG+5EO) (1500 g), MMA (2300 g, 22.97 mol) and MEHQ (1.3 g, 10.4 mmol). The reaction mixture was subsequently heated to 115 °C with an air sparge at a constant rate of 300 mL min<sup>-1</sup>. Water/MMA distillate was periodically removed from the still head until the headspace reached a constant temperature (~100 °C) after 2 h. The reactor was periodically topped up with MMA to maintain a constant reaction volume. Titanate catalyst (2.0 g) was added by syringe and transesterification commenced. The reaction was run for 2 h under partial take-off conditions. At this point, the head temperature reached 95 °C and the reaction was

switched to ‘run and bump’ conditions. This means the still head was allowed to fill for a period of time before draining in order to concentrate methanol in the distillate. The still head was drained every 20 min for 2 h, after which transesterification was deemed complete. The reaction mixture was allowed to cool overnight. The following day, MMA was stripped from the same rig at 80 °C under vacuum for 2 h. Deionised water (400 g) was added to deactivate the titanate catalyst and allowed to react for 1 h at 80 °C. Then the precipitate was removed by filtration and the water was stripped under vacuum at 80 °C for 2 h. The resulting colourless liquid (IPGEO5MA, 1500 g) had a water content of 0.01 % w/w and an OH number of 2.63 mg KOH g<sup>-1</sup>. If full conversion were achieved and no water was present an OH number of 0 mgKOH g<sup>-1</sup> would be expected, this measured value indicates high conversion for this reaction.

#### *Acidic Deprotection of IPGEO5MA*

IPGEO5MA (1500 g) was treated with a resin (Ambersep 900 OH) (150 g) to remove MEHQ inhibitor. The reaction solution was stirred for 20 min at 20 °C, then the resin was removed by filtration. The residual level of MEHQ was determined to be 25 ppm using UV-visible absorption spectroscopy and this was subsequently topped up to 100 ppm by addition of fresh MEHQ (0.115 g, 0.92 mmol). Deionised water (300 g) and concentrated HCl (11 g) were added to the IPGEO5MA in a 3 L flask. This reaction mixture was stirred for 48 h using a 300 mL min<sup>-1</sup> air sparge, while water was periodically topped up to maintain a constant reaction volume. The resulting homogeneous solution was neutralised using an ion exchange resin (150 g), which was then removed by filtration. Finally, water was removed from the reaction solution at 50 °C under vacuum for 4 h prior to analysis. The resulting yellowish liquid had a water content of 0.3 % w/w and an OH number of 289 mg KOH g<sup>-1</sup>. If full conversion were achieved and no water was present an OH number of 294 mg KOH g<sup>-1</sup> would be expected, this measured value indicates high conversion for this reaction.

#### *Oxidative cleavage of cis-diol group using sodium periodate*

The reaction of GEO5MA with NaIO<sub>4</sub> was performed at 10 % solids as follows: GEO5MA (1.00 g, 2.6 mmol) was diluted with D<sub>2</sub>O (9.0 g) to give a 10 % monomer solution. NaIO<sub>4</sub> (0.56 g, 2.6 mmol) was added and the solution was stirred for 16 h. The product was analysed by <sup>1</sup>H NMR spectroscopy, which indicated that more than 99 % conversion had been achieved. This was determined by comparing the integral of new aldehyde and hydrated aldehyde signals at

9.5 and 5.1 ppm respectively with the vinyl protons at 5.7 and 6.1 ppm which should remain constant. Purification of the resulting aldehyde-functional monomer was attempted by extraction into diethyl ether. This produced a yellow oil and removed some of dimethacrylate impurities. However, the isolated yield was rather low (~ 10 %).

#### *Synthesis of PGEO5MA brushes from planar silicon wafers using ARGET ATRP*

Silicon wafers were cut and prepared as reported in the literature.<sup>4</sup> The resulting wafers were then immersed in a 1 % solution of APTES in toluene for 1 h. The APTES-treated wafers were immersed in solutions of fresh toluene, 1:1 toluene/ethanol and fresh ethanol and sonicated for 15 min each using an ultrasonic bath. Finally, wafers were annealed for 30 min under vacuum at 120 °C before being sonicated in a 10 % aqueous surfactant solution (Decon90). Finally, the wafers were rinsed with water and IPA before being dried using a stream of N<sub>2</sub> gas. Wafers were then functionalised with ATRP initiator sites by immersion in a 0.1 M solution of BiBB in dichloromethane overnight, before being rinsed with this solvent and dried using a stream of N<sub>2</sub> gas.

Stock solutions of ATRP catalyst comprising Cu(II)Cl<sub>2</sub> (29.2 mg, 0.22 mmol) and bpy ligand (77.6 mg, 0.50 mmol) in water (10 mL) and reducing agent (100 mg ascorbic acid in 10 mL water) were made up. GEO5MA (3.00 g, 7.9 mmol) was dissolved in water (8.0 mL) and 1.0 mL of the catalyst stock solution plus 0.10 mL of the reducing agent stock solution were added to this aqueous monomer solution. The resulting reaction solution changed colour from brown to blue, indicating formation of the active Cu(I) ATRP catalyst. Silicon wafers were carefully immersed within this reaction solution for desired time periods. After a given reaction time, wafers were removed using tweezers, washed with ethanol and dried using a stream of N<sub>2</sub> gas. The resulting PGEO5MA brushes were analysed by ellipsometry and FT-IR spectroscopy.

#### *Characterisation Techniques*

*<sup>1</sup>H NMR Spectroscopy.* All spectra were recorded in either deuterated methanol or D<sub>2</sub>O using a 400 MHz Bruker Avance-400 spectrometer (64 scans averaged per spectrum).

*Gel Permeation Chromatography (GPC).* Molecular weight distributions were assessed using an Agilent 1260 Infinity GPC system equipped with both refractive index and UV-visible



detectors. Two Agilent PL gel 5  $\mu\text{m}$  Mixed-C columns and a guard column were connected in series and maintained at 60 °C. HPLC-grade DMF containing 10 mM LiBr was used as an eluent and the flow rate was set at 1.0 mL min<sup>-1</sup> with DMSO being used as a flow-rate marker. The refractive index detector was used to calculate molecular weights and dispersities using a series of ten near-monodisperse poly(methyl methacrylate) calibration standards (with  $M_n$  values ranging from 625 to 2,200,000 g mol<sup>-1</sup>).

*Transmission Electron Microscopy (TEM).* As-prepared aqueous PGEO5MA-PPMA dispersions were diluted at 20 °C to generate 0.20 % w/w dispersions. Copper/palladium TEM grids (Agar Scientific, UK) were coated in-house to produce a thin film of amorphous carbon. These grids were then treated with a plasma glow-discharge for 30 seconds to create a hydrophilic surface. Each aqueous dispersion (12  $\mu\text{L}$ ; 0.20 % w/w) was placed on a freshly-treated grid for 1 min and then blotted with filter paper to remove excess solution. To stain the deposited latex particles, an aqueous solution of uranyl formate (9  $\mu\text{L}$ ; 0.75% w/w) was placed on the sample-loaded grid via micropipette for 20 s and then carefully blotted to remove excess stain. Each grid was then carefully dried using a vacuum hose. Imaging was performed using a FEI Tecnai Spirit TEM instrument equipped with a Gatan 1kMS600CW CCD camera operating at 120 kV.

*Viscosity and pH.* Solution viscosities were determined using internally-calibrated U-tube viscometers immersed in an aqueous ethylene glycol bath at 25 °C. Each solution viscosity was calculated by averaging three independent measurements. Solution pH was determined by immersing a calibrated Metrohm 744 pH meter directly into the aqueous polymer solution.

*OH Number and Water Content.* OH numbers were determined by titration according to ASTM E 326 on a Mettler Toledo T70 Titroprocessor. Water contents were determined by titration according to ASTM E 203 on a Metrohm 787 KF Titrator.

*MeHQ Content.* The MEHQ content was determined as per ASTM D 3125 using a Thermo Scientific Evolution 220 UV-VIS Spectrophotometer

*FT-IR Spectroscopy.* FT-IR spectra were recorded for solid samples using a Thermo Scientific Nicolet iS10 FT-IR spectrometer by passing the beam directly through the silicon wafer and polymer brush. Each spectrum was averaged over 500 scans at a resolution of  $4\text{ cm}^{-1}$

*Contact Angles.* Contact angle of deionized water drops were measured using a Ramé-Hart model 100-00 contact angle goniometer.

*Ellipsometry.* Ellipsometric studies were conducted using an alpha-SE ellipsometer (J. A. Woollam Co., Lincoln, NE, USA) equipped with a He-Ne laser ( $\lambda = 633\text{ nm}$ ) at an incident angle ( $\Phi$ ) of  $70^\circ$  from the normal. Ellipsometric thicknesses were calculated for polymer brushes grown from planar silicon wafers. Measurements were conducted from 300 to 700 nm, and modelling was performed using completeEASE software provided by the instrument manufacturer.

## **Results and Discussion**

The synthesis of GEO5MA is a multi-step process starting from isopropylidene glycerol (IPG). Protecting group chemistry is essential to prevent the formation of di- or tri-methacrylate side-products. IPG was used as an initiator to oligomerise EO using an in-house method at  $125\text{ }^\circ\text{C}$  under pressure of 5.5 bar to afford isopropylidene glycerol pentaethylene glycol ether (IPG+5EO). This intermediate product was characterised by OH number and viscosity measurements.

IPG+5EO was then subjected to transesterification with methyl methacrylate (MMA) (see Scheme 5.1). A typical transesterification rig was set up as shown in Figure 5.3. The reactor was charged with IPG+5EO, MMA and MEHQ inhibitor (1000 ppm), then heated up to  $115\text{ }^\circ\text{C}$  to remove water (which is detrimental to the catalyst). Water and MMA have boiling points of  $100\text{ }^\circ\text{C}$  and  $101\text{ }^\circ\text{C}$  respectively, but an MMA/water mixture forms a low-boiling azeotrope. The distillate was periodically removed until the pot temperature reached a constant temperature of around  $100\text{ }^\circ\text{C}$ . At this point, the titanium catalyst was added and transesterification commenced.

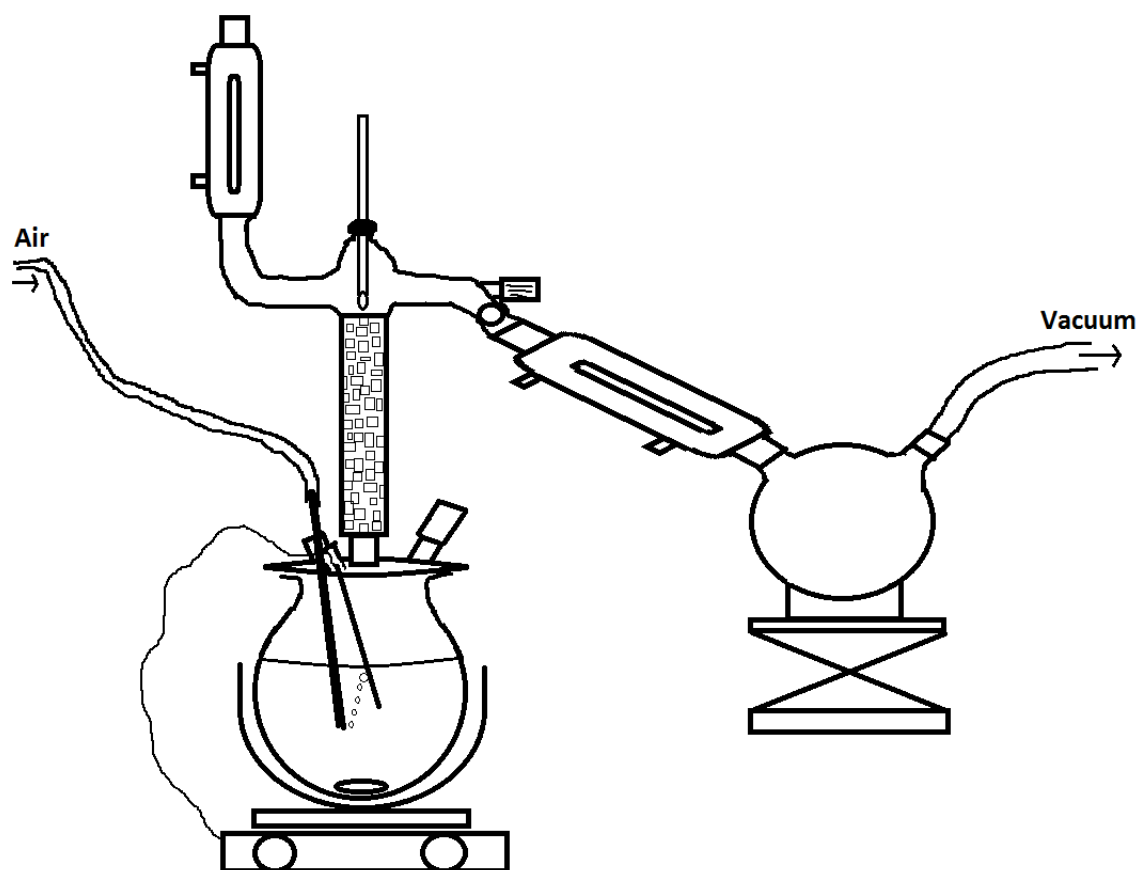
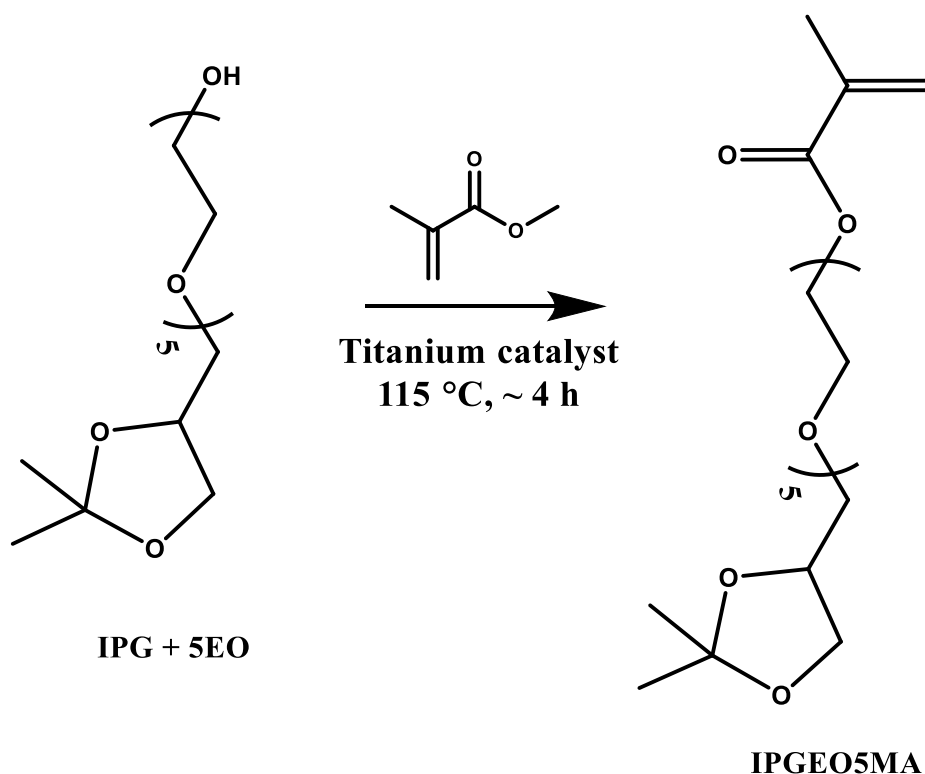


**Figure 5.3.** Schematic representation of a typical transesterification rig<sup>5</sup>

As transesterification continued, methanol and MMA were distilled into the top of the apparatus and periodically removed. Methanol has a boiling point of 65 °C. This is significantly lower than that of MMA, therefore the progress of the transesterification reaction can be monitored by measuring the temperature at the head of the distillation column. MMA was topped up periodically to account for that removed by distillation. Once the head temperature had reached close to 100 °C and remained constant, this indicated the end of the reaction.



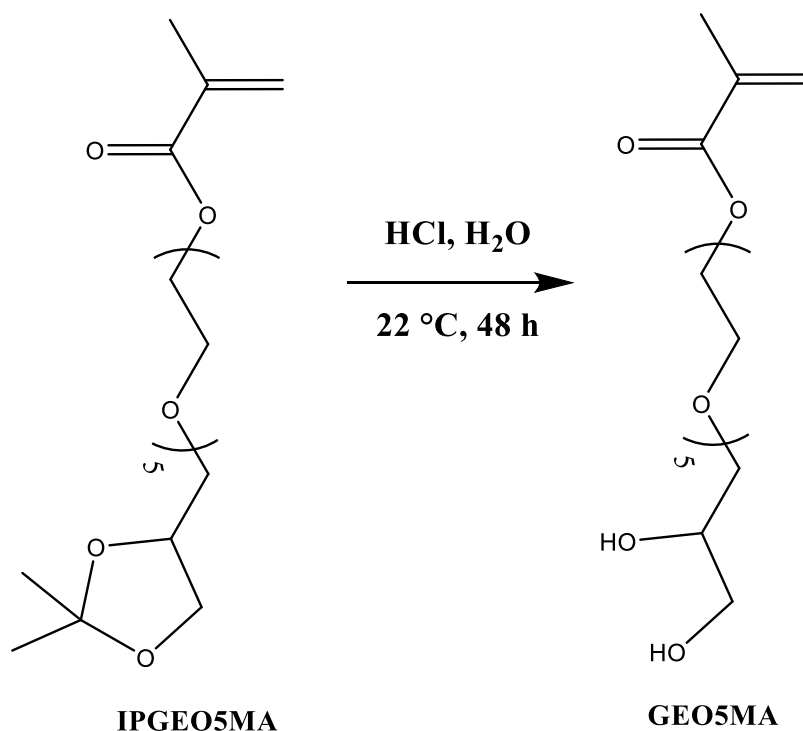
**Scheme 5.1.** Transesterification of IPG + 5EO with MMA to give IPGEO5MA using a titanate catalyst

A vacuum was applied to the rig in order to remove excess MMA from the pot. Once the MMA had been removed, the reactor was charged with water. The titanate catalyst reacts rapidly with water to form a precipitate. The reaction mixture was cooled and passed through a filter to remove insoluble catalyst residues. Finally, the product was stripped at 80 °C to remove unreacted water.

The resulting IPGEO5MA intermediate was analysed for its water content and OH number. If all product had reacted, a final OH number of zero would be expected, but small amounts of water lead to higher than expected values. The actual water content was 0.01 % w/w and the OH number was determined to be 2.63 mg KOH g<sup>-1</sup>. This non-zero OH number is fully consistent with the low water content, so the transesterification was deemed to be complete.

This IPGEO5MA was treated with Ambersep 900 OH resin for 20 min to reduce its inhibitor concentration to 100 ppm, as confirmed by UV-vis. Water and acid were added to facilitate the hydrolysis of the acetal group (see Scheme 5.2). The initially inhomogeneous reaction mixture was stirred for 48 h at 20 °C with an air sparge, while water was periodically topped up to allow for evaporation. After 48 h, a homogeneous aqueous solution was obtained, indicating the formation of a water-miscible product. The solution was neutralised using an Amberlyst A24

ion exchange resin and water was subsequently removed under vacuum. The OH number and water content of the product was analysed. If the reaction had gone to completion and no residual water remained, an OH number of 295 mg KOH g<sup>-1</sup> would be expected. An OH number of 289 mg KOH/g was observed with a water content of 0.3 % w/w. This suggested a high conversion of IPGEO5MA to GEO5MA.



**Scheme 5.2.** Acidic hydrolysis of IPGEO5MA at 20 °C for 48 h to afford GEO5MA

The GEO5MA monomer was subsequently analysed by <sup>1</sup>H NMR spectroscopy. The assigned spectrum shown in Figure 5.4b is consistent with that expected for GEO5MA, confirming that deprotection via acid hydrolysis had proceeded to high conversion (no IPG signals were observed at 1-2 ppm, see Figure 5.4b).

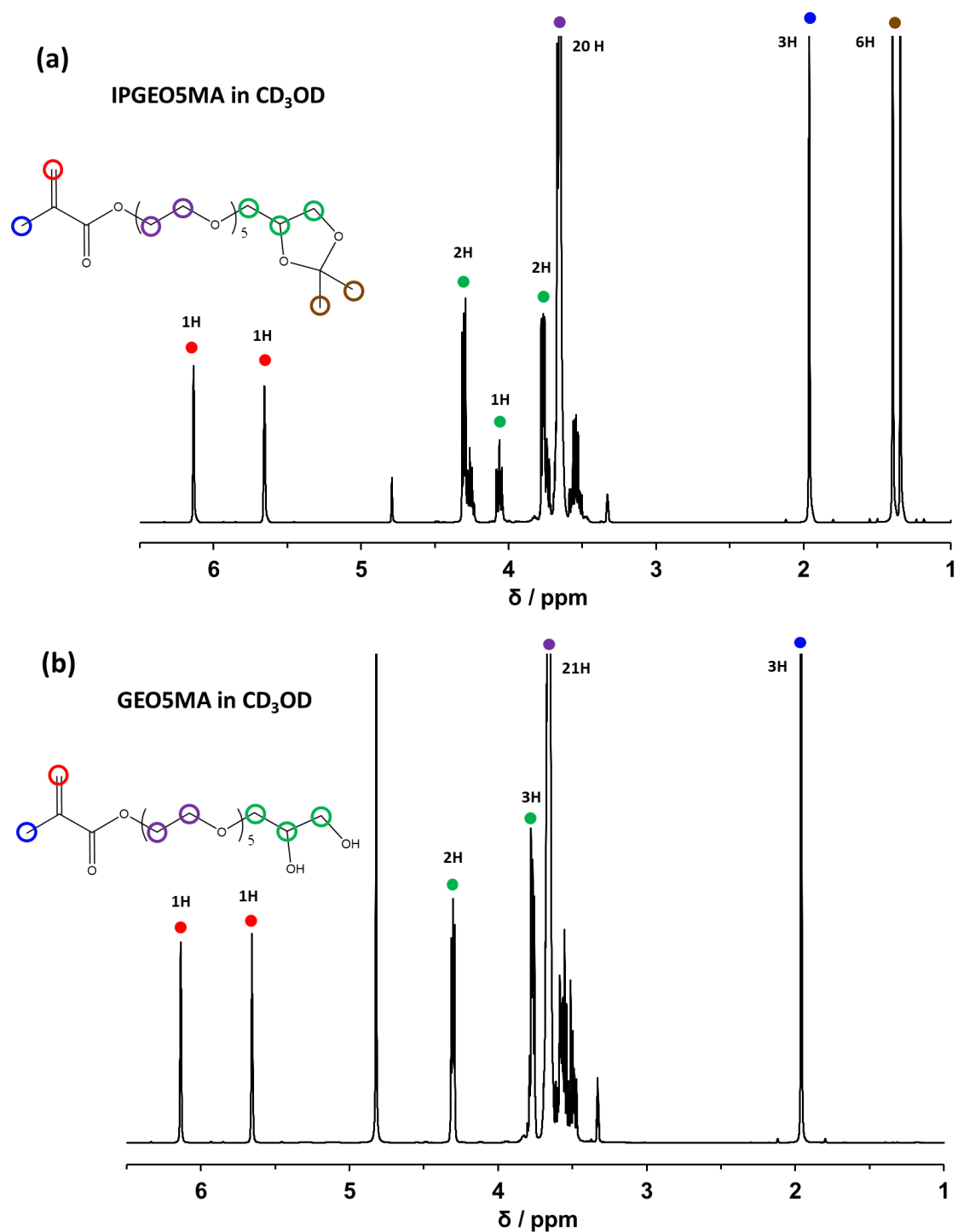


**Figure 5.4.** (a) <sup>1</sup>H NMR spectrum of IPGEO5MA in CD<sub>3</sub>OD and (b) <sup>1</sup>H NMR spectrum of GEO5MA in CD<sub>3</sub>OD confirming no visible IPG impurities.

### Previous work within the Armes group

A former group member (Dr. N. J. Warren) began to explore the reaction of sodium periodate with cis-diols to form aldehydes after noting that the analogous chemistry had been previously utilised to selectively cleave poly(vinyl alcohol) chains.<sup>6</sup> In principle, this chemistry offers an excellent opportunity to prepare new aldehydic vinyl monomers starting from either GMA or GEO5MA. Accordingly, GMA was reacted with one equivalent of NaIO<sub>4</sub> in D<sub>2</sub>O at a concentration of 20 g dm<sup>-3</sup> (see Figure 5.5). The reaction solution was analysed by <sup>1</sup>H NMR to confirm product formation and determine the overall conversion.

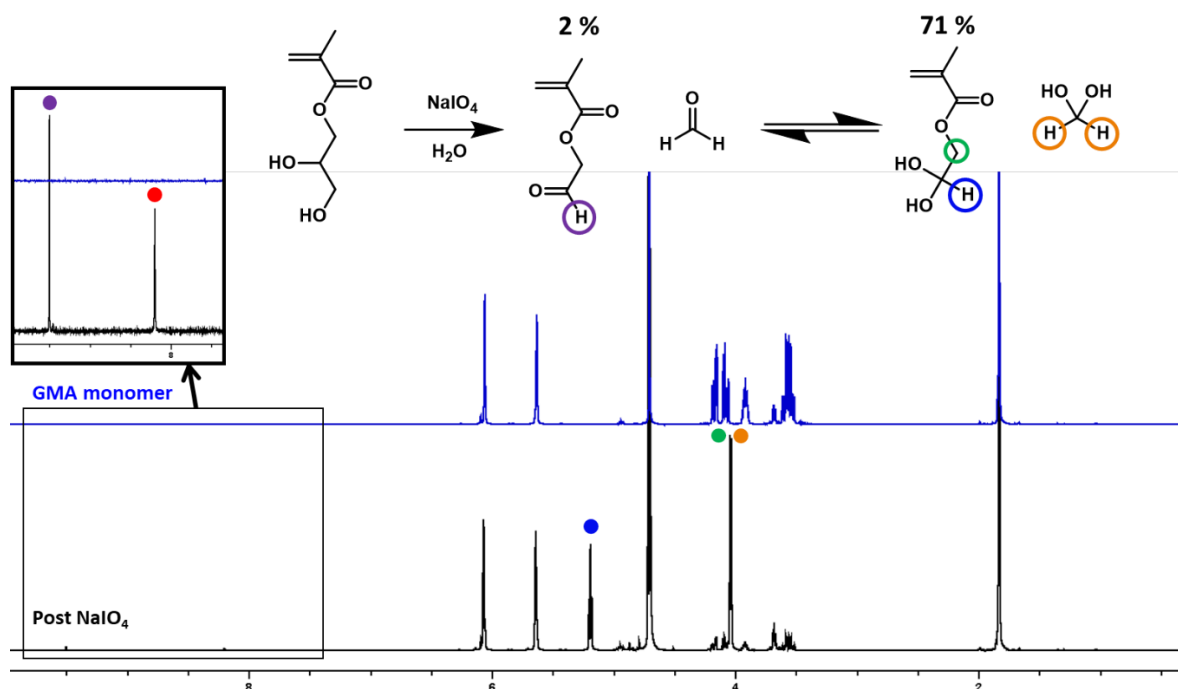
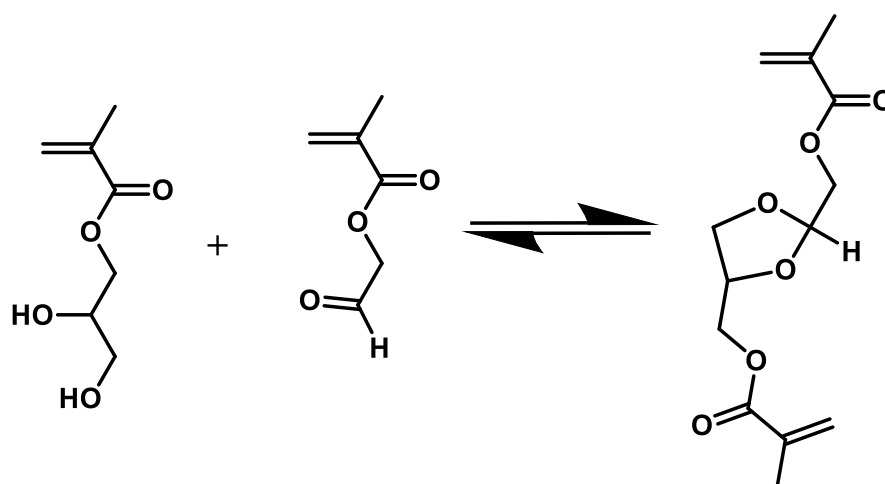


**Figure 5.5.** <sup>1</sup>H NMR spectra recorded in D<sub>2</sub>O showing the reaction of GMA with NaIO<sub>4</sub> to give a (hydrated) aldehyde product.

Periodate oxidation proceeded smoothly at 20 °C over the course of 20 h. In aqueous solution, aldehydes undergo a reversible reaction to form a gem-diol.<sup>1-2, 7</sup> The final NMR spectrum indicated the formation of 2 % of the target aldehyde and 71 % of its hydrated gem-diol form. It is well-known that aldehydes and ketones undergo a pH-reversible reaction with cis-diols to form acetal linkages.<sup>1-2, 7</sup> Thus, an additional signal at 8.1 ppm was attributed to dimethacrylate formation arising from acetal formation (see Scheme 5.3); this side-product was present at a level of approximately 1 mol % relative to the final product.



**Scheme 5.3.** Formation of a dimethacrylate side-product by the pH-reversible reaction of GMA with ethanal methacrylate

The same periodate oxidation reaction was used to derivatise a PGMA macro-CTA (for characterisation see Chapter 2, Figure 2.1) with a  $DP_n$  of 50. This water-soluble precursor was treated with either 0.1 or 1.0 equivalent of  $NaIO_4$  in  $D_2O$  at a concentration of  $20\text{ g dm}^{-3}$ . In both cases, a precipitate was formed within 20 h at  $20\text{ }^\circ\text{C}$ . This phase separation was attributed to the formation of a cross-linked water-insoluble product via the same chemistry that led to the production of the dimethacrylate side-product (see above). Dissolution of this precipitate was achieved by adjusting the solution pH to 3 using  $DCl/D_2O$ .  $^1H$  NMR spectroscopy studies confirmed the formation of the hydrated gem-diol product (see Figure 5.6).

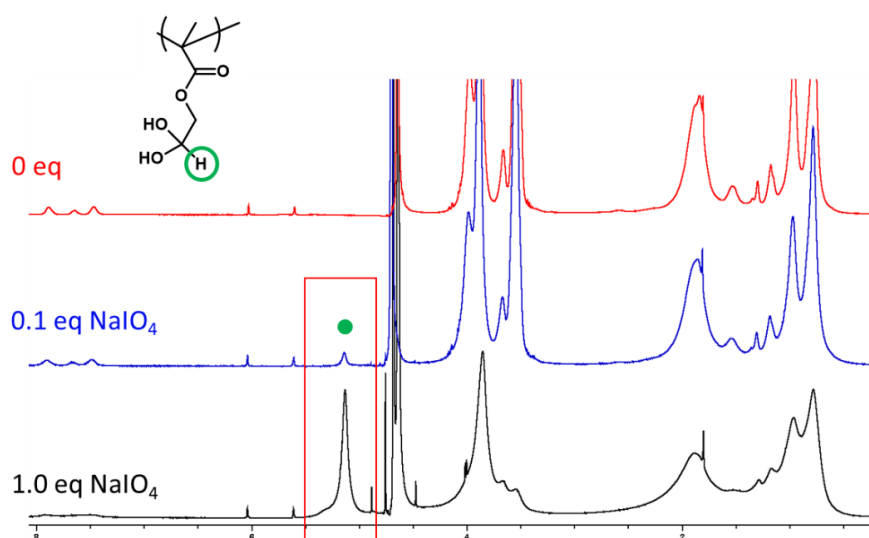


**Figure 5.6.**  $^1H$  NMR spectra recorded in  $DCl/D_2O$  for  $PGMA_{50}$  treated with either zero, 0.1 or 1.0 equivalents of  $NaIO_4$ . Conditions:  $22\text{ }^\circ\text{C}$ , 22 h.



In order to functionalise these aldehydic monomer/polymers with nucleophiles, it may be necessary to convert them into their more reactive aldehyde form. Removing water from the system should drive the equilibrium from the hydrated gem-diol towards the aldehyde. As such, the product was purified by dialysis and freeze-dried. However, attempts to dissolve this product in  $D_2O$ ,  $CD_3OD$  or  $CDCl_3$  proved unsuccessful, suggesting a high degree of crosslinking via acetal formation.

### Periodate oxidation of GEO5MA monomer and PGE05MA homopolymer

Given that PGMA became water-insoluble after treatment with sodium periodate, the same reaction was performed on GEO5MA to see whether the additional OEG moiety enabled aqueous solubility to be retained. Thus, a  $20\text{ g dm}^{-3}$  solution of GEO5MA in  $D_2O$  was treated with one equivalent of  $NaIO_4$ . The reaction mixture was stirred at  $20\text{ }^\circ\text{C}$  for 20 h before being analysed by  $^1H$  NMR spectroscopy. A relatively high conversion was observed under these conditions, with 88 % hydrated gem-diol and 3 % unhydrated aldehyde being observed (see Figure 5.7). Interestingly, unlike the reaction of GMA monomer with  $NaIO_4$ , no dimethacrylate side-products were detected.

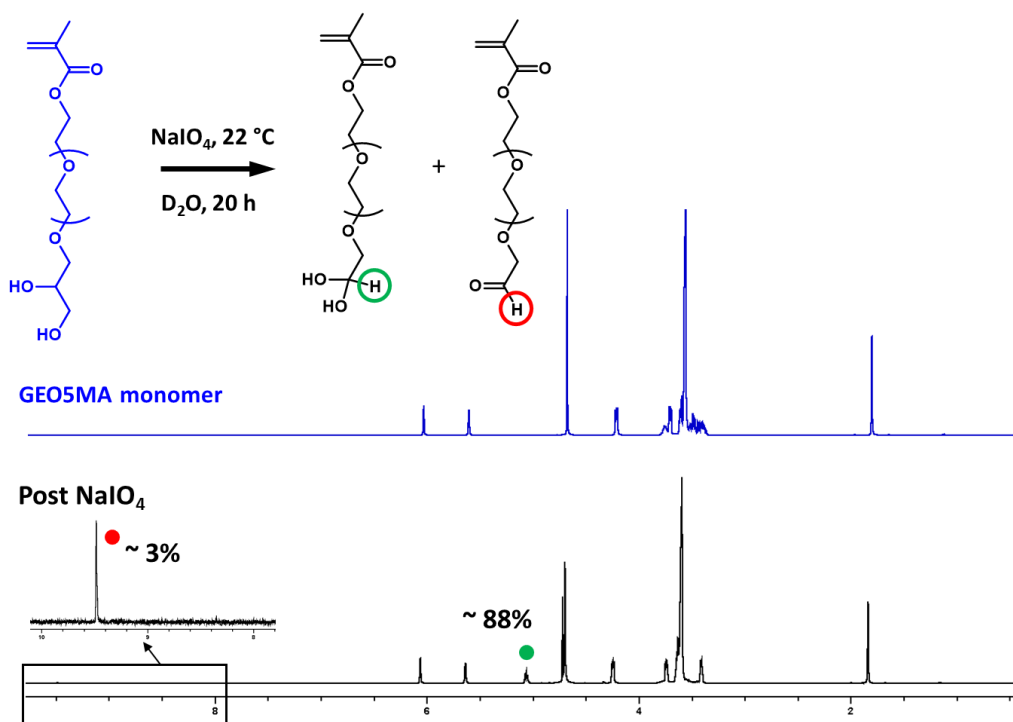


**Figure 5.7.**  $^1H$  NMR spectra recorded for GEO5MA in  $D_2O$  before and after treatment with  $NaIO_4$ . Conditions: one equivalent of  $NaIO_4$ ,  $22\text{ }^\circ\text{C}$ , 22 h

The same reaction was repeated using a PGEO5MA<sub>21</sub> macro-CTA. This precursor was treated with either 0.1 or 1 equivalent of NaIO<sub>4</sub> in D<sub>2</sub>O at a polymer concentration of 20 g dm<sup>-3</sup>. In both cases, the derivatised polymer remained water-soluble but a colour change from pink to orange was observed. This almost certainly indicates concomitant oxidation of the RAFT end-group. Each reaction yielded both hydrated gem-diol and unhydrated aldehyde products, but acetal crosslinks were observed when using a higher concentration of NaIO<sub>4</sub> (see Figure 5.8). Importantly, this does not seem to be the case when using 2.1 equivalents of NaIO<sub>4</sub>.

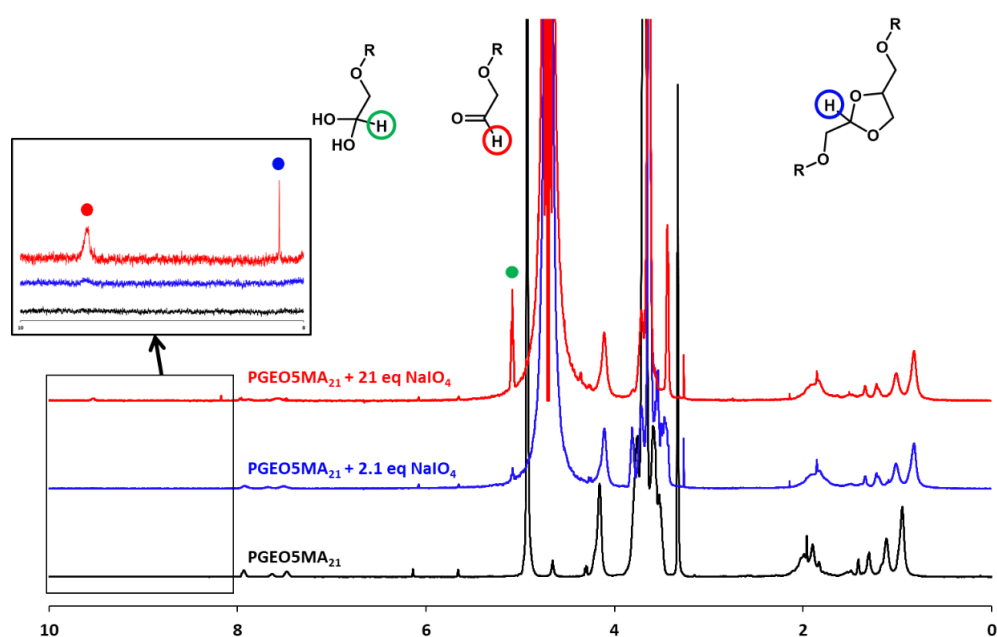


**Figure 5.8.** <sup>1</sup>H NMR spectra recorded for the oxidation of PGEO5MA<sub>21</sub> using either 2.1 or 21 equivalents of NaIO<sub>4</sub>. Conditions: 20 g dm<sup>-3</sup>, 22 °C, 16 h, D<sub>2</sub>O. The PGEO5MA<sub>21</sub> spectrum was recorded in CD<sub>3</sub>OD whereas the spectra recorded after the oxidation reactions were recorded in D<sub>2</sub>O.

There have been numerous literature reports of the synthesis of diblock copolymer nanoparticles via the RAFT aqueous dispersion polymerisation of HPMA.<sup>8-10</sup> For example, when using PGMA as the water-soluble stabiliser block, either spheres worms or vesicles can be produced by adjusting the DP of the PHPMA block and the copolymer concentration.<sup>9, 11-13</sup> In principle, water-soluble GEO5MA should also act as a suitable steric stabiliser in place of PGMA and also allow the formation of diblock copolymer nanoparticles. Thus, a phase diagram was constructed by chain-extending PGEO5MA<sub>21</sub> using varying amounts of HPMA over a range of copolymer concentrations, with the *post mortem* copolymer morphology being determined by TEM (see Figure 5.9).

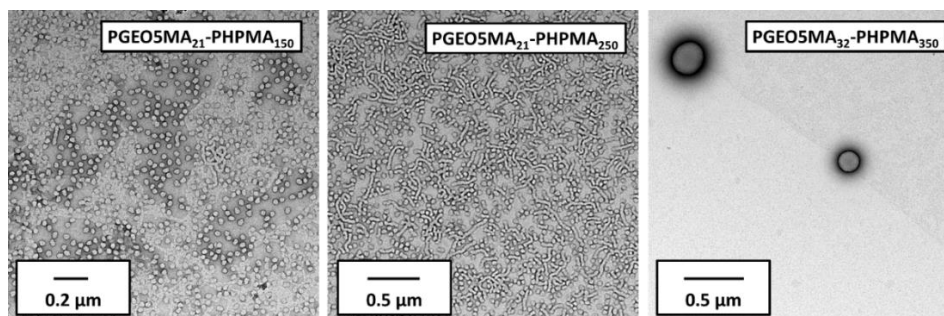
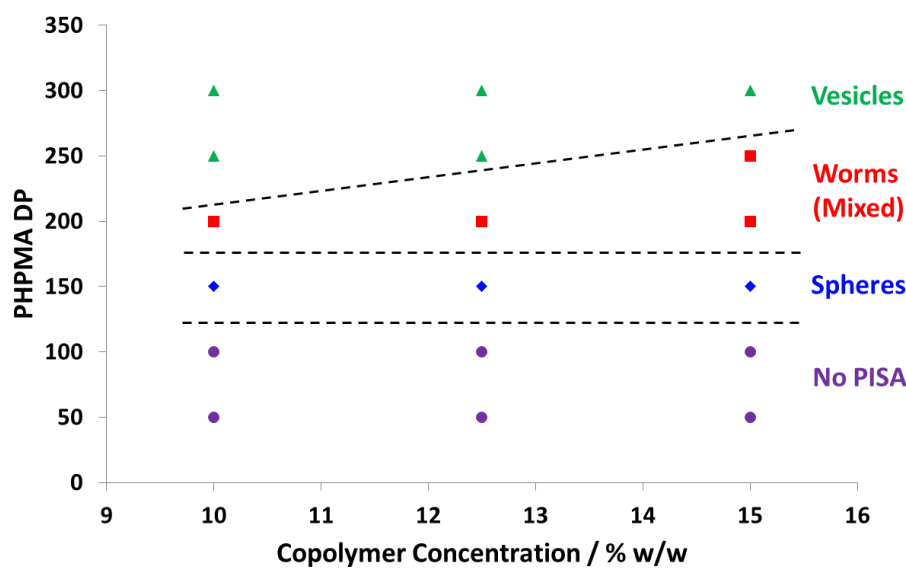


**Figure 5.9.** Phase diagram for PGE05MA<sub>21</sub>-PPHMA<sub>x</sub> diblock copolymer nanoparticles formed via RAFT aqueous dispersion polymerisation of HPMA using a PGE05MA<sub>21</sub> macro-CTA. Conditions: 70 °C, 5 h. Copolymer morphologies were assigned by TEM studies. Three representative TEM images for spherical, worm-like and vesicular particles are shown below the phase diagram.

In principle, functional nanoparticles with aldehyde groups expressed at the surface of the nanoparticles could be readily labelled with a fluorescent dye or used for protein conjugation reactions.<sup>14-15</sup> Accordingly, PGE05MA<sub>21</sub>-PPHMA<sub>x</sub> spheres ( $x = 150$ ) and vesicles ( $x = 300$ ) were derivatised in turn using 0.1 equivalents of NaIO<sub>4</sub> per cis-diol group at 10 % w/w solids. In each case, <sup>1</sup>H NMR spectroscopy studies confirmed the presence of aldehyde groups and the nanoparticles appeared to remain colloidally stable (as judged by visual inspection). In many cases, converting 10 % of the initial cis-diols to aldehyde groups may be sufficient. Nevertheless, it would be interesting to target an aldehyde-functional water-soluble polymer containing the maximum aldehyde content. However, performing this derivatisation leads to low levels of acetal crosslinking. In principle, an alternative route to the desired product would be to synthesise the corresponding water-soluble aldehyde monomer and subsequently perform

the corresponding RAFT solution polymerisation. Accordingly, GEO5MA was treated with an equimolar amount of NaIO<sub>4</sub> at a monomer concentration of 10 % w/w (see Figure 5.10).

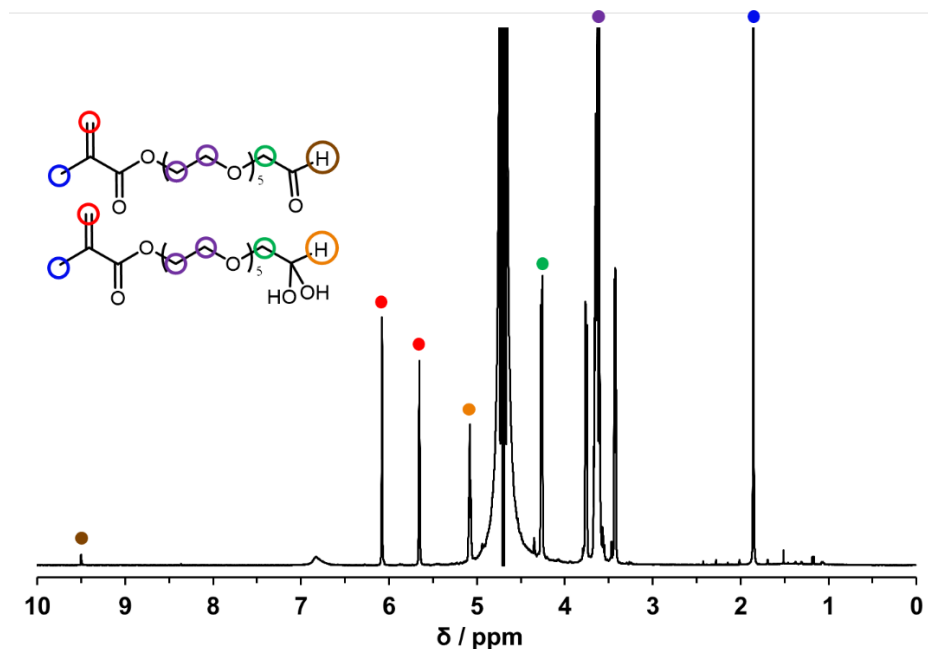


**Figure 5.10.** <sup>1</sup>H NMR spectrum recorded in D<sub>2</sub>O for the aldehyde-functionalised GEO5MA monomer formed from the reaction of GEO5MA with one equivalent of NaIO<sub>4</sub> conducted in D<sub>2</sub>O. Conditions: 10 % w/w, 22 °C, 16 h.

Under these conditions the periodate oxidation reaction proceeds very efficiently, with more than 95 % gem-diol and 4 % aldehyde being formed. Unfortunately, the higher concentration also led to the formation of approximately 0.5 mol % of the acetal-bridged dimethacrylate. Extraction with ether was used to isolate the desired product prior to freeze-drying, affording a yellow oil. Pleasingly, this purification protocol reduced the dimethacrylate side-product to almost undetectable levels. However, only a rather low purified yield (~10 %) of the desired aldehyde-functional vinyl monomer was obtained (approx. 0.1 g from 1.0 g of GEO5MA). Nevertheless, this oxidation reaction was repeated on a larger scale in order to obtain enough aldehyde-functional GEO5MA to perform a polymerisation. In this case, 10 g of GEO5MA yielded 0.75 g of the desired product. Unfortunately, time constraints prevented investigation of the RAFT solution polymerisation of this aldehyde-functionalised GEO5MA monomer. However, subsequent research within the Armes group undertaken by a PhD student (Emma

Brotherton) has confirmed that this is indeed a valid route to well-defined aldehyde-functional water-soluble polymers.

### **Growth of PGEO5MA brushes from planar silicon wafers using ARGET ATRP**

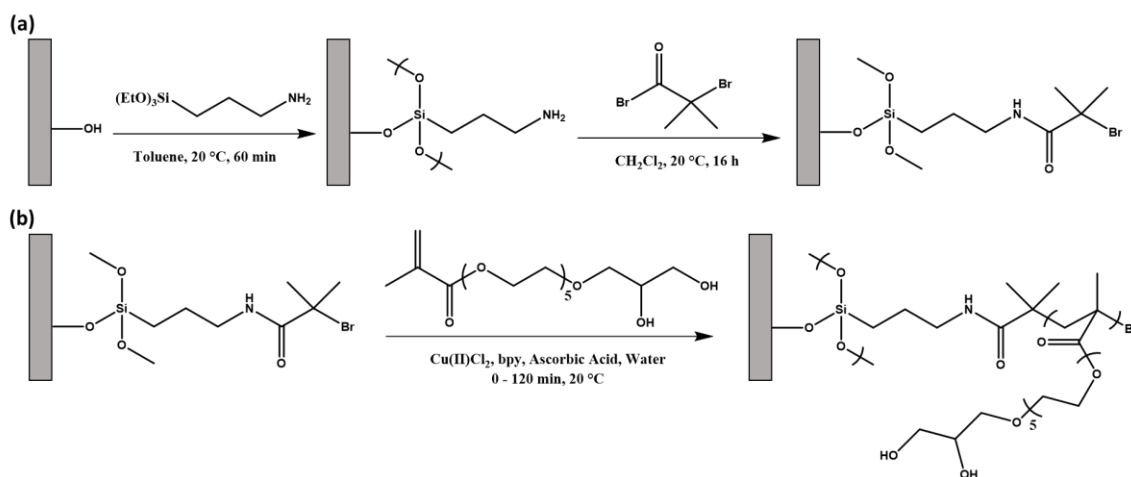
A further promising research avenue is aldehyde-functional polymer brushes. The growth of many methacrylic polymer brushes from planar silicon wafers is well-established via surface ATRP.<sup>16-17</sup> In principle, aldehyde-functional polymer brushes could be prepared either (i) by directly polymerising the aldehyde-functional monomer or (ii) by first growing PGEO5MA brushes followed by their selective oxidation via immersion in an aqueous solution of sodium periodate.

In this thesis, the second route was briefly explored. First, silicon wafers were cut using a diamond-tipped knife and placed into individual vials. The vials were then submerged in piranha solution (7 parts 98 % H<sub>2</sub>SO<sub>4</sub> solution: 3 parts 30 % H<sub>2</sub>O<sub>2</sub> solution) for 45 min, before thoroughly washing the vials and tubes (ten times) with distilled water. This cleaning is essential to remove any organic impurities which may impact further surface functionalisation and brush growth. Following this protocol, the slides were then immersed in RCA solution (5 parts distilled water : 1 part 30 % H<sub>2</sub>O<sub>2</sub> solution : 1 part 35 % NH<sub>3</sub>) and heated at 370 °C for 30 min. This treatment removed any excess piranha solution and also activated the surface. The slides were allowed to cool for 1 h before being washed seven times with distilled water and then stored in a clean oven at 120 °C overnight.<sup>4</sup>

The following morning, the slides were wrapped in foil and allowed to cool slowly. This precaution is essential to prevent dust contamination of the wafer surface. The resulting clean wafers were immersed in a 1 % APTES solution in toluene for 1 h. The siloxane groups on the APTES react with the silanol groups on the wafer to form a thin layer of primary amine surface groups (see Scheme 4a). The slides were then sonicated in toluene, a 1:1 solution of toluene and ethanol and finally ethanol for 15 min each. This treatment has been carefully optimised to produce approximately one monolayer of APTES at the silicon wafer surface. The APTES-treated slides were annealed in a vacuum oven for 30 min at 120 °C before being sonicated using an aqueous surfactant solution (Decon 90). Finally the wafers were rinsed with distilled water and IPA before being dried using a stream of nitrogen gas.

According to the literature, an APTES monolayer should give a water contact angle of 45°.<sup>18</sup> Contact angle measurements on the APTES-treated wafers prepared in this Thesis gave an

average value of  $35^\circ$ , indicating a reasonable monolayer. The wafers were then functionalised with 2-Bromoisobutyryl Bromide (BiBB) initiator by immersing them in a 0.1 M BiBB solution in dichloromethane for 16 h at  $20^\circ\text{C}$ . The BiBB reacts with the pendant amine groups to produce pendant amide-based ATRP initiators on the wafer surface (see Scheme 5.4a).



**Scheme 5.4.** (a) Functionalisation of surface silanol groups on a planar silicon wafer with APTES and BiBB in order to form surface initiator sites. (b) ARGET ATRP of GEO5MA from such initiator sites on a planar silicon wafer to grow PGEO5MA brushes.

Four individual wafers were subsequently placed into vials containing GEO5MA monomer (3.0 g),  $\text{CuCl}_2$  (2.92 mg), 2,2'-bipyridine (7.76 mg), ascorbic acid (1.0 mg) and water (9.1 mL). PGEO5MA brushes were grown from these surface initiator groups via ARGET ATRP (see Scheme 5.4b). Each slide was removed from the solution at different time points (10 min, 30 min, 1 h or 2 h) in order to monitor the rate of growth from the surface. The resulting PGEO5MA brush-coated wafers and one unfunctionalised wafer were then analysed by ellipsometry and FT-IR spectroscopy.

Assuming a refractive index of 1.35 for the PGEO5MA brush, the ellipsometry data confirmed an increase in brush thickness with time up to 60 nm (see Figure 5.11a). In each case the model was a good fit to the data with MSE (mean squared error) values less than 1 and the surface roughness was measured at less than 5 nm. The IR spectra showed no discernible difference between brushes of different thicknesses but did reveal the presence of ester carbonyl bands at  $1740\text{ cm}^{-1}$  and also C-O linkages at lower wavenumbers (see Figure 5.11). These preliminary results confirm that it is possible to grow relatively thick PGEO5MA brushes from the surface of silicon wafers.

Unfortunately, time constraints did not allow periodate oxidation of the PGEO5MA brushes grown from planar silicon wafers. In principle, this should be readily achieved simply by immersing the brush layer in an aqueous periodate solution for a given time, followed by rinsing with deionised water to remove excess periodate (and formaldehyde by-product). The success of this surface modification reaction could be studied by FT-IR spectroscopy and X-ray photoelectron spectroscopy (XPS). In the latter case, the surface aldehyde groups could be reacted with 2,2,2-trifluoroethylamine to produce a Schiff base, thus introducing a convenient  $F_{1s}$  label for quantification purposes.

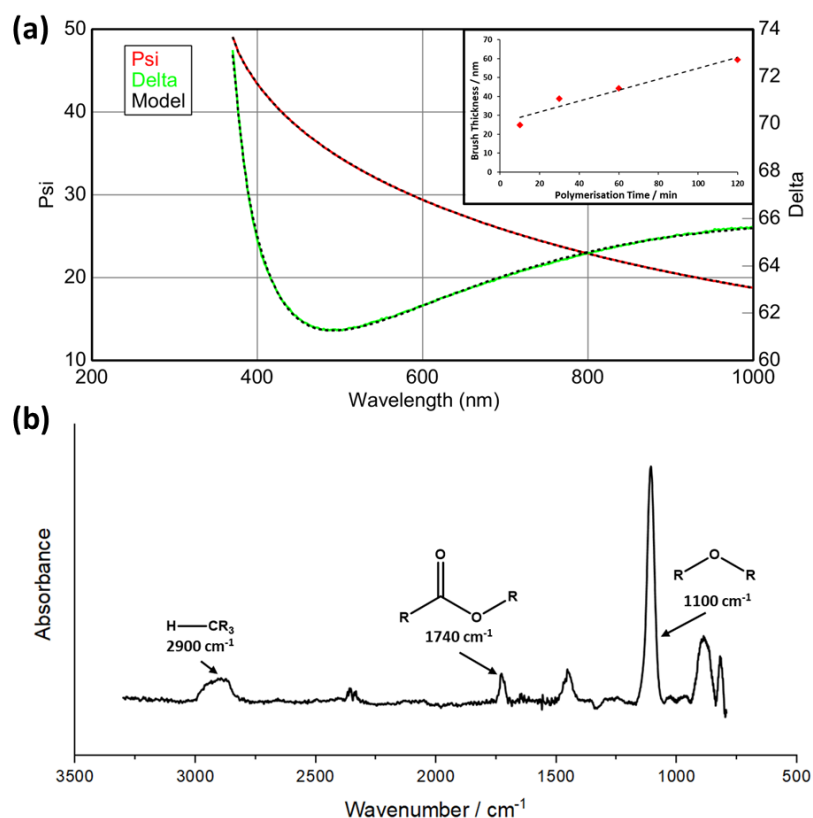


**Figure 5.11.** (a) Ellipsometric analysis of an ARGET ATRP-synthesised PGEO5MA brush of 60 nm dry thickness fitted using completeEASE software. The inset graph shows the monotonic evolution of dry brush thickness with polymerisation time. (b) Fourier transform infra-red spectrum recorded for a PGEO5MA brush of 39 nm dry thickness after subtraction of a background spectrum recorded for the pristine planar silicon wafer. Weak ester carbonyl (C=O) and C-O bands and a strong C-O ether band are observed at  $1740\text{ cm}^{-1}$ ,  $1450\text{ cm}^{-1}$  and  $1100\text{ cm}^{-1}$ , respectively, confirming the presence of PGEO5MA chains at the silicon wafer surface.

### Conclusions

A new water-soluble methacrylic monomer (GEO5MA) with a hybrid chemical structure lying between that of GMA and OEGMA was synthesised on a kilo scale during my six-month secondment at GEO Specialty Chemicals. This monomer is water-soluble in all proportions and is readily polymerised by RAFT solution polymerisation to afford a low-dispersity homopolymer precursor.

In principle, treating either GMA or GEO5MA with an aqueous solution of sodium periodate enables the selective oxidative cleavage of the cis-diol unit under mild conditions (20 °C, pH 6-7) to afford the corresponding aldehyde-functional methacrylic monomers. In practice, treating GMA with NaIO<sub>4</sub> in D<sub>2</sub>O gave a hydrated gem-diol product in high yield but also produced low levels of an acetal-bridged dimethacrylate impurity. When applied to a water-soluble PGMA precursor, this chemistry produced an insoluble precipitate that could be solubilised via treatment with HCl. The oligo(ethylene glycol) groups in GEO5MA ensured that this monomer and its corresponding homopolymer remained water-soluble. Moreover, no detectable dimethacrylate side product was formed when this derivatisation was conducted at relatively low concentration. However, the side-product for both such monomer syntheses is formaldehyde, which is a known carcinogen.

As expected, PGEO5MA acted as an effective steric stabiliser for diblock copolymer nanoparticles produced by the RAFT aqueous dispersion polymerisation of HPMA. By varying the copolymer concentration and the PHPMA block DP, either spheres, worms or vesicles could be reproducibly targeted. By determining the copolymer morphology by TEM, a preliminary phase diagram could be constructed. Finally, 10 % w/w copolymer dispersions of either spheres or vesicles were treated with 0.1 equivalents of NaIO<sub>4</sub> and the desired aldehyde groups were detected by <sup>1</sup>H NMR spectroscopy.

GEO5MA monomer could be treated with equimolar quantities of sodium periodate at concentrations as high as 10 % w/w. The resulting aldehyde-functionalised product contained dimethacrylate impurities but these could be significantly reduced by ether extraction, with freeze-drying yielding the final purified aldehyde-functional methacrylic monomer.

Finally, GEO5MA can be polymerised from planar silicon wafers via ARGET ATRP to produce PGEO5MA brushes. FT-IR spectroscopy studies confirmed the presence of PGEO5MA chains at the silicon wafer surface while ellipsometry confirmed that these brushes were relatively thick (up to 60 nm).



### **Future Work**

Promising proof-of-concept experiments have been conducted, but substantial further studies are now required to establish the true scope and limitations of this new route to aldehyde-functional monomers, water-soluble homopolymers and nanoparticles. For example, the periodate oxidation reaction requires further optimisation with regard to the reagent concentration, temperature, solution pH, reaction time and molar ratio of reactants. Ideally, such studies will enable suitable conditions to be identified that enable minimisation, and hopefully elimination, of the formation of acetal-bridged dimethacrylate impurity.

It would be interesting to prepare a series of diblock copolymer nanoparticles containing surface aldehyde groups in aqueous solution. Such nanoparticles could be conjugated to various dyes or proteins. In principle, such nanoparticles could be prepared by first synthesising and then polymerising an aldehyde-functional GEO5MA monomer. Alternatively, aqueous dispersions of PGEO5MA-stabilised nanoparticles could be directly treated with (sub-)stoichiometric quantities of NaIO<sub>4</sub>. The first route may lead to crosslinking via the aldehyde groups. Moreover, periodate functionalization of the PGEO5MA precursor is likely to lead to premature oxidative destruction of the RAFT end-group. Thus periodate treatment of the sterically-stabilised nanoparticles with NaIO<sub>4</sub> may be the best option, possibly immediately after their aqueous PISA synthesis. If desired, using a slight excess of periodate could also remove the RAFT end-groups, which would provide an alternative approach to the H<sub>2</sub>O<sub>2</sub> protocol developed in Chapter 2. In principle, the kinetics and extent of such periodate end-group removal could also be monitored by UV spectroscopy.

Being able to synthesise and purify the aldehyde-functionalised GEO5MA-based monomer should enable the preparation of new aldehyde-functionalised water-soluble homopolymers, statistical copolymers or block copolymers. Although the periodate oxidation of GEO5MA appears to work efficiently, further optimisation is desirable in terms of reaction time, temperature, pH and monomer concentration. Particular attention should be paid to the purification/work-up protocol as the current method only yields approximately 10 % of the desired product.

PGEO5MA brushes can be grown directly from planar silicon wafers, although this protocol requires further optimisation. In principle, selective oxidation of the cis-diol groups within such brushes should be readily achieved simply by dipping the brush-functionalised silicon wafer into an aqueous solution of sodium periodate, followed by removal of the silicon wafer after a

desired reaction time and copious rinsing with deionised water. In this context, it would be interesting to see whether such brushes could be first collapsed by addition of a water-miscible poor solvent (or an appropriate salt) and then reacted with sodium periodate to afford aldehyde-functionalised brushes that bear aldehyde groups only at their near-surface.<sup>19</sup> Such brush derivatisation should be amenable to monitoring by ellipsometry, FT-IR spectroscopy and/or X-ray photoelectron spectroscopy (XPS). A further possibility would be to grow aldehyde-functionalised GEO5MA monomer directly from such wafers. This method may enable the spatial placement of aldehyde groups within brush layers but would require further optimisation of the synthesis of the aldehyde-based methacrylic monomer.

### References

1. Smith, M. B.; March, J., *March's advanced organic chemistry: reactions, mechanisms, and structure*. John Wiley & Sons: Hoboken, NJ, 2007.
2. Clayden, J.; Greeves, N.; Warren, S. G., *Organic chemistry*. Oxford University Press: Oxford; New York, 2012.
3. Pritchard, J. G., *Poly(vinyl Alcohol): Basic Properties and Uses*. Macdonald & Company: London, New York, 1970.
4. Alang Ahmad, S. A.; Wong, L. S.; ul-Haq, E.; Hobbs, J. K.; Leggett, G. J.; Micklefield, J., Micrometer- and Nanometer-Scale Photopatterning Using 2-Nitrophenylpropyloxycarbonyl-Protected Aminosiloxane Monolayers. *Journal of the American Chemical Society* **2009**, *131* (4), 1513-1522.
5. Otera, J., Transesterification. *Chemical Reviews* **1993**, *93* (4), 1449-1470.
6. Harris, H. E.; Pritchard, J. G., Determination of 1,2-glycol units in polyvinyl alcohol. *Journal of Polymer Science Part A*, **1964**, *2* (8), 3673-3679.
7. Taylor, P. G.; Clark, G.; Smart, L. E., *Mechanism and Synthesis*. The Open University: Milton Keynes, 2007.
8. Sugihara, S.; Armes, S. P.; Blanazs, A.; Lewis, A. L., Non-spherical morphologies from cross-linked biomimetic diblock copolymers using RAFT aqueous dispersion polymerization. *Soft Matter* **2011**, *7* (22), 10787-10793.
9. Blanazs, A.; Ryan, A. J.; Armes, S. P., Predictive Phase Diagrams for RAFT Aqueous Dispersion Polymerization: Effect of Block Copolymer Composition, Molecular Weight, and Copolymer Concentration. *Macromolecules* **2012**, *45* (12), 5099-5107.

10. Warren, N. J.; Mykhaylyk, O. O.; Mahmood, D.; Ryan, A. J.; Armes, S. P., RAFT Aqueous Dispersion Polymerization Yields Poly(ethylene glycol)-Based Diblock Copolymer Nano-Objects with Predictable Single Phase Morphologies. *Journal of the American Chemical Society* **2014**, *136* (3), 1023-1033.
11. Warren, N. J.; Armes, S. P., Polymerization-Induced Self-Assembly of Block Copolymer Nano-objects via RAFT Aqueous Dispersion Polymerization. *Journal of the American Chemical Society* **2014**, *136* (29), 10174-10185.
12. Blanazs, A.; Madsen, J.; Battaglia, G.; Ryan, A. J.; Armes, S. P., Mechanistic Insights for Block Copolymer Morphologies: How Do Worms Form Vesicles? *Journal of the American Chemical Society* **2011**, *133* (41), 16581-16587.
13. Blanazs, A.; Verber, R.; Mykhaylyk, O. O.; Ryan, A. J.; Heath, J. Z.; Douglas, C. W. I.; Armes, S. P., Sterilizable Gels from Thermoresponsive Block Copolymer Worms. *Journal of the American Chemical Society* **2012**, *134* (23), 9741-9748.
14. Sangsuwan, R.; Tachachartvanich, P.; Francis, M. B., Cytosolic Delivery of Proteins Using Amphiphilic Polymers with 2-Pyridinecarboxaldehyde Groups for Site-Selective Attachment. *Journal of the American Chemical Society* **2019**, *141* (6), 2376-2383.
15. Fishman, J. M.; Zwick, D. B.; Kruger, A. G.; Kiessling, L. L., Chemoselective, Postpolymerization Modification of Bioactive, Degradable Polymers. *Biomacromolecules* **2019**, *20* (2), 1018-1027.
16. Johnson, A.; Bao, P.; Hurley, C. R.; Cartron, M.; Evans, S. D.; Hunter, C. N.; Leggett, G. J., Simple, Direct Routes to Polymer Brush Traps and Nanostructures for Studies of Diffusional Transport in Supported Lipid Bilayers. *Langmuir* **2017**, *33* (15), 3672-3679.
17. Dunderdale, G. J.; Urata, C.; Miranda, D. F.; Hozumi, A., Large-Scale and Environmentally Friendly Synthesis of pH-Responsive Oil-Repellent Polymer Brush Surfaces under Ambient Conditions. *ACS Applied Materials & Interfaces* **2014**, *6* (15), 11864-11868.
18. Zeng, X.; Xu, G.; Gao, Y.; An, Y., Surface Wettability of (3-Aminopropyl)triethoxysilane Self-Assembled Monolayers. *The Journal of Physical Chemistry B* **2011**, *115* (3), 450-454.
19. Alswieleh, A. M.; Cheng, N.; Leggett, G. J.; Armes, S. P., Spatial Control over Cross-Linking Dictates the pH-Responsive Behavior of Poly(2-(tert-butylamino)ethyl methacrylate) Brushes. *Langmuir* **2014**, *30* (5), 1391-1400.

## **Chapter Six - Conclusions and Prospect**

### Conclusions and Prospect

The radical nature of RAFT polymerisation means that it is exceptionally tolerant of monomer functionality.<sup>1-3</sup> Moreover, such polymerisations can be conducted in various media.<sup>1-3</sup> Thus, RAFT-mediated PISA is a powerful technique for the reproducible synthesis of a wide range of diblock copolymer nano-objects simply by varying the target diblock composition and copolymer concentration.<sup>4-5</sup> In recent years, considerable effort has been devoted to developing functional nanoparticles for various applications. For example, PGMA-PHPMA worm gels are promising media for the long-term storage of human stem cells without loss of pluripotency or for 3D cell culture.<sup>6-7</sup> Similarly, stimulus-responsive diblock copolymer vesicles can be used to encapsulate model payloads (e.g. silica nanoparticles or globular proteins) during PISA and release such payloads on demand (e.g. on adjusting the temperature or solution pH).<sup>8</sup> However, the colour and malodour of the RAFT chain-ends are a potential barrier for such biomedical applications, not least because their hydrolytic instability may compromise biocompatibility over long time scales (weeks).<sup>9</sup> Many studies have shown that RAFT end-groups can be readily removed from soluble polymer chains.<sup>10</sup> However, removing RAFT end-groups from diblock copolymer nanoparticles is much less well-researched, although some encouraging results have been obtained using ozone by Zard and co-workers.<sup>11</sup> For most PISA syntheses, the organosulfur RAFT end-groups are located within the nanoparticle cores. Thus, any reagent used to remove such groups must be able to diffuse into the nanoparticles to access the RAFT end-groups. In Chapter 2, hydrogen peroxide is demonstrated to be an effective reagent for the effective removal of RAFT end-groups from PGMA-PHPMA spheres, worms or vesicles in aqueous media. In principle, various alternative reagents such as amines or excess free radical initiators can also be used to remove such end-groups. However, in practice only hydrogen peroxide enables the physical properties of the nanoparticles to be retained. This is a particularly important consideration for PGMA-PHPMA worms because their rheological behaviour is rather sensitive to such chemical derivatisation. The hydrated nature of the core-forming PHPMA block enables rapid diffusion of the hydrogen peroxide and RAFT chain-end removal can be readily achieved in the case of dithiobenzoate RAFT end-groups. Perhaps surprisingly, the rate of end-group removal appears to be independent of either the size or morphology of the PGMA-PHPMA nanoparticles. However, a rather slower rate of end-group removal is observed for PGMA-PBzMA nanoparticles, which is attributed to the significantly greater hydrophobic character of the PBzMA chains. Moreover, the rate of removal of trithiocarbonate-based end-groups is significantly slower than for the equivalent

dithiobenzoate-based end-groups. This is consistent with the greater hydrolytic stability for the former RAFT end-groups.<sup>12</sup> One important aspect of this RAFT end-group removal study is the development of a robust protocol for monitoring the extent of end-group removal based on UV GPC. This technique is much more reliable than UV spectroscopy because the chromatographic fractionation that is achieved between the copolymer chains and the small molecule by-products ensures that any UV-active by-products such as benzoic acid do not interfere with the UV signal corresponding to the RAFT groups on the as-yet unreacted copolymer chains. This analytical protocol is recommended for monitoring the kinetics of removal of all RAFT end-groups, whether from soluble chains or from nanoparticles.

Recent work within the Armes group has established an effective method for the removal of trithiocarbonate end-groups from diblock copolymer nanoparticles prepared in *n*-tetradecane.<sup>13</sup> Importantly, the UV GPC protocol developed in this Thesis was used to confirm essentially complete end-group removal within 3 h by addition of excess initiator (lauroyl peroxide) at 70 °C. Under such conditions, the PTFEMA-based nanoparticle cores are appreciably solvated, which aids ingress of the initiator-derived radicals. Similarly, in unpublished work by Penfold and co-workers trithiocarbonate end-groups have been removed from aqueous dispersions of PEG-PPMA worms via reaction with excess water-soluble azo initiator at 70 °C. In this case, hydrogen peroxide cannot be used for end-group removal because this reagent degrades the PEG block. Nevertheless, UV GPC again proved to be an extremely useful analytical technique for verifying that a high degree of end-group removal can be achieved within short reaction times. These two examples suggest that the UV GPC protocol developed in this Thesis is likely to become the preferred technique for monitoring the rate of RAFT end-group removal. In summary, removing RAFT chain-ends directly from diblock copolymer nano-objects without affecting the physical properties of the original particles remains an important research topic because such chemical derivatisation is likely to be desirable for the majority of potential commercial applications.

In principle, the marked rate acceleration that occurs after micellar nucleation suggest that PISA should offer a decisive advantage for the efficient production of high molecular weight copolymer chains in the form of low-viscosity nanoparticles. Indeed, there are several reports in the PISA literature of copolymer molecular weights of up to  $10^6$  g mol<sup>-1</sup> (DP ~ 10,000).<sup>14</sup> PISA requires a soluble block and an insoluble block. It is rather obvious that these conflicting

requirements cannot be achieved by the same block, i.e. by a homopolymer. Instead, a diblock copolymer architecture is essential. However, if highly asymmetric diblock copolymers are targeted then the volume fraction of stabiliser block can be minimised. For example, Cunningham and co-workers used a relatively short PGMA block ( $DP = 63$ ) to grow relatively long PNMEP chains ( $DP = 5000$ ).<sup>15</sup> By generating the PNMEP chains above their LCST, sterically stabilised nanoparticles are formed at 70 °C that dissolve to form water-soluble diblock copolymer chains. Although these copolymer chains are certainly PNMEP-rich, they are not true homopolymers. Chapter 3 takes advantage of protecting group chemistry to produce high molecular weight PGMA homopolymer via sterically stabilised diblock copolymer nanoparticles prepared in water. More specifically, RAFT emulsion polymerisation of IPGMA at 70 °C affords well-defined, low-viscosity  $PGMA_{39}$ - $PIPGMA_x$  spheres at 20 % w/w solids. The hydrophobic PIPGMA block is then deprotected on addition of mineral acid at 70 °C to afford a PGMA homopolymer with a molecular weight of up to 250 kg mol<sup>-1</sup>. By utilising the much faster kinetics offered by RAFT emulsion polymerisation, a significantly shorter overall reaction time can be achieved for this wholly aqueous two-step one-pot protocol compared to that achieved via RAFT aqueous solution polymerisation of GMA.

As noted above, RAFT polymerisation is not more widely used in industry because of the intrinsic colour and malodour of RAFT agents, as well as their relatively high cost. Thus conventional aqueous emulsion polymerisation is explored in Chapter 4 as a synthetic route to high molecular weight PIPGMA (and hence PGMA). This approach utilises an anionic surfactant to stabilise the growing PIPGMA latex particles rather than the PGMA block employed in Chapter 3. Conventional free radical polymerisation of IPGMA under emulsion conditions enables high molecular weight PIPGMA precursor chains to be obtained ( $M_w > 700$  kg mol<sup>-1</sup>), albeit with reduced control over the molecular weight distribution. Utilising a monomer-starved protocol eliminated the initial problem of gel fractions observed for ‘one-shot’ batch formulations. The precursor PIPGMA latexes remained in their low-viscosity particulate form if stored at around pH 6-7. Deprotection was achieved under acidic conditions to yield a highly viscous aqueous solution of PGMA chains. Optimisation of the reaction conditions enabled access to PGMA molecular weights of more than 10<sup>6</sup> g mol<sup>-1</sup> with reasonably good control over the molecular weight distribution ( $M_w/M_n < 2.0$ ). Nevertheless, this promising formulation would probably benefit from further optimisation in terms of monomer, initiator and surfactant concentrations, reaction time, rate of monomer addition,

solution pH and reaction temperature. In particular, the possibility of performing such aqueous emulsion polymerisations at higher concentration (up to 40-50 % w/w) would make for a more intensive process. If successful, such concentrated latexes should offer significant cost and time savings and could be diluted as required prior to acid deprotection. High molecular weight water-soluble polymers have many commercial applications. For example, one potential customer for the industrial sponsor of this PhD project (GEO Speciality Chemicals) has expressed an interest in using high molecular weight PGMA in one of its proprietary cleaning products, which contains a substantial quantity of free surfactant(s). For such formulations, it would be interesting to explore using the desired surfactant(s) instead of SDS for the emulsion polymerisation of PIPGMA. Thus, any excess surfactant that is not adsorbed during the latex synthesis would ultimately contribute to the final commercial product, hence minimising waste and eliminating the need to remove excess SDS from the highly viscous water-soluble PGMA chains.

Finally, an interesting water-miscible methacrylic monomer (GEO5MA) has been prepared on a 1.2 kg scale during a six-month secondment at GEO Specialty Chemicals, as outlined in Chapter 5. This monomer, which had been previously synthesised within GEO but never commercialised, can be considered as a hybrid of two other GEO monomers, GMA and OEGMA. A series of PGEO5MA homopolymers were prepared via RAFT ethanolic solution polymerisation and subsequently utilised as a steric stabiliser for the RAFT aqueous dispersion polymerisation of HPMA. This new PISA formulation yielded spheres, worms or vesicles, depending on the target DP of the PHPMA block. Moreover, the pendant *cis*-diol moieties on the PGEO5MA precursor can be rapidly and selectively oxidised using sodium periodate in aqueous solution at ambient temperature to yield a new aldehyde-functional water-soluble homopolymer, for which there are remarkably few such examples in the literature. In contrast, if PGMA is treated with the same oxidant under the same conditions, only an insoluble crosslinked product is obtained. In this case, loss of the *cis*-diol units leads to progressively less hydrophilic (and ultimately water-insoluble) chains, with cross-linking occurring at intermediate conversions owing to hemiacetal formation between the aldehyde groups and the remaining *cis*-diol groups. Thus, the retention of water-solubility for the periodate derivatisation of PGEO5MA is related to the additional hydrophilic character conferred by the five ethylene oxide units in each monomer repeat unit. In principle, this same selective oxidation protocol can be applied to PGEO5MA-PHPMA nano-objects to yield aldehyde-



functional spheres, worms or vesicles. Moreover, GEO5MA monomer can be converted into a new water-miscible aldehyde-functional methacrylic monomer, but in this case a more efficient purification protocol is required for this small molecule reaction. Clearly, further studies are warranted to establish the scope and limitations of this convenient new route to aldehyde-functional monomers, water-soluble homopolymers and nanoparticles. For example, aldehyde groups offer tremendous potential for further reaction with amines via Schiff base chemistry,<sup>16-17</sup> which should be useful for protein functionalisation and/or dye conjugation directly in aqueous solution. Of particular interest is the growth of PGEO5MA brushes from planar surfaces (e.g. silicon wafers) via ARGET ATRP.<sup>18</sup> In principle, such brushes could be readily converted into aldehyde-functional brushes simply by immersion in an aqueous solution of sodium periodate, followed by copious washing to remove excess oxidant (and the toxic formaldehyde by-product). In principle, such brushes could be easily decorated with various enzymes for surface catalytic reactions. If the purification/isolation of the aldehydic methacrylic monomer can be optimised, then its surface polymerisation from silicon wafers would produce polymer brushes with maximum aldehyde functionality (i.e. one aldehyde group per monomer repeat unit). In either case, XPS should be a useful surface analytical technique for brush characterisation, particularly if the aldehyde groups can be reacted with 2,2,2-trifluoroethylamine to produce a convenient and highly specific spectroscopic label.

### References

1. Moad, G.; Rizzardo, E.; Thang, S. H., Living Radical Polymerization by the RAFT Process. *Australian Journal of Chemistry* **2005**, *58* (6), 379-410.
2. Moad, G.; Rizzardo, E.; Thang, S. H., Living Radical Polymerization by the RAFT Process – A Second Update. *Australian Journal of Chemistry* **2009**, *62* (11), 1402-1472.
3. Moad, G.; Rizzardo, E.; Thang, S. H., Living Radical Polymerization by the RAFT Process – A Third Update. *Australian Journal of Chemistry* **2012**, *65* (8), 985-1076.
4. Blanazs, A.; Ryan, A. J.; Armes, S. P., Predictive Phase Diagrams for RAFT Aqueous Dispersion Polymerization: Effect of Block Copolymer Composition, Molecular Weight, and Copolymer Concentration. *Macromolecules* **2012**, *45* (12), 5099-5107.
5. Warren, N. J.; Derry, M. J.; Mykhaylyk, O. O.; Lovett, J. R.; Ratcliffe, L. P. D.; Ladmiral, V.; Blanazs, A.; Fielding, L. A.; Armes, S. P., Critical Dependence of Molecular

Weight on Thermoresponsive Behavior of Diblock Copolymer Worm Gels in Aqueous Solution. *Macromolecules* **2018**, *51* (21), 8357-8371.

6. Canton, I.; Warren, N. J.; Chahal, A.; Amps, K.; Wood, A.; Weightman, R.; Wang, E.; Moore, H.; Armes, S. P., Mucin-Inspired Thermoresponsive Synthetic Hydrogels Induce Stasis in Human Pluripotent Stem Cells and Human Embryos. *ACS Central Science* **2016**, *2* (2), 65-74.

7. Simon, K. A.; Warren, N. J.; Mosadegh, B.; Mohammady, M. R.; Whitesides, G. M.; Armes, S. P., Disulfide-Based Diblock Copolymer Worm Gels: A Wholly-Synthetic Thermoreversible 3D Matrix for Sheet-Based Cultures. *Biomacromolecules* **2015**, *16* (12), 3952-3958.

8. Mable, C. J.; Gibson, R. R.; Prevost, S.; McKenzie, B. E.; Mykhaylyk, O. O.; Armes, S. P., Loading of Silica Nanoparticles in Block Copolymer Vesicles during Polymerization-Induced Self-Assembly: Encapsulation Efficiency and Thermally Triggered Release. *Journal of the American Chemical Society* **2015**, *137* (51), 16098-16108.

9. Pissuwan, D.; Boyer, C.; Gunasekaran, K.; Davis, T. P.; Bulmus, V., In Vitro Cytotoxicity of RAFT Polymers. *Biomacromolecules* **2010**, *11* (2), 412-420.

10. Willcock, H.; O'Reilly, R. K., End group removal and modification of RAFT polymers. *Polymer Chemistry* **2010**, *1* (2), 149-157.

11. Quiclet-Sire, B.; Zard Samir, Z., Fun with radicals: Some new perspectives for organic synthesis. In *Pure and Applied Chemistry*, 2010; Vol. 83, p 519.

12. Thomas, D. B.; Convertine, A. J.; Hester, R. D.; Lowe, A. B.; McCormick, C. L., Hydrolytic Susceptibility of Dithioester Chain Transfer Agents and Implications in Aqueous RAFT Polymerizations. *Macromolecules* **2004**, *37* (5), 1735-1741.

13. Cornel, E. J.; van Meurs, S.; Smith, T.; O'Hora, P. S.; Armes, S. P., In Situ Spectroscopic Studies of Highly Transparent Nanoparticle Dispersions Enable Assessment of Trithiocarbonate Chain-End Fidelity during RAFT Dispersion Polymerization in Nonpolar Media. *Journal of the American Chemical Society* **2018**, *140* (40), 12980-12988.

14. Truong, N. P.; Dussert, M. V.; Whittaker, M. R.; Quinn, J. F.; Davis, T. P., Rapid synthesis of ultrahigh molecular weight and low polydispersity polystyrene diblock copolymers by RAFT-mediated emulsion polymerization. *Polymer Chemistry* **2015**, *6* (20), 3865-3874.

15. Cunningham, V. J.; Derry, M. J.; Fielding, L. A.; Musa, O. M.; Armes, S. P., RAFT Aqueous Dispersion Polymerization of N-(2-(Methacryloyloxy)ethyl)pyrrolidone: A

Convenient Low Viscosity Route to High Molecular Weight Water-Soluble Copolymers. *Macromolecules* **2016**, *49* (12), 4520-4533.

16. Clayden, J.; Greeves, N.; Warren, S. G., *Organic Chemistry*. Oxford University Press: Oxford; New York, 2012.

17. Smith, M. B.; March, J., *March's advanced organic chemistry: reactions, mechanisms, and structure*. John Wiley & Sons: Hoboken, NJ, 2007.

18. Dunderdale, G. J.; Urata, C.; Miranda, D. F.; Hozumi, A., Large-Scale and Environmentally Friendly Synthesis of pH-Responsive Oil-Repellent Polymer Brush Surfaces under Ambient Conditions. *ACS Applied Materials & Interfaces* **2014**, *6* (15), 11864-11868.

**Chapter Seven – Appendix**

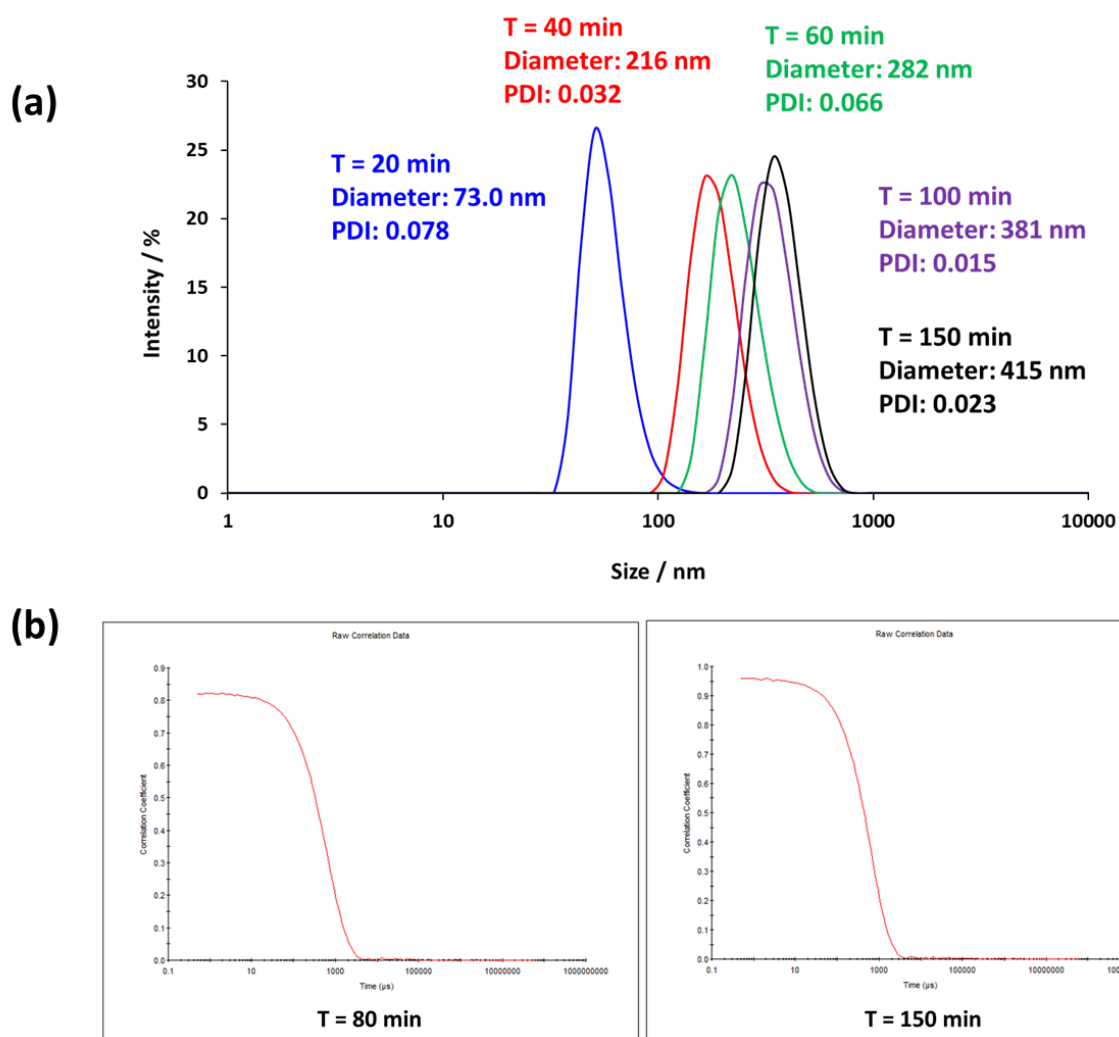


**Figure 7.1.** Analysis of aliquots extracted during the PISA synthesis of PGMA<sub>39</sub>-PIPGMA<sub>1000</sub> via RAFT emulsion polymerisation of IPGMA at 70 °C showing: (a) the development of the intensity-average size distribution during the polymerization and (b) representative DLS correlograms indicating good monodispersity of samples. Conditions: 20 % w/w solids; ACVA initiator; macro-CTA/ACVA molar ratio = 4.0.

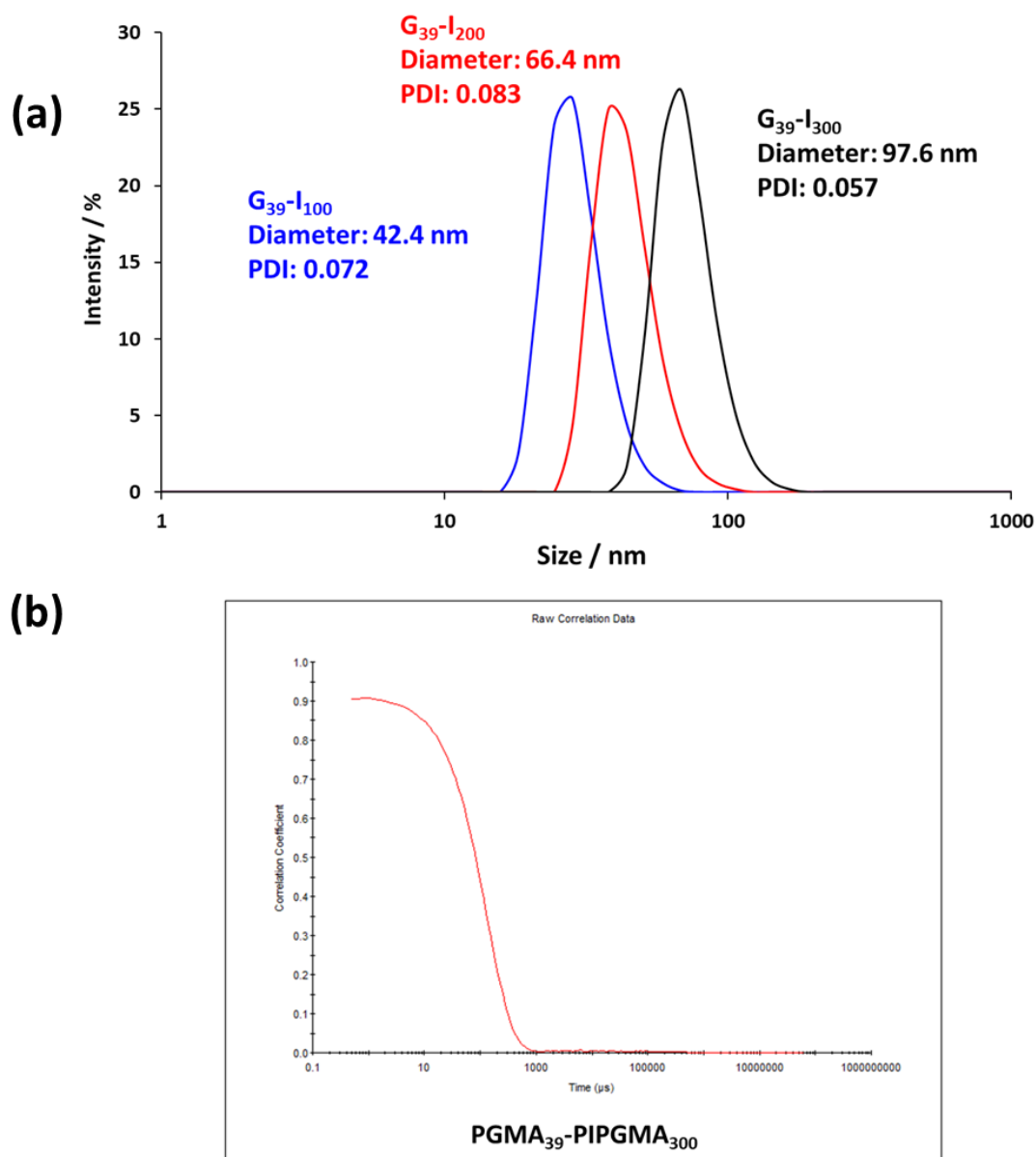


**Figure 7.2.** (a) Representative DLS intensity-average size distributions for a series of PGMA<sub>39</sub>-PIPGMA<sub>x</sub> spherical nanoparticles prepared via RAFT aqueous emulsion polymerisation of IPGMA at 70 °C (see Table 3.1). (b) Representative correlogram for such DLS distributions showing good monodispersity.